Functional Analysis of *Insl5* and *Insl6* Genes and Verification of Interactions between Pelota and its Putative Interacting Proteins

Dissertation

zur Erlangung des Doktorgrades

der Mathematisch-Naturwissenschaftlichen Fakultäten

der Georg-August-Universität zu Göttingen

vorgelegt von

Ozanna Burnicka-Turek

aus Bydgoszcz, Polen

Göttingen, 2009

D7

Referent: **Prof. Dr. W. Engel**

Korreferentin: **Prof. Dr. S. Hoyer-Fender**

Tag der mündlichen Prüfung:

To my husband, family and friends for their support, encouragement and love.

The more you know, the harder it is to take decisive action. Once you become informed, you start seeing complexities and shades of gray. You realize that nothing is as clear and simple as it first appears. Ultimately, knowledge is paralyzing.

Bill Watterson *(1958 -), Calvin & Hobbes (THERE'S TREASURE EVERYWHERE)*

TABLE OF CONTENTS

ABBREVIATIONS

aa	amino acids
Ab.	antibody
ABI	Applied Biosystem Instrument
Abs.	absolute
Amp	ampicillin
Ampuwa	aqua ad iniectabilia
ANOVA	Analysis of Variances
AP	alkaline phosphatase
APS	ammonium persulfate
ATP	adenosine triphosphate
BAC	bacterial artificial chromosome
BCIP	5-bromo-4-choro-3-indolyl-phosphate
BCP	1-bromo-3-chloropropane
bp	base pair
BSA	bovine serum albumin
bw	body weight
°C	degree Celsius
CA	chloramphenicol
CASA	computer assisted sperm analysis
Ccna1	cyclin A1
Cdk2ap1	cyclin-dependent kinase 2-associated protein 1
cDNA	DNA complementary to RNA
CMV	cytomegalovirus
Cy3	indocarbocyanine
DAPI	4',6-diamidino-2-phenylindole dihydrochloride
dATP	deoxyadenosine triphosphate
dCTP	deoxycytidine triphosphate
DEPC	diethylpyrocarbonate
dH_2O	distilled water
DMEM	Dulbecco´s Modified Eagles Media
DMSO	dimethyl sulfoxide

DNA	deoxyribonucleic acid
DNase	deoxyribonuclease
dNTP	deoxyribonucleotide phosphate
dpc	day post coitus
DTT	1,4-dithio-DL-threitol
E	embryonic day
E. coli	*Escherichia coli*
EDTA	ethylene diamine tetraacetic acid
Eif3g	eukaryotic translation initiation factor 3, subunit G
EGFP	enhanced green fluorescent protein
ES	embryonic stem
et al.	et alii or 'and others'
EtBr	ethidium bromide
EtOH	ethanol
F	filial generation or forward
FCS	fetal calf serum
FITC	fluorescein isothiocyanate
g	gravity
gm	gram
GMC	German Mouse Clinic
GSC	germline stem cell
GST	glutathione S-transferase
HBS	HEPES buffered saline
HBSS	Hanks' balanced salt solution
HE	heterozygote
H&E	hematoxylin and eosin stain
HEPES	N-(-hydroxymethyl)piperazin,N'-3-propansulfoneacid
HO	homozygote
hr(s)	hour(s)
Insl3	Insulin-like 3
Insl4	Insulin-like 4
Insl5	Insulin-like 5
Insl6	Insulin-like 6
IPTG	isopropyl-ß-thiogalactopyranoside

Kan	kanamycin
kb	kilobase
kDa	kilodalton
L	liter
LB	Luria-Bertani medium
M	molarity (moles per litre)
m	milli
MeOH	methanol
min	minute
µ	micro
MOPS	3-[N-morpholino]-propanesulfate
mRNA	messenger ribonucleic acid
n	nano
NaAc	sodium acetate
NaCl	sodium chloride
NaOH	sodium hydroxide
NBT	nitroblue tetrazolium
NCBI	National Center for Biotechnology Information
Neo	neomycin
ng	nanogram
NLS	nuclear localization sequence
OD	optical density
ON	overnight
ORF	open reading frame
Pa	Pascal
PAGE	polyacrylamide gel electrophoresis
PCR	polymerase chain reaction
PBS	phosphate buffer saline
PBT	phosphate buffer saline + Tween 20
PFA	paraformaldehyde
pH	preponderance of hydrogen ions
PMSF	phenylmethylsulfonyl fluoride
′ (prime)	denotes a truncated gene at the indicated side
RNA	ribonucleic acid

RNase	ribonuclease
RNasin	ribonuclease inhibitor
rpm	revolutions per minute
RT	room temperature
RZPD	the Resource Center and Primary Database
RT-PCR	reverse transcriptase polymerase chain reaction
SDS	sodium dodecyl sulfate
SDS-PAGE	SDS-polyacrylamide gel electrophoresis
sec	second
SEM	standard error of the mean
S.O.C	sodium chloride medium
Srpx	sushi-repeat-containing protein, X-linked
SV40	Simian Virus 40
Taq	*Thermus aquaticus*
TBE	tris-borate-EDTA electrophoresis buffer
TE	tris-EDTA buffer
TEMED	tetramethylethylenediamine
TK	thymidine kinase
Tris	trihydroxymethylaminomethane
Tween 20	polyoxyethylene-sorbit-monolaurate
U	unit
UV	ultraviolet light
V	voltage
Vol.	volume
w/v	weight/volume
Wt	wild type
X-Gal	5-bromo-4-chloro-3-indolyl-β-galactosidase

Amino acids symbols

A	Ala	Alanine
B	Asx	Asparagine or Aspartic acid
C	Cys	Cysteine

D	Asp	Aspartic acid
E	Glu	Glutamic acid
F	Phe	Phenylalanine
G	Gly	Glycine
H	His	Histidine
I	Ile	Isoleucine
K	Lys	Lysine
L	Leu	Leucine
M	M	Methionine
N	Asn	Asparagine
P	Pro	Proline
Q	Gln	Glutamine
R	Arg	Arginine
S	Ser	Serine
T	Thr	Threonine
V	Val	Valine
W	Trp	Tryptophan
Y	Tyr	Tyrosine
Z	Glx	Glutamine or Glutamic acid

Nucleotides symbols

A	Adenosine
C	Cytidine
G	Guanosine
T	Thymidine
U	Uridine

1. INTRODUCTION

For a better understanding this thesis should be divided into two parts: one concerning the analysis of the expression and function of two insulin-like genes namely *Insl5* and *Insl6*, and the second part about the verification of interactions between PELO and its putative interacting proteins.

1.1. Expression and function of insulin-like genes

The insulin superfamily encompasses the insulin (INS), insulin-like growth factors I and II (IGF-I and II), relaxin-1 to 3 (RLN1-3); and the insulin-like (INSL) peptides, INSL3, INSL4, INSL5, and INSL6 (Blundell und Humbel, 1980; Adham *et al*., 1993; Laurent *et al.,* 1998; Conklin *et al*., 1999; Hsu, 1999, Lok *et al*., 2000; Bathgate *et al.,* 2002a, 2002b; Sherwood, 2004; Halls *et al.,* 2007b).

Members of this family share conserved cysteine residues as well as a similar primary peptide structure, which consists of a signal sequence, a B-chain, a connecting C-peptide and an A-chain (Conklin *et al*., 1999; Wilkinson *et al.,* 2005; Bathgate *et al.,* 2006a) (Fig. 1). The signal peptide facilitates the translocation of the prohormone into the endoplasmic reticulum and the connecting C-peptide mediates correct folding of the protein and the formation of the two inter-chain and one intra-chain disulfide bonds between six invariant cysteine residues in the active hormone (Sherwood, 2004; Wilkinson *et al.,* 2005). In proinsulin, prorelaxin and proinsulin-like peptides, the B- and A-chains are located at the N- and C-terminal, respectively, and are separated by a long C-peptide. The active insulin, relaxin (Sherwood 2004), relaxin-3 (Bathgate *et al.,* 2002a) and INSL3 (Bullesbach and Schwabe, 2002) are formed by the cleavage and removal of the C-peptide and the formation of two disulfide bridges between the B- and A-chains (Bathgate *et al.,* 2006a). In contrast, the proIGF-I and proIGF-II contain a small C-peptide and two additional domains (D and E) at the C-terminus of which the E-peptide is removed during processing while the C-peptide is maintained in the active protein (Blundell and Humbel, 1980; Fawcett and Rabkin, 1995; Duguay *et al.,* 1998). Based on primary sequence similarity, the native structures of INSL4, INSL5 and INSL6 should be similar to insulin and relaxin, but to date this has not been confirmed (Wilkinson *et al.,* 2005; Wilkinson and Bathgate, 2007).

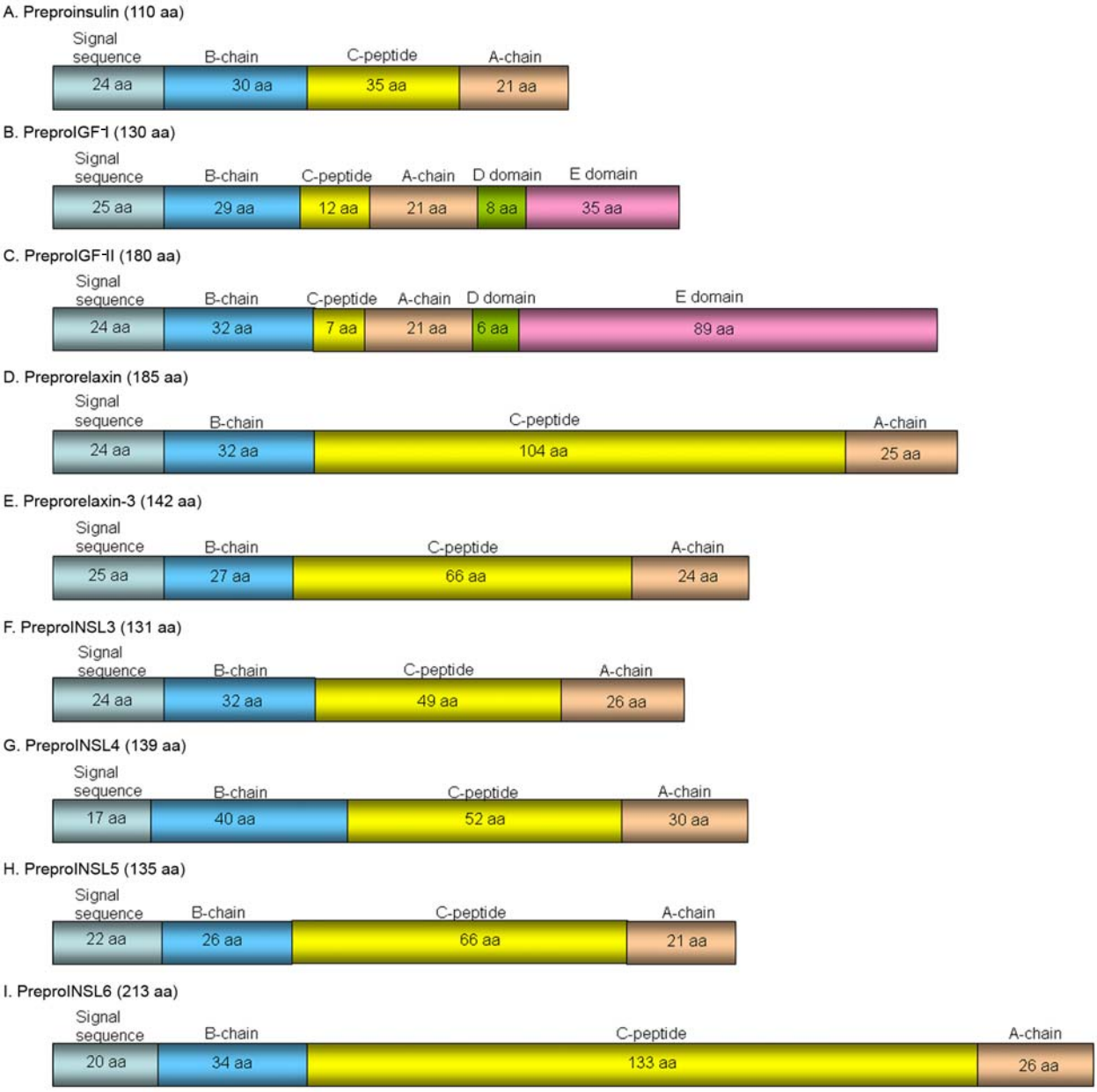

Fig. 1. The members of the insulin superfamily. Primary structure organization (preprohormone) of the human insulin (A) (Bell *et al.,* 1979), IGF-I (B) (Jansen *et al.,* 1983), IGF-II (C) (Bell *et al.,* 1984), relaxin (D) (Hudson *et al.,* 1983, Hudson *et al.,* 1984), relaxin-3 (E) (Bathgate *et al.,* 2002; Kizawa *et al.,* 2003), INSL3 (F) (Burkhardt *et al.,* 1994), INSL4 (G) (Chassin *et al.,* 1995), INSL5 (H) (Conklin *et al.,* 1999) and INSL6 (I) (Lok *et al.,* 2000) are shown.

The expression analysis of the genes belonging to the insulin superfamily revealed that some of them are ubiquitously expressed such as relaxin, IGF-I and IGF-II (Sherwood, 1994; Daughaday and Rotwein, 1998; Sherwood, 2004; Bathgate *et al.,* 2006a; Bondy *et al.,* 2006). Others genes show tissue-specific expression such as insulin, which is expressed in β–cells of pancreas (Pictet and Rutter, 1972; Chan and Steiner, 2000; Bondy *et al.,* 2006), or relaxin 3, which is expressed in the brain (Burazin *et al.,* 2000; Tanaka *et al.,* 2005).

Members of the insulin superfamily are known to have regulatory role in cell growth and differentiation, metabolism, and reproduction (Adham *et al.,* 1993; de Pablo and de la Rosa, 1995; Conklin *et al.,* 1999; Liu and Leroith, 1999; Lok *et al.,* 2000; Bathgate *et al.,*2006a). Insulin regulates peripheral energy homeostasis by acting on multiple tissues to control carbohydrate, lipid and protein metabolism (Chan and Steine, 2000; Cantley *et al.,* 2007). The IGF-I and IGF-II are involved in cell growth and differentiation as autocrine/paracrine factors (O'Dell and Day, 1998; Reinecke and Collet, 1998; Liu and Leroith, 1999). Relaxins (RLN) are multifunctional hormones, which play important role in growing of reproductive tissues, collagen remodeling, regulation of cardiovascular function, and allergic responses (Chan and Steine, 2000; Hsu *et al.,* 2002, Bathgate *et al.,* 2003; Sherwood, 2004**;** Bathgate *et al.,* 2006a). Females deficient for RLN1 exhibited undeveloped mammary gland nipples and increased parturition time during pregnancy (Zhao *et al.*, 1999). Male-specific abnormalities were detected in renal and cardiac function of the older RLN1-deficient animals. Furthermore, the testes, epididymes, and prostate of *Rln1*$^{-/-}$ mice showed delayed tissue maturation and growth associated with increased collagen deposition (Bathgate *et al.,* 2003; Samuel *et al.,* 2005). INSL3 is essential for testicular descent and gubernacular development (Zimmermann *et al.,* 1999; Nef and Parada, 1999). It has also role in oocyte maturation and suppression of male germ cell apoptosis in rats (Kawamura *et al.,* 2004). INSL3-deficient male mice showed bilateral cryptorchidism with abnormal spermatogenesis and gubernaculums feminization during embryogenesis (Zimmermann *et al*., 1999; Nef and Parada, 1999). Female *Insl3*$^{-/-}$ mice exhibited impaired fertility associated with extension of the estrous cycle length (Nef and Parada, 1999; Ivell and Bathgate, 2002; Gambinari *et al.,* 2007) and accelerated follicular atresia and luteolysis, with the premature loss of corpora lutea in ovaries, probably due to increased apoptosis (Spaniel-Borowski *et al.,* 2001; Gambinari *et al.,* 2007). The insulin-like 4 gene is highly expressed in the human placenta but a role of its peptide has not been determined. Janneau *et al.* (2002) suggested that INSL4 can play a significant role in trophoblast development. The functions of *Insl5* and *Insl6* genes are not known, therefore our work was concentrated to study their expression and functions.

1.2. The pelota gene

The *Pelo* gene was first identified in *Drosophila melanogaster* in 1993 (Castrillon *et al.,* 1993) and then the orthologe gene has been isolated and characterized in several species including *Methanococcus jannaschii* (Bult *et al.,* 1996), *Sulfolobus solfataricus* (Ragan *et al.,* 1996), *Saccharomyces cerevisiae* (Davis and Engebrecht, 1998), *Caenorhabditis elegans* (Gen Bank, Accession No.Z36238), *Arabidopsis thaliana* (Gen Bank, Accession No.T20628), *Homo sapiens* (Shamsadin *et al.,* 2000) and *Mus musculus* (Shamsadin *et al.,* 2002). Comparison of the predicted amino acid and nucleotide sequences of the *Pelo* reveals that the pelota gene is highly conserved during evolution. The amino acid sequence of archaebacteria, yeast, *A. thaliana, C. elegans, D. melanogaster* and mouse protein are 23%, 36%, 51%, 57%, 70%, 90% identical to human pelota, respectively (Adham *et al.,* 2003). The expression analysis of *Pelo* in *Drosophila*, mouse and human revealed that the gene is widely expressed in adult tissues as well as during embryonic development (Eberhart and Wasserman, 1995; Shamsadin *et al.,* 2000 and 2002).

Davis and Engebrecht (1998) reported that the pelota of *S. cerevisiae* contains three regions that display similarity to conserved motifs (Fig. 2): (1) A putative nuclear localization signal (NLS) is located at residues 173-177 of the yeast protein. This sequence PKKKR (nuclear localization signal) is similar to PKKKRK of simian virus 40 (SV40) large T antigen. (2) PELO protein contains three eEF1α-like domains. The eEF1α-like domain is present in several proteins such as the translation elongation factor eEF1α and the translation release factors eRF1 and eRF3, which are involved in the termination step of protein synthesis (Frolova *et al.,* 1994).(3) A putative leucine zipper motif is located at the C-terminus of *S. cerevisiae* protein. Leucine zippers have been suggested to mediate protein-protein interactions in a diverse set of functionally unrelated proteins (Busch and Sassone-Corsi, 1990). Alignment of PELO from different species revealed that the pelota proteins share the NLS, eRFI and leucine zipper motifs (Sallam, 2001).

Fig. 2. Schematic representation of human PELO protein structure. PELO protein contains three regions that display similarity to conserved motifs: (1) Residues 1-131, 136-268 and 271-371 are highly similar to a portion

of eukaryotic peptide chain release factor subunit 1 (eRF1). (2) A putative nuclear localization signal (NLS) is located at residues 168-172. This sequence is similar to that of simian virus 40 (SV40) large T antigen NLS (DOM34, PKKKR; SV40, PKKKRKV). (3) A putative leucine zipper (LZ) motif is located at the C-terminus of PELO protein.

A phylogenetic analysis of Pelo primary amino acid sequences from different species using the TreeFam database supports of the idea that all *Pelo* genes are derived from the same ancestral gene (Buyandelger, 2006).

The function of *Pelo* gene was first studied in *Drosophila.* Male mutants were found to be infertile (Eberhart and Wasserman, 1995). During *Drosophila* spermatogenesis, germ cells undergo four rounds of mitosis, an extended premeiotic G2 phase and two meiotic division. In male homozygous for mutations in pelota, the germline mitotic divisions are normal. The 16 spermatocytes undergo a premeiotic S-phase and duplicate their DNA content. However, spermatocytes in the mutant arrested prior to full chromosome condensation, spindle pole organization, and nuclear breakdown. Metaphase and anaphase figures of the meiotic divisions, which are clearly recognized in squashed preparations of wild type testis, were not observed in testis of the *Pelo* mutant. Although meiotic division arrests in *Pelo*-deficient spermatocytes, germ cell differentiation continues, resulting in 4*N* spermatids with head and tail structures. These results indicate that the *Pelo* is required for the meiotic cell division during the G2/M transition (Eberhart and Wasserman, 1995). Beside the effect of the mutation concerning the progression of spermatogenesis, the eyes of the *Pelo* homozygotes are up to 30% smaller than those of wild type siblings. These results suggest that *Pelo* is required for *Drosophila* eye development (Castrillon *et al.,* 1993; Eberhart and Wasserman, 1995). Also, the ovaries of *Pelo* homozygous flies are very small. The mitotic zone of ovaries appears disorganized and often contains degenerating cells. Later stages of oogenesis are also affected. The female mutants produce less than 50% eggs compared with wild type. These result suggest that pelota is also required for mitotic division in the ovary (Eberhart and Wasserman, 1995).

Analysis of mitotic and meiotic division in the *Dom34* mutant of *Saccharomyces cerevisiae*, which has a mutation in the *Pelo* orthologous gene, reveals that deletion of *Dom34* causes growth retardation, defective sporulation and reduces polyribosomes. The yeast mutant also fails to segregate chromosomes properly (Davis and Engebrecht, 1998). Introduction of the

Drosophila wild type *Pelo* transgene into a *Dom34* mutant was found to result in substantial rescue of the *Dom34* growth and sporulation defects (Eberhart and Wasserman, 1995).
To analyze the function of pelota in mammalian species, *Pelo* gene was disrupted by homologous recombination in the mouse (Adham *et al.,* 2003). This knock-out causes early embryonic lethality of the $Pelo^{-/-}$ pups between E3.5 and E7.5. However, heterozygous $Pelo^{+/-}$ mice show no apparent abnormalities in development or fertility, indicating that one functional copy of the pelota gene is sufficient for normal development (Adham *et al.,* 2003).

To get more information about the possible function of *Pelo*, we have started to identify the putative interaction partners of PELO protein. In order to find out putative interaction partners of human PELO protein, the yeast two-hybrid screening was performed by Linda Ebermann (Ebermann, 2005). The human prostate expression library was screened using human PELO protein as bait. Several PELO binding partners were identified. They were classified according to their structure and function into three categories:

- Cytoskeleton associated proteins [Filamin A, α-Actinin 1, Filamin C, Fibulin 4]
- LIM-domain containing proteins, which play a role in actin polymerization [Four and a half LIM domains 2 (FHL2)]
- Proteins, which are involved in cell cycle control or cancerogenesis [Cyclin-dependent kinase 2 associated protein 1 (CDK2AP1), Eukaryotic translation initiation factor 3, subunit G (EIF3G) and Sushi-repeat-containing protein, X-linked (SRPX)]

The most interesting putative pelota interaction partners were proteins involved in the cell cycle control. Therefore in the present thesis we have been concentrated to verify the interactions between PELO and CDK2AP1, EIF3G and SRPX.

1.3. Objectives of this study

1. The functional analysis of the *Insl5* and *Insl6* genes. Scientific approaches undertaken in this study were as follows:

- Expression analysis of *Insl5* gene during the pre- and postnatal life using RT-PCR
- Generation and characterization of the *Insl5*-deficient mice
- Expression analysis of *Insl6* gene during the pre- and postnatal life using RT-PCR and Northern blot
- Generation and characterization of the *Insl6*-deficient mice
- Identification of the cause of male infertility in the *Insl6*-deficient mice

2. Verification of the interactions between PELO and CDK2AP1, EIF3G and SRPX. The specific topics of the study were:

- Colocalization of PELO and its putative interaction partners in HeLa cells
- Coimmunoprecipitation of PELO protein and its putative interaction partners
- GST Pull-down assay to determine which domain of PELO is responsible for binding to CDK2AP1, EIF3G and SRPX
- Subcellular localization of PELO-interacting protein complexes using Bimolecular Fluorescence Complementation (BiFC) assay

2. MATERIALS AND METHODS

2.1. Materials

2.1.1. Chemicals and reagents

Acetic acid	Merck, Darmstadt
Acrylamide/Bisacrylamide	Roth, Karlsruhe
Agar	Roth, Karlsruhe
Agarose	Invitrogen, Karlsruhe
Ammonium acetate	Fluka, Neu Ulm
Ammonium persulfate	Sigma, Deisenhofen
Ampicillin	Sigma, Deisenhofen
Ampuwa	Fresenius, Bad Homburg
Aqua Poly/Mount	Polysciences, Inc, USA
Aprotinin	Sigma, Deisenhofen
Bacto-tryptone	Roth, Karlsruhe
Bacto-Yeast-Extract	Roth, Karlsruhe
BCIP	Applichem, Darmstadt
Benzonase	Merck, Darmstadt
Blocking powder	Roth, Karlsruhe
Bromophenol blue	Sigma, Deisenhofen
BSA	Biomol, Hamburg
Cell culture media	Gibco-BRL, Karlsruhe
Chemiluminescent substrate	Pierce, Rockford, IL
Chloromphenicol	Sigma, Deisenhofen
Chloroform	Merck, Darmstadt
Coomassie G-250	Sigma, Deisenhofen
Crystal violet	Sigma, Deisenhofen
Dextran sulfate	Amersham, Freiburg
Dextrose (glucose)	Fisher, Schwerte
Diethylpyrocarbonate (DEPC)	Sigma, Deisenhofen
Dimethylformamide	Sigma, Deisenhofen

Dimethyl sulfoxide (DMSO)	Merck, Darmstadt
Dithiothreitol	Sigma, Deisenhofen
DNA markers	Invitrogen, Karlsruhe
dNTPs (100 mM)	Invitrogen, Karlsruhe
Ethanol	Baker, Deventer, NL
Ethidium bromide	Roth, Karlsruhe
Eukitt-quick hardening mounting medium	Fluka, Neu Ulm
FCS	Invitrogen, Karlsruhe
Ficoll 400	Applichem, Darmstadt
Formaldehyde	Merck, Darmstadt
Formamide	Sigma, Deisenhofen
Glutaraldehyde	Sigma, Deisenhofen
Glycerol	Invitrogen, Karlsruhe
Glycine	Biomol, Hamburg
Goat serum	PAN-Systems, Nürnberg
HCl	Roth, Karlsruhe
HEPES	Merck, Darmstadt
H_2O_2	Merck, Darmstadt
Horse serum	PAN-Systems, Nürnberg
Ionophore A23187	Calbiochem, Bad Soden
IPTG	Biomol, Hamburg
Isoamyl alcohol	Fluka, Neu Ulm
Isopropanol	Merck, Darmstadt
IVF media	Medicult, Berlin
Kanamycin	Sigma, Deisenhofen
KCl	Merck, Darmstadt
Klenow DNA polymerase	Amersham, Braunschweig
L.A.B. solution	Polysciences, Inc., Warrington, USA
Leupeptin	Sigma, Deisenhofen
Lipofectamine 2000 TM	Invitrogen, Karlsruhe
Lysozyme	Sigma, Deisenhofen
Methanol	Merck, Darmstadt
Methyl benzoate	Fulka, Neu Ulm
$MgCl_2$	Merck, Darmstadt

Milk powder	Roth, Karlsruhe
MOPS	Applichem, Darmstadt
β-Mercaptoethanol	Serva, Heidelberg
NaCl	Merck, Darmstadt
$NaHCO_3$	Merck, Darmstadt
Na_2HPO_4	Merck, Darmstadt
NaH_2PO_4	Merck, Darmstadt
NaN_3	Merck, Darmstadt
NaOH	Merck, Darmstadt
NBT	Applichem, Darmstadt
Nonidet P40	Fluka, Neu Ulm
NuPAGE LDS sample buffer (4x)	Invitrogen, Karlsruhe
NuPAGE Novex Bis-Tris 4-12% Gel	Invitrogen, Karlsruhe
NuPAGE MES running buffer (20x)	Invitrogen, Karlsruhe
NuPAGE MOPS running buffer (20x)	Invitrogen, Karlsruhe
NuPAGE SDS sample buffer	Invitrogen, Karlsruhe
OptiMEM I	Invitrogen, Karlsruhe
Orange G	Sigma, Deisenhofen
Paraformaldehyde	Merck, Darmstadt
PBS	PAN-Systems, Nürnberg
Penicillin/Streptomycin	PAN-Systems, Nürnberg
Peptone	Roth, Karlsruhe
Phalloidin	Sigma, Deisenhofen
Phenol	Biomol, Hamburg
Phosphoric acid	Merck, Darmstadt
Picric acid	Fulka, Neu Ulm
Protein A/G PLUS agarose	Santa Cruz Biotechnology, Heidelberg
Protease cocktail	Sigma, Deisenhofen
Protein marker	Invitrogen, Karlsruhe
Proteinase K	Applichem, Darmstadt
$[\alpha^{32}P]$-dCTP	Amersham, Braunschweig
RediprimeTM II	Amersham, Freiburg
RNase A	Qiagen, Hilden
RNAse away	Biomol, Hamburg

RNase Inhibitor	Boehringer, Mannheim
RNA length standard	Invitrogen, Karlsruhe
Saccharose (Sucrose)	Roth, Karlsruhe
Salmon sperms DNA	Sigma, Deisenhofen
SDS	Serva, Heidelberg
Select peptone	Invitrogen, Eggenstein
S.O.C medium	Invitrogen, Karlsruhe
sodium acetate	Merck, Darmstadt
sodium citrate	Merck, Darmstadt
SuperScript II	Invitrogen, Karlsruhe
T4 DNA ligase	Promega, Mannheim
TEMED	Serva, Heidelberg
TRI reagent	Sigma, Deisenhofen
Tris base	Sigma, Deisenhofen
Triton X-100	Serva, Heidelberg
Trypsin	PAN-Systems, Nürnberg
Tween-20	Sigma, Deisenhofen
Vectashield (DAPI)	Vector, Burlingame
X-Gal	Biomol, Hamburg
Xylene	Merck, Darmstadt

All those chemicals, which are not mentioned above, were ordered from either Merck, Darmstadt or Roth, Karlsruhe.

2.1.2. Buffers and solutions

2.1.2.1. Agarose gel electrophoresis

5X TBE buffer	450 mM Trisbase 450 mM Boric acid 20 mM EDTA (pH 8.0)
Glycerol loading buffer	10 mM Tris/HCl (pH 7.5)

	10 mM EDTA (pH 8.0) 0.025% Orange G 30% Glycerol

2.1.2.2. SDS-PAGE

40% Acrylamide stock solution	Acrylamide 29.2% (w/w) Bis-acrylamide 0.8% (w/w) 10% Ammonium persulfate solution in H_20

10% Ammonium persulfate solution in H_20

Coomassie solution: (staining solution)	30% (v/v) Methanol 10% (v/v) Acetic Acid 0.5% (w/v) Coomassie G-250
Coomassie Blue (destaining solution)	45% Methanol 10% Acetic acid
Running buffer (5x)	25 mM Tris/HCl (pH 8.3) 192 mM Glycine 0.1% SDS
Separating gel buffer (4x)	1.5 M Tris/HCl (pH 8.3) 0.4% SDS
Stacking gel buffer (4x)	0.5 M Tris/HCl (pH 6.8) 0.4% SDS

2.1.2.3. Frequently used buffers and solutions

All standard buffers and solutions were prepared according to Sambrook *et al.* (1989).

AP buffer	100 mM Tris-HCl (pH 9.5) 100 mM NaCl 50 mM $MgCl_2$
BCIP-Solution	50 mg/ml BCIP 70% Dimethylformamide
Blocking solution I (immunostaining)	60 µl of Horse serum, 150 µl of 10%Triton X-100 2790 µl PBS
Blocking solution II (immunostaining)	10% Goat serum in 0.2% PBT
Bouin's solution	15 volume of Picric acid (in H_2O) 5 volume Formaldehyde 1 volume Acetic acid
Carrier DNA	sonicated salmon sperm DNA, 5 mg/ml
dNTP-Mix (10 mM)	10 mM dATP 10 mM dGTP 10 mM dCTP 10 mM dTTP
Denaturation solution	1.5 M NaCl 0.5 M NaOH
Denhardt´s solution (50x)	1% BSA

	1% Polyvinylpyrrolidon 1% Ficoll 400
Depurization solution	0.25 M HCl
E-buffer (10x)	300 mM NaH_2PO_4 50 mM EDTA
Elution buffer	1.5 M NaCl 20 mM Tris/HCl (pH 7.5) 1 mM EDTA
Hybridization Solution	5x SSC 5x Denhardt´s solution 10% Dextran sulfate 0.1% SDS
IPTG	0.1 M in ddH_2O filter sterilized and stored at 4°C
Ligation buffer (10x)	600 mM Tris/HCl (pH 7.5) 80 mM $MgCl_2$ 100 mM DTT
Lysis buffer I	100 mM Tris/HCl (pH 8.0) 100 mM NaCl 100 mM EDTA 0.5% SDS
Lysis buffer II	100 mM Tris/HCl (pH 8.0) 5 mM EDTA 200 mM NaCl 0.2% SDS 100 µg/ml Proteinase K

Lysis buffer A	10 mM Tris/HCl (pH 8.0) 1 mM EDTA 2.5% SDS 1 mM PMFS
Lysis buffer B	50 mM Tris/HCl, (pH 7.5) 150 mM NaCl 1% Nonidet P40 0.5% Sodium deoxycholate 1 Protease inhibitor cocktail tablet
10X MOPS buffer	41.8 gm MOPS 16.6 ml 3 M Sodium acetate 20 ml 0.5 M EDTA in 1 liter of DEPC water adjust pH to 6.75
NBT- Solution	75 mg/ml NBT 70% Dimethylformamide
Neutralization solution	1.5 M NaCl 1 M Tris/HCl (pH 7.0)
P1 buffer (Mini prep)	50 mM Tris/HCl, pH 8.0 10 mM EDTA 100 µg/ml RNase A
P2 buffer (Mini prep)	200 mM NaOH 1% SDS
P3 buffer (Mini prep)	3.0 M Natrium acetate (pH 5.5)

PBS buffer	130 mM NaCl 7 mM Na_2 HPO_4 4 mM NaH_2 HPO_4
PBT buffer I	0.2% Tween-20 in PBS (1x)
PBT buffer II	0.02% Tween-20 in PBS (1x)
Protein lysis buffer	150 mM NaCl 10 mM EDTA 50 mM Tris/HCl pH7.6 1% Triton X-100 1% Sodium deoxycholate
Semidry transfer buffer (1x)	25 mM Tris pH 8.3 150 mM Glycin 10 % Methanol
SSC (20x)	3 M NaCl 0.3 M Trisodium citrate (pH 7.0)
Stop-Mix	15% Ficoll 400 200 mM EDTA 0.1% Orange G
TE buffer (10x)	10 mM Tris/HCl (pH 8.0) 100 mM EDTA
Washing solution I	2x SSC 0.1% SDS
Washing solution II	0.2x SSC 0.1% SDS

2.1.3. Laboratory materials

The laboratory materials, which are not listed here, were bought from Schütt and Krannich (Göttingen).

Cell culture flask	Greiner, Nürtingen
Culture slides	BD Falcon, Heidelberg
Dialysis hoses	Serva, Heidelberg
Disposable filter Minisart NMI	Sartorius, Göttingen
Filter paper 0858	Schleicher and Schüll, Dassel
Hybond C	Amersham, Braunschweig
Hybond N	Amersham, Braunschweig
Microcentrifuge tubes	Eppendorf, Hamburg
Petri dishes	Greiner, Nürtingen
Pipette tips	Eppendorf, Hamburg
RotiPlast paraffin	Roth, Karlsruhe
Superfrost slides	Menzel, Giser
Transfection flask	Lab-Tek/Nalge, Nunc, IL, USA
Whatman blotting paper (GB 002, GB 003 and GB 004)	Schleicher and Schüll, Dassel
X-ray films	Amersham, Braunschweig

2.1.4. Sterilization of solutions and equipment

All solutions that are not heat sensitive were sterilized at 121°C, 10^5 Pa for 60 min in an autoclave (Webeco, Bad Schwartau). Heat sensitive solutions were filtered through a disposable sterile filter (0.2 to 0.45 μm pore size). Plastic wares were autoclaved as above. Glassware were sterilized overnight in an oven at 220°C.

2.1.5. Media, antibiotics and agar-plates

2.1.5.1. Media for bacteria

LB Medium (pH 7.5):
1% Bacto-trypton
0.5% Yeast extracts
1% NaCl

LB-Agar:
1% Bacto-trypton
0.5% Yeast extracts
1% NaCl
1.5% Agar

The LB medium was prepared with distilled water, autoclaved and stored at 4°C.

2.1.5.2. Media for cell culture

HeLa or 15P1 cells medium:

Dulbecco´s Modified Eagles Media (DMEM)
2 mM L-Glutamine
10% FCS
1% Penicillin/Streptomycin

HepG2 cells medium:

RPMI 1640 medium
2 mM L-Glutamine
10% FCS
1% Penicillin/Streptomycin

For long time storage of the cells in liquid nitrogen, the following freezing medium was used:

Freezing medium
30% culture medium
50% FCS
20% DMSO

2.1.5.3. Antibiotics

Stock solutions were prepared for the antibiotics. The stock solutions were then filtered through sterile disposable filters and stored at –20°C. The antibiotic was added to the autoclaved medium after cooling down to a temperature lower than 55°C.

Antibiotics	Master solution	Solvent	Final concentration
Ampicillin	50 mg/ml	H_2O	50 µg/ml
Chloroamphenicol	12,5 mg/ml	ethanol	12,5 µg/ml
Kanamycin	25 mg/ml	H_2O	50 µg/ml
Penicillin	0.1 mg/ml	PBS	10 µg/ml
Streptomycin	0.1 mg/ml	PBS	10 µg/ml

2.1.5.4. IPTG/X-Gal plate

LB-agar with 50 µg/ml ampicillin, 100 µM IPTG and 0.4% X-Gal was poured into Petri dishes. The dishes were stored at 4°C. All other antibiotic plates were prepared similarly.

2.1.6. Bacterial strains

E. coli BL21 (DE3)	B strain, F-*omp*T *hsd*SB(rB-mB-) *gal, Dcm* Novagen, Darmstadt
E. coli DH5α	K-12 strain**,** F- Φ80d lacZΔM15 endA1 recA1 hsdR17 (rk-, mk+) sup E44 *thi*-1 d- gyrA96 Δ(lacZYA-arg) Invitrogen, Karlsruhe

2.1.7. Cell lines

15P1	Sertoli cell line ,Rassoulzadegan *et al.,* 1993
HeLa	Human cervical adenocarcinoma cell line, ATCC, Rockville, USA
HepG2	Human hepatocellular liver carcinoma cell line, ATCC, Rockville, USA

MA10 Mouse Leydig tumor cells, Ascoli, 1981

2.1.8. Plasmids

FPCA-V1	Prof. Dr. S. Hoyer-Fender, Göttingen
FPCA-V2	Prof. Dr. S. Hoyer-Fender, Göttingen
pBluesript SK (+/-)	Stratagene La Jolla, USA
pcDNA^{TM} 3.1/myc-His A(+)	Invitrogen, Darmstadt, Germany
pCMV-HA	BD Biosciences, Heidelberg
pCMV-Myc	BD Biosciences, Heidelberg
pGEM-T Easy	Promega, Wisconsin, USA
pET 41a(+)	Novagen, Darmstadt, Germany
pPNT	Tybulewicz *et al.,* 1991
pZERO-2	Invitrogen, Darmstadt, Germany

2.1.9. Synthetic oligonucleotide primers

The synthetic oligonucleotide primers used in this study were obtained from OPERON (Köln, Germany) and dissolved in water (Ampuwa) to a final concentration of 100 pmol/µl.

Primer name	Sequence
CDK2AP1_LF	5’ AGG CAA GCT TTG TCT TAC AAA CCG AAC TTG GC 3’
CDK2LIV	5’ TCC TGG ATC CGT GTT ACA GGT CTG GCT CAT TTC 3’
CDK2AP1_LR	5’ GGG AGA TCT CTA GGA TCT GGC ATT CCG TTC CG 3’
CDK2AP1_LVI_F1	5’ GGG CTC GAG ATG TCT TAC AAA CCG AAC TTG GCC 3’
CDK2AP1_LVI_R1	5’ TCC TGG ATC CGA TCT GGC ATT CCG TTC CGT TTC 3’
C-Insl5-FcDNA	5’ GCT GAC CAC ATT GCT TCT CA 3’
C-Insl5-RcDNA	5’ TTT TGC ACA GCA CTC GAA AC 3’
eIF3g_F1	5’ CGA CTT TGA CTC GAA GCC CAG 3’
eIF3g_R1	5’ GCT TTC TGT CTG TCC TGA GGG 3’
eIF3F2	5’ GCC ACC ATC CGT GTC ACT AAC 3’
eIF3R2	5’ GCT TTC TGT CTG TCC TGA GGG 3’
eIF3F1anew	5’ CGT GAG CCT GTA CTT TCA GCC 3’

eIF3R1anew	5’ CCA CGC ATA CTC AAA GTC GCC 3’
eIF3G_pPNT_linker_F2	5’ GGC CAA CTC GAG AGT CGA CAG CGG CCG CA 3’
eIF3G_pPNT_linker_R2	5’ TTG AGC TCT CAG CTG TCG CCG GCG TAG CT 3’
eIF3_LF	5’ AGG CAA GCT TTG CCT ACT GGA GAC TTC GAT TCG 3’
eIF3_LR	5’ GGG AGA TCT CTA GTT GGT GGA CGG CTT GGC CCA C 3’
hPelo_F20	5’ CCC TCT AGA CTT CCT TGG CCA TGA AGC TCG 3’
hPelo_LR	5’ TCC TGG ACT CTC CTC TTC AGA ACT GGA ATC ACC 3’
HPelo_LVI_F2	5’ GCC CTC GAG ATG AAG CTC GTG AGG AAG AAC ATC 3’
HPelo_LVI_R2	5’ TCC TGG ATC CTC CTC TTC AGA ACT GGA ATC ACC 3’
hPelo_R20	5’ GGG TCT AGA CTT GCA GCT TTC TGT CAC AAG 3’
I5KO-F1	5’ CCA CTA GAG GTC TTA GGA TCC 3’
Insl5F	5’ GCT GAC CAC ATT GCT TCT CA 3’
Insl5-F8	5’ CGG ATC TCT CAG GAL AGG AG 3’
Insl5R	5’ TTT TGC ACA GCA CTC GAA AC 3’
Insl5-R9	5’ ACC TCA GCA CAG GGA GAA GA 3’
Insl6_ext4_F	5’ GGA CCA ATG TGC TGA GTG TG 3’
Insl6_ext4_R	5’ GGT ACA GAA TGC CAC CTG CT 3’
Insl6_ext5_F	5’ TGA GTC TTG ATG GGG ATG AC 3’
Insl6_ext5_R	5’ TCT CCA TGA AGG AAA GTG ATG 3’
Insl6_F2	5’GTG CTA GAG GGA GAG ATG GTG 3’
Insl6_R2	5’CGA ACT CAG AAA TCC GCC TGC 3’
Insl6_F2cDNA	5’ AGA GGA AGA GGA ATC CAG ACC 3’
Insl6_R1cDNA	5’ CGA GCA TAG TTC CTA CGA CAG 3’
Insl6_TA_F1	5’ TCT AGA GAT GAA GCA GCT GTG CTG TTC 3’
Insl6_TA_R1	5’ AAG CTT ACA TCT CTA TCA CCA GTG ATG 3’
Insl6_TA_R1a	5’ TTC GAA ACA TCT CTA TCA CCA GTG ATG 3’
Insl6TR_genF1:	5’ TTT GGA CTA TAA AGC TAG TGG 3’
Insl6TR_genR1:	5’ CGT CTT TTC AAA CTG ATA GTC 3’
KO6F	5’ GGG TCA GTA TCG GCT TAT CGG 3’
KO6R	5’ CCC AGT CAT AGC CGA ATA GCC 3’
LOXP_S1	5’ CTA GTG AAT TCA TAA CTT CGT ATA GCA TAC ATT ATA CGA AGT TAT A 3’
LOXP_A1	5’ CTA GTA TAA CTT CGT ATA ATG TAT GCT ATA CGA AGT TAT GAA TTC A 3’

mCcna1_F	5’ GAG AAG AAC CTG AGA AGC AGG 3’
mCcna1_R	5’ GTG TCG ACT TCA TAC ACA TCC 3’
mGAPDH_F	5’ CAC CAC CAA CTG CTT AGC C 3’
mGAPDH_R	5’ CGG ATA CAT TGG GGG TAG G 3’
mHPRT_F:	5’ CCT GCT GGA TTA CAT CAA AGC ACT G 3’
mHPRT_R:	5’ GTC AAG GGC ATA TCC TAC AAC AAA C 3’
pcDNApeloF1	5’ GTG GAA TTC TCC TTG GCC ATG AAG CTC GTG 3’
pcDNApeloR1	5’ AGA CTC GAG ATC CTC TTC AGA ACT GGA ATC ACC 3’
Pelo_LZ	5’ CAC TGT CCC ACT GTT TCT TGG 3’
Pelo_pET_F2	5’ CCC CGA ATT CGA TGT GGC AGC TGT GGT CAT G 3’
Pelo_pET_R2	5’ CTC GAG TTA ATC CTC TTC AGA ACT TGA ATC C 3’
PET_PELOLZ_F	5’ CCC GAA TTC AAG CTC GTG AGG AAG GAT ATC GAG 3’
PET_PELOLZ_R	5’ GCT TCC CAG TGC CAG AAC TTT AAC TCG AGC CC 3’
PGK-1	5’ TCT GAG CCC AGA AAG CGA AGG 3’
PGK-3	5’ GGA TGT GGA ATG TGT GCG AGG 3’
Relaxin1_F	5’ CCA GCA GAT TTT TGC TCC AGC 3’
Relaxin1_R	5’ GGG AAC AGA AAG AGG CCA TCA 3’
Riken_F	5’ GGG ACA CTC CTG TTT GCC TTC 3’
Riken_R	5’ CCC TTC TGG CTT TCT CAA GGC 3’
SP6	5’ AGG TGA CAC TAT AGA ATA C 3’
SRPX_AsSaBH_S1	5’ GTA CCA AGT CGA CG 3’
SRPX_AsSaBH_A1	5’ GAT CCG TCG ACT TG 3’
SRPX_IN_F1	5’ GCT TTA GAG GCT CTG TCT CAC 3’
SRPX_IN_F2	5’ CTG CTG CTG CCT CAA GTA CTG 3’
SRPX_IN_R1	5’ GGG TCT GAT GTA CAA CCT CTG 3’
SRPX_IN_R2	5’ CTC AGC CTG CAG GAT CAT CTC 3’
SRPX_KOF1	5’ CCG GTT TCC AGA AAG AAG GGG 3’
SRPX_KOF2	5’ CGG GCAGAG AAT TCT ATC TGG- 3’
SRPX_KOR1	5’ GGA GCC ACA CTC CTC TTT CAG 3’
SRPX_KOR2	5’ GCT GAT TCA GCG AGT CTT GGG 3’
SRPX_LF	5’ AGG CAA GCT TTC AAT GCC CCA GAG AAT GGT TAC 3’
SRPX_LF2	5’ GGG AGA TCT TCA GGT GTT ACA GTT CTG GCT CA 3’
SRPX_LR2	5’ GGG AGA TCT TCA GTA ACC ATT CTC TGG GGC ATT GA 3’
SRPX_LR3	5’ GGG AGA TCT TCA ACT GGT GGG CTC CGT GCC AGA 3’

SRPX_LVI_F1	5’ CTC CTC GAG ATG AAT GCC CCA GAG AAT GGT TAC 3’
SRPX_LVI_F2	5’ GCG CTC GAG ATG CTG CTG CTG CTG CTG CCG CCT 3’
SRPX_LVI_R1\R2	5’ TCC TGG ATC CGT GTT ACA GGT CTG GCT CAT TTC 3’
SRPX_RNA_Full_F	5’ CTT AAG TGA GCT GTG CAG CCT 3’
SRPX_RNA_Full_R	5’ CAG CAC ATC AGA CGT TGG AAG 3’
SRPX_RNA_ISOF_R	5’ TCT CAC TTG GGC ACT TGA TTC 3’
SRPX_SpXhNo_S1	5’ CTA GTA ACT CGA GGC 3’
SRPX_SpXhNo_A1	5’ GGC CGC CTC GAG TTA 3’
SRY_F	5’ AAG ATA AGC TTA CAT AAT CAC ATG GA 3’
SRY_R	5’ CCT ATG AAA TCC TTT GCT GCA CAT GT 3’
Sycp1_F	5’ CCG TTT AAA CTG TTC GTG CCG 3’
Sycp1_R	5’ GGT GTT CTC TGC TTG CAC ACG 3’
Sycp2_F	5’CCA GTG AGA CCA GAC CTC CAA 3’
Sycp2_R	5’GCT TCC ACA ATG CCT ACC TGT 3’
Sycp3_F2	5’ CCA GGT TTC CTC AGA TGC TTC 3’
Sycp3_R2	5’ CGA ACA TTT GCC ATC CTC TGC 3’
T7	5’ TAA TAC GAC TCA CTA TAG GG 3’

2.1.10. Genomic and cDNA probes

Acr cDNA probe	Kremling *et al.,* (1991)
β-actin cDNA probe	Clontech, France
Ccna1 cDNA probe	generated in present study
Eif3g cDNA probe	generated in present study
*Eif3g*_pZero probe	generated in present study
*Insl6*_4 external probe	generated in present study
Insl6 cDNA probe	generated in present study
Neo probe	generated in present study
Pgk2 cDNA probe	Chen *et al.,* (2004)
Sycp3 cDNA probe	Lammers *et al.,* (1994)
Tnp2 cDNA probe	Meetei *et al.,* (1996)

2.1.11. Mouse strains

Mouse strains C57Bl/6J, 129/Sv, CD-1 and NMRI were initially ordered from Charles River Laboratories, Wilmington, USA and further bred in the Animal Facility of Institute of Human Genetics, Göttingen.

2.1.12. Antibodies

Goat anti-mouse IgG alkaline phosphatase conjugate	Sigma, Deisenhofen
Goat anti-mouse IgG Cy3 and FITC conjugate	Sigma, Deisenhofen
Goat anti-rabbit IgG alkaline phosphates conjugate	Sigma, Deisenhofen
Goat anti-rabbit IgG Cy3 and FITC conjugate	Sigma, Deisenhofen
Goat anti-rabbit IgG horse radish preoxidase conjugate	Sigma, Deisenhofen
Mouse monoclonal anti-c-Myc	Santa Cruz Biotechnologie, Heidelberg
Mouse monoclonal anti-GCNA1	Santa Cruz Biotechnologie, Heidelberg
Mouse monoclonal anti-Insulin	Sigma, Deisenhofen
Mouse monoclonal anti-α-Tubulin	Sigma, Deisenhofen
Rabbit anti-mouse IgG horse radish preoxidase conjugate	Sigma, Deisenhofen
Rabbit polyclonal anti-Apg1	Santa Cruz Biotechnologie, Heidelberg
Rabbit polyclonal anti-Glucagon	Chemicon, Schwalbach
Rabbit polyclonal anti-GLUT2	Chemicon, Schwalbach
Rabbit polyclonal anti-HA-tag	BD Biosciences, Heidelberg
Rabbit polyclonal anti-Insl5	The Antibody Facility at the Medical University of South Carolina,USA
Rabbit polyclonal anti-Pelota	Institute of Human Genetics
Rabbit polyclonal anti-Prm3	Grzmil *et al.,* 2008
Rabbit polyclonal anti-SCP3 (Syp3)	Abcam, Cambridge, UK

Polyclonal anti-Pelota antibodies were generated in the Institute of Human Genetics by immunization of rabbits with GST-Pelota.

2.1.13. Enzymes

Alkaline phosphatase	New England Biolabs, Frankfurt am Main
Collagenase (Type II)	Sigma, Deisenhofen
DNase	Qiagen, Hilden
Immolase DNA Polymerase	Bioline, Luckenwalde
Klenow Fragment	Invitrogen, Karlsruhe
Platinum *Taq* polymerase	Invitrogen, Karlsruhe
Proteinase K	Sigma, Deisenhofen
Restriction enzymes (with supplied buffers)	Invitrogen, Karlsruhe
RNase A	Qiagen, Hilden
RNase H	Invitrogen, Karlsruhe
RNase inhibitor	Invitrogen, Karlsruhe
Superscript-II	Invitrogen, Karlsruhe
T4 DNA ligase	Promega, Mannheim
Trypsin	Invitrogen, Karlsruhe

2.1.14. Radioactive substances

α-^{32}P-dCTP	Amersham, Braunschweig

2.1.15. Kits

ApoAlert DNA fragmentation Kit	BD Clontech, Palo Alto
Endo Free Plasmid Maxi Kit	Qiagen, Hilden
BugBuster™ GST-bind™ Purification Kit	Novagen, Darmstad
Immunoprecipitation Kit (protein G)	Roche, Penzberg
In Situ Cell Death Detection Kit, POD	Roche, Penzberg
Maxi Plasmid Kit	Qiagen, Hilden
Megaprime DNA Labeling Kit	Amersham Pharmacia, Freiburg

Midi Plasmid Kit	Invitrogen, Karlsruhe
Mini Plasmid Kit	Qiagen, Hilden
Montage PCR clean-up columns	Millipore, USA
QIAquick Gel Extraction Kit	Qiagen, Hilden
PCR Purification Kit	Qiagen, Hilden
pET GST Fusion Systems 41	Novagen, Darmstad
pGEM-T Easy cloning system	Promega, Mannheim
Protein Refolding Kit	Novagen, Darmstadt
RediprimeTM II Random Prime Labeling System	Amersham Pharmacia, Freiburg

2.1.16. Instruments

Autoclave	Webeco, Bad Schwartau
Biophotometer	Eppendorf, Hamburg
CASA system	Hamilton Thorne Research
Centrifuge 5415D	Eppendorf, Hamburg
Centrifuge 5417R	Eppendorf, Hamburg
Cryostat™	Leica, Solms
DNA Sequencer Modell Megabace 1000	Amersham, Freiburg
GeneAmp PCR System 9600	Perkin Elmer, Berlin
Histocentre 2 embedding machine	Shandon, Frankfurt aM.
Inverted Microscope IX81	Olympus, München
Microscope BX60	Olympus, München
Microtiterplate-Photometer	BioRad laboratories, München
Microtom Hn 40 Ing.	Nut hole
Molecular Imager FX	BioRad laboratories, München
Neubauer cell chamber	Schütt Labortechnik, Goettingen
Phosphoimager Screen	BioRad laboratories, München
Pipette	Eppendorf, Hamburg
Refrigerated Superspeed Centrifuge RC-5B	Sorvall, Langenselbold
Semi-Dry-Blot Fast Blot	Biometra, Göttingen
Spectrophotometer Ultraspec 3000	Amersham, Freiburg

SpeedVac concentrator SVC 100H	Schütt, Göttingen
Thermomixer 5436	Eppendorf, Hamburg
TurboblotterTM	Schleicher & Schüll, Dassel
UV StratalinkerTM1800	Leica, Nußloch
Video-Documentation system	Herolab, Heidelberg
X-Ray Automatic Processor Curix 60	Agfa, München

2.2. Methods

2.2.1. Isolation of nucleic acids

2.2.1.1. Isolation of plasmid DNA

2.2.1.1.1. Small - scale isolation of plasmid DNA (Mini preparation, adapted from Birnboim and Doly, 1979)

A single *Escherichia coli* colony was inoculated in 5 ml of LB medium with the appropriate antibiotic and incubated in a shaker for 8 - 12 hrs at 37°C with a speed of 160 rpm. 0.7 ml of this culture was used for making glycerol stocks and rest of the culture was centrifuged at 5000 x g at 4°C for 20 min. The pellet was resuspended in 100 µl of resuspension solution P1. Then, the bacterial cells were lysed with 200 µl of lysis solution P2, incubated at RT for 5 min and neutralized with 150 µl of neutralization solution P3. The precipitated solution was incubated at RT for 5 min and centrifuged at 13000 x g at RT for 15 min. The supernatant was transferred into a new tube and centrifugation was done again. The supernatant was transferred again into a new tube and 1 ml of 100% ethanol was added to precipitate the DNA. Mixture was then incubated at -20°C for 1 hr, centrifuged at full speed for 30 min, and finally the pellet was washed with 0.5 ml of 70% ethanol and after air-drying it was dissolved in 30 - 50 µl of Ampuwa. DNA was stored at -20°C.

P1:	50 mM	Tris/HCl, pH 8.0
	10 mM	EDTA
	100 µg/ml	RNase A

P2:	200 mM	NaOH
	1%	SDS
P3:	3.0 M	KAc, pH 5.5

2.2.1.1.2. Preparation of bacterial glycerol stocks

Bacterial glycerol stocks were made suspending 700 µl bacteria in 300 µl of 80% (v/v) sterile glycerol. The suspension was mixed well and stored at –80°C.

2.2.1.1.3. Large - scale preparation of plasmid DNA (Midi preparation)

QBT:	750 mM	NaCl
	50 mM	MOPS pH 7.0
	15 %	Ethanol
	0.5 %	Triton X-100
QC:	1 mM	NaCl
	50 mM	MOPS pH 7.0
	15%	Ethanol
QF:	1.25 M	NaCl
	50 mM	Tris/HCl pH 8.5

A single clone was inoculated in 5 ml LB medium with appropriate antibiotic as a preculture for 8 hrs at 37°C in a shaker. This preculture was added in a dilution 1:100 fold into 100 ml LB medium with appropriate antibiotic and incubated overnight at 37°C with shaking. Next day, the culture was centrifuged at 6000 x g for 15 min at 4°C. The pellet was resuspended in 4 ml of solution P1 and cells were then lysed with 4 ml of P2 buffer. After incubation on ice for 5 min, reaction was stopped by adding 4 ml of P3 buffer and incubation 15 min on ice. The precipitated solution was centrifuged at 20000 x g for 30 min at 4°C. Meanwhile, the provided column (Qiagen, Hilden) was equilibrated with 10 ml of QBT solution. After centrifugation, the lysate was poured into this equilibrated column to allow the DNA to bind

with the resin present in the bed of the column. The column was then washed twice with 10 ml of solution QC. Finally, the DNA was eluted with 5 ml of QF solution. To precipitate the DNA, 3.5 ml of isopropanol was added to the eluent and mixed thoroughly. The mixture was then centrifuged at 14000 x g for 30 min at 4°C. The DNA pellet was washed with 70% ethanol, air-dried and dissolved in 50 - 100 µl of TE buffer. DNA was stored at -20°C and was further used for transfection, sequencing, restriction analysis and subcloning.

2.2.1.1.4. Endotoxin free preparation of plasmid DNA

Endotoxins, also known as lipopolysaccharides (LPS), are cell membrane components of Gram-negative bacteria (e.g. *E.coli*). During lysis of bacterial cells for plasmid preparations, endotoxin molecules are released from the outer membrane into the lysate. Endotoxins strongly influence transfection of DNA into primary cells and sensitive cultured cells like embryonic stem (ES) cells. Increased endotoxin levels lead to sharply reduced transfection efficiencies. EndoFree plasmid preparation kit integrates endotoxin removal into standard plasmid preparation procedure. For this isolation, a single clone was inoculated in 5 ml LB medium with appropriate antibiotic as a preculture for 8 - 12 hrs at 37°C in a shaker. The preculture was diluted 1:500 into 200 ml LB medium with appropriate antibiotic, and incubated overnight at 37°C with shaking. The saturated culture was centrifuged at 6000 x g for 15 min. The pellet was resuspended in 5 ml of solution P1 and cells were lysed with P2 and P3 as described above. The precipitated solution was centrifuged at 20000 x g for 30 min at 4°C and supernatant was filtered through a QIAfilter cartridge (provided in kit). Then, it was incubated on ice for 30 min with a specific Endotoxin Removal buffer (patented by Qiagen). After incubation, sample was poured into an equilibrated column (QIAGEN-tips) to allow the DNA to bind with the resin present in the bed of the column. The column was then washed twice with 10 ml of solution QC. Finally, the DNA was eluted with 5 ml of QF solution. To precipitate the DNA, 3.5 ml of isopropanol was added, mixed thoroughly and then centrifuged at 14000 x g for 30 min at 4°C. The DNA pellet was washed with 70% ethanol and dissolved in 100 µl of TE buffer. DNA was stored at -20°C and was further used for electroporation of ES cells.

2.2.1.2. Isolation of genomic DNA

2.2.1.2.1. Isolation of genomic DNA from mouse tails (Laird *et al.,* 1991)

Routinely, 0.5 to 1 cm of the mouse tail was incubated overnight in 700 µl of lysis buffer I containing 35 µl proteinase K (10 µg/µl) at 55°C in thermomixer. The tissue lysate was centrifuged at 13000 x g for 10 min at RT and the supernatant was transferred into a new e-cup. After transferring, DNA was precipitated by adding an equal volume of isopropanol and mixed by inverting several times and centrifuged at 13000 x g for 20 min at RT. Pellet was washed with 0.5 ml of 70% ethanol, dissolved in 50 - 100 µl of Ampuwa and incubated at 60°C for 10 min. DNA was stored at 4°C.

2.2.1.2.2. Isolation of genomic DNA from tissue samples

100 mg of the mouse tissue was incubated overnight in 700 µl of lysis buffer I containing 35 µl proteinase K (10µg/µl) at 55°C in thermomixer. Then, the equal volume of phenol was added to the tissue lysate, mixed by inverting several times, and centrifuged at 13000 x g for 15 min at RT. After transferring the upper aqueous layer into a new tube, the same procedure was repeated, first with 1:1 ratio of phenol and chloroform, and then with chloroform alone. Finally, the DNA was precipitated with 0.7 volume of isopropanol, washed with 70% ethanol, and dissolved in 50 - 100 µl of Ampuwa and incubated at 60°C for 15 min. DNA was stored at 4°C.

2.2.1.2.3. Isolation of genomic DNA from ES cells

The Es cells grown in a 24-well plate were washed with PBS and incubated overnight in 500 µl of lysis buffer II at 37°C. After transferring into a new e-cup, DNA was precipitated by adding an equal volume of isopropanol and incubation for 15 min at RT. Then, it was centrifuged for 20 min at maximal speed and washed with 70% ethanol. Pellet was dissolved in 80 – 100 µl of Ampuwa H_2O and incubated at 60°C for 10 min. DNA was stored at 4°C and used for Southern blot.

2.2.1.3. Isolation of total RNA

2.2.1.3.1. Isolation of total RNA from tissue samples and cultured cells

Total RNA isolation reagent is an improved version of the single-step method for total RNA isolation described first by Chomczynski and Sacchi (1987). The composition of reagent includes phenol and guanidine thiocyanate in a monophase solution. In order to avoid any RNase activity, homogenizer used for RNA isolation was previously treated with RNase away and DEPC-dH_2O and special RNase free Eppendorf cups were used during the procedure. 100 - 200 mg of tissue sample was homogenized in 1 - 2 ml of cold TRI Reagent by using a glass-Teflon homogenizer. The sample volume should not exceed 10% of the volume of reagent used for the homogenization. The homogenate was mixed and incubated on ice for 5 min to permit the complete dissociation of nucleoprotein complexes. Then, 0.2 ml of cold chloroform was added, mixed vigorously, and stored on ice for 10 min. After centrifugation at 12000 x g for 15 min at 4°C, the colourless upper aqueous phase was transferred into a new tube. The RNA was precipitated by adding 0.5 ml of cold isopropanol and centrifugation at 14000 x g for 15 min at 4°C. Finally, the pellet was washed twice with cold 75% ethanol and dissolved in 30 - 100 µl of RNase free water or DEPC-dH_2O. RNA was stored at -80°C.

Total RNA from eukaryotic cultured cells was isolated with the RNeasy Mini Kit (Qiagen, Hilden) according to the supplier's instructions. The total RNA was treated with RNase-free DNase I (Qiagen, Hilden) according to the user manual and resuspended in 30 -100 µl RNase-free water. It was stored at -80°C.

2.2.2. Determination of nucleic acid concentration

The concentration of nucleic acids was determined spectrophotometrically by measuring absorption of the samples at 260 nm. The quality of nucleic acids i.e. contamination with salt and protein was checked by measurements at 230, 280, and 320 nm. The concentration was calculated according to the formula:

$$C = (E\ 260 - E\ 320)fc$$

C = concentration of sample (µg/µl)

E 260 = ratio of extinction at 260 nm

E 320 = ratio of extinction at 320 nm

f = dilution factor

c = concentration (standard)/absorption (standard)

For double stranded DNA: c = 0.05 µg/µl

for RNA : c = 0.04 µg/µl

for single stranded DNA : c = 0.03 µg/µl

2.2.3. Gel electrophoresis

Gel electrophoresis is a technique by which mixtures of charged macromolecules, especially nucleic acids and proteins, are resolved in an electrical field according to their mobility which is directly proportional to macromolecule's charge to mass ratio.

2.2.3.1. Agarose gel electrophoresis of DNA

Agarose gels are used to electrophorese nucleic acid molecules from as small as 50 bases to more than 20 kb, depending on the concentration of the agarose. Usually, 1 gm of agarose was added to 100 ml of 0.5x TBE buffer and boiled in the microwave to dissolve the agarose, then cooled down to about 60°C before adding 3 µl of ethidium bromide (10 mg/ml). This 1% agarose gel was poured into a horizontal gel chamber. 0.5x TBE buffer was used as electrophoresis buffer. The samples were mixed with about 0.1 volume of loading buffer, loaded into the wells of the gel and electrophoresis was carried out at a steady voltage (50 - 100 V). Size of the DNA fragments on agarose gels was determined using 1 kb DNA ladder, which was loaded with samples in parallel slots. DNA fragments were observed and photographed under UV light.

2.2.3.2. Agarose gel electrophoresis of RNA (Hodge, 1994)

Single-stranded RNA molecules often have complementary regions that can form secondary structures. Therefore, RNA was run on a denaturing agarose gel that contained formaldehyde, and before loading, the RNA was pre-treated with formaldehyde and formamide to denature the secondary structure of RNA. 2 mg of agarose was added to 20 ml of 10x MOPS buffer

and 148 ml DEPC-H_2O, and dissolved by heating in a microwave. After cooling it to about 50°C, 33.2 ml of formaldehyde (37%) was added, stirred and poured into a horizontal gel chamber. RNA samples were prepared as follows:

10 – 20 µg RNA
2 µl 10x MOPS buffer
3 µl Formaldehyde
7 µl Formamide (40%)
6 µl Loading buffer

Samples were denatured at 65°C for 10 min and chilled down on ice before loading into the gel. The gel was run at 30 V at 4°C for 12 - 16 hrs.

2.2.3.3. DNA and RNA molecular weight ladders

To determine the size of the nucleic acid fragments on agarose gels, molecular weight ladders were loaded in parallel.

1 kb DNA ladder Invitrogen, Karlsruhe
100 bp DNA ladder Invitrogen, Karlsruhe
0.24-9.5 bp RNA ladder Invitrogen, Karlsruhe

2.2.4. Cloning techniques

2.2.4.1. Enzymatic modifications of DNA

2.2.4.1.1. Restriction enzyme digestion of DNA

Restriction enzyme digestions were performed by incubating double-stranded DNA with an appropriate amount of restriction enzyme in its respective buffer as recommended by the supplier, and at the optimal temperature for the specific enzyme. Standard digestions included 2 - 10 U enzyme per microgram of DNA. These reactions were usually incubated for 1 - 3 hrs or overnight (genomic DNA) to ensure complete digestion at the optimal temperature for enzyme activity, which was typically 37°C.

2.2.4.1.2. Filling-up reaction (Costa and Weiner, 1994)

To blunt overhanging ends, 0.1 - 4 µg of digested DNA was mixed with 0.05 mM dNTPs and 1 - 5 U of Klenow fragment with reaction buffer in a total volume of 50 µl. The reaction was incubated at 37°C for 15 min, then stopped by heating at 75°C for 10 min. DNA was subsequently purified by phenol/chloroform extraction and ethanol precipitation.

2.2.4.1.3. Dephosphorylation of 5' ends of DNA

To prevent the recircularization of linearized plasmids without the insertion of foreign DNA, alkaline phosphatase treatment was performed. Alkaline phosphatase catalyses the hydrolysis of 5'-phosphate residues from DNA. The following items were mixed:

1 - 5 µg vector DNA,
5 µl 10 x reaction buffer,
1 µl alkaline phosphatase (1 U)

in a total volume of 50 µl and incubated at 37°C for 1 h. The reaction was then stopped by heating at 85°C for 15 min. The dephosphorylated DNA was purified by phenol/chloroform extraction and ethanol precipitation.

2.2.4.2. Purification of DNA

2.2.4.2.1. Purification of DNA by phenol/chloroform extraction and ethanol precipitation

Protein impurities were removed by vigorous shaking of nucleic acid solution with an equal volume of phenol/chloroform mixture (1:1). The emulsion was then centrifuged for 10 min at 13000 x g at RT, and the upper aqueous phase was collected, mixed with an equal volume of chloroform and centrifuged as above. Finally, the upper aqueous phase was collected, mixed with NaAc (final conc. 0.3 M) and 2.6 volume of absolute ethanol and centrifuged for 30 min at 4°C with maximal speed. The pellet was washed with 70% ethanol and centrifuged at 13000 x g for 5 min at 4°C. The pellet was air-dried and resuspended in 10 - 100 µl Ampuwa.

2.2.4.2.2. Purification of DNA fragments from agarose gel

2.2.4.2.2.1. QIAquick gel extraction method

This method is designed to extract and purify DNA of 70 bp to 10 kb in length from agarose gels. Up to 400 mg agarose can be processed per spin column. The principle of this method depends on selective binding of DNA to uniquely designed silica-gel membranes.

After electrophoresis, a fragment of agarose gel containing the desired DNA was excised with a scalpel, weighed and incubated with 3 volumes of QG buffer at 50°C for 10 min. After the gel slice was dissolved completely, the solution was applied over a QIAquick column and centrifuged for 1 min. The flow-through was discarded and the column was washed with 0.75 ml of PE buffer. After drying the column, it was placed into a fresh microcentrifuge tube. To elute DNA, 30 - 50 µl of EB buffer was applied to the centre of the QIAquick membrane and centrifuged for 1 min. DNA was stored at -20°C, further checked on agarose gels and used for subcloning or as a probe for Northern or Southern blot experiments.

2.2.4.3. Ligation of DNA fragments

The ligation of an insert DNA into a vector (digested with appropriate restriction enzyme) was carried out in the following reaction mix:

30 ng vector DNA (digested)
50 - 100 ng insert DNA (1:3, vector: insert ratio)
1 µl ligation buffer (10x)
1 µl T4 DNA ligase (5 U/µl)
in a total volume of 10 µl

Blunt-end ligations were carried out at 16°C for overnight, whereas overhang-end ligations were carried out at 4°C overnight.

2.2.4.4. TA-Cloning (Clark, 1988; Hu, 1993)

Taq polymerase and other DNA polymerases have a terminal transferase activity that results in the non-template addition of a single nucleotide to the 3' ends of PCR products. In the presence of all 4 dNTPs, dATP is preferentially added. This terminal transferase activity is the basis of the TA-cloning strategy. For cloning of PCR products, the pGEMTeasy vector system that has 5‘ dT overhangs was used. The following substances were mixed:

50 ng of pGEMTeasy vector
150 ng PCR product
5 µl of T4 DNA Ligase buffer (2x)
1 µl of T4 DNA Ligase
in a total volume of 10 µl

The substances were mixed by pipetting and reaction was incubated overnight at 4°C. For transformation of the ligation reaction, DH5α competent cells were used (Invitrogen).

2.2.5. Preparation of competent *E. coli* bacteria (Dagert and Ehrlich, 1979)

The competent bacterial cells are generated by a physical cell wall modification that facilitates DNA uptake. LB medium (100 ml) was inoculated with a single colony of *E.coli* (strain DH5α) and the culture was grown at 37°C to OD600 = 0.6. Bacteria were centrifuged (10 min, 4°C, 3000 x g), and the pellet was resuspended in 50 ml of sterile 50 mM $CaCl_2$ solution (4°C) and incubated on ice for 30 min. The suspension of bacteria was centrifuged (10 min, 4°C, 3000 x g) and the pellet was resuspended in 10 ml of sterile 50 mM $CaCl_2$ (4°C) with 15% glycerol. The mixture was dispensed into aliquots of 100 µl, the cups were frozen quickly in liquid nitrogen and stored at -80°C. Mostly, competent DH5α were purchased from Invitrogen.

2.2.6. Transformation of competent bacteria

Transformation of bacteria was done by gently mixing one aliquot of competent bacteria (50 µl) with 5 - 10 µl of ligation reaction. After incubation for 30 min on ice, bacteria were heat

shocked for 45 sec at 37°C or 42°C, cooled down for 2 min on ice and 450 - 900 µl of S.O.C medium were added. Bacteria were subsequently incubated with shaking for 1 – 2 hrs at 37°C. 50 µl and 100 µl cell suspensions, respectively, were plated out on LB-agar plates containing appropriate antibiotic (50 µg/ml), and whenever required 1 mM IPTG and X-Gal 40mg/ml, X-Gal for "Blue - White" selection. The plates were then incubated overnight at 37°C. The single colonies were picked and inoculated into 5 ml LB medium supplemented with 50 µg/ml appropriate antibiotic. The cell suspension was further used for plasmid preparations or preparation of bacterial glycerol stocks.

2.2.7. Polymerase Chain Reaction (PCR)

The polymerase chain reaction (PCR) represents an important technique in the field of molecular biology. It is a very sensitive, powerful technique (Saiki *et al.,* 1988) which is widely used for the exponential amplification of specific DNA sequences in vitro by using sequence specific synthetic oligonucleotides (primers). The general principle of PCR starts from a pair of oligonucleotide primers that are designed so that a forward or sense primer directs the synthesis of DNA towards a reverse or antisense primer, and vice versa. During the PCR, the *Taq* DNA polymerase (a heat stable polymerase) (Chien *et al.,* 1976) catalyses the synthesis of a new DNA strand that is complementary to a template DNA from the 5' to 3' direction by a primer extension reaction, resulting in the production of the DNA region flanked by the two primers. It allows the rapid and unlimited amplification of specific nucleic acid sequences that may be present at very low concentrations in very complex mixtures.

2.2.7.1. PCR amplification of DNA fragments

The amplification cycles were performed in an automatic thermocycler. In general, the PCR reaction contains the following substances:

5 - 10 ng	template DNA
1 µl	forward primer (10 pmol/µl)
1 µl	reverse primer (10 pmol/µl)
1 µl	10 mM dNTPs
5 µl	10x PCR buffer

1.5 µl	50 mM $MgCl_2$
0.5 µl *Taq*	DNA polymerase (5 U/µl)
Up to 50 µl	Ampuwa H_2O

The reaction mixture was placed in a 200 µl reaction tube and placed in a thermocycler. A standard PCR program is shown as follows:

Initial denaturation	94°C	5 min
Elongation	94°C	30 sec (denaturation)
30-35 cycles	51 - 65°C	45 sec (annealing, time depends on primer's Tm value)
	72°C	1 min (extension, time depends on the PCR product, as 1 min for 1 kb DNA)
Final extension	72°C	10 min

The simplest formula for calculating the Tm (melting temperature) of the primers is:

Tm = 4°C x (number of G's and C's in the primer) + 2°C x (number of A's and T's in the primer)

2.2.7.2. Genotyping of knock-out mice using PCR

The genotypes of all offspring of *Insl5* and *Insl6* knock-out mutant mice were analysed by PCR. For amplification of the wild type and the mutant allele, the DNA was extracted from mouse tails as described in 2.2.1.2.1. and pipetted to the following reaction mixture:

	The *Insl5* KO mice	The *Insl6* KO mice
DNA (300-500 ng)	0.5 µl	0.5 µl
Forward primer I (10 pmol/µl)	0.5 µl C-Insl5-F8	1 µl Insl6_F2

Forward primer II (10 pmol/µl)	0.5 µl I5KO-F1	-
Reverse primer I (10 pmol/µl)	0.5 µl C-Insl5-R9	1 µl Insl6_R2
Reverse primer II (10 pmol/µl)	0.5 µl PGK_3	1 µl PGK_1
dNTPs (10 mM)	0.5 µl	1 µl
Taq polymerase buffer (10x)	5 µl	2.5 µl
Taq polymerase (5 U/µl)	0.5 µl	0.25 µl
$MgCl_2$ 50 mM	1.5 µl	0.75 µl
Ampuwa H_2O	Up to 25 µl	Up to 50 µl

The mixture was subjected to the following program in the thermocycler:

	The *Insl5* KO mice		The *Insl6* KO mice
Initial denaturation	94°C for 5 min		94°C for 5 min
Elongation	94°C for 30 sec	Denaturation	94°C for 30 sec
(for 35 cycle)	58°C for 30 sec	Annealing	60°C for 45 sec
	72°C for 45 sec	Elongation	72°C for 1 min
Extension	72°C for 7 min		72°C for 10 min

2.2.7.3. Reverse transcription PCR (RT-PCR)

2.2.7.3.1. Reverse transcription or cDNA synthesis

RT-PCR is a technique, that generates cDNA fragments from RNA templates, and thereafter amplifies it by PCR. It is very useful to determine the expression of genes in specific tissues or in different development stages. 1 - 5 µg of total RNA was mixed with 1 µl of oligo $(dT)_{18}$ primer (10 pmol/µl) in a total volume of 12 µl. To avoid the possible secondary structure of the RNA, which might interfere with the synthesis, the mixture was heated to 70°C for 10 min, and then quickly chilled on ice. After a brief centrifugation, the following components were added to the mixture:

4 µl 5x first strand buffer
2 µl 0.1 M DTT
1 µl 10 mM dNTPs
1 µl RNasin (10 U/µl)

The content of the tube was mixed gently and incubated at 42°C for 2 min. Then, 1 µl of reverse transcriptase enzyme (Superscript II) was added and incubated at 42°C for 50 min for the first strand cDNA synthesis. Next, the reaction was inactivated by heating at 70°C for 15 min. 1 µl of the first strand reaction was used for the further PCR reactions.

2.2.7.3.2. One-Step RT-PCR

To obtain specific RT-PCR products, the QIAGEN One-Step RT-PCR kit was employed which contains optimized components that allow both reverse transcription and PCR amplification to take place in what is commonly referred to as a ”one-step” reaction.

Master mix:	Per reaction:
5x Qiagen One-Step RT-PCR buffer	10 µl
dNTP mix (containing 10 mM of each dNTP)	2 µl
Forward primer (10 pmol/µl)	1 µl
Reverse primer (10 pmol/µl)	1 µl
Qiagen One-Step RT-PCR Enzyme Mix	2 µl
RNase inhibitor (20 U/µl)	1 µl
RNase-free water	31 µl

2 µl (2 µg) of total RNA isolated from mammalian cultured cells and mouse tissues was added to 48 µl of prepared master mix in a PCR tube. The sample was placed in the thermocycler and the RT-PCR program was followed according to the user manual. Reverse transcription reaction was performed at 50°C for 30 min. To denaturate the DNA-RNA hybrid molecules, the reaction was heated to 94°C for 10 min. Thermal cycling was carried out for 35 cycles with denaturation at 94°C for 30 sec, annealing at 54 - 60°C for 40 sec and extension at 72°C for 1 min. After the amplification, the presence of a product was checked on an agarose gel.

2.2.8. Non-radioactive dye terminator cycle sequencing

The non-radioactive sequencing was performed with the Dye Terminator Cycle Sequencing-Kit (ABI PRISM). The reaction products were analysed with automatic sequencing equipment, MegaBase DNA Sequencer. For the sequencing reaction, four different dye labelled dideoxy nucleotides were used (Sanger *et al.,* 1977), which, when exposed to an argon laser, emit fluorescent light which can be detected and interpreted. The reaction was carried out in a total volume of 10 µl containing 1 µg plasmid DNA or 100 - 200 ng purified PCR products, 10 pmol primer and 4 µl reaction mix (contains dNTPs, dideoxy dye terminators and *Taq* DNA polymerase). Elongation and chain termination take place during the following program in a thermocycler: 4 min denaturation followed by 25 cycles at 95°C, 30 sec; 55°C, 15 sec, annealing; 60°C, 4 min, elongation. After the sequencing reaction, the DNA was precipitated with 1/10 volume 3 M sodium acetate and 2.5 volume 100% ethanol and washed in 70% ethanol. The pellet was dissolved in 4 µl of loading buffer, denaturated at 95°C for 3 min, and finally loaded on the sequence gel.

2.2.9. Nucleic acids blotting techniques

2.2.9.1. Southern blotting of DNA to nitrocellulose filters (Southern, 1975)

In Southern blotting, the transfer of denaturated DNA from agarose gels onto nitrocellulose membrane is achieved by capillary flow. 20x SSC buffer, in which nucleic acids are highly soluble, is drawn up through the gel onto nitrocellulose membrane, taking with it the single-stranded DNA that becomes immobilized in the membrane matrix. After electrophoresis of DNA, the gel was treated with 0.25 M HCl for depurination. It was followed by denaturation solution for 30 min and 45 min in neutralization solution. The transfer of the DNA to the nitrocellulose membrane was done in a Turbo-Blot apparatus (Schleicher & Schuell, Dassel). 27 Whatman filter papers (GB 003) were layered on a Stack Tray, followed by 3 Whatman filter papers (GB 002) and 1 Whatman filter paper (GB 002) soaked with 20x SSC. The equilibrated nitrocellulose filter that was soaked with 2x SSC was laid on the top. The agarose gel rinsed with 20x SSC, was placed on the filter and was covered with 3 Whatman filter papers GB 002 soaked with 20x SSC. The buffer tray was placed and filled with 20x SSC. Finally a wick, which was also soaked with 20x SSC, and the wick cover were put on top of

the blot. The transfer was carried out for overnight. Finally, after disassembling of the blot, the filter was dried on the air and the DNA was fixed onto the filter by either baking it at 80°C for at last 2 hrs or by UV-crosslinking in UV Stratalinker 1800.

2.2.9.2. Dot blot of DNA to nitrocellulose filters (colony hybridization)

The colony hybridization is a rapid and effective technique that detects recombinant sequences isolated directly from cells grown on plates and transferred to membranes. 88 mm nitrocellulose or nylon membranes (Optitran BA-S85, Schleicher & Schuell) were placed on plates for 1 - 2 min to transfer the colonies to the filters, whereas reference position points were marked to identify later the positive colonies. The culture plate was incubated at 37°C, so the colonies grow again. The marked membranes were placed on surfaces with the following solutions:

5 min 10% (w/v) SDS
7 min denaturation solution
10 min neutralisation solution
10 min 2 x SSC

Finally, the filter was dried on air for 10 - 15 min and baked at 80°C for at least 2 hrs. Then, the membrane was ready for hybridization with a ^{32}P-labeled probe (2.2.10). After hybridization, the positive colonies were localized.

2.2.9.3. Northern blotting of RNA onto nitrocellulose filters

For the transfer of RNA onto a nitrocellulose filter, the same procedure as described above (2.2.9.1) was performed. In this case, however, the gel does not need to be denaturated, but was transferred directly onto the filter as explained in section 2.2.9.1.

2.2.10. Random Prime method for generation of ^{32}P labeled DNA (Denhardt, 1966; Feinberg and Vogelstein, 1984)

RediprimeTM II Random Prime Labeling System (Amersham Pharmacia) was used for labelling of DNA probes. The method depends on the random priming principle developed by Feinberg and Vogelstein (1984). The reaction mix contained dATP, dGTP, dTTP, Klenow fragment (4 - 8 U) and random oligodeoxyribonucleotides. Firstly, 25 - 50 ng of DNA were denaturated in a total volume of 46 µl at boiling water for 10 min and quick chilled on ice for 5 min. After pipetting the denaturated probe in RediprimeTM II Random Prime Labelling System cup, 4 µl of [α-32P] dCTP (3000 Ci/mmol) was added to the reaction mixture. The labelling reaction was carried out at 37°C for 0.5 - 1 hr. The labelled probe was purified from uncorporated [α-32P] dCTP by using microspin columns (Amersham Pharmacia) and the specific radioactivity was measured by using a scintillation counter (Tri-Carb 1600TR, Packard Instruments, Warrenville, USA) and varied between 4 to 10 x 10^7 cpm.

2.2.11. Hybridization of nucleic acids (Denhardt, 1966)

The membrane to be hybridized was equilibrated in 2x SSC and transferred to a hybridization tube. After adding 12 ml of hybridization solution (Rapid-hyb buffer, Amersham) and 250 µl of sheared denaturated salmon DNA, the membrane was incubated for 2 - 4 hrs in the hybridization oven at an appropriate temperature, which is usually 65°C. After that, the labelled probe was denaturated at 95°C for 10 min, chilled on ice for 5 min, and then added to the hybridization solution. The hybridization was carried out overnight in the oven. Next day, the filter was washed for 10 min with 2x SSC at RT. Finally, the membrane was washed with 2x SSC containing 0.1 % SDS and then with 0.2x SSC containing 0.1% SDS at the hybridization temperature. After air-drying the filter, it was sealed in saran wrap and exposed to autoradiography overnight at -80°C or to phosphoimager screen for 1 - 4 hrs. The film was developed in X-Ray Automatic Processor Curix 60 or the screen was scanned in phosphoimager. For quantification of detected bands, the program Quantity One (Bio-Rad) was used. If membrane has to be used again, it was stripped in 0.2x SSC at 80°C, until radioactive signal was no longer detected.

2.2.12. Protein analysis methods

2.2.12.1. Isolation of total proteins from mouse tissues

Proteins were extracted from 100 mg of fresh or frozen mouse tissues after homogenization in 500 µl lysis buffer A containing protease inhibitors (1µg/µl leupeptin, 3µg/µl aprotinin). Lysates were sonicated on ice 2 x 2 min, and centrifuged at 14000 x g for 20 min at 4°C. Supernatant, containing membranes, organelles and cytosol proteins was collected, quantified and stored at -80°C, or used immediately.

2.2.12.2. Isolation of total protein from eukaryotic cells

5 x 10^6 cells/ml were washed with PBS and resuspended in 70 - 100 µl of lysis buffer B. The whole cell lysate was collected with a cell scraper, transferred to a separate Ependorf cup and incubated on ice for 30 min. After that, cells were sonicated gently on ice (2 x 30 sec) and centrifuged at 14000 x g for 20 min at 4°C. The total protein concentration of the supernatant was quantified and stored at -80°C in aliquots until use.

2.2.12.3. Determination of protein concentration (Bradford, 1976)

To determine the protein concentration, Bio-Rad protein assay was employed which is a dye-binding assay based on the differential color change of a dye in response to various concentrations of protein. The assay is based on the observation that the absorbance maximum for an acidic solution of Coomassie Blue G-250 shifts from 494 to 595 nm when the binding to protein occurs. The BSA stock solution of 1 mg/ml was diluted in order to obtain standard dilutions in range of 10 µg/ml to 100 µg/ml. The Bio-Rad's color reagent was diluted 1:5 with Ampuwa H_2O and filtered through 0.45 µm filter. In a 96-well microtiter plate, 20 µl of each standard dilution and the samples to be measured were pipetted with 280 µl of the color reagent. The absorption of the color reaction was measured at 595 nm in a microplate reader (Microplate Reader 450, Bio-Rad) and the protein concentration was determined by extrapolating to the standard curve plotted with the values obtained from the known concentrations of the BSA.

2.2.12.4. SDS-PAGE for the separation of proteins (Laemmli, 1970)

The NuPAGE® Pre-Cast Gel System (Invitrogen) is a polyacrylamide gel system for high performance gel electrophoresis and is based on SDS-PAGE gel chemistry. It consists of NuPAGE® Bis-Tris Pre-Cast Gels and specially optimized buffers which have an operating pH of 7.0, giving the system advantages over existing polyacrylamide gel systems with an operating pH of 8.0. The neutral pH increases the stability of the proteins and provides better electrophoretic results.
To 15 µl of whole protein lysate 5 µl of 4x LDS sample buffer and 3 µl of DTT were added. The samples were denaturated by boiling in the water bath for 10 min, cooled to RT for 5 min and loaded in SDS-PAGE (NuPage 4 - 12% Bis-Tris gel). The gel electrophoresis was run in 1x MOPS or 1x MES buffer (Invitrogen). To determine the molecular weight of the proteins on the gel, 10 µl of a pre-stained molecular weight standard (See Blue Plus2, Invitrogen) was also loaded. The gel was run at 80 - 100 V for 2 hrs at RT.

2.2.12.5. Western blotting of protein onto PVDF membrane (Gershoni and Palade, 1982)

Transfer buffer	5.8 gm Tris-Cl
pH 9.2	2.92 gm Glycine
	3.7 ml 10% SDS
	20% methanol
	dH_2O to 1000 ml

After electrophoresis of proteins on a polyacrylamide gel, the gel and the nitrocellulose membrane Hybond-C (Amersham), which was cut at the size of the gel, were equilibrated in transfer buffer for 10 min. Four sheets of Whatman GB003 filter paper (Schleicher & Schull, Dassel) were cut and soaked in the transfer buffer. The gel was placed on the membrane and subsequently on the presoaked filter papers. Another four sheets of presoaked filter paper were applied to complete the sandwich model, and it was placed into an electro-blotter (Biometra, Göttingen). The transfer was carried out at 10 W (150 - 250mA, 39 V) for 1-2 hrs at RT. After that, the blotted membrane was blocked and incubated with antibodies.

2.2.12.6. Staining of polyacrylamide gel

To confirm transfer efficiency of proteins onto nitrocellulose membranes, the gel was incubated overnight in Coomassie Blue staining solution. The methanol and acetic acid in the staining solution cause the proteins to precipitate and thus be fixed in the gels. In acidic solution Coomassie Blue dye interacts chiefly with arginine residues of the proteins, resulting in colour development in the gel. Gel was destained in Coomassie destaining solution for 3 - 8 hrs at RT.

2.2.12.7. Incubation of protein-bound membranes with antibodies

The blotted membrane was first incubated with 5% non-fat milk in PBT for 1 - 2 hrs at RT, in order to block unspecific binding sites, and then it was incubated overnight at 4°C with a primary antibody at the recommended antibody dilution in 2% non-fat milk in PBT. Next day, membrane was washed 3 x 10 min with 2% non-fat milk in PBT and incubated 2 hrs at RT with horse radish peroxidase conjugate secondary antibody diluted 1:10000 in PBT containing 2% non-fat milk. Then, the membrane was washed three times for 10 min at RT in PBT with 2% non-fat milk and one time for 5 min at RT in PBS. Finally, the proteins from the membrane were visualized by using SuperSignal® West Pico Chemiluminescent Substrate (Pierce, USA). Shortly, the membrane was incubated for 3 – 5 min with 1 ml of developing mixture (0.5 ml stable peroxidase solution and 0.5 ml luminal/enhancer solution) and then was wrapped in saran foil and exposed to Roentgen Films (Hyperfilm MP, Amersham, Braunschweg) for 0.5 to 30 min. The films were developed in X-Ray Automatic Processor Curix 60 and air-dried.

2.2.13. Expression of recombinant proteins in the pET vector

2.2.13.1. Production of the GST-PELOTA fusion proteins

Plasmids with recombinant GST-PELO (GST-PELO, GST-PELOΔ5', GST-PELOΔ3' and ST-PELOΔLZ) constructs were transformed to expression in the host bacterial strain *E.coli* BL-21(DE3). A single bacterial colony containing the pET41a vector with fusion constructs was picked from a freshly streaked plate into 50 ml of LB culture medium containing

kanamycin (50 μg/ml) and incubated for overnight culture at 37°C with shaking. Next day, overnight cultures were diluted into 500 ml fresh LB medium with 50 μg/ml kanamycin and cultured further at 37°C until OD600 reached 0.6 - 0.8. Non-induced samples were collected for control. IPTG from a 100 mM stock was added to a final concentration of 1 mM and the incubation step was continued for 4 – 6 hrs. Then, the induced samples were removed and flasks were placed on ice for 5 min. Cells were harvested by centrifugation at 5000 x g for 15 min at 4°C, and stored as a frozen pellet at –80°.

2.2.13.2. Isolation and purification of GST-PELOTA fusion proteins

2.2.13.2.1. Preparation of cell extracts with BugBuster™ protein extraction reagent

Soluble fraction

Frozen cell pellet was slowly thawed on ice for 10 – 30 min and resuspended in the BugBuster solution at RT, using 20 ml reagent for cells from a 500 ml culture. Cell suspension was incubated on a shaking platform at a slow setting for 10 min at RT and for next 10 min on ice. Then, lysate was sonicated on ice 6 times, 1 min each with an interval of 2 min to avoid heat. Insoluble cell debris (pellet) was removed by centrifugation at 16000 x g for 20 min at 4°C and saved for inclusion body purification as described below. Supernatant (soluble extract) was transferred into a fresh tube, purified and after checking on SDS-PAGE gel, it was used for further experiments.

Inclusion body

Pellet after isolation of soluble protein fraction was resuspendend by vortex in the same volume of BugBuster reagent that was used to suspend the cell pellet above. Then, lysozyme was added to a final concentration of 200 μg/ml and the sample was mixed by vortexing and incubated at room temperature for 5 min. After that, 4.6 volumes of 1:10 diluted BugBuster reagent (in deionized water) was added to the suspension and vortexed for 1 min. Suspension was centrifuged at 16000 x g for 15 min at 4°C to collect the inclusion bodies. Supernatant was removed and inclusion bodies were resuspended in ½ the original culture volume of 1:10 diluted BugBuster. The sample was mixed by vortexing and centrifuged at 16000 x g for 15 min at 4°C. This washing step was repeated 2 times more and the final pellet of purified

inclusion bodies was resuspended in 1x PBS. Sample was stored at -80°C for GST Pull-down assay.

2.2.13.2.2. Purification of GST fusion proteins

GST-fusion proteins were purified from bacterial cell extracts using the GST-binding kit (Novagen) according to the manufacturer's instruction. Shortly, bacterial cell extracts were filtrated through 0.45 µm filter and incubated with pre-equilibrated glutathione-agarose (Sigma) for 1 hr at 4°C with gentle mixing. The bound resin was washed four times with PBT at 4°C. Thereafter, fusion protein was eluted with 3 ml elution buffer (10 mM reduced glutathione in 50 mM Tris/HCl, pH 7.5) and the eluate was collected into three fractions. Purified protein was dialyzed overnight at 4°C against PBS. Protein quality and quantity were checked by SDS-PAGE analysis.

2.2.14. Techniques used for interaction studies

2.2.14.1. GST Pull-down assay

GST-fusion proteins were purified from bacterial cell extract using the GST-binding kit (Novagen, Darmstadt). Following reagent were combined in a 1.5 ml microcentrifuge tube on ice. Glutathione-agarose beads were mixed gently by inverting several times. A sufficient volume of beads was transferred to a clean 1.5 ml microcentrifuge tube. The beads were washed 3 times with 250 µl of GST Bind/Wash Buffer (4.3 mM Na_2HPO_4, 1.47 mM KH_2PO_4, 137 mM NaCl, 2.7 mM KCl, pH 7.3) in a microcentrifuge tube and centrifuged at 800 x g for 30 sec. The supernatant was removed by aspiration with a micropipette. Steps were repeated and finally, the beads were resuspended to their original volume (i.e., the original beads volume was transferred to microcentrifuge tube) by adding GST Bind/Wash Buffer. Then, the 50 µl GST fusion protein (100 µg) was added to the GST-beads. To ensure adequate mixing, the reaction tube was rotated at room temperature for 30 min. The tube was centrifuged at 800 x g for 1 min and the supernatant discarded. Beads were washed 2 times with lysis buffer B. 100 µl of tissue extract (300 - 500 µg) were added to the reaction tube and the mixture was incubated for additional 2 hrs at 4°C on a rocking platform. Beads were washed 3 times with 250 µl of lysis buffer B for 10 min at 4°C. Finally, the beads were resuspended in 40 - 50 µl

SDS-PAGE-Loading buffer, denatured with 6 µl DTT at 75°C for 15 min and loaded onto a SDS-PAGE minigel.

2.2.14.2. Co-immunoprecipitation

Immunoprecipitation is a technique that permits the purification of specific proteins for which an antibody has been raised. This primary antibody is either already bound to dynabeads or can be bound to the protein/dynabeads during the procedure in order to physically separate the antibody-antigen complex from the remaining sample.

Total cell extract (2.2.12.2) was used to analyze putative protein-protein interactions in eukaryotic cells. Human cervical adenocarcinoma cells (HeLa) were cotransfected with the appropriate expression vectors by using Lipofectamin 2000 transfection reagent (2.2.15.5.). Transfected cells were grown for 48 hrs at 37°C, then collected, homogenized in 70 – 100 µl lysis buffer B, and total protein was isolated as described above (2.2.12.2). Co-immunoprecipitation was done according to the manufacturer's instruction (Roche, Mannheim). Shortly, to reduce background caused by non-specific adsorption of irrelevant cellular proteins to protein A/G-agarose, a preclearing step was done by incubation 350 - 500 µg of lysate protein with 50 µl A/G-agarose suspension for at least 3 hrs. Then, the samples were centrifuged at 5000 x g for 30 sec and supernatants were transferred into fresh tubes. 10 – 20 µl of c-Myc monoclonal antibody or HA-Tag polyclonal antibody was added and mixtures were incubated at 4°C for 2–3 hrs. After that, mixtures were incubated overnight at 4°C with fresh prepared protein G or A beads. The next day, samples were centrifuged at 5000 x g for 30 sec, and the beads were washed 3 x for 20 min with washing buffer 1. Finally, the beads were resuspended in 40 - 50 µl SDS-PAGE-Loading buffer, 6 µl DTT, and then denatured and loaded onto a SDS-PAGE minigel. Integrity of the resulting proteins was checked by SDS-PAGE analysis (2.2.12.).

2.2.14.3. Bimolecular fluorescence complementation (BiFC) assay

The bimolecular fluorescence complementation (BiFC) assay have been developed for the simple and direct visualization of protein interactions in living cells (Hu *et al.* 2002). It is based on the principle of protein fragment complementation, in which two non-fluorescent fragments derived from a fluorescent green protein (GFP) are fused to a pair of interacting

partners. When the two partners interact, the two non-fluorescent fragments are brought into proximity and an intact fluorescent protein is reconstituted. Hence, the reconstituted fluorescent signals reflect the interaction of two fused proteins under study. This method enables visualization of the subcellular locations of specific protein interactions in the normal cellular environment.

Vectors (FPCA-V1 and FPCA-V2) used for these studies have been generated by Prof. Dr. S. Hoyer-Fender (Department of Developmental Biology GZMB, University of Göttingen, Göttingen) and they contain a EGFP molecule which was split between amino acid 157 and 158. cDNA fragments containing the coding sequence of our candidate genes were used for generation of BiFC assay constructs. cDNAs were amplified (2.2.7.3.) using primers with 5' overhang restriction sites sequences. PCR condition was as follows:

94 °C	5 min	
94 °C	30 sec	35 cycles
60°C	45 sec	
72°C	1 min	
72°C	10 min	

The PCR products were sequenced (2.2.8.) and digested either with *XhoI*/*Bam*HI enzymes for subcloning into FPCA-V1 vector, or with *HindIII*/*BglI* enzymes for subcloning into FPCA-V2 vector (2.2.4.). Then, the constructs were transformed into competent *E.coli* DH5α cells, and after large scale plasmid DNA preparation (2.2.1.1.3.) they were used for transient transfection of HeLa cells (2.2.15.5). 48 hrs after transfection, cells were fixed by incubation with cold 4% paraformaldehyde for 15 min. After washing steps (3 x 5 min) they were mounted with DAPI (Vector, Burfingame). Slides were stored at 4°C. Finally, fluorescent cells were visualized with Olympus BX60 microscope using 20X or 60X Neofluor lens, photographed using digital camera and analyzed by analysis 3.0 soft imaging system.

HeLa cells cotransfected with FPCA-Pelota-V1 and FPCA-Cops5-V2 constructs were used as negative control for our BiFC assay.

2.2.15. Eukaryotic cell culture methods

2.2.15.1. Cell culture conditions

All procedures such as culturing and transfection of cell lines were done under sterile conditions using sterile hood (Heraeus, Hamburg). Solutions and media were sterilized by autoclaving or filtration and were prewarmed before use (37°C water bath). All glassware items like pipettes and bottles were autoclaved, and bottles with liquids were cleaned each time before placing under the sterile hood by whipping with 70% ethanol. All cells were grown in their respective growth media with L-glutamin containing 10% FCS and 1% penicillin/streptomycin solution. The cells were cultured at 37°C in a humidified incubator with 5% CO_2 and grown to 80% confluency.

2.2.15.2. Trypsinisation of eukaryotic cells

Cells were washed twice with 2 – 5 ml sterile PBS and incubated in minimal amount trypsin-EDTA (0.5 gm/l trypsin, 0.2 gm/l EDTA) at 37°C until they had detached from the dish. The process was controlled under an inverted microscope. Trypsin activity was inhibited by addition of growth medium in which the cells were subsequently resuspended. The trypsin was removed by centrifugation at 1000 x g for 5 min. Cells were resuspended in an appropriate volume of cell culture medium and transferred into a new flask with medium. Cell counting was performed, when necessary, using an improved Neubauer chamber, and the cells were plated out or harvested for cryopreservation.

2.2.15.3. Cryopreservation and thawing of eukaryotic cells

Trypsinised cells were spun down (1000 x g for 5 min at 4°C) in 4 ml of growth medium. The supernatant was aspirated and the cells were resuspended (1 - 5 x 10^7 cells/ml) in ice cold medium (DMEM or RPMI, 20% FCS, 10% DMSO). Aliquots of the cells were kept for 2 days at -80°C and then stored in liquid nitrogen. For revitalization, frozen cells were quickly thawed at 37°C in water bath, gently transferred to disposable Falcon (BD Falcon, USA) tubes containing 4 ml growth medium and spun down as described above. Supernatant was

discarded by aspiration and cells were plated out after being resuspended in a suitable amount of prewarmed growth medium.

2.2.15.4. Transient transfection of the eukaryotic cells with plasmid

The transfection involves the introduction of foreign DNA into mammalian cells for its expression. The reagent used in this study was "Lipofectamine 2000 TM" (Invitrogen, Karlsruhe, Germany). For transfection, approximately 0.5 x 10^6 HeLa cells were plated in small flasks with 5 ml of complete DMEM medium and incubated overnight at 37°C, 5% CO_2. 12 µl of Lipofectamine 2000 TM reagent and 4 µg of the DNA of interest were diluted each in a total volume of 100 µl, respectively, with OptiMEM I reduced serum medium (Invitrogen, Karlsruhe, Germany) and incubated at RT for 10 min. Subsequently, we have mixed diluted Lipofectamine and DNA together in a reaction tube and then incubated at RT for 30 min to allow DNA complex formation. Meanwhile, the DMEM containing cells were washed twice with PBS. After DNA complex formation, 800 µl of OptiMEM I medium was added to the reaction tube, mixed vigorously, and applied drop-by-drop to the cells in culture flask and incubated for 2.5-3 hrs at 37°C. Then, 1ml of OptiMEM I medium with 20% FCS was added and further incubated for next 3 hrs. The cells were then incubated for 24 - 48 hrs at 37°C and 5% CO_2.

2.2.15.5. Immunofluorescence staining of eukaryotic cells

The culture media was removed from the cells in microscopical chambers and they were rinsed with PBS. After that, 1 ml cold 4% PFA (fresh made) per chamber was added and incubated for 15 min at RT for fixing the cells. Then, the cells were washed 3 times for 5 min with PBS and blocked for 1 hr at RT with blocking solution containing 0.5% Triton X-100 and 10% horse serum in PBS. After that, cells were incubated overnight at 4°C in humidified chamber with the respective diluted primary antibody in a buffer containing PBS and 5% horse serum. Finally, the cells were incubated with the secondary antibody for 2 hrs at RT, rinsed 3 x 10 min with PBS and mounted with DAPI (Vector, Burfingame). Slides were stored at 4°C. Fluorescent cells were visualized with Olympus BX60 microscope using 20X or 60X Neofluor lens, photographed using digital camera and analyzed by analysis 3.0 soft imaging system.

2.2.16. Techniques for production of targeted mutant mice (Joyner, 2000)

The discovery that cloned DNA introduced into cultured mouse embryonic stem cells can undergo homologous recombination at specific loci has revolutionized our ability to study gene function *in vitro* and *in vivo*. In theory, this technique will allow us to generate any type of mutation in any cloned gene. Over twenty years ago, pluripotent mouse embryonic stem cells (ES) derived from inner cell mass (ICM) of mouse blastocysts were isolated and cultured (Martin, 1981; Evans and Kaufman, 1981). Using stringent culture conditions, these cells can maintain their pluripotent developmental potential even after many passages and following genetic manipulations. Genetic alterations introduced into ES cells in this way can be transmitted into the germline by producing chimeric mice. Therefore, applying gene targeting technology to ES cells in culture gives the opportunity to alter and modify endogenous genes and study their functions *in vivo*.

2.2.16.1. Production of targeted embryonic stem cell clones

2.2.16.1.1. Preparation of EMFI feeder layer

A frozen vial of EMFI cells was quickly thawed at 37°C and transferred to 10 ml EMFI medium. After centrifugation at 270 x g for 5 min, the cell pellet was gently resuspended in 10 ml EMFI medium and plated on a 50 mm culture flask. Cells were incubated at 37°C in 5% CO_2. When the cells formed a confluent monolayer (three days), they were trypsinised, transferred to five 150 mm dishes and grown until they formed confluent monolayer or directly treated with mitomycin C. To treat the EMFI with mitomycin C, the medium was removed and 10 ml fresh medium containing 100 µl mitomycin C (1mg/ml) was added. After 2-3 hrs of incubation, the monolayer of cells was washed twice with 10 ml PBS. The cells were then resuspended with 10 ml medium and gentle pipetting. The cells were centrifuged, resuspended in EMFI medium and plated onto dishes, which have been treated with 0.1% gelatine for 30 min. The feeder cells were allowed to attach by incubation overnight at 37°C, 5% CO_2 or used after 2 hrs of incubation. Before adding ES cells on the feeder layer, the medium was changed to ES cell medium.

2.2.16.1.2. Growth of ES cells on feeder layer

One vial of frozen ES cells was quickly thawed at 37°C and cells were transferred to a 12 ml tube containing 6 ml ES cell medium. After centrifugation, the cell pellet was resuspended in 5 ml ES cell medium and plated on 6 cm dishes containing EMFIs at 37°C, 5% CO_2. Next day, the medium was changed. The second day, cells were washed with PBS, treated with 2 ml trypsin/EDTA at 37°C, 5% CO_2, for 5 min. The cells were gently pipetted up and down to dissolve cell clumps, resuspended with 5 ml ES medium and centrifuged. The cell pellet was resuspended in 10 ml ES cell medium and distributed either to 5 or 6 dishes (6 cm) or to 2 dishes (10 cm) containing feeder layers. The cells were passaged every second day as described above.

2.2.16.1.3. Electroporation of ES cells

ES cells which have grown for two days in 10 cm dishes were trypsinised. The cell pellet was resuspended in 20 ml PBS and centrifuged. The cell pellet was then resuspended in 1 ml PBS. The 0.8 ml of cell suspension was mixed with 40 µg of linearised DNA-construct and transferred into an electroporation cuvette. The electroporation was performed at 240V, 500 µF with the Bio-Rad gene pulser^{TM} apparatus. After electroporation, the cuvette was placed on ice for 20 min. The cell suspension was transferred from cuvette into 20 ml of ES cell medium and plated onto two 10 cm dishes containing feeder layers. The medium was changed every next day. Two days after the electroporation, the drugs for selection were added (active G418 at 400µg/ml and gancyclovir at 2 µM). The medium was changed every day. After about eight days of selection, drug resistant colonies have appeared and were ready for screening by Southern blot analysis.

2.2.16.1.4. Growing ES cells for Southern blot analysis

The drug resistant colonies that were formed after about eight days of selection were picked with a drawn-out Pasteur pipette under a dissecting microscope. Each colony was transferred into a 24-well plate containing feeders and ES cell medium. After 2 days, the ES cells were trypsinised with 100 µl trypsin for 5 min and resuspended in 500 µl ES cell medium. Half of the cell suspension in each well was transferred to a well on two different 24-well plates, one

gelatinised plate, and the other containing feeder cells (master plate). The gelatinised plate was used for preparing DNA and the master plate was kept frozen.

2.2.16.2. Production of chimeras by injection of ES cells into blastocysts

The ability of mammalian embryos to incorporate foreign cells and develop as chimeras has been exploited for a variety of purposes including the perpetuation of mutations produced in embryonic stem (ES) cells by gene targeting and the subsequent analysis of these mutations. The standard procedure is to inject 10 - 20 ES cells from 129/Sv, which are recombinant for the targeted locus, into the blastocoel cavity of recently cavitated blastocysts that have been recovered by flushing the uteri of day 4 pregnant mice (C57Bl/6J). After injection, embryos are cultured for a short period (2 - 3 hrs) to allow re-expansion of the blastocoel cavity and then transferred to the uterine horns of day three pseudopregnant mice. Pseudopregnant females are obtained by mating 6 - 8 weeks old oestrous females with vasectomised males.

2.2.16.3. Detection of chimerism and mice breeding

The most convenient and readily apparent genetic marker of chimerism is coat color. Chimeric males are bred to wild type mice to ascertain contribution of the ES cells to germline. Once a germline chimera has been identified, the first priority will be to obtain and maintain the targeted allele in living animals. The chimeras were bred with C57Bl/6J and with 129/Sv mice, respectively, to compare the phenotypes in two different genetic backgrounds.

2.2.17. Generation of transgenic mice

Generation of transgenic mice was performed by “Transgenic Service” of Max Planck Institute for Experimental Medicine in Göttingen by pronuclear microinjection of DNA. Method for transgenic animal production was based on Hogan *et al.* (1994).

2.2.17.1. Preparation of DNA for pronuclear microinjection

Transgenic constructs were released from cloning vector by restriction digestion. Digested fragments were separated by agarose gel electrophoresis (without EtBr) in the way that 25 µg

of digested plasmid was loaded to many slots of the gel. After separation, outer lanes were cut out and stained with EtBr. After staining, gel was reconstructed and appropriate gel slices were cut out from the rest of the gel under UV light. DNA was then eluted from gel with QIAquick extraction kit and filtered through 0.45 μm microfilter (Milipore). Concentration of DNA was estimated by EtBr electrophoresis of DNA aliquots in comparison with Smart ladder marker (defined DNA amounts in each band). For microinjection, DNA was diluted to 4 ng/μl in microinjection buffer (10 mM Tris, pH 7.5; 0.1 mM EDTA, pH 8.0).

2.2.18. Determination of sperm parameters

2.2.18.1 Sperm count in epididymes, uterus and oviduct

Epididymes of wild type and KO mice were dissected under aseptic condition and put in 0.5 ml of in vitro fertilization (IVF) medium. Spermatozoa were allowed to swim out of the epididymes for 1 hr at 37°C, 5% CO_2. Sperm suspension was diluted 10 - 40 times with PBS before counting, when necessary. 5 μl of this suspension was put into Neubauer counting chamber and spermatozoa were counted in 8 independent fields (each having an area of 0.0025 mm^2) under the microscope (Olympus BX60) with 20x magnification. Total spermatozoa were calculated by following formula:

Total Sperm = average No. of sperm x 10 x 500 x D (D is the dilution factor)

For determination of sperm number in the uterus and the oviduct female wild type mice were mated with KO males. The uteri and oviduct of those mice, which were positive for vaginal plug, were dissected in IVF medium and the sperm were flushed out. The number of spermatozoa was calculated as described above.

2.2.18.2 Determination of sperm abnormalities

For the determination of sperm abnormalities, sperm suspensions from wild type and KO mice were spread onto Superfrost slides, air-dried and fixed in cold 4% PFA for 10 min at RT. Slides were then washed in H_2O for 1 min and then stained in hematoxylin for 15 min. Next, slides were washed in running tap water for approximately 10 min and finally stained with

eosin (0.1% + 2% acetic acid) for a 1 min and again washed in H_2O for 1 min. 200 spermatozoa were counted and percentage of normal or abnormal (normal or unusual sperm head shape) sperm was determined.

2.2.18.3 Sperm motility analysis

10 µl of sperm suspension from wild type and KO mice was put on a dual sided sperm analysis chamber. Sperm motility was quantified using the computer assisted semen analysis (CASA) system (CEROS version 10, Hamilton Thorne Research). Then, 6000 - 10000 spermatozoa from mutant and wild type males were analyzed using the following parameters: average path velocity (VAP), straight line velocity (VSL), curvilinear velocity (VCL), lateral head amplitude (ALH), beat frequency (BCF) and straight forward movement (STR). Frequencies of these six sperm motility parameters were examined by probability plots categorized by mouse type (wild-type/mutant) and by time of observation (1.5, 3.5 and 5.5 hrs after preparation) for statistical analysis.

2.2.18.4 Acrosome reaction

Spermatozoa were isolated and capacitated by incubating for 1 hr at 37°C with 5 % CO_2. Sperms were transferred into two microcentrifuge tubes and centrifuged for 2 min at 3000 x g. The supernatant was aspirated, leaving only 50 µl for resuspension of sperms. 2.5 µl of Ionophore A23187 (final concentration 10 µm in DMSO) was added to sperm suspension. For negative control, 2.5 µl of phosphoric acid (5 mM) was added and incubated at 37°C for 1 hr. The sperms were then fixed in 500 µl of 2 % formaldehyde (in PBS) for 30 min at 4°C. After completion of fixation, sperms were centrifuged at 4000 x g for 2 min. Sperms were further washed twice with 0.15 mM ammonium acetate. Finally, sperms were resuspended in 100 µl of PBS and 30 µl of suspension was spread on superfrost slides and air-dried. The slides were stained with Coomasie G-250 in 3.5 % H_2O_2 for 2.5 min. Unbound dye was removed by washing several times with water. The slides were mounted with 30% glycerol and observed under microscope. At least 200 sperms with and without blue head were counted. Here, blue head sperms represent those sperms, which failed to undergo acrosome reaction. The acrosome reaction was calculated as follows:

$$\text{Acrosome reaction (in percentage)} = \frac{\text{Number of sperms without blue head}}{\text{Total numbers of sperms}} \times 100$$

2.2.19. Studies of estrus cycle

2.2.19.1. Vaginal cytology

Monitoring of vaginal cytology was performed with virgin female mice (3 months old) for at least 4 consecutive estrus cycles prior to the mating test. Vaginal smears were collected daily between 09:00 and 10:00 a.m. for identification of the estrus cycle phase. The mean duration of the estrus cycle of young adult female mouse is 4 days, comprising the 4 phases; proestrus (P), estrus (E), metestrus (M), and diestrus (D) that are characterized *via* changes in the vaginal cytology (Fig. 3). Vaginal cells were collected with a plastic pipette tip filled with 200 µl of 0.9% NaCl. The vagina was flushed 2 - 3 times, or until the saline became milky. The vaginal fluid containing the suspended cells was then transferred onto Superfrost slides and closed with cover slide. To determine the estrus cycle phase, the unstained native vaginal cell suspension was evaluated under a light microscope (Zeiss, Germany) by using the 20x objective. In the vaginal samples three types of cell populations are present: -proestrus: round-shaped, nucleated, large epithelial cells (Fig. 3A); -estrus: large irregular shaped, anucleated, cornified cells (Fig. 3B); -metestrus and diestrus: leukocytes (Fig. 3C and D).

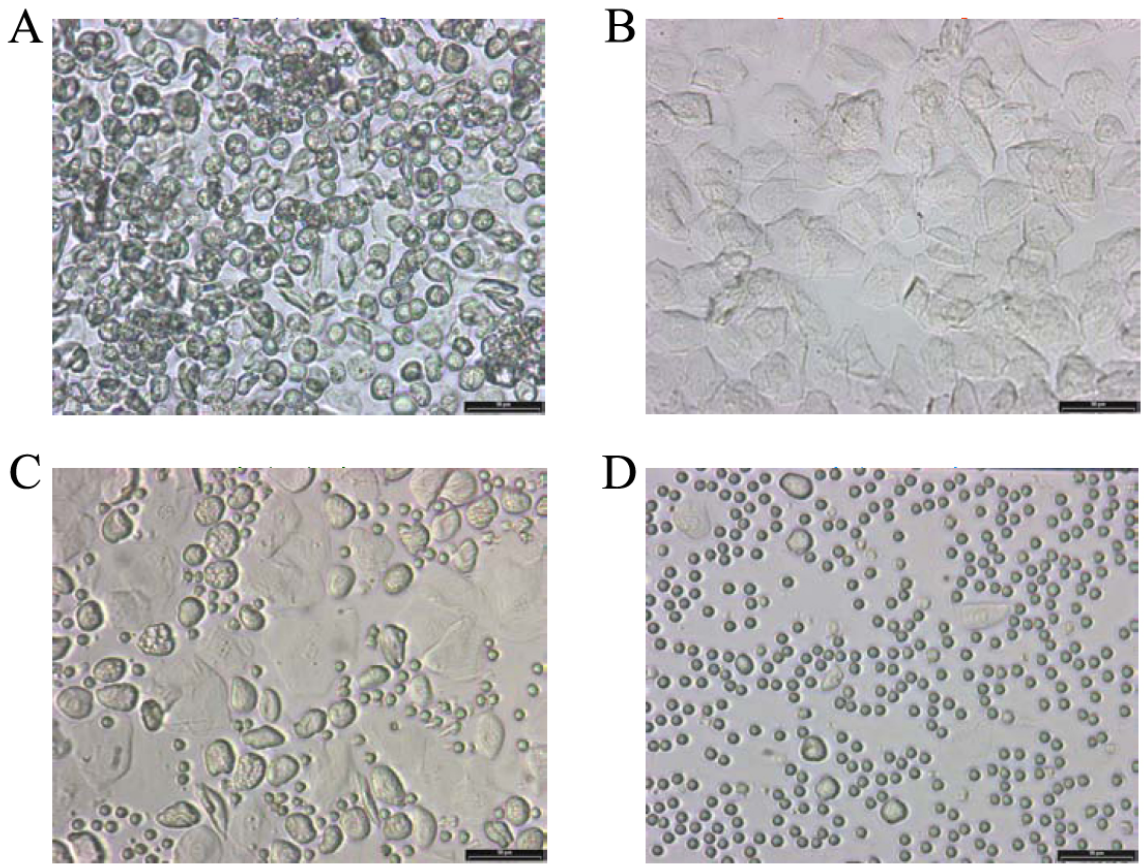

Fig 3. Photomicrographs of the vaginal smears collected from female mice at proestrus (A); estrus (B); metestrus (C); and diestrus (D). All photos were taken at the same magnification (20x). Scale bar = 50 µm.

2.2.19.2. Mating behavioral testing procedure

Five 4-month old wild type and Insl5$^{-/-}$ females were mated with ten infertile adult *Insl3*-deficient males (ratio 1:1), for least 35 days. During this time, the mating pairs were observed for sexual activity and every morning, females were checked for the presence of a vaginal plug. In this study, the presence of a vaginal plug was used as an indicator of positive mating behavior as previously described (Cicero *et al.,* 2002).

2.2.19.3. Superovulation and isolation of oocytes

Seven to twelve-week old female mice were superovulated by intraperitoneal injections of 5 IU of pregnant mare's serum gonadotropin (PMSG), followed 44 - 48 hrs later by 5 IU of human chorionic gonadotrophin (HCG; Sigma). After the second injection, females were

housed overnight with males and were checked by a vaginal plug the following morning. The E0.5 was considered to be 12:00 noon at the day of vaginal plug.

2.2.20. Histological and immunocytochemical analysis

2.2.20.1. Tissue preparation for electron microscopy

For conventional electron microscopy, freshly isolated mouse testes were fixed with 1% paraformaldehyde and 3.5% glutaraldehyde in 0.1 M cacodylate buffer (pH 7.4) for 8 - 12 hrs at 4°C. Fixed testes were cut into small pieces and thoroughly washed over 3-4 days at 4 °C in 0.1 M cacodylate buffer containing 0.1 M saccharose. After that, testes were treated with 1% OsO_4 in cacodylate buffer for 2 hrs, washed three times, dehydrated and embedded in epoxy resin. Ultrathin sections were contrasted using uranyl acetate and lead citrate and examined with a Leo 906 electron microscope.

2.2.20.2. Tissue preparation for paraffin embedding

The freshly prepared tissues were fixed in Bouin's solution or 4% (w/v) paraformaldehyde for 24 - 72 hrs to prevent alterations in the cellular structure. The tissue to be embedded in paraffin should be free of water. The dehydration process was accomplished by passing the tissue through a series of increasing alcohol concentrations. For this purpose, the tissue was let in 70%, 80%, 90%, 95% and 100% ethanol for at least 2 hrs at RT. Later, the alcohol was removed from the tissue by incubating it in isopropanol or methylbenzoat for overnight. Tissue was then washed in different mixtures of isopropanol/xylol (histoclear) in ratios 3:1, 1:1 and 1:3 for 30 min to 1 hr at RT. After that, tissue was incubated overnight in 100% xylol. Further, tissue was incubated in paraplast at 60°C overnight. Before embedding, paraplast was changed at least three times. Finally, the tissue was placed in embedding mould and melted paraffin was poured into the mould to form a block. The block was allowed to cool and was then ready for sectioning or stored at 4°C.

2.2.20.3. Sections of the paraffin block

The paraffin blocks were pre-cut to the optimal size and clamped into the microtome (Hn 40 Ing., Nut hole, Germany). The cut-thickness of the sections was 7 µm. The sections were floated on 40°C water to allow actual spread and subsequently put onto Superfrost slides. A fine brush was used to transfer the sections to the slides. After complete evaporation at 37°C for 1 - 3 days, slides were stored at RT for further analysis.

2.2.20.4. Immunostaining of mouse tissues

Fixation and subsequent treatment of mouse tissue were performed as described in section 2.2.20.2. Tissue sections (7 µm) were incubated twice for 5 min in xylol to remove the paraffin. Then, sections were rehydrated in a decreasing ethanol series (100%, 95%, 80%, 70%, and 50%) for 2 min each. For immunstaining, slides were washed in PBS and then incubated with a blocking solution containing 10% goat serum in PBT for 1 hr at RT. After blocking, sections were incubated overnight with primary antibodies in a humidified chamber at 4°C. Tissue sections were rinsed three times for 5 min in PBT and subsequently incubated with appropriate secondary antibody for 2 hrs in a humidified chamber at RT. Finally, sections were washed three times for 5 min in PBT and mounted with DAPI or AquaMount medium. Immunostaining of the sections was examined using a fluorescence equipped microscope (BX60; Olympus).

2.2.20.5. Immunocytochemical staining of germ cell suspensions

Germ cell suspensions were prepared from mouse testes by using the collagenase/trypsin method according to published procedure (Romrell *et al.,* 1976). Testes from 60 days old mice were collected in serum-free culture medium, rinsed in 0.1 M PBS, pH 7.2. After removal of the tunica albuginea, seminiferous tubules were enzymatically dissociated by the addition of 1 ml collagenase (1mg/ml). The slurry maintained at 37°C for 30 min was triturated every 5 min. 5 ml of Hank's solution was added and then spun at 350 x g to sediment the dissociated cells. The pellet was resuspended in 3 ml trypsin, incubated for 5 – 10 min and then trypsin was inactivated by adding 5 ml FKS. The slurry was passed through 80 µm nylon mesh. The filtrate was spun at 350 x g to sediment the cells. Cells were

resuspended in 1 ml PBS and spread onto superfrost slides, air-dried and fixed in 4% PFA for 10 min at RT. Next, they were washed twice in PBS and immunostained as described above (2.2.15.5).

2.2.20.6. Hematoxylin-eosin (H&E) staining of the histological sections

Tissue sections were first incubated three times in xylol for 3 min each, followed by incubation three times in 100% for 3 min, 95%, 80% and 70% ethanol for 2 min each. Thereafter slides were washed in dH_2O for 5 min and stained for 3 min in hematoxylin. This staining was followed by rinsing with deionised water and washing in running tap water for 10 min. The treated slides were dipped fast in acid ethanol (1ml concentrated HCl in 400 ml 70% ethanol) for 8 - 12 times to destain, rinsed in running tap water for 2 min and in deionised water for 2 min, stained in eosin for 15 - 30 sec and then incubated in 70%, 80% 90%, 95% and 100% ethanol for 3 min each. Finally, the stained slides were incubated two times in xylol for 15 min and mounted with Eukitt-quick hardening mounting medium.

2.2.20.7. TUNEL-assay for detection of apoptotic cells

Testes were fixed in 4% paraformaldehyde and embedded in paraffin. Sections were cut at 5µm. TdT- mediated nick labeling (TUNEL) staining was performed using the In Situ Cell Death Detection Kit (Roche Diagnostic GmbH, Mannheim) according to the manufacturer's instructions. After rehydration, the sections were incubated in 2x SSC at 80°C for 20 min followed by washing twice with water and once with proteinase K buffer (29 mM Tris/HCl, pH7.5, 2mM CaCl) for 5 min each. The slides were then treated with proteinase K (10µg/ml) at 37°C for 30 min. An aliquot of 3'-end labeling reaction mixture containing 4 µl of 5x terminal deoxynucleotidyl transferase (TdT) buffer, 0.1 µl of digoxigenin-11-ddUTP (10 nmol/µl) 0,2 µl of ddATP (5 mM), 1 µl of TdT and 14.7 µl nuclease-free water was applied to one section. The slides were kept in a humidified box, incubated at 37°C for 1 hr, and then washed three times with TBST buffer (10mM Tris/HCl, pH-8.0, 100mM NaCl, and 0.1%Tween-20) for 20 min each. An anti-digoxigenin-horseradish peroxidase monoclonal antibody (DAKO, 1:200 dilution in TBST containing 1% BSA) was applied, and the slides were incubated in the humidified box at RT for 1 hr and then washed three times with TBST for 5 min each time. Finally, the labeled cells were visualized by 3,3'-diaminobenzidine tetrahydrochloride for 0.5 - 2 min.

2.2.21. German Mouse Clinic (GMC) screen

27 *Insl5*$^{-/-}$ and 30 wild type males and females were subjected to general set up of the screen, husbandry, and multiparameter analysis in the German Mouse Clinic (GMC, Munich, Germany) as previously described (Gailus-Durner *et al.,* 2005).

2.2.21.1. Behavioral Screen

In the behavioral screen we tested the spontaneous exploration of a novel environment by Insl5$^{-/-}$ and Insl5$^{+/+}$ animals to assess locomotor activity, anxiety-related behaviour, exploratory pattern, arousal and object recognition memory in a single short test. To this end we used our standard procedure of the modified Hole Board test as previously described in detail (Galy *et al.,* 2006; Kallnik *et al.,* 2007; and Bender *et al.,* 2008).

2.2.21.2. Neurological Screen

In the primary neurological analysis a modified SHIRPA-protocol for the general assessment of basic neurological functions was used as described previously (Schneider *et al.,* 2006).

2.2.21.3. Nociceptive Screen

In the nociceptive screen we tested the pain reactivity of *Insl5*$^{-/-}$ and Insl5$^{+/+}$ animals to different type of pain stimuli. We studied the reaction of the intact animals to thermal pain (Hargreaves, hot plate and tail flick tests) and to mechanical (von Frey test) stimulus.
The hot plate test was performed as previously described (Eddy and Limbach, 1953) using a hot plate analgesia meter (TSA GMBH, Germany) heated to 50°C (±0.2ºC). The cut-off time was 60 s. The latency until mice showed first signs of discomfort (paw shaking, licking or lifting) was recorded.
The Hargreaves test was performed with an apparatus which consists of multiple chambers with transparent glass floors, under which a mobile radiant heat source can be focused accurately on a mouse paw (Hargreaves *et al.,* 1988). The animals were first acclimatized to the apparatus for approximately 60 min one day before measurement and 30 min on the test day. The light source was than moved using a targeting system directly under the paw. The

intensity of the heat source was set to produce the desired (RI=40) baseline response time (7 sec). To prevent tissue injury, 15 sec cut-off time was used. The test was repeated for 3-5 times at any animal.

To determine the tail flick latencies the Hargreaves apparatus was used. The procedure was identical with that described above, but the tail was targeted instead of the paw, and the intensity of the used stimulus was larger (RI = 70). The response latency is determined to the nearest 0.1sec. When the tail of a mouse is exposed to a noxious heat, a spinally-mediated withdrawal reflex (a vigorous flexion of the tail) is elicited at the nociceptive threshold (D'Amour and Smith, 1941). Although the behavioral response consists of a spinal reflex, it is affected by descending pain-modulating inputs.

With the help of von Frey filament test, we examined the responses of the animals to mechanical noxious stimuli. For this measurement, we used an apparatus of Ugo-Basile (Italy). This instrument consists of a mobile pressure-actuator, which can exert a user-defined force, or a continuously increasing force on the mouse paw. For the test, mice were placed in the transparent test chamber with a wire mash floor and allowed to acclimatize for approximately 30 min. The tip of the filaments or force actuator was applied to the middle of the plantar surface of the mouse. Withdrawal threshold was measured 4 times pro trial and expressed as tolerance level in gram (Chaplan *et al.,* 1994; Hofmann *et al.,* 2003).

2.2.22. Glucose and insulin tolerance tests

For intraperitoneal glucose tolerance tests (IPGTT), animals were fasted overnight (12-16 hrs) and then injected with glucose (2 g/kg body weight, i.p.). Glucose was measured in the tail vein blood at 0, 20, 40, 60, and 120 min after injection using Haemogluco-Test (Boehringer-Mannheim, Germany).

For insulin tolerance tests, mice were fasted for 5 hours and then injected with human recombinant insulin (0.75 U/kg of body weight i.p.; Novo-Nordisk, Copenhagen, Denmark) The tail vein blood glucose was measured at 0, 20, 40, 60, and 120 min after injection.

2.2.23. Computer analysis

For the analysis of the nucleotide sequences, programs like BLAST, BLAST2, MEGABLAST and other programs from National Center for Biotechnology Information

(NCBI) were used (www.ncbi.nlm.nih.gov). And for restriction analysis of DNA NEBcutter V2.0 programm was used (http://tools.neb.com/NEBcutter2/index.php). Information about mouse alleles, phenotypes and strains were used from Jackson Laboratory webpage (www.informatics.jax.org). For protein studies ExPASy tools (www.expasy.ch) and Promega Biomath calculator (http://www.promega.com/biomath/) were used. Mouse genome sequence and other analysis on mouse genes, transcripts and putative proteins were downloaded from Celera discovery system (www.celera.com). Statistical analysis was performed using Statistica software (Statsoft®, http://www.statsoftinc.com).

3. RESULTS

3.1. Expression and functional analysis of *Insl5* gene

3.1.1. Expression analysis of mouse *Insl5* gene by RT-PCR

In previous studies, the tissue-specific expression of the mouse Insulin-like 5 gene (*Insl5)* was detected in thymus and colon (Conklin *et al.,* 1999). In order to confirm these results, a more sensitive method (RT-PCR) was used. RT-PCR was performed on total RNA from different tissues (brain, thymus, colon, rectum, heart, lung, liver, kidney, spleen, stomach, testis, and ovary) using primers Insl5F and Insl5R amplifying a 650-bp fragment of *Insl5* gene. The quality of RNA was checked using HPRT primers (Fig. 4A, B). The *Insl5* transcript was detectable in almost all of the investigated tissues, except heart and liver (Fig. 4A, B). To examine the expression of the *Insl5* gene during prenatal development, RNA was extracted from embryos at 9.5 to 15.5 *dpc* and analyzed for the presence of *Insl5* transcript by RT-PCR. *Insl5* expression was detected from E11.5 to E15.5 (Fig. 4C).

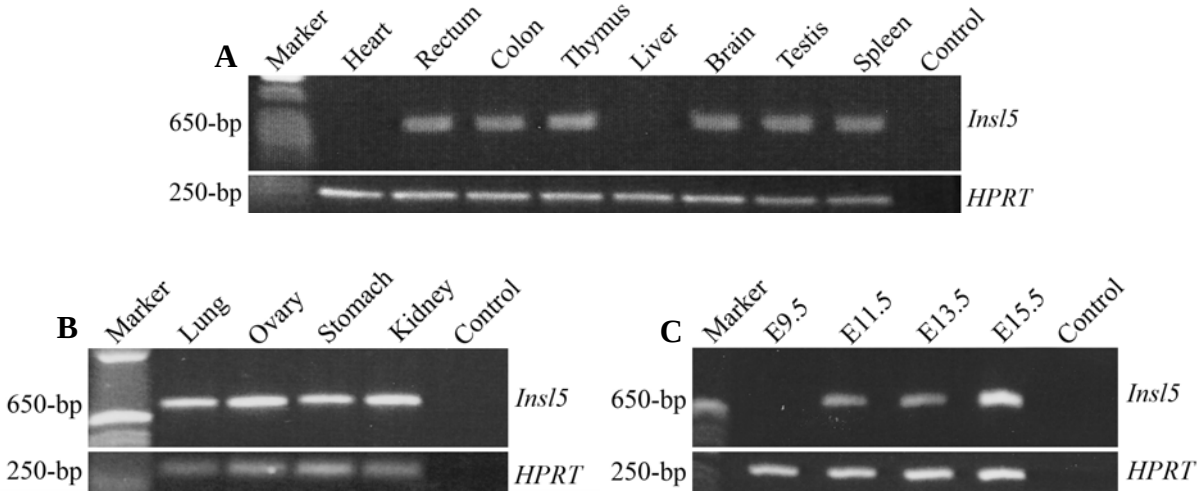

Fig. 4. RT-PCR expression analysis of *Insl5* in different tissues **(A, B)**, and prenatal developmental stages **(C)**. *Insl5*-specific primers Insl5F and Insl5R were used to amplify a 650-bp fragment of *Insl5* transcript. Expression was detected in all of the investigated tissues, except heart and liver. The level of *Insl5* transcript is increased during prenatal development. RT-PCR for HPRT transcript was performed for control of RNA quality. Control: negative control (no-template probe).

3.1.2. Generation and analysis of *Insl5*-deficient mice

Insl5 knock-out construct and *Insl5*-deficient mice on a C57BL/6J x 129/Sv hybrid genetic background were generated by Dr. K. Shirneshan (Shirneshan, 2005). The targeting construct was designed to replace a genomic fragment containing sequence of exon 2, encoding amino acids of the A- and C-chain regions, by the *Neomycin* resistance gene (*neo*^{r}) under the control of the *Phosphoglycerate kinase (Pgk)* promoter (Fig. 5).

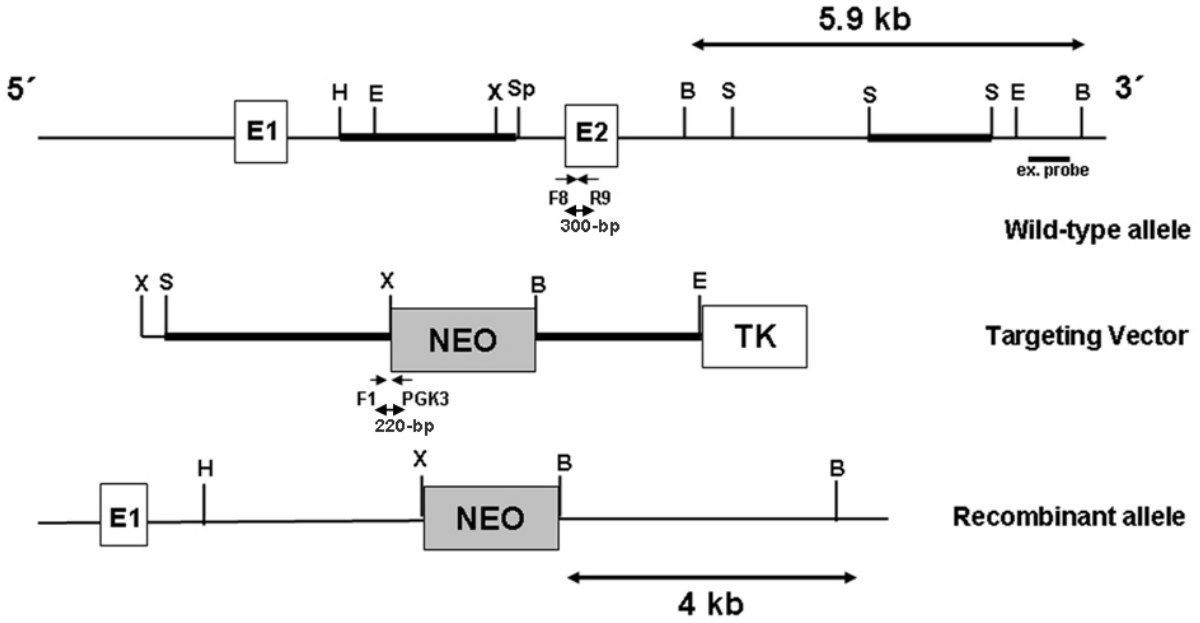

Fig. 5. Targeted disruption of the *Insl5* gene. Structures of the wild type allele, targeting vector and recombinant allele are shown together with the relevant restriction sites. The construct contains 4.2-kb of the 5'and 2.8-kb of the 3' region of *Insl5* gene. A *pgk-neo* selection cassette (NEO) replaces exon 2. The 3' external probe used to identify wild type and targeted allele in Southern blot analysis and the predicted length of the detected fragments are also shown. The primers F8, R9, F1 and PGK3, which were used to amplify the wild type and targeted allele by PCR are also indicated by arrows. Abbreviations: TK: *Thymidine kinase* cassette; E1: exon 1; E2: exon 2; B: *Bam*HI; E: *Eco*RI; S: *Sal*I; Sp: *Spe*I; X: *Xho*I; F8: primer Insl5-F8; R9: primer Insl5-R9; F1: primer I5KO-F1.

3.1.2.1. Phenotypic analysis of *Insl5* knock-out mice

Primary analysis of *Insl5* mutant mice on a C57BL/6J x 129/Sv hybrid genetic background did not show obvious abnormalities (Shirneshan, 2005), therefore we analyzed the phenotype of *Insl5*-deficient mice in collaboration with the German Mouse Clinic (GMC). In the GMC *Insl5*$^{-/-}$ and wild type mice were subjected to an open access platform for standardized phenotyping (Gailus-Durner *et al.,* 2005)**.** Several hundred parameters including analysis of

morphology, organ pathology, neurology, behavior, cardiovascular and lung function, immunological status, vision and eye and nociceptive behavior were assessed.

In the behavioral screen, homozygous *Insl5*$^{-/-}$ mutants displayed a significant reduction of rearing activity characterized by reduced rearing frequency (*Insl5*$^{-/-}$ vs. *Insl5*$^{+/+}$, 11.4±2 vs. 22.19±2.57, $p< 0.01$) and increased rearing latency (*Insl5*$^{-/-}$ vs. *Insl5*$^{+/+}$, 122.25±17.53 vs. 53.93±4.13, $p< 0.001$) as well as increased risk assessment behavior characterized by an increased number of stretched attend postures (*Insl5*$^{-/-}$ vs. *Insl5*$^{+/+}$, 2.1±0.61 vs. 0.7±0.17, $p < 0.05$). The analysis of *Insl5*-deficient mice with the modified SHIRPA-protocol in the neurological screen revealed less transfer arousal ($p< 0.05$) in the arena and diminished tail elevation ($p< 0.05$) (Tab. 1). The most interesting differences between *Insl5*$^{-/-}$ mice and their wild type littermates were observed in the nociceptive behavior.

Tab. 1. Significant differences in transfer arousal and tail evaluation in *Insl5*-deficient mice.

Genotype of mice	Transfer arousal			Tail elevation		
	Extended freeze	Brief freeze	Immediate movement	Dragging	Horizontally extension	Elevated/ Straub tail
Insl5$^{+/+}$	6	8	1	0	4	11
Insl5$^{-/-}$	7	8	0	2	6	7

3.1.2.1.1. Nociceptive behavior in *Insl5*-deficient mice

The nociceptive screen was performed (2.2.21.3) on 7-month old *Insl5*$^{+/+}$ and *Insl5*$^{-/-}$ mice. We examined the response to noxious thermal stimuli using hot plate, Hargreaves and tail flick tests and to mechanical stimuli by von Frey filament test. The hot plate and Hargreaves test was used to examine a supraspinal and spinal involvement in nociception, respectively, and the tail flick test was used to evaluate the spinal reflexes at the lumbar and sacral levels. In these screen, *Insl5*-deficient mice showed significant delay of hind paw licking ($p< 0.001$; n = 27-30 animals for each genotype) and hind paw shaking ($p< 0.05$) in response to hot plate test as compared with wild type mice (Fig. 6A, B). Paw withdrawal responses of *Insl5*$^{-/-}$ mice in Hargreaves test was slightly faster than that of wild type mice ($p< 0.05$; n = 29-30 animals for each genotype; Fig. 6C), while nociceptive response in the tail flick test demonstrated no significant difference ($p> 0.05$) between wild type (n = 29) and mutant mice (n = 30) (Fig. 6D). Also no differences were found between genotypes in response to mechanical stimuli (Fig. 6E). Thus, *Insl5*$^{-/-}$ mice showed delayed latency for antinociceptive behavior and showed faster paw withdrawal latency what could indicate impairment of descending inhibitory antinociceptive inputs to the spinal cord.

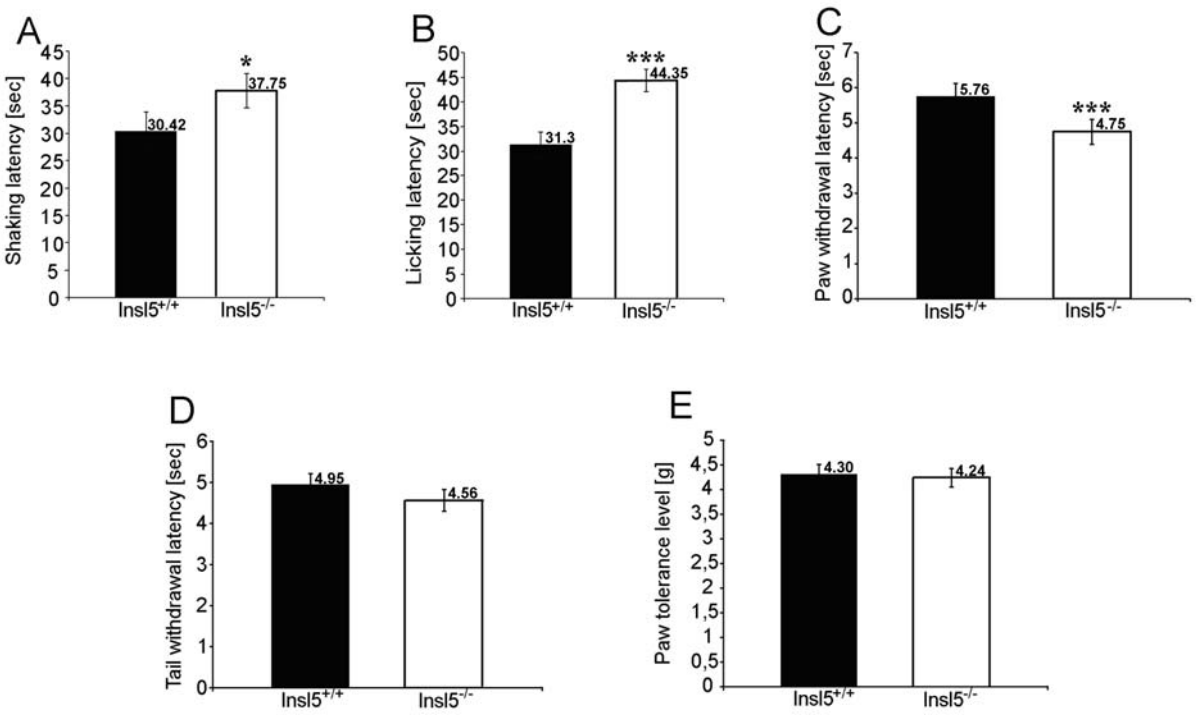

Fig. 6. Responses of *Insl5*$^{+/+}$ and *Insl5*$^{-/-}$ mice to noxious stimuli. Responses of *Insl5*$^{+/+}$ and *Insl5*$^{-/-}$ mice to noxious stimuli were determined in the hot plate **(A, B),** Hargreaves **(C),** tail flick **(D)** and von Frey filament tests **(E)**. Shaking **(A)** and licking **(B)** latencies in hot plate test were significantly increased in *Insl5*$^{-/-}$ mice. In contrast, paw withdrawal latency in the Hargreaves test **(C)** was highly decreased in *Insl5*$^{-/-}$ mice. **(D)** Tail flick latency was similar between both genotypes. No significant differences were shown between *Insl5*$^{+/+}$ and *Insl5*$^{-/-}$ in pain response to mechanical stimuli in the von Frey filament test **(E).** Data are presented as the mean±SD. *, $p< 0.05$; ***, $p< 0.001$; $n = 27$-30 for each genotype.

To provide a complete picture of the pain reactivity of *Insl5* mutant mouse line, we have repeated hot plate and Hargreaves tests on younger (3-month old) wild type and *Insl5* knock-out mice (20 animals per genotype). Nociceptive response in both tests demonstrated no significant differences between young wild type and mutant mice ($p> 0.05$) (Fig. 7).

Summarizing these data, we have observed that in younger animals there were no significant differences in nociception response between *Insl5*$^{-/-}$ and *Insl5*$^{+/+}$ mice ($p> 0.05$, Fig. 7), whereas in older mice the differences were clearly visible ($p< 0.05$, Fig. 6).

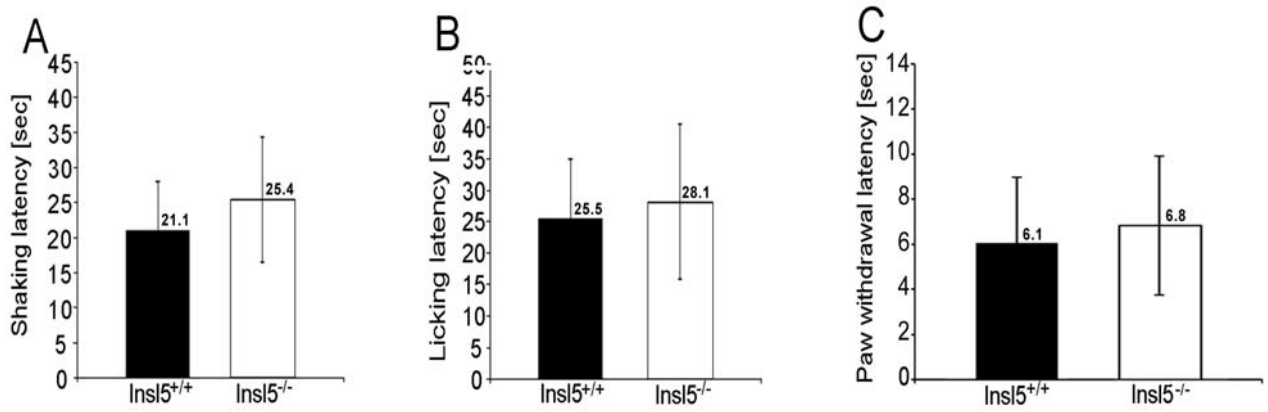

Fig. 7. Responses of 3-month old *Insl5*$^{+/+}$ and *Insl5*$^{-/-}$ mice to noxious stimuli were determined in repeated hot plate **(A, B)** and Hargreaves **(C)** tests. *Insl5* knock-out mice showed no different pain reactivity in both tests.

3.1.2.1.2. Expression of INSL5 in brain and spinal cord

To determine the expression pattern of INSL5 in the mouse hypothalamus and to confirm the inactivation of *Insl5* at protein level, an immunohistochemical analysis was performed.
Immunohistochemical staining of brain sections revealed that the INSL5 is densely expressed in the regions of the anterior hypothalamus overlapping with the preoptic area and in the paraventricular hypothalamus (Fig. 8A), while no immunostaining could be detected in these regions of INSL5-deficient brain (Fig. 8B). The expression profile of INSL5 in these areas of brain confirmed the results of previous studies using other polyclonal anti-Insl5 antibodies (Dun *et al.,* 2006). We further analyzed the expression of INSL5 in the brain nuclei that are involved in the processing of painful stimuli, such as midbrain, pons, medulla oblongata and spinal cord. A particular dense expression of INSL5 was observed in the ventral nuclei of the periaqueductal gray locating in the midbrain (Fig. 8C), and the pontine Kölliker-Fuse nucleus and lateral parabrachial nuclei of the pons (Fig. 8D). Other areas within the medulla oblongata including the medullary raphe nuclei, the lateral reticular nucleus and the nucleus of the solitary tract showed only weak expression of INSL5. In contrast, the dorsal horn of the spinal cord did not show Insl5-immunoreactivity (data not shown).

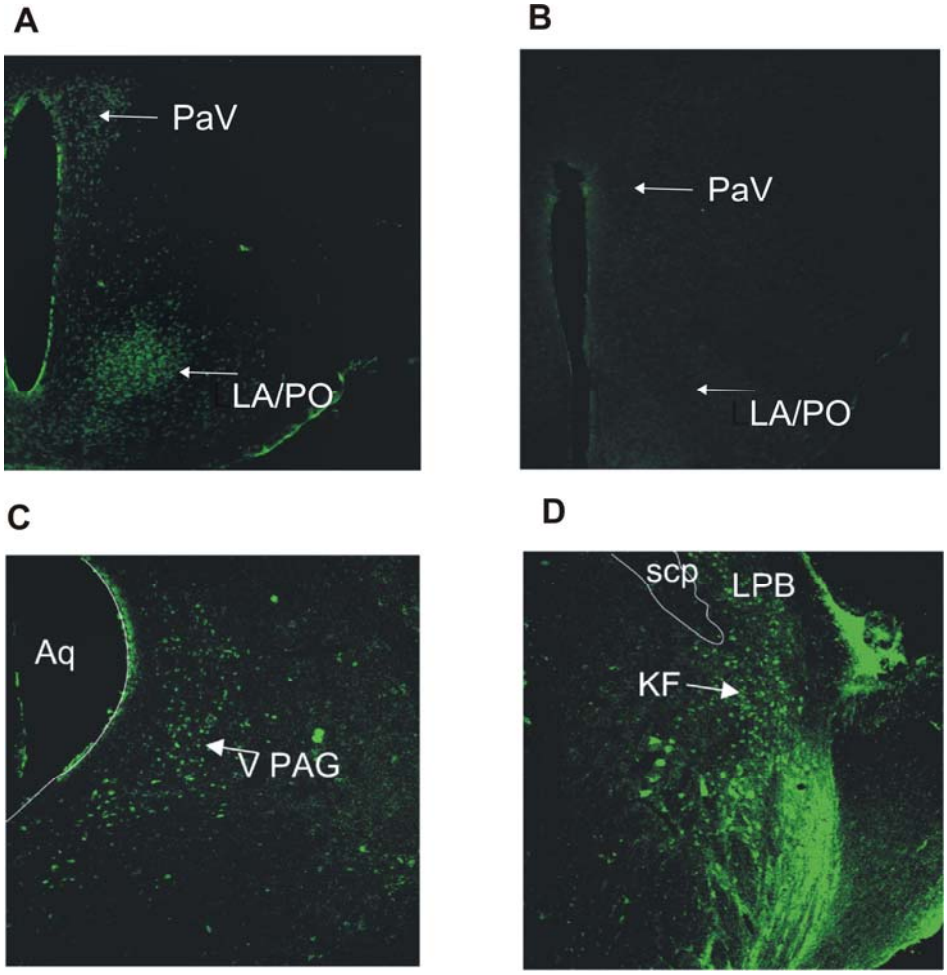

Fig. 8. Confocal scanning images of mouse brain section labeled with anti-Insl5 antibody. INSL5-possitive neurons appear green. **(A)** Expression of INSL5 in the anterior hypothalamus/preoptic area (LAH/PO) and paraventricular hypothalamus (PaV) in WT mice. **(B)** In *Insl5*$^{-/-}$ mice no expression of INSL5 in the hypothalamus/preoptic area and paraventricular hypothalamus was observed. **(C)** Expression of INSL5 in the ventral nuclei of the periaqueductal gray (vPAG) in WT mice. **(D)** Expression of INSL5 in the pontine Kölliker-Fuse nucleus (KF) and lateral parabarachial nuclei (LPB) in WT mice. *Abbreviations*: Aq = aqueduct, scp = superior cerebral peduncle. Sections were photographed at 10-fold magnifications.

3.1.3. Generation and analysis of *Insl5*-deficient mice on 129/Sv inbred genetic background

To analyze the effect of disruption of *Insl5* gene on 129/Sv inbred genetic background, *Insl5*$^{-/-}$ homozygous line was generated. To establish this line, *Insl5*$^{-/-}$ homozygous mice on a C57BL/6J x 129/Sv hybrid genetic background were backcrossed with wild type mice of mouse strain 129/Sv. Heterozygous offspring in the first backcross generation (B_1) were intercrossed with 129/Sv mice to give the second backcross generation (B_2). This breeding strategy was pursued till generation B7. Then, heterozygous mice in the seventh backcross

generation were intercrossed to give *Insl5*$^{-/-}$ mice, which genome contains 99.1% of 129/Sv genetic background.

Genotyping of progeny for *Insl5* was performed by PCR assay (2.2.7.2). A 300-bp fragment of the wild type allele was amplified with primer pair Insl5-F8/Insl5-R9, whereas the primer pair I5KO-F1/PGK3 amplified a 220-bp fragment of the mutant allele (Fig. 9).

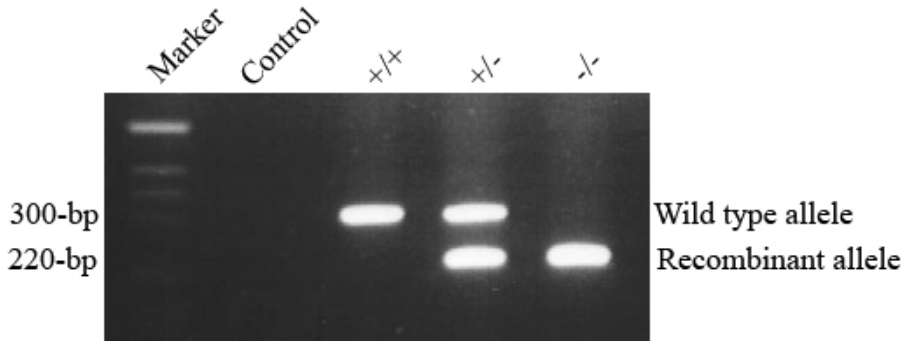

Fig. 9. Genotyping results of *Insl5* knock-out animals. Genomic DNA was extracted from mouse tails. PCR was performed using primers Insl5-F8 and Insl5-R9, which detect the wild type allele, and I5KO-F1 and PGK3 amplify the recombinant allele. In wild type animals (+/+) a 300-bp product was obtained, in homozygous (-/-) animals only a 220-bp product was detected, while both products were visible when DNA from heterozygous mice was used (+/-). The PCR products were electrophoresed on 1.5% agarose gel and stained with EtBr. Control: negative control (no-template probe).

3.1.3.1. Phenotypic analysis of *Insl5*$^{-/-}$ mice on 129/Sv inbred genetic background

Heterozygous F_1 mice (129/Sv inbred genetic background) were intercrossed to obtain F_2 generation. PCR analyses showed a distribution of 21.4% *Insl5*$^{+/+}$, 53.4% *Insl5*$^{+/-}$, and 25.2% *Insl5*$^{-/-}$ mice within 103 offspring analyzed. The ratio of three genotypes in F_2 generation was consistent with Mendelian transmission, indicating that INSL5 is not essential for embryonic development.

3.1.3.1.1. Analysis of fertility of *Insl5*-deficient mice

3.1.3.1.1.1. Fertility test experiments

To establish the *Insl5*$^{-/-}$ homozygous line on a 129/Sv inbred genetic background, homozygous males and females were intercrossed. Seven of twelve breeding pairs were infertile during a 4-month mating period, while the remaining five pairs gave only one or two

litters with reduced litter size compared to that of their wild type littermates (2.1±1.0 versus 5.9±2.4). Therefore, the fertility of homozygous mutant mice of both sexes was more accurately monitored using the following protocol.

In mating test, 15 sexually mature homozygous mutant males and 15 sexually mature homozygous mutant females were bred with wild type mice of mouse strain CD-1. During the 2-month mating period, females were checked for the presence of vaginal plugs and pregnancy. The number and size of litters sired by each group of males and females were determined. The control for *Insl5*$^{-/-}$ males in mating test was wild type cross between 5 males of mouse strain 129/Sv and 5 females of mouse strain CD-1, while wild type cross between 5 females of mouse strain 129/Sv and 5 males of mouse strain CD-1 was the control in mating test for *Insl5*$^{-/-}$ females.

As summarized in Table 2, fertility of both male and female *Insl5*$^{-/-}$ mice showed significant differences in comparison with wild type mice, indicating that *Insl5*$^{-/-}$ mice have reduced reproductive capacity. Approximately 80% (12 of 15) of homozygous mutant males had impaired fertility. Eight of them did not produce a single litter during the 2-months mating period, while the remaining four males showed significantly reduced litter size compared to that of wild type control breeding (2.1±1.5 versus 9.6±2.5, $p< 0.05$). Only 20% of *Insl5*$^{-/-}$ males (3 of 15) appeared to be normally fertile, since the average litter size (8.5±2.7) observed was not significantly different from that observed with the wild type control intercrosses ($p> 0.05$).

The fertility of *Insl5*$^{-/-}$ females was also affected. Seven of fifteen homozygous *Insl5*-deficient females (46%) had dramatically impaired fertility. Five of them did not produce a single litter during the 2-month period, and the remaining two females showed dramatically reduced litter size compared to the control cross (2.3±1.3 versus 7.6±2.8, $p< 0.05$). The other eight *Insl5*-deficient females (53.3%) produced normal litter size compared to that observed with the control (5.8±2.1versus 7.6±2.8, > 0.05).

Our results indicate that the fertility of *Insl5*-deficient mice is heterogeneous.

Tab. 2. Fertility test analysis of wild type and *Insl5*-deficient mice on 129/Sv inbred genetic background

Genotype and group	No of matings (%)	Average litter size
Wild type males (129/Sv) [a]	5 (100%) [a]	9.6±2.5 [a]
Insl5$^{-/-}$ infertile males	8 (53.3%)	0
Insl5$^{-/-}$ subfertile males	4 (26.7%)	2.1±1.5
Insl5$^{-/-}$ fertile males	3 (20%)	8.5±2.7
Wild type females (129/Sv) [b]	5 (100%) [b]	7.6±2.8 [b]
Insl5$^{-/-}$ infertile females	5 (33.4%)	0
Insl5$^{-/-}$ subfertile females	2 (13.3%)	2.3±1.3
Insl5$^{-/-}$ fertile females	8 (53.3%)	5.8±2.1

[a], wild type breeding between male of mouse strain 129/Sv and female of mouse strain CD-1

[b], wild type breeding between female of mouse strain 129/Sv and male of mouse strain CD-1

Insl5-deficient males and females were intercrossed with wild type mice of strain CD-1

3.1.3.1.1.2. Histological analysis of *Insl5*-deficient gonads

To search for a cause of the decreased fertility of *Insl5*-deficient mice, ovaries and testes were isolated from wild type and *Insl5*$^{-/-}$ mature animals, and histological analysis was performed (2.2.20).

Testes and ovaries of *Insl5*-deficient mice were of normal size and weight. No abnormalities were noticed in their shape. Analysis of hematoxylin-eosin (H&E) stained sections revealed normal spermatogenesis in *Insl5*-deficient testis compared to that of wild type (Fig. 10). Histological analysis of ovaries from *Insl5*$^{-/-}$ mice revealed the presence of all stages of follicle development (Fig. 11). These results suggest that the impairment of male and female fertility is not due to defects in germ cell development.

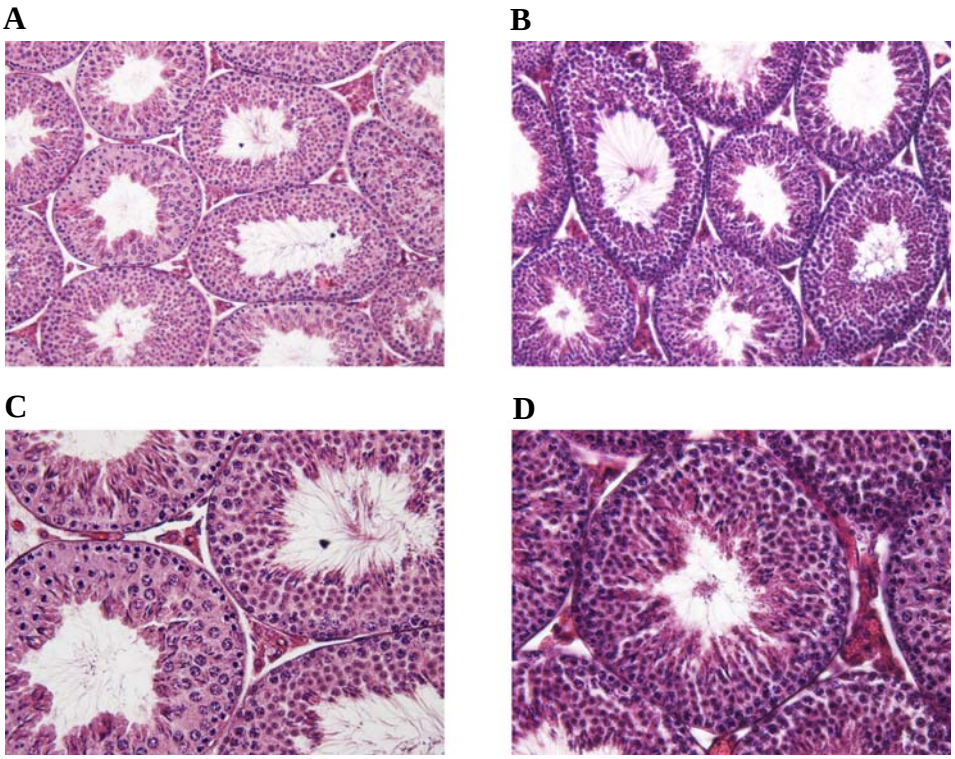

Fig. 10. Histological examination of *Insl5* knock-out and wild type testes. The testicular sections from mutant males did not show any abnormalities, as compared with wild type sections. Germ cells from all stages of spermatogenesis are present in the seminiferous tubules of *Insl5*$^{-/-}$ testes. A, C: testis sections of infertile *Insl5* mutant male; B, D: wild type control. A, B: 10-fold magnification; C, D: 20-fold magnification.

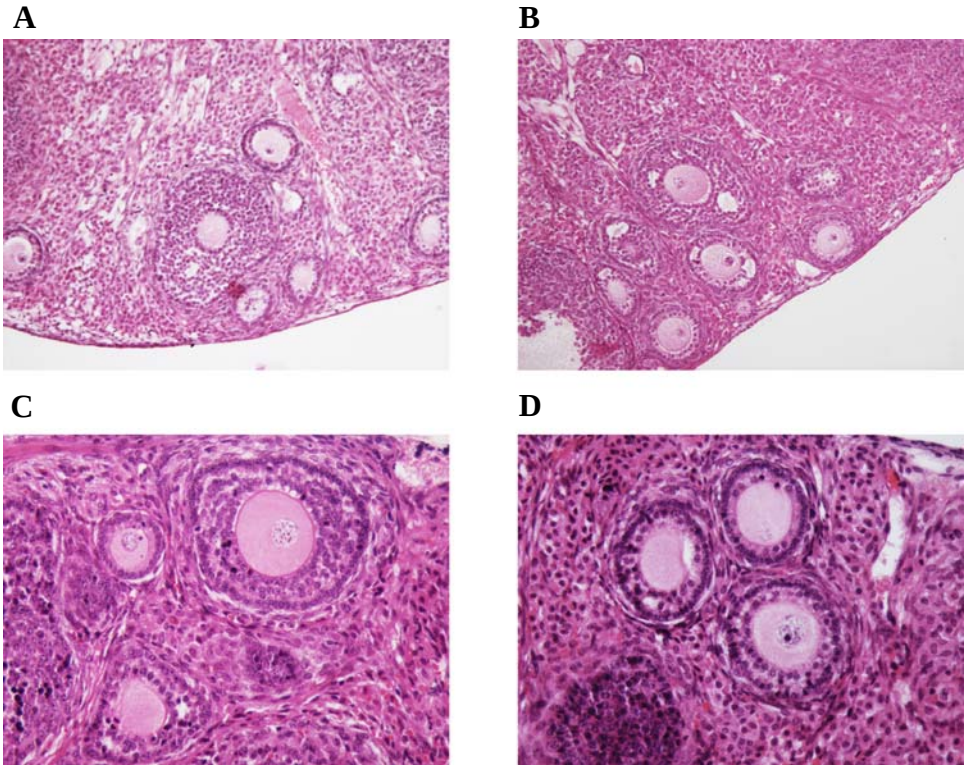

Fig. 11. Histological examination of wild type and *Insl5* knock-out ovaries. Paraffin sections from infertile mutant females (A, C) did not show obvious abnormalities, as compared with wild type (B, D) sections. A, B: 10-fold magnification; C, D: 20-fold magnification.

3.1.3.1.1.3. Determination the number of 2-cell stage embryos recovered from breeding of *Insl5*$^{-/-}$ males with impaired fertility

To further determine the cause of *Insl5*$^{-/-}$ male infertility on 129/Sv inbred genetic background, 20 eight week-old wild type females of mouse strain CD-1 were superovulated (2.2.19.3.) and mated with 5 wild type and 5 infertile mutant males, respectively. Oocytes from oviduct of females with a copulatory plug were isolated at E0.5 (2.2.19.3), cultured overnight in M16 medium and number of 2-cell stage embryos was counted (Fig. 12). As shown in Table 3, significant differences were found between wild type and knock-out males ($p< 0.05$). 328 of 442 embryos (74.2%) harvested from females inseminated by wild type males were at 2-cell stage, whereas only 4 of 419 cells (0.9%) isolated from females inseminated by *Insl5*$^{-/-}$ males were at 2-cell stage.

Tab. 3. E1.5 embryos collected from wild type females inseminated by *Insl5*$^{+/+}$ or *Insl5*$^{-/-}$ males.

Genotype of males used for insemination	Total no. of E1.5 embryos	No. of E1.5 embryos at one cell stage	No. of E1.5 embryos at two cell stage	No. of degraded cells
Insl5$^{+/+}$	442	79	328	35
Insl5$^{-/-}$	419	331	4	84

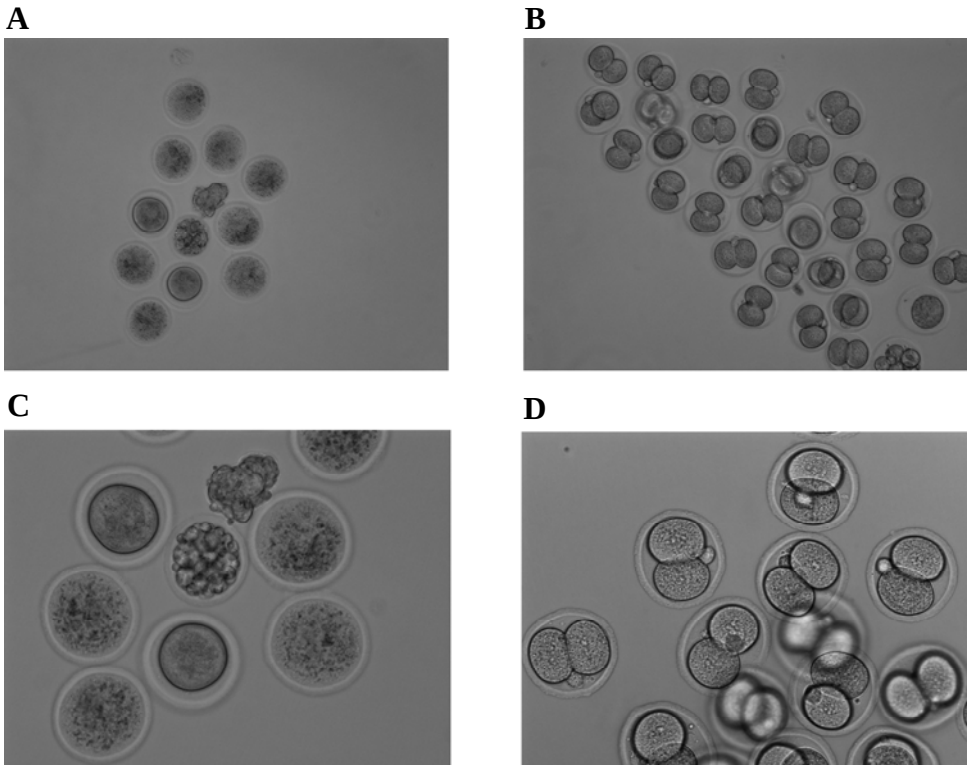

Fig. 12. Light microscope images of E1.5 embryos collected from wild type females inseminated by *Insl5*$^{-/-}$ (A, C) or *Insl5*$^{+/+}$ (B, D) males. A, B: 10-fold magnification; C, D: 20-fold magnification.

3.1.3.1.1.4. Sperm analysis of *Insl5* knock-out mice

To study the causes of *Insl5*$^{-/-}$ male infertility, different sperm parameters were analyzed (2.2.18). Sperm number was determined in the cauda epididymidis of 4 wild type and 5 infertile mutant males as well as in uteri and oviducts of wild type females inseminated by 6 infertile *Insl5*$^{-/-}$ and 6 wild type males, respectively. As shown in Table 4, no statistically significant differences ($p > 0.05$) in epididymal sperm number and sperm number in uterus were found. However, in oviducts of females mated with *Insl5*$^{-/-}$ males no sperm was observed. This result let us to suggest that the migration of *Insl5*-deficient spermatozoa through the female genital tract is disturbed. Therefore, spermatozoa from 3 wild type and 3 mutant males were isolated and their motility was measured after 1.5 hr of incubations *in vitro* (2.2.18.3). Highly significant differences ($p < 0.001$) between the motility of spermatozoa of wild type and knock-out mice were observed (Tab. 5). Proportion of motile spermatozoa of *Insl5*$^{-/-}$ mice was reduced compared with wild type (31.8±7.3% versus 61.8±6.8%) and proportion that exhibited progressive movement in sperm of *Insl5*-deficient mice was also significantly reduced compared with those of wild type mice (16.6±4.2% versus 41±5.3%) (Tab. 5). For further investigation of sperm motility, the following parameters were evaluated: curvilinear velocity (VCL), average path velocity (VAP), straight line velocity (VSL), beat cross frequency (BCF), straightness (STR) and lateral head displacement (ALH) (Fig. 13). Mann-Whitney U-Test was done and statistically significant differences were observed for VCL, VAP, VSL, and ALH ($p < 0.05$) (Fig. 13).

Tab. 4. Sperm analysis of the *Insl5*$^{+/+}$ and Insl5$^{-/-}$ mice on 129/Sv inbred genetic background.

Genotype of mice	No. of sperm in:		Oviduct	Percentage of abnormal spermatozoa	Percentage of acrosome reacted spermatozoa
	Cauda epididymidis (10^7)	Uterus (10^6)			
Insl5$^{+/+}$	1.4±0.4	2.9±1.5	724±186.8	3.6±2.5	95.2±3.4
Insl5$^{-/-}$	0.9±0.2	2.8±1.5	0*	4.5±1.8	74.1±3.1*

Data for sperm analysis represent the means±SD for the numbers of individual measurements.

*, value in *Insl5*$^{-/-}$ mice is significantly different from that in *Insl5*$^{+/+}$ mice ($p < 0.05$ by Student's *t* test).

Tab. 5. Motility analysis of sperm from *Insl5*-deficient males on 129/Sv genetic background. Highly significant differences (p> 0.001) in motility and progressive movement between mutant and wild type mice were observed**.**

Genotype of mice	Percentage of motile spermatozoa	Percentage of spermatozoa with progressive movement
Insl5$^{+/+}$	61.8±6.8	41±5.3
Insl5$^{-/-}$	31.8±7.3*	16.6±4.2*

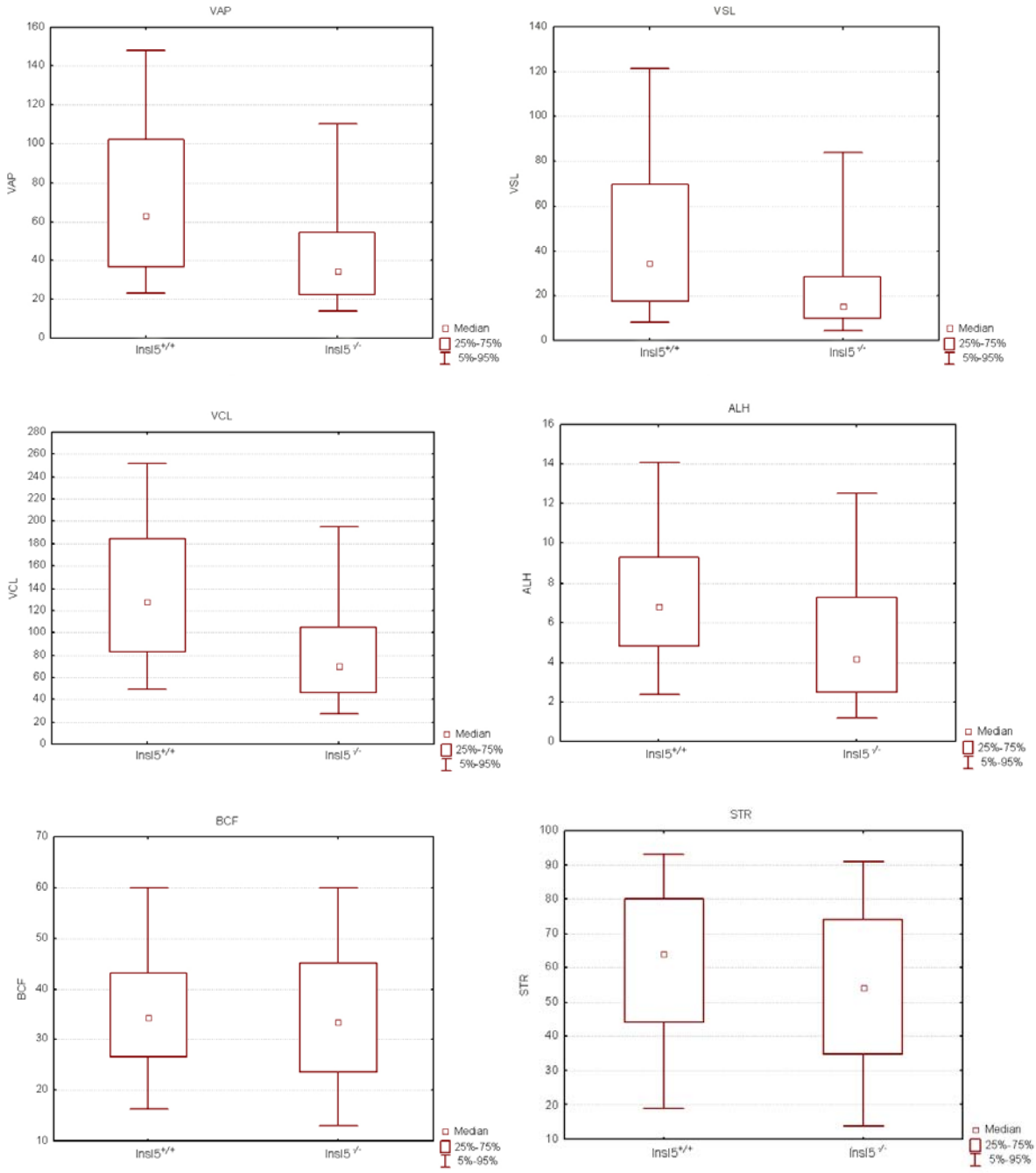

Fig. 13. Computer-assisted analysis of sperm motility. The results of analyses of wild type and *Insl5*$^{-/-}$ spermatozoa on 129/Sv inbred background are shown. Sperm velocities (micrometers/second), forward movement (percent), lateral head displacement (micrometers), and beat cross frequency (hertz) were measured after 1.5hr incubation *in vitro*. For all parameters the medians and percentiles are shown. The *Insl5*-deficient

spermatozoa exhibit statistically significantly reduced velocities and lateral head displacement in comparison to wild type sperm (p<0.05 by Mann-Whitney U-Test). Middle points represent median value, boxes represent 25% -72% percentiles range and the whiskers represent 5% - 95% percentiles of the nonoutliers range. Abbreviations: VAP: Average Path Velocity; VSL: Straight Line Velocity; VCL: Curvilinear Velocity; ALH: Lateral Head Displacement; BCF: Beat Cross Frequency; STR: Straightness.

To determine whether the *Insl5*-deficient spermatozoa have structural abnormalities, light microscope analysis was performed (2.2.18.2). No abnormalities were observed in sperm head shape in *Insl5* infertile mutants as compared to wild type controls (Tab. 4).

To address the question whether the fertility of *Insl5*$^{-/-}$ mice might be influenced by defect in acrosome reaction, we examined the response of spermatozoa from infertile mutant and wild type mice to the calcium ionophore A23187 (2.2.18.4) (Fig. 14). As shown in Table 4, percentage of acrosome reacted spermatozoa of *Insl5*$^{-/-}$ mice was significantly reduced compared to wild type controls (74.1±3.1% versus 95.2±3.4%, p< 0.05).

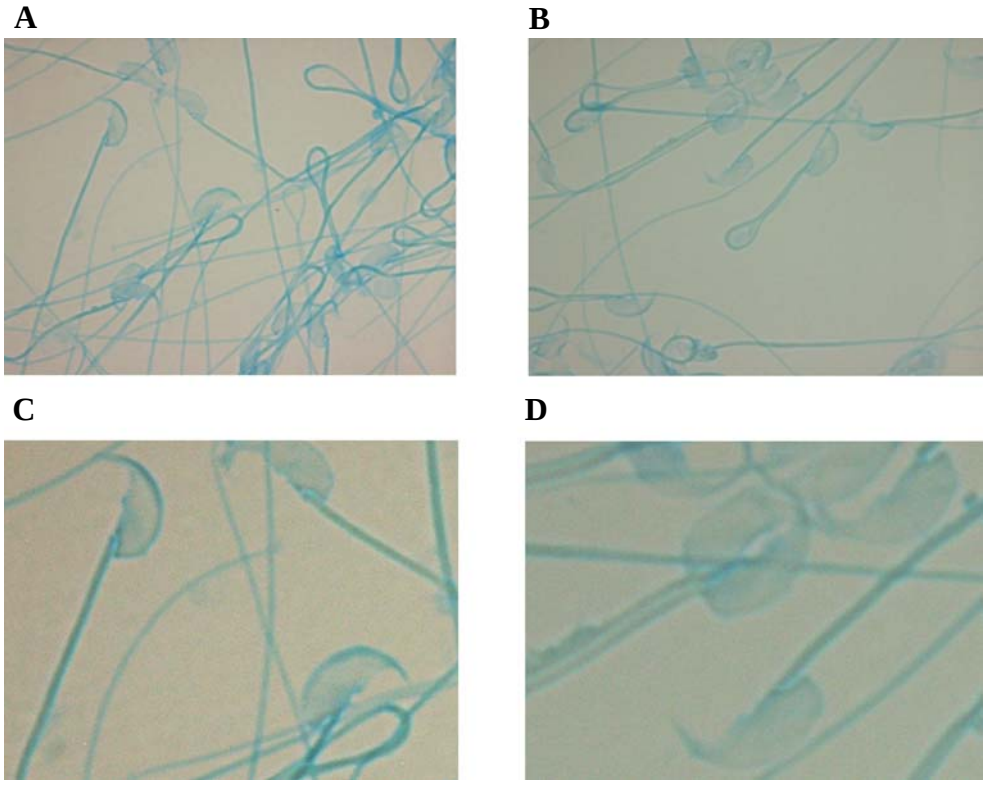

Fig. 14. Examination the response of spermatozoa from *Insl5*$^{-/-}$ (A, C) and wild type (B, D) mice to the calcium ionophore A23187. Significant differences in the assay of acrosome reaction between *Insl5*$^{-/-}$ and wild type spermatozoa were found (p< 0.05). A, B: 10-fold magnification; C, D: 20-fold magnification.

3.1.3.1.1.5. Ovulation studies of *Insl5*-deficient mice

To further analyse the reproductive defect in infertile *Insl5*$^{-/-}$ females on the 129/Sv inbred background, the number of oocytes, which were collected from superovulated and not superovulated wild type and *Insl5*-deficient females, were calculated. No significant differences ($p > 0.05$) between mice of both groups were observed (Tab. 6).

Tab. 6. Number of oocytes collected from superovulated and not superovulated females.

Genotype of mice	No. of oocytes collected from:	
	Superovulated mice	Not superovulated mice
Insl5$^{+/+}$	55.7±3.8	6.8±2.1
Insl5$^{-/-}$	51.7±20.8	3.2±2.2

To verify whether *Insl5*-deficient females have normal sexual behaviour, five 3-month old *Insl5*$^{-/-}$ and *Insl5*$^{+/+}$ females were mated with sterile *Insl3* mutant males during a 5-week period. The presence of vaginal plug was checked and noticed every day. One of five homozygous mutant females did not mate during the 5-week period, whereas the remaining four *Insl5*$^{-/-}$ females mated irregularly. In contrast, *Insl5*$^{+/+}$ females mated every 10 days (Fig. 15).

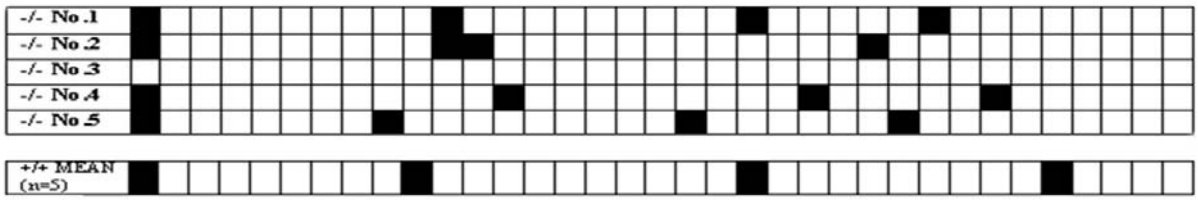

Fig. 15. Seminal vaginal plug frequency in *Insl5*$^{-/-}$ and *Insl5*$^{+/+}$ animals. *Insl5*$^{-/-}$ females mated individually to sterile *Insl3* mutant males were checked daily for seminal vaginal plug, indicated by a filled box corresponding to the day on which the plug was found. Five irregular vaginal plug patterns for *Insl5*$^{-/-}$ mice were found (lines 1 to 5). Mean data representative of the pattern obtained from the mating of five *Insl5*$^{+/+}$ females to sterile males are shown below.

The irregular mating pattern of mutant females (Fig. 15) can indicate an alteration of oestrous cycle. Therefore, to determine whether *Insl5* knock-out females present normal oestrous cycle, monitoring of vaginal cytology was performed with five 4-month old wild type and knock-out females (2.2.19.1). *Insl5*-deficient mice exhibited altered oestrous cycle as compared with wild type controls. In one of five knock-out females estrus stage was not

detected during a 5-week period while in the remaining four homozygous mutant females, estrus phase was found irregularly. In contrast, *Insl5*$^{+/+}$ female mice had estrus phase every 4 days (Fig. 16).

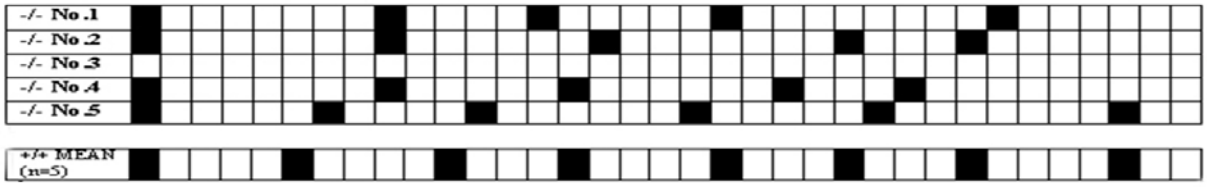

Fig. 16. Estrus stage frequency in female ovulation cycle of *Insl5*$^{-/-}$ and *Insl5*$^{+/+}$ mice determined by vaginal smear. Black squares demonstrate the day on which estrus was found.

3.1.3.1.2. Glucose homeostasis in *Insl5*-deficient mice

During breeding of *Insl5*-deficient mice on 129/Sv inbred genetic background, we found in the three cages with *Insl5*$^{-/-}$ mice an increased amount of urine, which may be due to diabetes. Measurement of fasted blood glucose level from these three animals revealed increased glucose level, which was more than 500 mg/dL. Therefore, the blood glucose level and body weight were measured from 1-, 3-, 6-, 9-, and 12-month old fasted wild type and *Insl5*-deficient mice (six to eight mice per group). No significant difference was observed in fasted blood glucose concentration in 1-month old *Insl5*$^{-/-}$ mice compared to control mice. However, at 3 months of age, the blood glucose level of *Insl5*-deficient mice in the fasted state was significantly higher than in control mice (117.6±14.94 versus 84.16±5.74, $p< 0.05$). This difference increased after 6, 9, and 12 months of age (Fig. 17A). In contrast, no significant differences in body weight were observed between mutant and wild type animals at different postnatal stages (Fig. 17B).

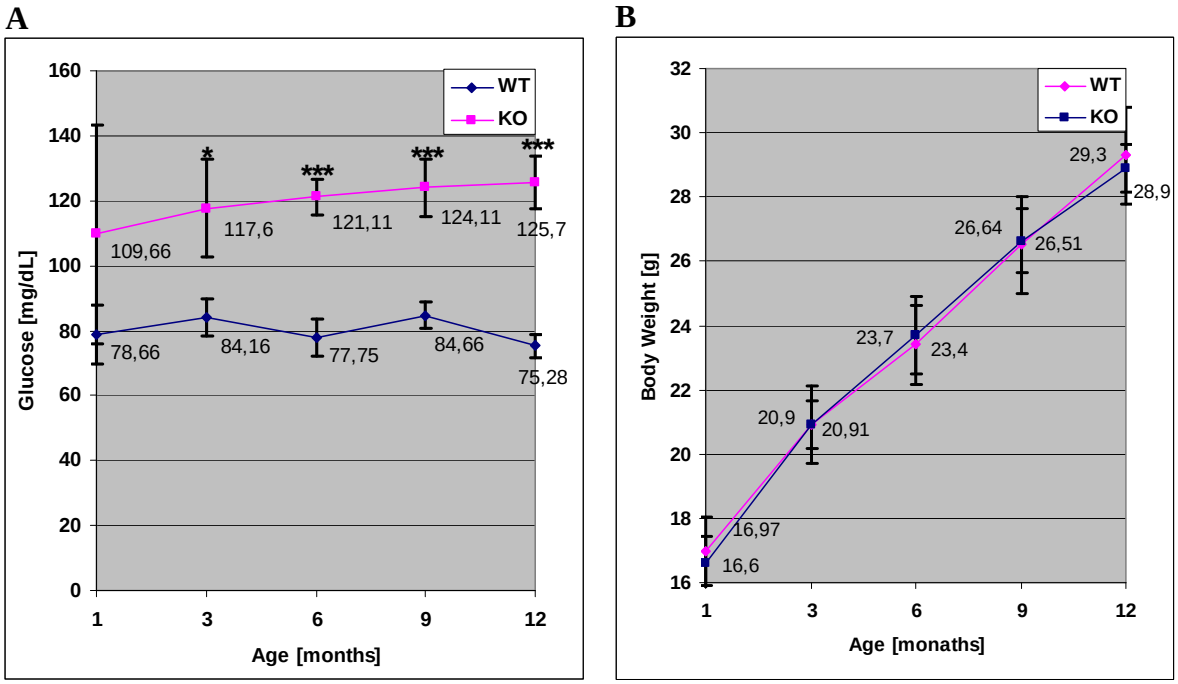

Fig. 17. Fasted blood glucose concentration (A) and body weight curves (B) for wild type and *Insl5*-deficient mice at the indicated ages. Graphs show mean±SD from at least six *Insl5*$^{+/+}$ and I*nsl5*$^{-/-}$ mice in each age. WT, wild type mice; KO, *Insl5*-deficient mice; *, $p< 0.05$; ***, $p< 0.001$.

The ability of *Insl5* knock-out mice to handle a glucose load was assessed by intraperitoneal glucose tolerance test (IPGTT). It was performed on 1-, 3-, 6-, 9-, and 12-month old *Insl5*-deficient and wild type mice (six to eight mice per group) (2.2.22), which were fasted for 12 hrs. The glucose concentration in tail blood was measured immediately before glucose injection (defined as time zero) and at 20, 40, 60, 90, and 120 min after injection (Fig. 18).

A trend toward glucose intolerance was found in *Insl5*-deficient mice at all ages. However, in younger *Insl5*$^{-/-}$ animals (1- and 3-month old) significantly higher blood glucose levels, compared with wild type animals, were noticed only at 20 and 120 min after glucose injection (Fig. 18A and B, respectively). Whereas, in older *Insl5* mutant mice (6-, 9- and 12- month old) blood glucose levels were significantly higher, compared with wild type mice, at 20 min after an intraperitoneal glucose injection and remained significantly higher at the all tested time-points during IPGTT (Fig. 17C, D, and E, respectively). These results suggest that older *Insl5* mutant mice are less able to metabolize glucose from the bloodstream than younger *Insl5*$^{-/-}$ mice and that progressive impairment of glucose tolerance in *Insl5*-deficient mice is an age-dependent.

A

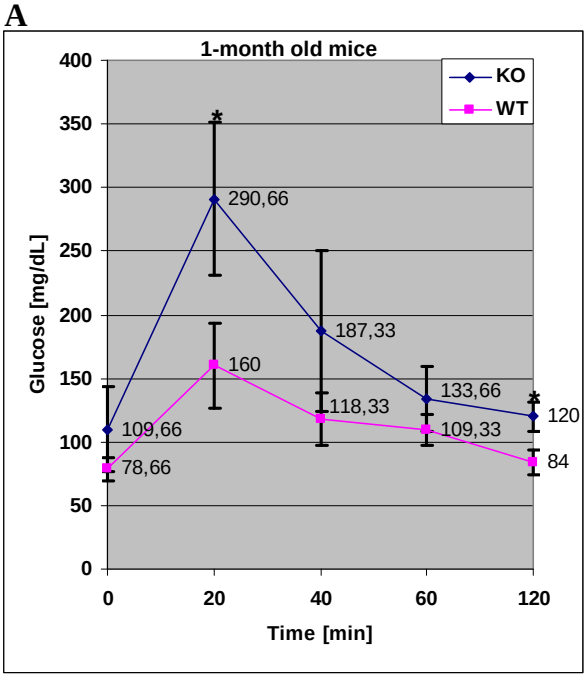
1-month old mice
KO
WT
Glucose [mg/dL]
Time [min]
290,66
187,33
133,66
120
109,66
160
118,33
109,33
84
78,66

B

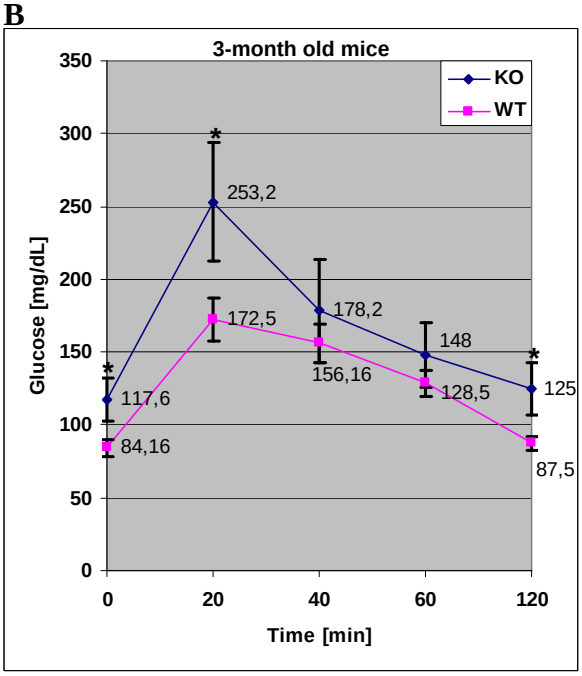
3-month old mice
KO
WT
Glucose [mg/dL]
Time [min]
253,2
178,2
148
125
117,6
172,5
156,16
128,5
87,5
84,16

C

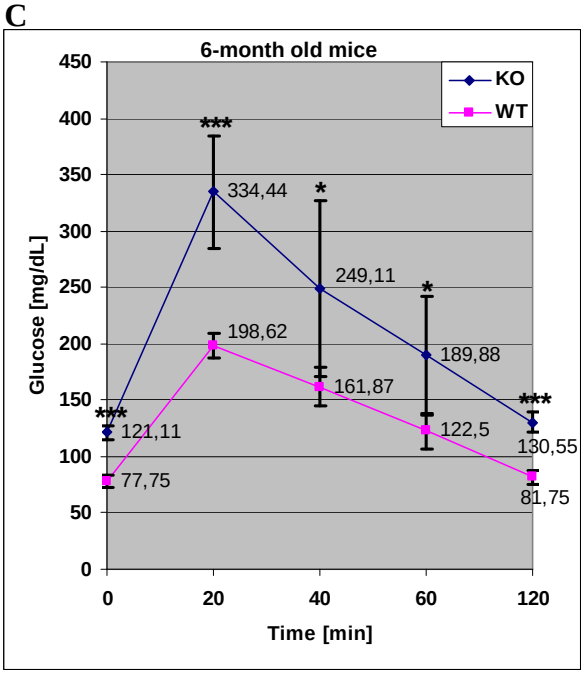
6-month old mice
KO
WT
Glucose [mg/dL]
Time [min]
334,44
249,11
189,88
130,55
121,11
198,62
161,87
122,5
81,75
77,75

D

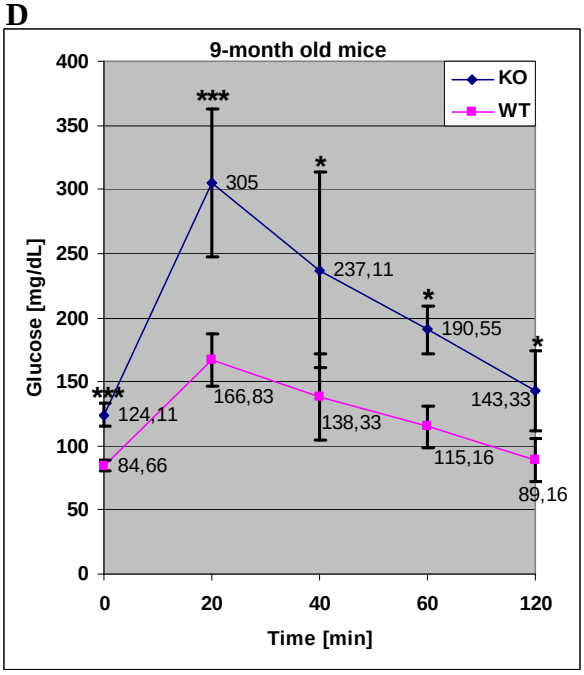
9-month old mice
KO
WT
Glucose [mg/dL]
Time [min]
305
237,11
190,55
143,33
124,11
166,83
138,33
115,16
89,16
84,66

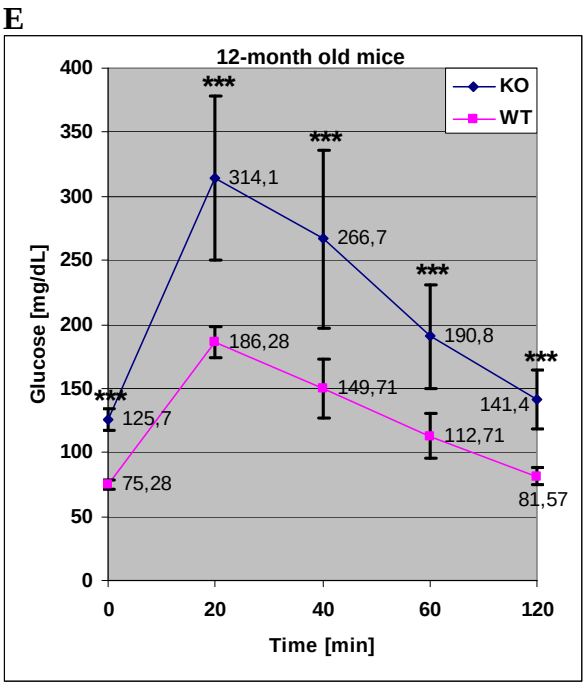

Fig. 18. Intraperitoneal glucose tolerance tests, results at one (A), three (B), six (C), nine (D) and twelve (E) months of age in *Insl5*-deficient and wild type mice. Values are means±SD; n=6 to 8 mice per group in each age; WT, wild type mice; KO, *Insl5*-deficient mice; *, $p< 0.05$; ***, $p< 0.001$.

To determine whether impairment of glucose homeostasis in *Insl5*-deficient mice is associated with lower insulin level or systemic resistance to insulin, we have done insulin tolerance tests (ITT) on 3- and 9-month old wild type and *Insl5* knock-out mice (six to eight mice per group) (2.2.22). Animals were intraperitoneally injected with insulin and blood glucose levels were measured immediately before insulin injection (defined as time zero) and at 15, 30, 45, 60, 90 and 120 min after injection (Fig. 19).

During insulin tolerance test, *Insl5*$^{-/-}$ mice showed normal response to insulin injection compared to control mice. In both genotypes of 3- and 9-month old mice were observed decreases in plasma glucose concentration at 15, 30, 45, and 60 min after intraperitoneal administration of insulin (Fig. 19). Admittedly, blood glucose concentration in 3- and 9-month old *Insl5*-deficient mice was still significantly higher at the all tested time points compared with control mice, but trend toward decrease of blood glucose level in *Insl5* mutant mice was similar to that observed in wild type animals (Fig. 19A and B, respectively). These observations suggest that sensitivity to insulin is not altered in *Insl5*-deficient mice, which in turn suggests that the higher glucose levels observed in IPGTT might reflect reduced insulin secretion in *Insl5* knock-out mice.

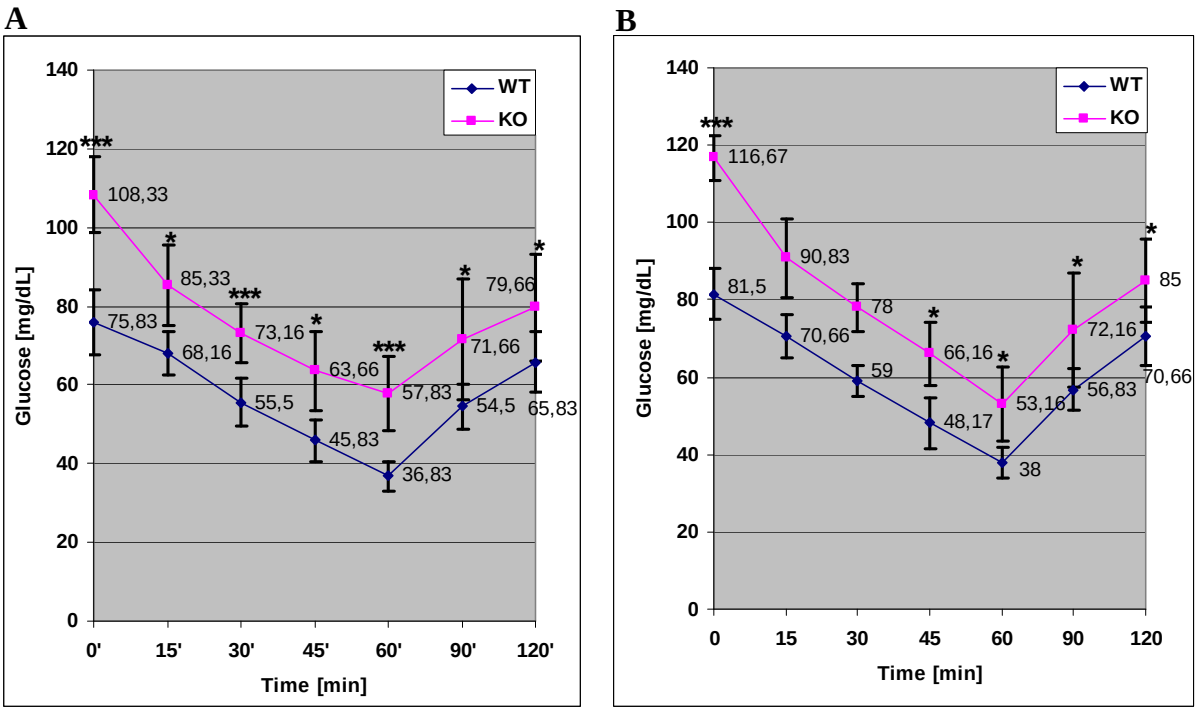

Fig 19. Intraperitoneal insulin tolerance tests, results at 3 (A) and 9 (B) months of age in *Insl5*$^{+/+}$ and *Insl5*$^{-/-}$ mice. Values represent mean±SD; n= 6 to 8 mice per group; WT, wild type mice; KO, *Insl5*-deficient mice; *, $p< 0.05$; ***, $p< 0.001$.

Impairment of glucose homeostasis is often associated with alterations in organization and morphology of pancreatic islets of Langerhans. Therefore, to determine whether these parameters are affected in *Insl5*-deficient mice, we examined the histology and number of pancreatic islets in three serial pancreatic sections from 9-month old *Insl5*$^{+/+}$ and *Insl5*$^{-/-}$ mice (4 animals per group). Furthermore, area of at least 15 randomly chosen islets from each section was measured to estimate mean area of pancreatic islets (Fig. 20 and 21).

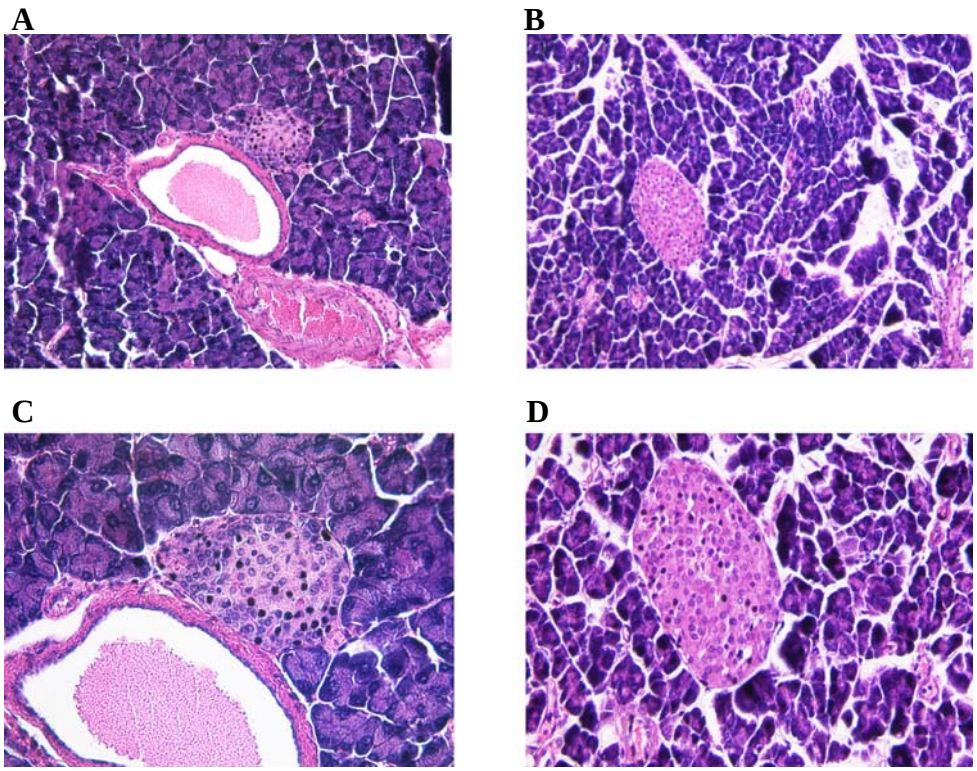

Fig. 20. Histological analysis of pancreatic islets of *Insl5*-deficient mice. Representative histological sections were obtained from 9-month old *Insl5*$^{-/-}$ (A, C) and *Insl5*$^{+/+}$ (B, D) mice and stained with hematoxylin-eosin. A, B, 10-fold magnifications; C, D, 20-fold magnifications.

No significant alterations in pancreatic islet morphology of *Insl5*$^{-/-}$ mice were observed compared to wild type animals (Fig. 20). However, mean islets area in *Insl5*-deficient mice was 1.6-fold smaller than in wild type controls (85.8±49.3 versus 141.9±64.3). Moreover, significant differences ($p< 0.05$) in number of islets in *Insl5*$^{-/-}$ mice compared to that in control mice were noticed (49.2±20.1 versus 112.8±14.4, Fig. 20 and 21).

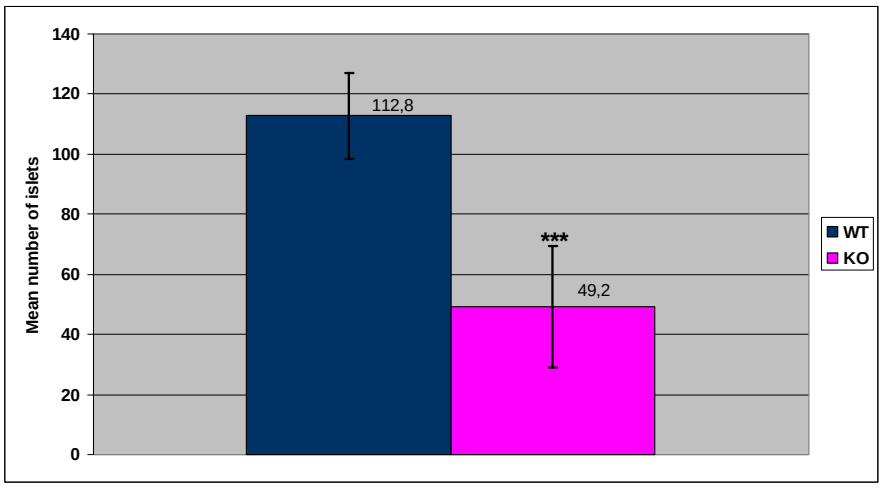

Fig. 21. Reduction in the number of pancreatic islets in *Insl5*-deficient mice. In *Insl5*$^{-/-}$ mice (KO) nearly 1.3-fold less pancreatic islets was observed compared with wild type controls (WT). Graph shown means±SD from at least four 9-month old mice of each genotype. ***, $p< 0.001$.

To estimate alterations in islets organization and number of α- and β-cells in pancreas of *Insl5*-deficient mice, double immunofluorescence staining was performed (2.2.20). Sections from 9-month old *Insl5*$^{+/+}$ and *Insl5*$^{-/-}$ mice (3 animals per genotype) were stained with anti-glucagon (green signal) and anti-insulin (red signal) antibodies, which are markers for α- and β-cells, respectively. Number and percentage of glucagon-positive and insulin-positive cells were calculated from the total number of stained cells from at least 10 islets from each three mice of each genotype (Fig. 22 and Tab. 7).

Double immunostaining revealed the presence of insulin-producing cells in pancreas of *Insl5*$^{-/-}$ mice. However, the number of insulin-positive β-cells was decreased in the islets of *Insl5*$^{-/-}$ mice compared with wild type controls, and the proportion of α-cells to β-cells, seem to be affected by *Insl5* deficiency (Fig. 22 and Tab. 7).

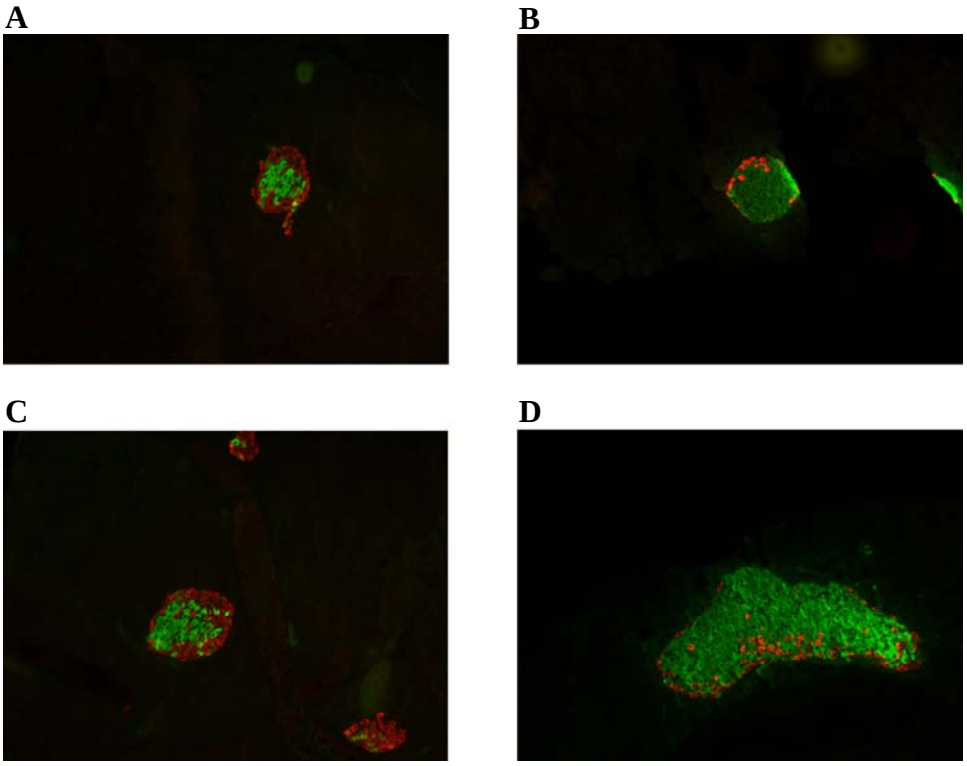

Fig. 22. Endocrine area in pancreas of *Insl5*-deficient mice. Representative sections were obtained from 9-month old *Insl5*$^{-/-}$ (A, C) and *Insl5*$^{+/+}$ (B, D) mice and double stained with anti-insulin (green) and anti-glucagon (red) antibodies. Sections were photographed at 10-fold magnifications.

Tab. 7. Percentage of insulin-positive cells and glucagon-positive cells in wild type and *Insl5*-deficient mice.

Genotype of mice	Percentage of glucagon-positive cells	Percentage of insulin-positive cells	Total no. of stained cells	No. of glucagon-positive cells	No. of insulin-positive cells
Insl5$^{+/+}$	39	62	3343	1303	2044
Insl5$^{-/-}$	58	42	2239	1296	943

Number of glucagon-positive cells and insulin-positive cells were counted in islet sections stained with anti-glucagon and anit-insulin antibodies, which are markers for α- and β-cells, respectively. Percentage of glucagon-positive or insulin-positive cells was calculated from the total number of stained cells. Cells from at least 10 islets from each of three mice of each genotype were counted.

3.2. Functional characterization of *Insl6* gene using mouse as a model system

3.2.1. Transcriptional analysis of mouse *Insl6* gene

To study the expression pattern of mouse *Insl6* gene, Northern and RT-PCR analysis were performed with total RNA samples isolated from different mouse tissues, ES cells, prenatal developmental stages (E8.5 to E14.5), testes of mouse at different postnatal developmental stages and testes of mutants with spermatogenesis defects at different stages of germ cell development (2.2.1.3). Northern blots were hybridized with a ^{32}P-labelled 577-bp *Insl6* cDNA probe, which was generated by Dr Shirneshan (Shirneshan 2005), and RT-PCRs were performed using Insl6_F2cDNA and Insl6_R1cDNA primers amplifying 577-bp fragment of *Insl6* gene. In order to exclude genomic contamination, our primers for RT-PCR were located in two different exons (exon 1 and 2). RNA quality and integrity was checked using a *β-actin* cDNA probe for rehybridization of Northern blots (Fig. 23A-C) or using HPRT primers for RT-PCR (Fig. 23D, E).

A Northern blot analysis revealed that *Insl6* was expressed only in testis; no expression in others adult tissues and in embryos at 10.5 to E14.5 *dpc* was detected (Fig. 23A and data not shown, respectively). However, *Insl6* transcript could be detected by RT-PCR assay in male and female embryos at different developmental stages (embryonic day E8.5 to E14.5) and in all analyzed postnatal tissues (Fig. 23B, C). These results demonstrated that *Insl6* is expressed in all of the investigated organs and prenatal developmental stages, but at low level, which is not detectable by Northern blot. Only in the testis expression of *Insl6* is strong enough to be detected by Northern blot hybridization.

Evaluation of *Insl6* expression during testis development revealed that *Insl6* transcript could be detected first at day 15 of postnatal development. Thereafter, an increased level of *Insl6* expression was observed (Fig. 23B). Moreover, *Insl6* transcript was present in the cryptorchid testes of *Insl3*$^{-/-}$ mutant mice, in which spermatogenesis is arrested at the stage of pachytene spermatocytes (Zimmermann *et al.,* 1999), and in testes of *olt/olt* and *qk/qk* mutant mice, in which spermatogenesis is arrested at the spermatid stage (Bennett *et al.,* 1971; Moutier, 1976). Whereas, no transcript could be detected in the testes of *W/W*^{v} mutant mice, which lack germ cells (de Rooij and Boer, 2003), and in testes of *Tfm/Y* mutant mice, in which the spermatogenesis is arrested at the primary spermatocyte stage (Lyon and Hawkes, 1970) (Fig.

23C). These results clearly demonstrated that the expression of *Insl6* gene in the testis is restricted to germ cells and starts at the pachytene spermatocyte.

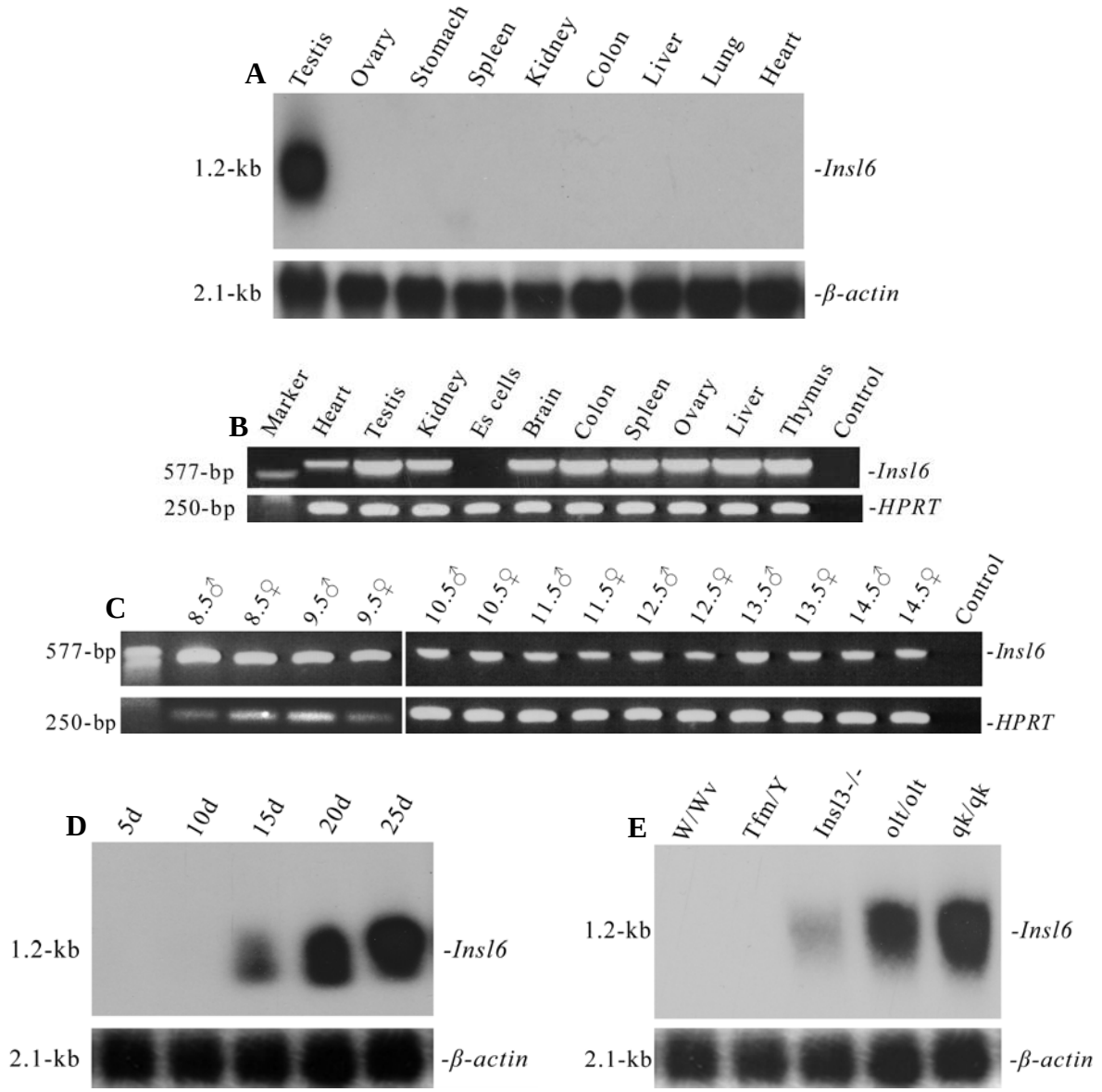

Fig. 23. Expression analysis of mouse *Insl6* gene. Northern blot expression analysis of *Insl6* gene in different tissues of adult mice (A), in postnatal developmental stages of mouse testis (D) and in testes of mutants with spermatogenesis arrests at different stages of germ cell development (E). Total RNA was hybridized with the mouse *Insl6* cDNA fragment and rehybridized with mouse *β-actin*, as a RNA quality control. RT-PCR expression analysis of *Insl6* in different mouse tissues (B) and prenatal developmental stages (C) was carried out using *Insl6* specific primers: Insl6_F2cDNA and Insl6_R1cDNA. RT-PCR for HPRT transcript was performed as positive control of RNA quality. Control: negative control (no-template cDNA).

3.2.2. Targeted inactivation of mouse *Insl6* gene

One of the best ways to elucidate gene function is analysis of an animal model deficient in the gene of interest. In this study such a model mouse has been generated by targeted inactivation of the *Insl6* gene. Phenotypic analysis would help us to understand the role of *Insl6* gene in spermatogenesis and fertilization.

3.2.2.1. Construction of the *Insl6* knock-out construct

Insl6 knock-out construct was generated by Dr. K. Shirneshan (Shirneshan, 2005). The targeting construct was designed to replace a 4.3-kb BamHI/EcoRI genomic fragment containing exon 1 by the *Neomycin* resistance gene (*neo*^{r}) under the control of the *Phosphoglycerate kinase (Pgk)* promoter (Fig. 24). The deletion of exon 1, which contains the translation initiation site ATG and the coding sequence of A-chain, is predicted to generate a null allele.

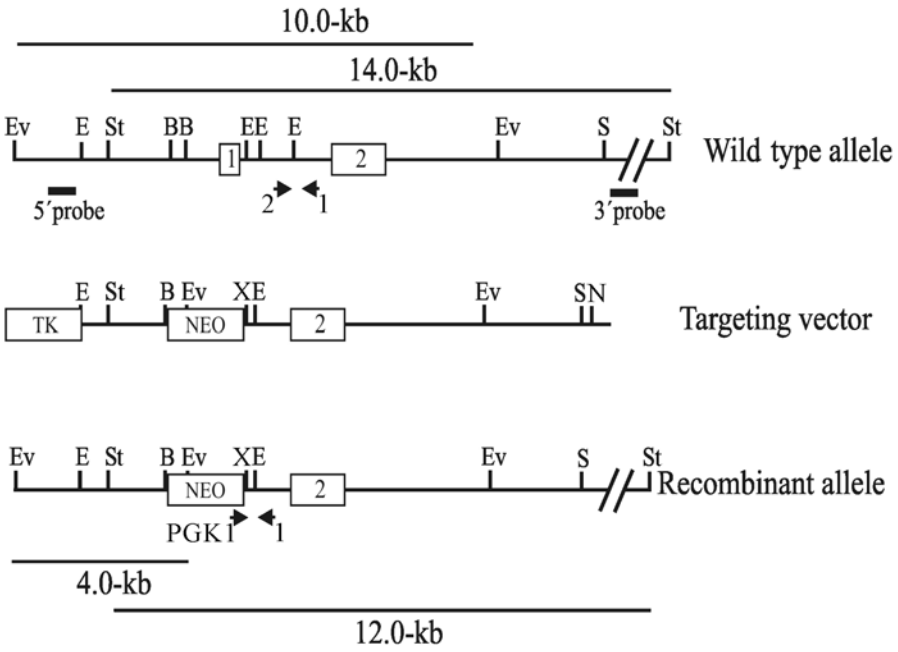

Fig. 24. Targeted disruption of the mouse *Insl6* gene. The structures of the wild type allele, targeting vector, and recombinant allele are shown together with the relevant restriction sites. The 4.3-kb Bam*HI/*Eco*RI fragment containing exon 1* of the gene *was replaced by the* pgk-neo *selection cassette (NEO).* The 5' and 3' external probes used and the predicted length of *Eco*RV and *Sst*I restriction fragments in Southern blot analysis are shown. The primers Insl6_1 (1), Insl6_2 (2), and PGK1 used to amplify the wild type and targeted allele by PCR are also indicated by arrows. Abbreviations: TK: *Thymidine kinase* cassette; E1: exon 1; E2: exon 2; B: *Bam*HI; E: *Eco*RI; Ev: *Eco*RV; N: *Not*I; S: *Spe*I; St: *Sst*I; X: *Xho*I.

3.2.2.2. Generation of a 5’ external probe

A 5’ external probe for screening of ES cells was generated to distinguish between wild type and recombinant clones. For this purpose, a 431-bp fragment located in the 5’ flanking region of the *Insl6* gene was amplified by PCR assay, using Insl6_ext5_F and Insl6_ext5_R primers and genomic DNA from 129/Sv mice as a template. The PCR product was subcloned into pGEM-T Easy vector, sequenced, and cut out with *Eco*RI restriction enzyme. Then, the 431-bp fragment was extracted from the agarose gel and used as a 5’ external probe. This external probe recognizes a 10-kb fragment in case of wild type and a 4-kb fragment in case of recombinant allele in Southern blot hybridization after digestion of genomic DNA with *EcoRV* enzyme (Fig. 24 and 25A).

3.2.2.3. Generation of a 3’external probe

A 3’ external probe for screening of ES cells was generated to distinguish between wild type and recombinant clones. For this purpose, a fragment of 652-bp downstream to *Insl6* gene was amplified by PCR, using primers Insl6_ext3_F and Insl6_ext3_R and genomic DNA from 129/Sv mice as a template. The PCR fragment was cloned in pGEM-T Easy vector, sequenced, then isolated using *Eco*RI restriction enzyme. Purified insert was used as a 3’ external probe. This external probe recognizes a 14-kb fragment in case of wild type and 12-kb in case of recombinant allele in Southern blot hybridization after digestion of genomic DNA with *Sst*I enzyme (Fig. 24 and 25B).

3.2.2.4. Electroporation and screening of RI ES cells for homologous recombination events

RI embryonic stem (ES) cells were grown in Dulbecco’s modified Eagle’s medium (2.2.16.1.2). The *Insl6* targeting vector was linearized with *Not*I enzyme and 40 μg of purified DNA was electroporated into RI embryonic stem cells, as it was described in section 2.2.16.1.3. The cells were plated on fibroblast feeder layer and after 10 days of selection around 600 drug-resistant clones were picked into 24-well plates and replicated. Genomic DNA was isolated from recombinant ES cell clones (2.2.1.2.3) and used for Southern blot hybridization (2.2.11). DNA from each clone was digested with *Eco*RV enzyme, electrophoresed and blotted onto Hybond-XL membrane (2.2.9.1). Blots were then hybridized

with radioactively labelled 5´external probe. Two bands were recognized in case of homologous recombination, 10-kb wild type allele and 4-kb recombinant allele. When no recombination has occurred or non-homologous recombination had taken place, only wild type band could be detected. After screening of all the ES cell clones, two putative recombinant clones were identified, namely Insl6-114 and Insl6-123 (Fig. 24 and 25A).

In order to confirm the successful targeting at the *Insl6* locus, DNA from putative heterozygous ES cells was digested with *Sst*I enzyme, electrophoresed and transferred onto a Hybond-XL membrane. This blot was hybridized with radioactively labelled 3´external probe, which detected two expected bands, 14-kb wild type allele and 12-kb recombinant allele (Fig. 24 and 25B). Then the blot was rehybridized with a ^{32}P-labelled *Neomycin* probe to rule out any multiple integration of targeting vector into the genome (Fig. 25C). The results of Southern blot analysis using 5' external probe, 3' external probe and *Neomycin* probe collectively confirmed the successful targeting of *Insl6* gene. Therefore, both clones, Insl6-114 and Insl6-123, were used for blastocyst injection.

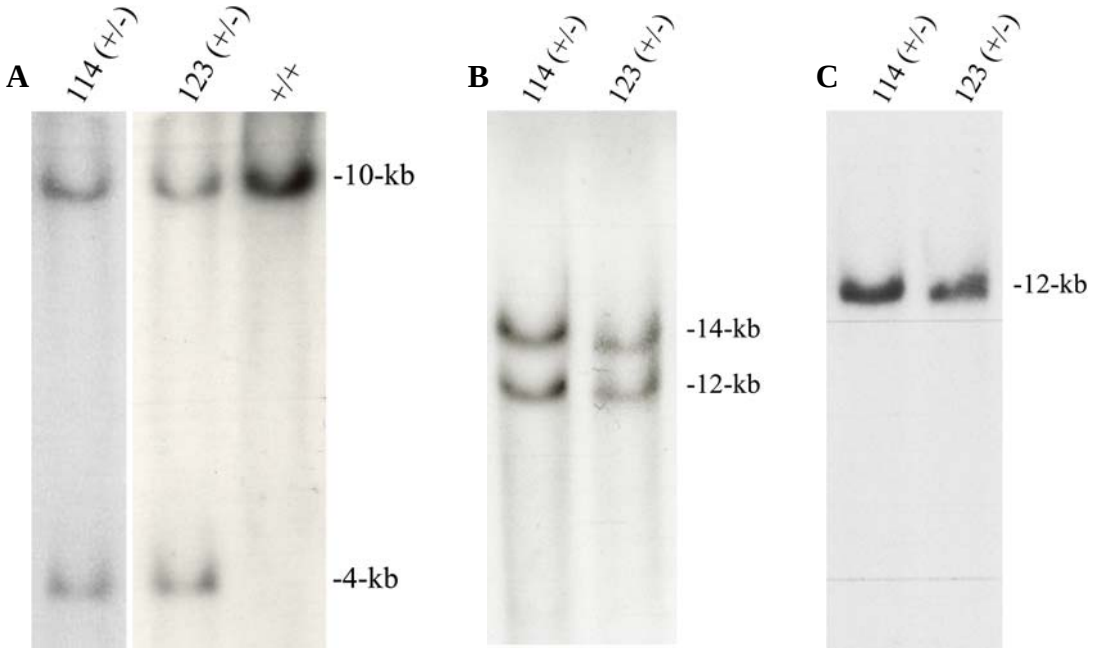

Fig. 25. Genomic Southern blot analysis for screening the ES cells. (A) Genomic DNA of ES cell clones was digested with *Eco*RV and hybridized with ^{32}P-labelled 5' external probe shown in Fig. 24. This probe detected 10-kb fragment (wild type allele) and 4-kb fragment (targeted allele). (B) Genomic DNA of Insl6-114 and Insl6-123 ES cell clones was digested with *Sst*I and hybridized with ^{32}P-labelled 3' external probe shown in Fig. 24. The external probe detected two expected bands in each clone (14-kb wild type allele and 12-kb recombinant allele). (C) The same blot was rehybridized with *Neomycin* resistance gene specific probe to prove if the construct was integrated into mouse genome by single homologous recombination. As expected for correct homologous recombination event, the probe only detected the 12-kb fragment.

3.2.2.5. Generation of chimeric mice

ES cells from two recombinant clones (Insl6-114 and Insl6-123) were injected into 3.5 dpc blastocysts derived from C57BL/6J female mice. Blastocysts were then transferred into pseudopregnant CD-1 females in order to generate chimeric mice. This work was performed in the Max Planck Institute for Experimental Medicine in Göttingen.

After three independent injections of ES cells from Insl6-114 and Insl6-123 recombinant clones, 16 male and 7 female chimeras were obtained. Their chimerism was estimated in percentage according to the coat colour: 100%, 2x 95%, 2x 90%, 70%, 25%, 2x 20%, 15%, 3x 10%, and 3x 5% for males and 55%, 40%, 2x 20%, and 3x 5% for females. Five high percentage male chimeras (100%, 2x 95%, and 2x 90%) were intercrossed with C57BL/6J and 129/Sv females in order to obtain F_1 generation on a C57BL/6J x 129/Sv hybrid background and on a 129/Sv inbred genetic background, respectively. All the five male chimeras transmitted *Insl6* recombinant allele to the germline on both backgrounds. Transmission was checked by PCR genotyping (2.2.7.2), using primers shown in Figure 24 and genomic DNA isolated from tail biopsies of mice. A 374-bp fragment of the wild type allele was amplified with primer pair Insl6_2/Insl6_1, whereas the primer pair PGK1/Insl6_1 amplified a 548-bp fragment of the mutant allele (Fig. 26).

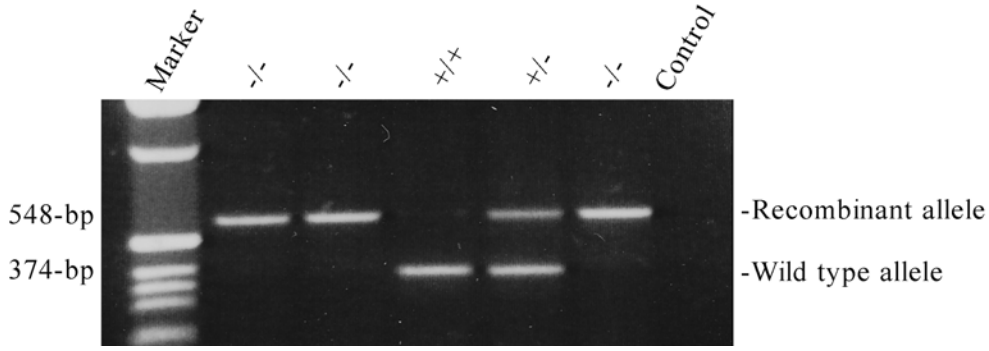

Fig. 26. PCR genotyping of progeny. Genomic DNA was extracted from mouse tails. PCR was performed using primers Insl6_2 and Insl6_1, which detect the wild type allele, and PGK1 and Insl6_1 were used for amplification of the recombinant allele. Product of 374-bp was obtained in case of wild type animal (+/+), 548-bp product was amplified in case of homozygous (-/-) animals, while both products were visible when DNA from heterozygous (+/-) mice was tested. The PCR products were electrophoresed on 1.5% agarose gel and stained with EtBr. Control: negative control (no-template probe).

3.2.3. Generation and analysis of the *Insl6*-deficient mice

F_1 animals, heterozygous for a null *Insl6* allele, were used for further crossing in order to obtain F_2 animals and establish *Insl6*$^{-/-}$ homozygous lines on both C57BL/6J x 129/Sv and 129/Sv backgrounds. F_2 animals were genotyped as described above (Fig. 26). The statistical analysis is summarized in Table 8.

In both genetic backgrounds mice heterozygous for the Insl6 mutant allele grew to adulthood, were fertile, and appeared phenotypically normal. PCR analyses (Fig. 26) showed that the ratio of the three genotypes in F_2 generation was consistent with Mendelian transmission of the two alleles. Among 186 offspring, 55 (30%) were wild type, 90 (48%) were heterozygous and 41 (22%) were homozygous mice (Tab. 8) in a C57BL/6J x 129/Sv hybrid genetic background, while in case of 129/Sv inbred background, 50 (30%) were wild type, 72 (48%) were heterozygous and 32 (22%) were homozygous mice out of 155 animals genotyped (Tab. 8). Also the sex ratio of these animals was not affected (as it was shown by χ^2 test, $p > 0.05$; Tab. 8). *Insl6*$^{-/-}$ mice were indistinguishable from their wild type littermates in appearance and gross behavior. These data demonstrate that *Insl6* is not essential for embryonic development in spite of its expression during embryogenesis (Fig. 23C).

Tab. 8. Statistical analysis of genotype distribution of *Insl6* null allele within mice from F_2 generation. χ^2 analysis clearly demonstrated that genotype distribution from +/- x +/- breedings on both backgrounds does not differ from expected Mendelian ratio ($p > 0.1$). Also no change in the sex ratio of offspring of heterozygous mice was noticed (χ^2 test, $p > 0.05$). χ^2, chi square; ♂, male; ♀, female.

Background	Total no. of progeny	No. of progeny with genotyping			Average litter size
		Insl6$^{+/+}$	*Insl6*$^{+/-}$	*Insl6*$^{-/-}$	
C57BL/6J x 129/Sv	186 104 ♂ 82 ♀	55 (30%) 28 ♂ 27 ♀	90 (48%) 54 ♂ 36 ♀	41 (22%) 22 ♂ 19 ♀	9.3±2.0
129/Sv	155 88 ♂ 67 ♀	50 (30%) 28 ♂ 22 ♀	72 (48%) 40 ♂ 32 ♀	33 (22%) 20 ♂ 13 ♀	6.9±2.1

3.2.3.1. Analysis of *Insl6* expression in knock-out mice

In wild type mice the strongest tissue-specific expression of mouse *Insl6* gene was detected in testis (Fig. 23). Therefore, to confirm that the engineered disruption of *Insl6* gene had

generated a null allele, Northern and RT-PCR analyses were performed with total RNA samples isolated from testes of mice of the three genotypes.

Insl6-cDNA probe (Shirneshan 2005) detected a strong testicular expression of *Insl6* gene in *Insl6*$^{+/+}$ mice, and weaker in *Insl6*$^{+/-}$ mice. No expression was detected in testes of *Insl6*$^{-/-}$ mice (Fig. 27A). Rehybridization with a *ß-actin* probe proved the integrity and the amount of RNA used in this experiment (Fig. 27A). RT-PCR with primers located in exons 1 and 2 confirmed the absence of *Insl6* transcript in testis of *Insl6*$^{-/-}$ mice, indicating that, due to the integration of the *Neomycin* cassette, the expression of *Insl6* gene is completely disrupted (Fig. 27B).

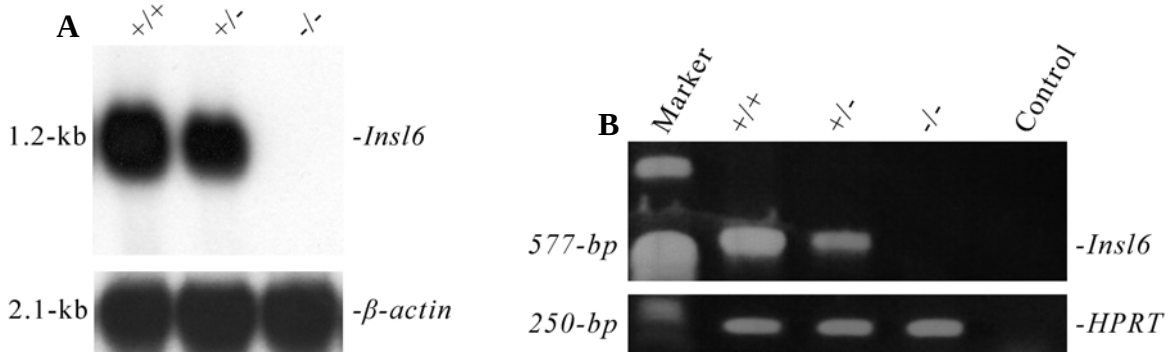

Fig. 27. Transcriptional analyses of *Insl6*-deficient mice. (A) Northern blot analysis of testicular RNA from three genotypes. Hybridization with mouse *Insl6* cDNA probe revealed a 1.2-kb specific transcript prominent in *Insl6*$^{+/+}$, reduced in *Insl6*$^{+/-}$ and absent in *Insl6*$^{-/-}$ mice. Rehybridization of the blot with *β-actin* probe confirmed integrity and amount of RNA used in this experiment. (B) RT-PCR analysis. RT-PCR using Insl6_F2cDNA and Insl6_R1cDNA primers was performed with testicular RNA from wild type (*Insl6*$^{+/+}$), heterozygous (*Insl6*$^{+/-}$) and homozygous for null allele (*Insl6*$^{-/-}$) animals. *Insl6* specific product (577-bp) was obtained from RNA of *Insl6*$^{+/+}$ and *Insl6*$^{+/-}$ animals, but no band was visible in case of *Insl6*$^{-/-}$ mice. Integrity of RNA was verified by HPRT primers amplification.

3.2.3.2. Reproductive functions of *Insl6* gene

Most studies were performed with homozygous mutants on a C57BL/6J x 129/Sv mixed genetic background.

3.2.3.2.1. Analysis of fertility of *Insl6*-deficient mice

During generation of *Insl6* knock-out line on a C57BL/6J x 129/Sv hybrid genetic background, homozygous males and females were intercrossed. Three of seven breeding pairs were infertile during a 4-month mating period, while the remaining four pairs produced

smaller litter size compared to that of their wild type littermates (3.6±1.2 versus 7.3±2.2, p<0.05). Therefore, the fertility of Insl6-null mice of both sexes was more accurately monitored by intercrossing with wild type mice of strain CD-1. The control for *Insl6*$^{-/-}$ males in mating test was wild type cross between 5 males of C57Bl/6J strain and 5 females of CD-1 strain, while wild type cross between 5 C57Bl/6J females and 5 CD-1 males was the control in mating test for *Insl6*$^{-/-}$ females. During the 3-month mating period, females were checked for the presence of vaginal plugs and pregnancy. The number and size of litters sired by each group of males and females were determined.

As summarized in Table 9, homozygous *Insl6*$^{-/-}$ females showed no reproductive defects and produced litters of approximately normal size (average litter size, 8.1±*1.7*; average wild type litter size*,* 9.4±2.0*,* p> 0.05). In contrast, approximately 57% (40 of 70 mice) *of Insl6*-null males in F_2 generation had impaired fertility. Nineteen of them did not produce a single litter during the 3-month mating period*,* while the remaining 21 *Insl6*-deficient males produced significantly reduced litter size compared to that of wild type control breeding (5.05±1.9 versus 14.1±2.1, p< 0.05). The other 30 *Insl6*-deficient males (43%) produced normal litter size compared to that observed with the control (12.1±1.7 versus 14.1±2.1, p> 0.05). These results revealed that male fertility was heterogeneous and that null mutant males fall into two classes, as follows: group I males were infertile, whereas group II males were fertile. Subfertile animals were included into the first group of males, because they became infertile during the lifetime. Therefore, we focused the subsequent experiments on infertile and fertile groups of males.

Tab. 9. Fertility test analysis of wild type and *Insl6*-deficient mice on C57BL/6J x 129/Sv hybrid background

Genotype and group	No of matings (%)	Average litter size
Wild type males (C57BL/6J) [a]	5 (100%) [a]	14.1±2.1 [a]
Insl6$^{-/-}$ infertile males	19 (27%)	0
Insl6$^{-/-}$ subfertile males	21 (30%)	5.05±1.9
Insl6$^{-/-}$ fertile males	30 (43%)	12.1±1.7
Wild type females (C57BL/6J) [b]	5 (100%) [b]	9.4±2.0 [b]
Insl6$^{-/-}$ females	10 (100%)	8.1±1.7

[a], wild type breeding between male of mouse strain C57BL/6J and female of mouse strain CD-1

[b], wild type breeding between female of mouse strain C57BL/6J and male of mouse strain CD-1

Insl6-deficient males and females were intercrossed with wild type mice of strain CD-1

3.2.3.2.2. Sperm analysis of *Insl6* knock-out mice

To study the causes of *Insl6*$^{-/-}$ male infertility, different sperm parameters were analyzed (2.2.18). Sperm number was determined in the cauda epididymidis of 4 wild type, fertile and infertile mutant males as well as in uteri and oviducts of wild type females inseminated by 2 wild type, 3 fertile *Insl6*$^{-/-}$ and 3 infertile *Insl6*$^{-/-}$ males, respectively (Tab. 10).

Tab. 10. Sperm analysis of *Insl6*$^{+/+}$ and *Insl6*$^{-/-}$ mice.

Genotype of mice	No. of sperm in:			Percentage of motile spermatozoa	Percentage of spermatozoa with progressive movement
	Cauda epididymidis (10^7)	Uterus (10^6)	Oviduct (10^2)		
Insl6$^{+/+}$	1.73±0.47 (4)	5.3±0.42 (2)	9.0±3.1 (2)	61.7±9.07 (3)	42±6.08(3)
Insl6$^{-/-}$					
fertile	0.34±0.26* (4)	2.4±1.42 (3)	3.91±3.1(3)	56.67±7.77(3)	31±8(3)
Infertile	0.06±0.03* (4)	0.49±0.34* (3)	0* (3)	24.56±11.26*(3)	12.56±7.83*(3)

Data for sperm analysis represent the means±SD for the numbers of individual measurements indicated in parentheses. *, value in *Insl6*$^{-/-}$ mice is significantly different from that in *Insl6*$^{+/+}$ mice ($p< 0.01$ by Student's *t* test).

As shown in Table 10, significant reduction ($p< 0.01$) in the mean number of spermatozoa collected from the cauda epididymides of both groups of fertile and infertile *Insl6*-deficient mice was observed. Sperm number in uteri and oviducts of females mated with fertile *Insl6* mutant males was not significantly different ($p> 0.05$) from that counted from females inseminated by age matched wild type males (Tab. 10). In contrast to that, sperm number in uteri of females inseminated by infertile *Insl6* knock-out males was decreased to about 9.2% of that in wild type controls. Moreover, in oviducts of the same females no sperm was observed (Tab.10). These results suggest that the migration of *Insl6*-deficient spermatozoa through the female genital tract might be disturbed. Therefore, spermatozoa from adult mutant (fertile and infertile) and control animals were isolated and their motility was measured using the CASA system after 1.5 h of incubations *in vitro* (2.2.18.3).

Highly significant differences ($p< 0.001$) between the motility of spermatozoa of wild type and *Insl6* knock-out mice were only observed in group of infertile *Insl6*$^{-/-}$ males (Tab. 10). Proportion of motile spermatozoa of *Insl6*$^{-/-}$ infertile mice was reduced compared with wild type (24.56±11.26% versus 61.7±9.07%) and proportion that exhibited progressive movement in sperm of infertile *Insl6*$^{-/-}$ mice was also significantly reduced compared with those of wild type mice (12.56±7.83% versus 42±6.08%), (Tab. 10). For further investigation of sperm

motility, following parameters were evaluated: curvilinear velocity (VCL), average path velocity (VAP), straight line velocity (VSL), beat cross frequency (BCF), straightness (STR) and lateral head displacement (ALH) (Fig. 25). Mann-Whitney U-Test was done and statistically significant differences ($p< 0.05$) were observed for VCL, VAP, VSL, and ALH between spermatozoa of infertile *Insl6*$^{-/-}$ and wild type males (Fig. 28).

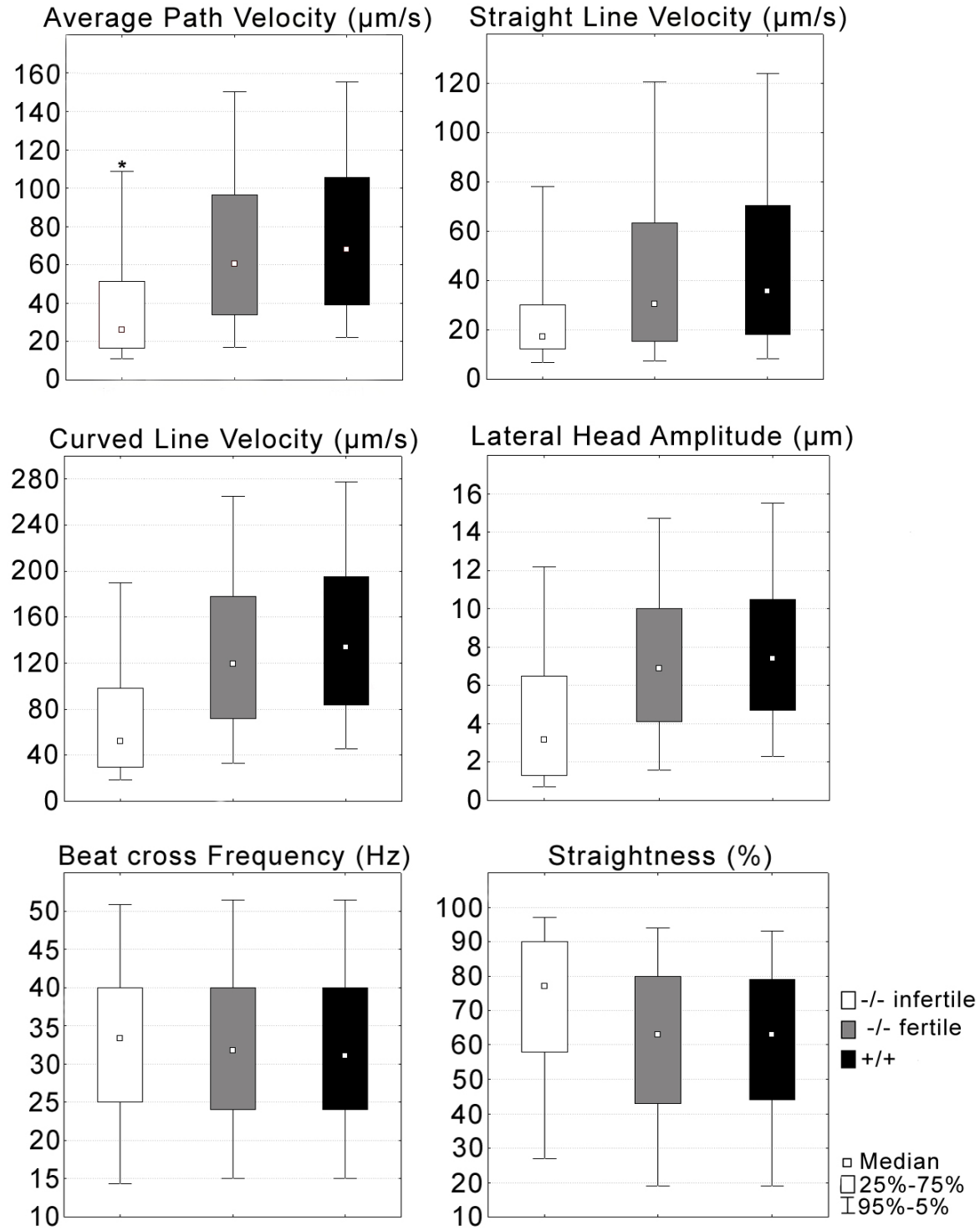

Fig. 28. Computer-assisted analysis of sperm motility. The results of analyses of wild type and *Insl6*$^{-/-}$ spermatozoa on C57BL x 129/Sv hybrid genetic background are shown. Sperm velocities (micrometers/second),

forward movement (percent), lateral head displacement (micrometers), and beat cross frequency (hertz) were measured after 1.5 h incubation *in vitro*. For all parameters the medians and percentiles are shown. The *Insl6*-deficient spermatozoa exhibit statistically significantly reduced velocities and lateral head displacement in comparison to wild type sperm ($p<0.05$ by Mann-Whitney U-Test). Middle points represent median value, boxes represent 25% -75% percentiles range and the whiskers represent 5% - 95% percentiles of the nonoutliers range. Abbreviations: VAP: Average Path Velocity; VSL: Straight Line Velocity; VCL: Curvilinear Velocity; ALH: Lateral Head Displacement; BCF: Beat Cross Frequency; STR: Straightness.

To determine whether the *Insl6*-deficient spermatozoa have structural abnormalities, light microscope analysis was performed (2.2.18.2). No abnormalities were observed in sperm head shape from both groups of *Insl6* mutants as compared to wild type mice (Tab. 11).

Tab. 11. Acrosome reaction and analysis of sperm morphology of *Insl6*-deficient mice.

Genotype of mice	Percentage of abnormal spermatozoa	Percentage of acrosome reacted spermatozoa
Insl6$^{+/+}$	4.03±3.02 (3)	95.1±5.8 (2)
Insl6$^{-/-}$		
fertile	2.87±0.5 (3)	93.25±3.18 (2)
infertile	7.33±3 (3)	81.03±8.61 (4)

Data for sperm analysis represent the means±SD for the numbers of individual measurements indicated in parentheses. Values in *Insl6* mutant mice are not significantly different from those in wild type mice ($p> 0.05$ by Student's *t* test).

To address the question whether the fertility of *Insl6*$^{-/-}$ mice might be influenced by defect in acrosome reaction, we examined the response of spermatozoa from infertile and fertile *Insl6* mutant and wild type mice to the calcium ionophore A23187 (2.2.18.4) (Fig. 29). This analysis showed that there is no significant difference in percentage of acrosome reacted spermatozoa between the mutant (fertile and infertile) and control strains (Tab. 11).

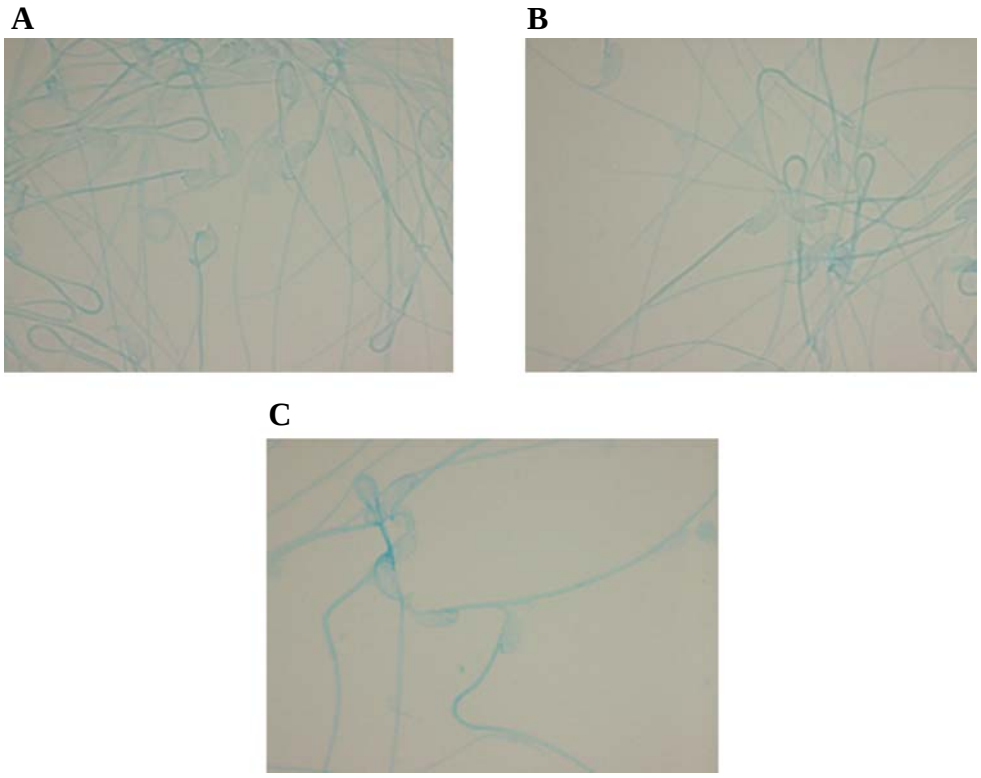

Fig. 29. Examination of the response of spermatozoa from wild type (A), fertile *Insl6*$^{-/-}$ (B) and infertile *Insl6*$^{-/-}$ (C) mice to the calcium ionophore A23187. No significant differences in percentage of acrosome reacted spermatozoa between the *Insl6*$^{-/-}$ mutant (fertile and infertile) and control mice were observed ($p > 0.05$). A, B, C: 10-fold magnification.

3.2.3.2.3. Histological analysis of *Insl6*-deficient mouse testes

To further define the causes of impaired fertility in *Insl6*-deficient males, testes were isolated from wild type and infertile *Insl6*$^{-/-}$ mature animals and morphological and histological analyses were performed (2.2.20).

Examination of infertile *Insl6*-deficient mice revealed that the Wolffian duct derivatives had differentiated normally (Fig. 30) and testes are descended in scrotum. However, testes from adult *Insl6*$^{-/-}$ males were much smaller than those of wild type mice and they weighed on average 48% less than wild type testes (68±4 mg versus 131±6 mg, $p < 0.01$, $n = 5$) (Fig. 30 and 32).

Fig. 30. Morphology of reproductive organs from infertile *Insl6* mutant and wild type mice. The seminal vesicle (white arrowhead), vasa differentia (white arrow) and epididymis (black arrow) differentiated normally and testes (black arrowhead) are descended. The testes from *Insl6*-deficient mice are markedly smaller than those from wild type controls.

Analysis of hematoxylin-eosin (H&E) stained sections revealed clear differences between testes of wild type and infertile *Insl6*$^{-/-}$ mice (Fig. 31). Seminiferous tubules from wild type animals showed a normal pattern of spermatogenesis, with the presence of all spermatogenic stages from spermatogonia to spermatozoa (Fig. 31 A and C). In contrast, testes of *Insl6* mutant mice exhibited seminiferous tubular degeneration (Fig. 31 B and D). Histological analyses showed that many seminiferous tubules were completely devoid of elongated spermatids and spermatozoa, whereas spermatogonia, spermatocytes and round spermatids were visible. The number of pachytene spermatocytes and round spermatids was far fewer in *Insl6*$^{-/-}$ than in that of *Insl6*$^{+/+}$. The percentage of postmeiotic-free tubules varied in different *Insl6*$^{-/-}$ mice from 30% to 80% (approximately 300 tubules from 5 adult *Insl6*$^{-/-}$ mice were analyzed), and corresponded to partially or completely impaired fertility of these animals. We frequently observed seminiferous tubules where meiosis does not progress beyond the first meiotic division. These tubules contained degenerated cells at prophase I, and bi- or multinucleated *giant* cells. The seminiferous epithelium was vacuolated, and immature germ cells were present in lumen (Fig. 31 B and D).

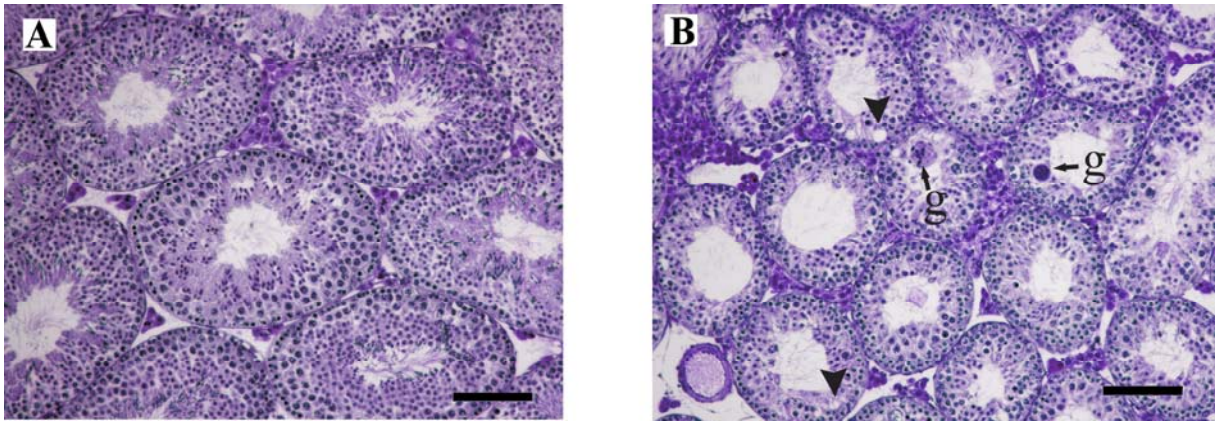

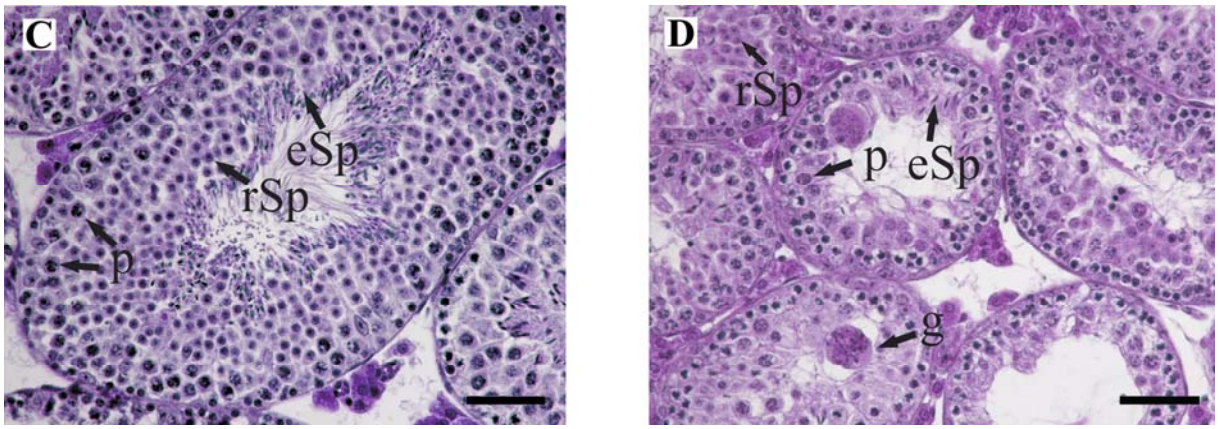

Fig. 31. Spermatogenesis of *Insl6*$^{+/+}$ and *Insl6*$^{-/-}$ infertile mice. Staining with hematoxylin-eosin reveals hypo spermatogenesis with a strongly reduced number of pachytene spermatocytes, round and elongated spermatid in the seminiferous tubules of *Insl6*$^{-/-}$ mice (B, D) compared to wild type littermates (A, C). Degenerated spermatogenic cells and vacuoles (arrows), a decreased diameter of tubules and the presence of multinucleated giant cells (arrowheads) were observed in testes of infertile *Insl6*$^{-/-}$ mice (B, D). Scale bars: panel A and B, 100 µm; panel C and D, 50 µm.

3.2.3.2.4. Stage specific histological analysis of *Insl6*-deficient mouse testes

To define the onset of the disruption of spermatogenesis in *Insl6*-deficient mice, the progression of the first wave of spermatogenesis was examined in wild type and *Insl6* mutant testes at different developmental stages (at least 4 testes from each age). Testes of 5- and 10-days old wild type and mutant mice were indistinguishable in weight (Fig. 32). In contrast, *Insl6*$^{-/-}$ testes from mice at 15-, 20-, 25- and 90-days of age weighted significantly less than testes from their control littermates (Fig. 32).

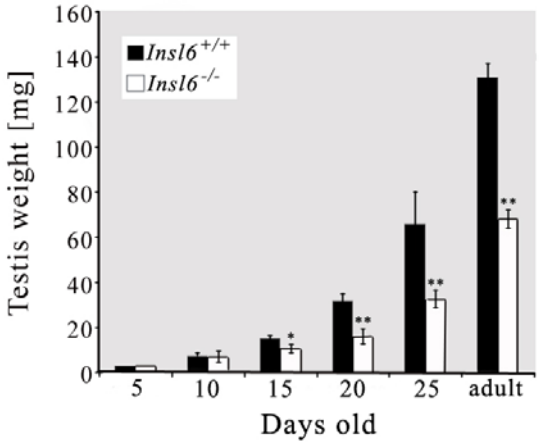

Fig. 32. Comparison of testes weights from 5-, 10-, 15-, 20-, 25- and 90-days old *Insl6*$^{+/+}$ and *Insl6*$^{-/-}$ mice. The testis weights of *Insl6*$^{-/-}$ are significantly smaller than those of *Insl6*$^{+/+}$ mice after postnatal day 15. Data are presented as the mean±SD of at least 4 testes from each age; *, $p < 0.05$; **, $p < 0.001$.

Examination of H&E stained tubular cross sections at postnatal day 5 and 10 revealed that the histology of wild type and *Insl6*$^{-/-}$ testes were similar, with seminiferous tubules containing only Sertoli cells and spermatogonia (data not shown). At day 15, when the spermatogenesis progresses to mid and late pachytene spermatocytes, in *Insl6*$^{-/-}$ testes drastically reduced number of pachytene spermatocytes was counted as compared to wild type controls (Fig. 33A and B). At day 20, the most advanced germ cells in seminiferous tubules of wild type were round spermatids (Fig. 33 C). However, progression of spermatogenesis was delayed in *Insl6*$^{-/-}$ testes, and the most advanced germ cells were primarily still at the pachytene spermatocyte stage (occasional tubules showed the presence of round spermatids) (Fig. 33 D). Early signs of Sertoli cell vacuolization were observed. At day 25, when tubules of wild type siblings contained germ cells at the elongated spermatid stage (Fig. 33 E), *Insl6*$^{-/-}$ testes displayed severe depletion of germ cells and Sertoli cell vacuolization was more evident. Very few round spermatids and no elongated spermatids were present in the epithelium of *Insl6*$^{-/-}$ males. Moreover, a drastically reduced number of spermatocytes (mainly pachytene spermatocytes) was visible in mutant testes (Fig. 33 F). Thus, absence of mouse INSL6 appears to induce the spermatogenesis arrest at first meiotic prophase of most of germ cells.

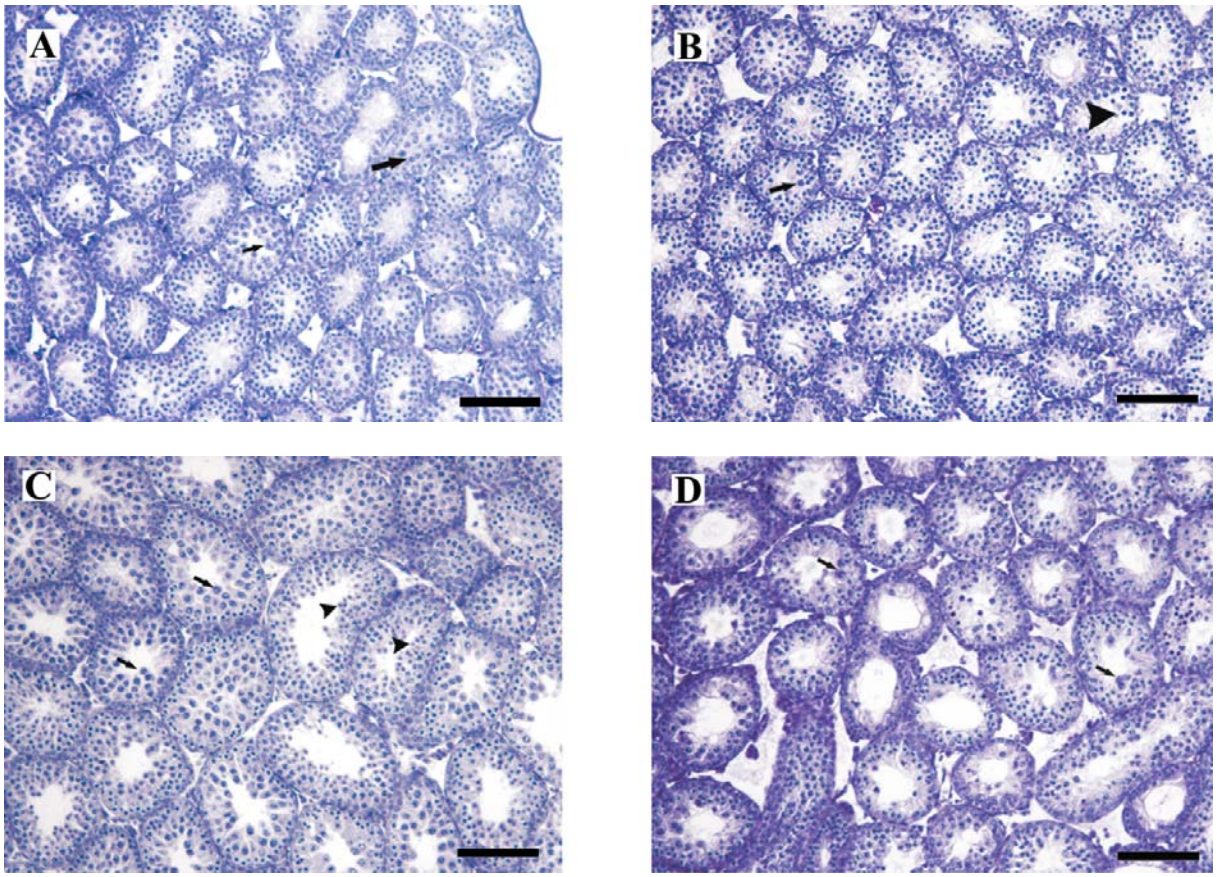

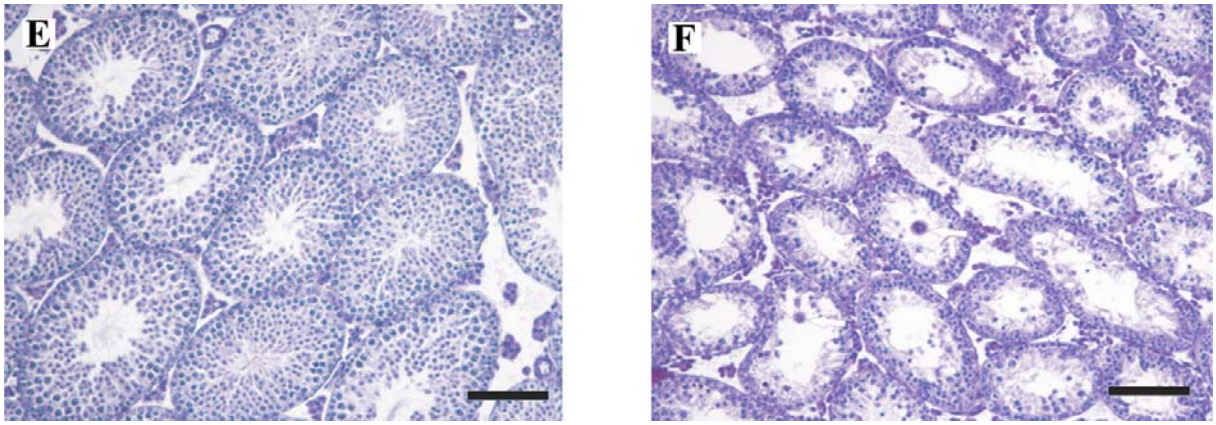

Fig. 33. Delayed and disrupted late meiotic prophase and subsequent meiotic division in the first wave of spermatogenesis in *Insl6*-deficient mice. Morphology of seminiferous tubules of testes from *Insl6*$^{+/+}$ *(A,* C, E) and *Insl6*$^{-/-}$ (B, D, F) mice at postnatal day 15 (A, B), 20 (C, D), and 25 (E, F) is shown. At day 15, germ cell development progressed to pachytene spermatocyte stage (arrows) in *Insl6*$^{+/+}$ mice (A), while very few pachytene spermatocytes could be observed in *Insl6*$^{-/-}$ mice (B). At day 20, meiosis has been completed and tubules were filled with spermatocytes and round spermatids (arrowhead) in *Insl6*$^{+/+}$ mice (C), while in *Insl6*$^{-/-}$, spermatogenesis was primarily still in pachytene spermatocyte stage and tubules displayed early signs of Sertoli cell vacuolization (D). At day 25, adluminal cells were primarily round and elongated spermatids in *Insl6*$^{+/+}$ mice (E), while in *Insl6*$^{-/-}$ adluminal cells were still primarily pachytene spermatocytes and tubules showed the presence of multinucleated cells similar to those present in adult *Insl6*$^{-/-}$ mice (F). Scale bar: 100 um.

3.2.3.2.5. Immunohistochemical analysis of *Insl6*-deficient mouse testes

To confirm our histological findings (Fig. 33) we investigated whether the depletion of germ cells in testes of *Insl6*$^{-/-}$ mice is due to the defect in spermatogonia or due to the arrest of germ cells development at later stage. For these studies, immunohistochemistry with polyclonal antibodies (dilution 1:200) against HSPA4, which is marker for spermatogonia and HSPA4L, whose expression begins in pachytene spermatocytes (Held et al., 2006), was performed. Testis cross-sections from three 10- and 15-days old wild type and *Insl6*-deficient mice were stained (2.2.20.4) with antibodies against HSPA4 or HSPA4L, respectively. Then, sections were examined under the light microscope (Fig. 34).

Immunohistochemistry detected no abnormalities in the number of HSPA4-positive spermatogonia in sections from 10-days old *Insl6*$^{-/-}$ males compared to *Insl6*$^{+/+}$ (Fig. 34A, B). In contrast, immunohistochemistry analysis of 15-days old testes revealed a strongly reduced number of HSPA4L-positive cells in *Insl6*$^{-/-}$ mice (only few labelled cells per microscope field), whereas in *Insl6*$^{+/+}$ testes most of tubules were filled with HSPA4L-positive pachytene

spermatocytes (Fig. 34C, D). These results confirm that the progression of spermatogenesis in infertile *Insl6*$^{-/-}$ mice is delayed and that pachytene spermatocytes are the first affected cells population.

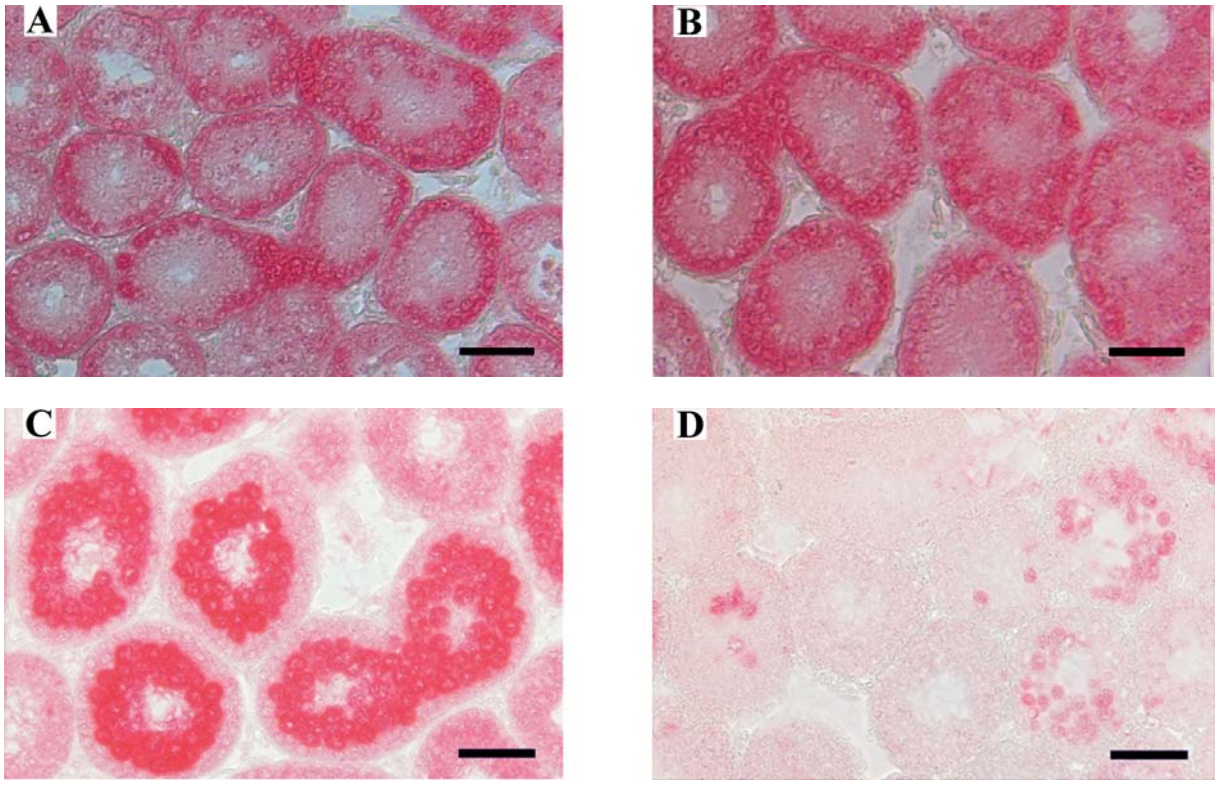

Fig. 34. Immunohistochemical analysis of *Insl6*-deficient mouse testes. Immunohistochemical detection of HSPA4-positive cells in testes of *Insl6*$^{+/+}$ (A) and Insl6$^{-/-}$ infertile (B) mice at postnatal day 10. No abnormalities in sections of *Insl6*-deficient mice were detected compared to wild type controls. Immunohistochemical analysis of HSPA4L in testes of *Insl6*$^{+/+}$ (C) and *Insl6*$^{-/-}$ infertile (D) mice at postnatal day 15. Only few HSPA4L-positive cells were visible in tubules of *Insl6*$^{-/-}$ mice (D). In contrast, most of tubules of *Insl6*$^{+/+}$ mice were filled with pachytene spermatocytes (C). Scale bar, 50 µm.

3.2.3.2.6. Detection of apoptotic cells in *Insl6* mutant males

To determine whether the germ cell depletion in adult *Insl6*$^{-/-}$ infertile testes is due to enhanced apoptosis, we performed a TUNEL assay (2.2.20.7) on cross-sections of juvenile (5-, 10-, 15-, 20-, and 25-days old) and adult testes. For each developmental stage, testes of three wild type and *Insl6* mutant mice were examined.

Analysis of spermatogenesis in juvenil animals revealed that the number of apoptotic cells in *5-, 10-* (data not shown) and 15-days old (Fig. 35B) *Insl6*$^{-/-}$ testes was not significantly different from that observed in sections of wild type testes (Fig.35A). In contrast, dramatically increased number of TUNEL-positive spermatocytes was observed in 20- and 25-days old

Insl6 mutants compared to wild type controls (Fig. 35C-F). The accumulation of apoptotic cells in these developmental stages coincides with the appearance of clearly impaired spermatogenesis in juvenile testes of *Insl6*$^{-/-}$ mice as detected by hematoxylin and eosin staining (Fig. 33C-F).

In 3-month old mice, the frequency of TUNEL-positive cells was variable among tubules, but overall we have observed significantly more apoptotic cells in the semineferous tubules of infertile *Insl6*$^{-/-}$ males than in those of wild type littermates (Fig. 35G, H). At higher magnification, most of these TUNEL-positive cells were seen to be in meiotic prophase, with a smaller number of late-stage germ cells. To confirm our observation, a statistical evaluation of apoptotic cells from 3-month old mice was performed by counting TUNEL-positive cells in at least 10 independent microscopic fields for each wild type and mutant mice (n = 3). As shown in Table 12, the mean value indicates significantly elevated numbers of apoptotic cells in *Insl6* mutant mice compared with wild type controls (9.6±1 versus 1.4±0.2, $p < 0.01$).

The above results suggest that the enhanced apoptosis is the cause for germ cell depletion in *Insl6*-null infertile testes.

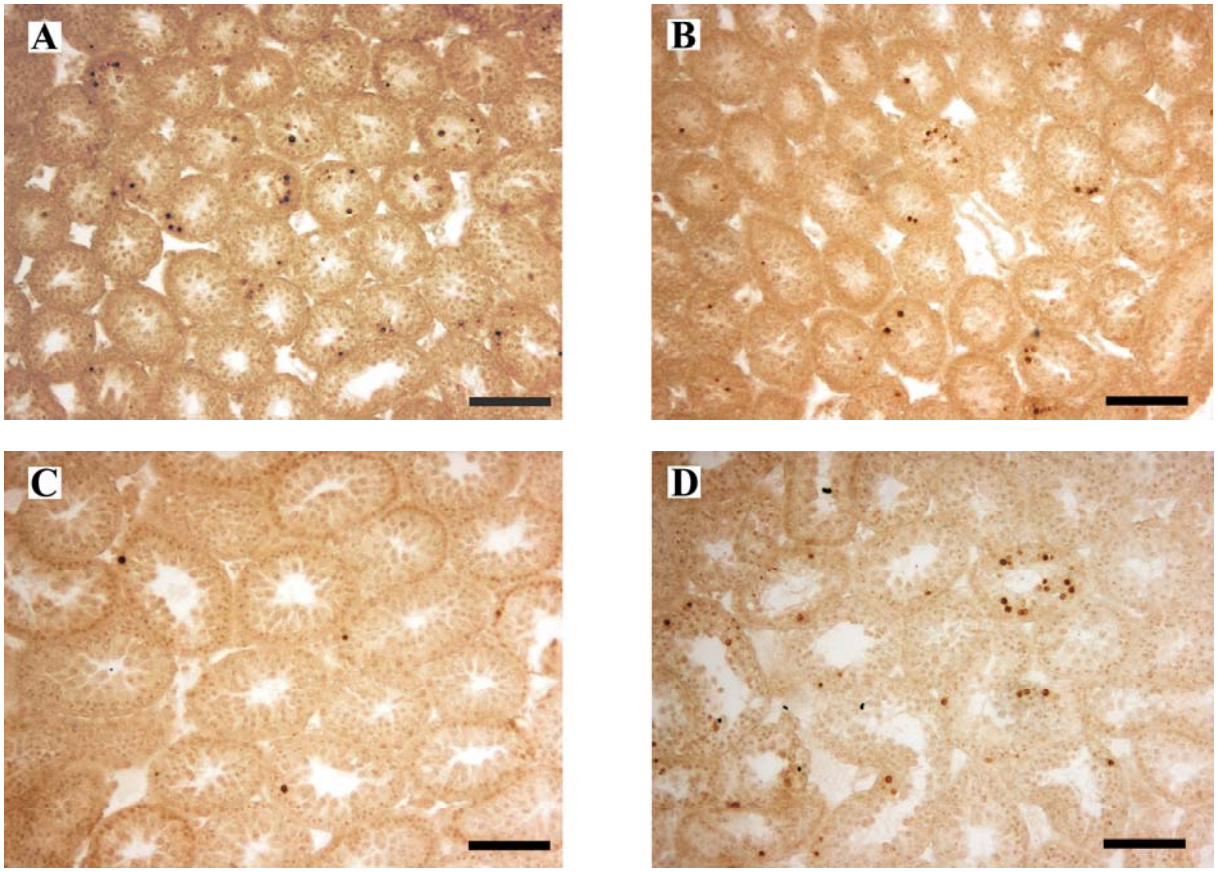

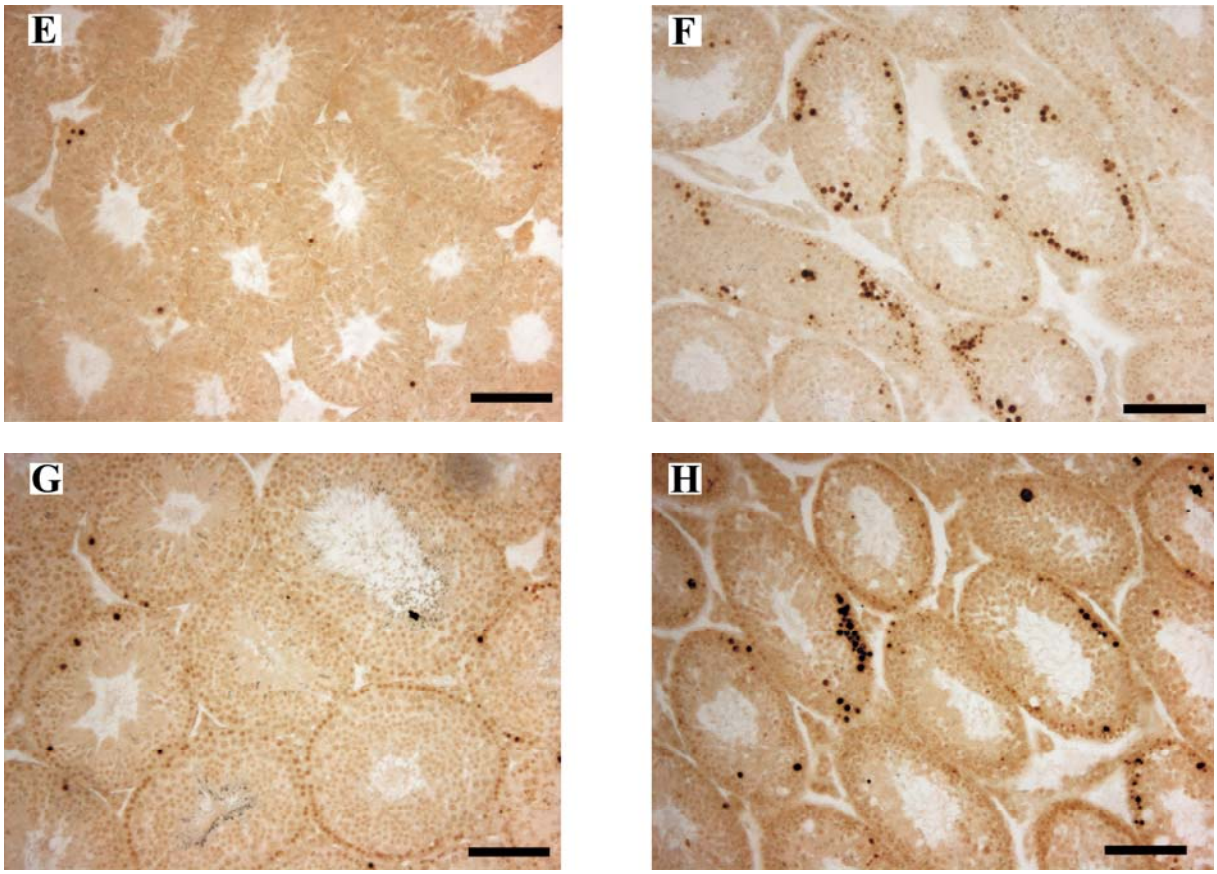

Fig. 35. Increased apoptotic germ cells during the first wave of spermatogenesis in juvenile infertile *Insl6*$^{-/-}$ mice. Detection of apoptotic cells in testes of *Insl6*$^{+/+}$ (A, C, E,G) and *Insl6*$^{-/-}$ (B, D, F, H) mice at postnatal days 15 (A, B), 20 (C, D), 25 (E, F) and 90 (G, H) was performed. At day 15, TUNEL staining for apoptotic cells (brown nuclei) was equal in seminiferous tubules from *Insl6*$^{+/+}$ (A) and *Insl6*$^{-/-}$ (B) mice. At day 20, apoptotic cells were more common in *Insl6*$^{-/-}$ (D) than in *Insl6*$^{+/+}$ (C) mice. At day 25, only few spermatocytes were apoptotic in *Insl6*$^{+/+}$ mice (E), while the majority of tubules from *Insl6*$^{-/-}$ mice had apoptotic spermatocytes (F). At day 90, TUNEL staining revealed massive apoptosis of spermatocytes in *Insl6*$^{-/-}$ testes (H) compared to *Insl6*$^{+/+}$ testes (G). Scale bar, 100 µm.

Tab. 12. Quantification of TUNEL-positive germ cells in adult wild type and *Insl6*$^{-/-}$ infertile mice.

Genotype of mice	Percentage of semineferous tubules containing at least one TUNEL-positive cell	No. of TUNEL-positive cell per tubule
Insl6$^{+/+}$	20.5±0.3 (3)	1.4±0.2 (3)
Insl6$^{-/-}$	77.7±6.3* (3)	9.6±1.0* (3)

Results represent the means±SD for the numbers of individual measurements indicated in parentheses. *, value in infertile *Insl6*$^{-/-}$ mice is significantly different from that in *Insl6*$^{+/+}$ mice (p<0.01 by Student's t test).

3.2.3.2.7. Expression analysis of germ cell marker genes in *Insl6*-deficient mouse testes

To further elucidate the defective stage of spermatogenesis in *Insl6*-deficient mice, we investigated the transcription level of germ cell marker genes that are transcribed in meiotic and postmeiotic stages. Testicular RNA was isolated (2.2.1.3) from 3-month old *Insl6*$^{+/+}$ males, fertile and infertile *Insl6*$^{-/-}$ males and probed with mouse *Sycp3, Pgk2, Ccna1, Acr,* and *Tnp2* cDNA (Kremling *et al.,* 1991; Lammers *et al.,* 1994; Meetei *et al.,* 1996; Sweeney *et al.,* 1996; Chen *et al.,* 2004). The integrity and the amount of RNA used in this experiment were proved by rehybridization with a *ß-actin* probe (Waters *et al.,* 1985) (Fig. 36).

In adult testis, *Sycp3* (encoding a synaptonemal complex protein 3) was found to be expressed from leptotene to diplotene spermatocytes (Parra *et al.,* 2003; Kuramochi-Miyagawa *et al.,* 2004), and expression of testis-specific *Pgk2* (encoding testis-specific phosphoglycerate kinase 2) begins in leptotene and peaks in pachytene spermatocytes (Goto *et al.,* 1990; McCarrey *et al.,* 1992; Yoshioka *et al.,* 2007). Our analysis revealed that expression of *Sycp3* and *Pgk2* genes in testes of fertile and infertile *Insl6*$^{-/-}$ animals was maintained at level comparable with that seen in wild type testes. Proacrosin transcript (*Acr*), which is expressed in pachytene spermatocytes and round spermatids (Nayernia *et al.,* 1994), was detected in testes of fertile and infertile *Insl6* mutants, but in decreased amounts. The expression of transition protein 2 (*Tnp2*), which is initially expressed in round spermatides (Saunders *et al.,* 1992; Shih *et al.,* 2002), was weaker in *Insl6*-deficient testes (Fig. 36).

In conclusion, our results suggest that development of most *Insl6*$^{-/-}$ germ cells is arrested just at the beginning of meiotic division (at meiotic prophase).

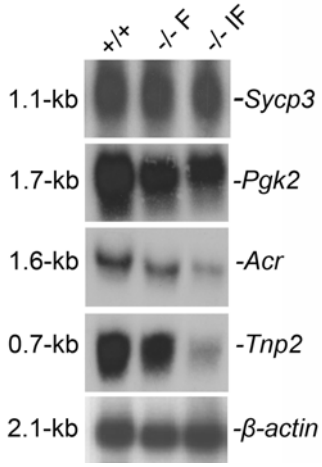

Fig. 36. Analysis of gene expression in *Insl6*-deficient mice. The expression of stage-specific genes during spermatogenesis was analyzed by Northern blot. Total testicular RNA (10 µg) derived from 3-month old wild type (+/+), fertile *Insl6* mutant (-/- F) and infertile *Insl6* mutant (-/- IF) animals were hybridized with mouse

Sycp3, Pgk2, Acr, and *Tnp2* cDNA fragments and rehybridized with mouse *β-actin*, as a control for equal RNA loading.

3.2.3.3. Generation of *Insl6* knock-out mice on C57BL/6J background

To further analyze the effect of the disruption of *Insl6* gene on C57BL/6J genetic background, *Insl6*$^{-/-}$ homozygous mice on a C57BL/6J x 129/Sv hybrid genetic background were backcrossed with wild type mice of mouse strain C57BL/6J. Heterozygous offspring in the first backcross generation (B_1) were intercrossed with C57BL/6J mice to give the second backcross generation (B_2). This breeding strategy was pursued till generation B_7. Then, heterozygous mice in the seventh backcross generation were intercrossed to give *Insl6*$^{-/-}$ mice, whose genome contains 99.1% of the mouse strain C57BL/6J.
Genotyping of progeny for *Insl6* was performed by PCR assay as it was described in sections 2.2.7.2 and 3.2.2.5 (Fig. 26). To date, only 2 *Insl6*$^{-/-}$ homozygous mice were identified out of 24 genotyped offspring, derived from the heterozygous intercrosses. However, a lot of animals (7 mice) failed to thrive and died between days 3 and 20 after birth (before PCR analysis). Therefore, more accurately phenotypic examination of *Insl6*-deficient mice on C57BL/6J background will be performed.

3.2.4. Creation of transgenic mouse models for *Insl6* gene

3.2.4.1. Construction of *RIP1-Insl6* transgenic construct

To study the result of the overexpression of *Insl6*, we generated a transgenic construct containing the mouse *Insl6* open reading frame (ORF) with SV40 polyadenylation signal under the control of *rat Insulin 1* promoter (*RIP1*) (Fig. 37). This transgenic line should also be used in rescue strategy of *Insl6*$^{-/-}$ infertile males. The *RIP1* is specifically expressed in pre- and postnatal ß-cells of the Langerhans islets (Ahlgren *et al.,* 1998; Herrera *et al.,* 1998). Therefore, we have expected that the *Insl6* would be expressed in ß-cells of *RIP1-Insl6* transgenic mice.

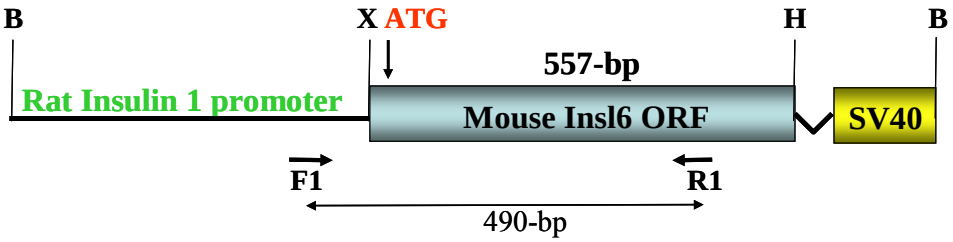

Fig. 37. Schematic representation of *RIP1-Insl6* transgenic construct. The construct contains the *rat Insulin 1* promoter (700-bp) fused to the mouse *Insl6* ORF (557-bp) and SV40 polyadenylation signal. The primers F1 and R1 (arrows) were used in PCR assay for genotyping the founder animals. Abbreviation: F1, Insl6_TA_F1 primer; R1, Insl6_TA_R1 primer; ORF, open reading frame; X, *Xba*I; H, *Hind*III; B, *Bam*HI.

To generate the transgenic construct, mouse *Insl6* cDNA was amplified (2.2.7.3) from mouse testis RNA using specific primers Insl6_TA_F1 and Insl6_TA_R1. A 557-bp *Insl6* ORF fragment containing *Xba*I and *Hind*III restriction sites was subcloned into pGEM-T Easy vector and sequenced. Subsequently, the 557-bp *Xba*I/*Hind*III fragment was isolated and cloned into *Xba*I/*Hind*III digested RIP1-DIPA vector.

3.2.4.2. Generation of *RIP1-Insl6* transgenic mice

The *RIP1-Insl6* fusion fragment was isolated from the vector backbone by digestion with *Bam*HI enzyme and purified as it was described in section 2.2.17.1. Then, a 1.7-kb *RIP-Insl6* *Bam*HI fragment was microinjected into the male pronuclei of the fertilized mouse oocytes of C57BL/6J genetic background. The oocytes were transferred into the uteri of foster mothers. In order to identify transgenic mice harbouring *RIP1-Insl6* transgenic allele, genomic DNA isolated from tail biopsies of founder mice were examined by PCR genotyping (2.2.7.) using Insl6TR_genF1 (F1) and Insl6TR_genR1 (R1) primers (Fig. 37and 38). A 490-bp fragment should be amplified in transgenic founders. Unfortunately, out of 9 genotyped pups, no transgenic founder was identified (Fig. 38).

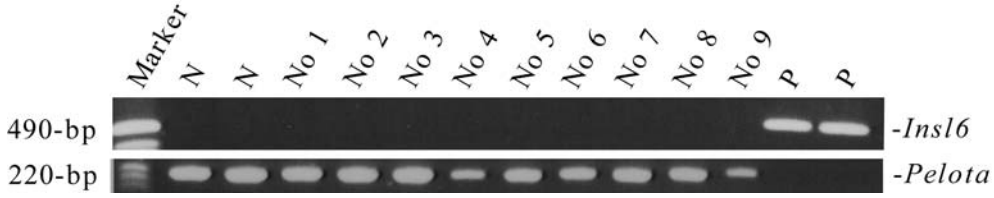

Fig. 38. Genotyping PCR of *RIP1-Insl6* founder mice. Primers Insl6TR_genF1 and Insl6TR_genR1 amplified a 490-bp transgenic allele. None transgenic founder was identified. DNA quality was checked by amplification a 220-pb fragment of *Pelota* (Sallam, 2001). N, negative control (wild type DNA), P, positive control (transgenic construct DNA).

3.3. Verification of interactions between PELO and its putative interacting proteins

My work was concentrated to verify the interactions between PELO and CDK2AP1, EIF3G and SRPX by colocalization study and using in vitro methods (coimmunopresipitation and GST Pull-down assay).

3.3.1. Colocalization of PELO and putative interaction partners in HeLa cells

3.3.1.1. Generation of pCMV-Myc-*CDK2AP1*, pCMV-Myc-*EIF3G* and pCMV-Myc-*SRPX* expression constructs

Plasmid DNA from clones identified in yeast two-hybrid screen as interaction partners of PELO was extracted. Inserts, containing a part of cDNA of analyzed genes (*CDK2AP1*, *EIF3G* and *SRPX*) were amplified by PCR using sequencing primers (Y2H_5cDNA and Y2H_3cDNA). Amplified cDNA clones encoding CDK2AP1 (1-115 aa), EIF3G (1-320 aa) and SRPX (265-464 aa) were used to generate expression vectors to produce fusion proteins (Fig.39).

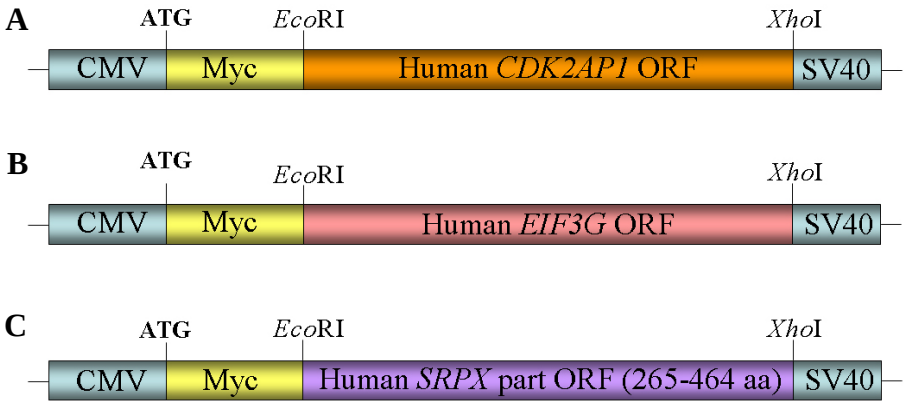

Fig. 39. Schematic representation of pCMV-Myc-*CDK2AP1* (A), pCMV- Myc-*EIF3G* (B) and pCMV-Myc-*SRPX* (C) expression constructs. Fusion proteins were expressed under the control of human cytomegalovirus promoter (CMV). ATG, start codon; Myc, myc epitop tag; ORF, open reading frame; SV40, SV40 polyadenylation signal.

The amplified cDNA fragments containing the coding sequences of putative interaction partners (*CDK2AP1*, *EIF3G*, and *SRPX*) were separately subcloned into pGEM-T Easy vector, sequenced, cut out with *Eco*RI and *Xho*I restriction enzymes and then inserted in frame

into the pCMV-Myc mammalian expression vector. Nucleotide sequences of generated pCMV-Myc-*CDK2AP1*, pCMV-Myc-*EIF3G* and pCMV-Myc-*SRPX* constructs (Fig. 39) were confirmed by sequencing.

3.3.1.2. Generation of pCMV-HA-PELO expression constructs

To generate a pCMV-HA-*PELO* expression construct, human *PELO* cDNA was amplified (2.2.7.3) from human testis RNA using specific primers PELO_HAF1 and PELO_HAR1. A 1.1-kb *PELO* ORF fragment containing *Eco*RI and *Xho*I restriction sites was subcloned into pGEM-T Easy vector and sequenced. Subsequently, the 1.1-kb *Eco*RI/*Xho*I fragment was isolated and cloned in frame into the *Eco*RI/*Xho*I digested pCMV-HA mammalian expression vector. Nucleotide sequence of generated pCMV-HA-*PELO* construct (Fig. 40) was confirmed by sequencing.

Fig. 40. Schematic representation of pCMV-HA-*PELO* expression constructs. 1.1-kb PCR product containing human *PELO* ORF was cloned in frame into the mammalian expression vector pCMV-HA using standard techniques (2.2.7.3). Fusion protein was expressed under the control of human cytomegalovirus promoter (CMV). ATG, start codon; HA, HA epitop tag; ORF, open reading frame; SV40, SV40 polyadenylation signal.

3.3.1.3. Immunofluorescence analysis of subcellular colocalization of PELO and putative interaction partners

To verify interactions between PELO and putative interaction partners identified in yeast two-hybrid assay, colocalization analysis was performed. Human HeLa cells were cultured onto coverslips and transiently cotransfected (2.2.15.4) with: pCMV-HA-*PELO* and pCMV-Myc-*CDK2AP1*; pCMV-HA-*PELO* and pCMV-Myc-*EIF3G* or pCMV-HA-*PELO* and pCMV-Myc-*SRPX* expression constructs, respectively. Then, 48 hrs after transfections, the expression of fusion proteins was determined by immunostaining (2.2.15.5) with mouse monoclonal anti-c-myc (dilution 1:200) and rabbit polyclonal anti-HA-tag (dilution 1:200) antibodies (Fig. 41). Reactivity with primary antibodies was visualized with FITC conjugated anti-mouse IgG (green colour, dilution 1:500) and Cy3-conjugated anti-rabbit secondary antibodies (red colour, dilution 1:1000), respectively. To prove that the labeling technique

was specific and that the primary antibodies were responsible for generation of the immunostaining, negative controls were performed. Untransfected HeLa cells were incubated with primary and secondary antibodies and observed under fluorescence microscope (Fig. 41).

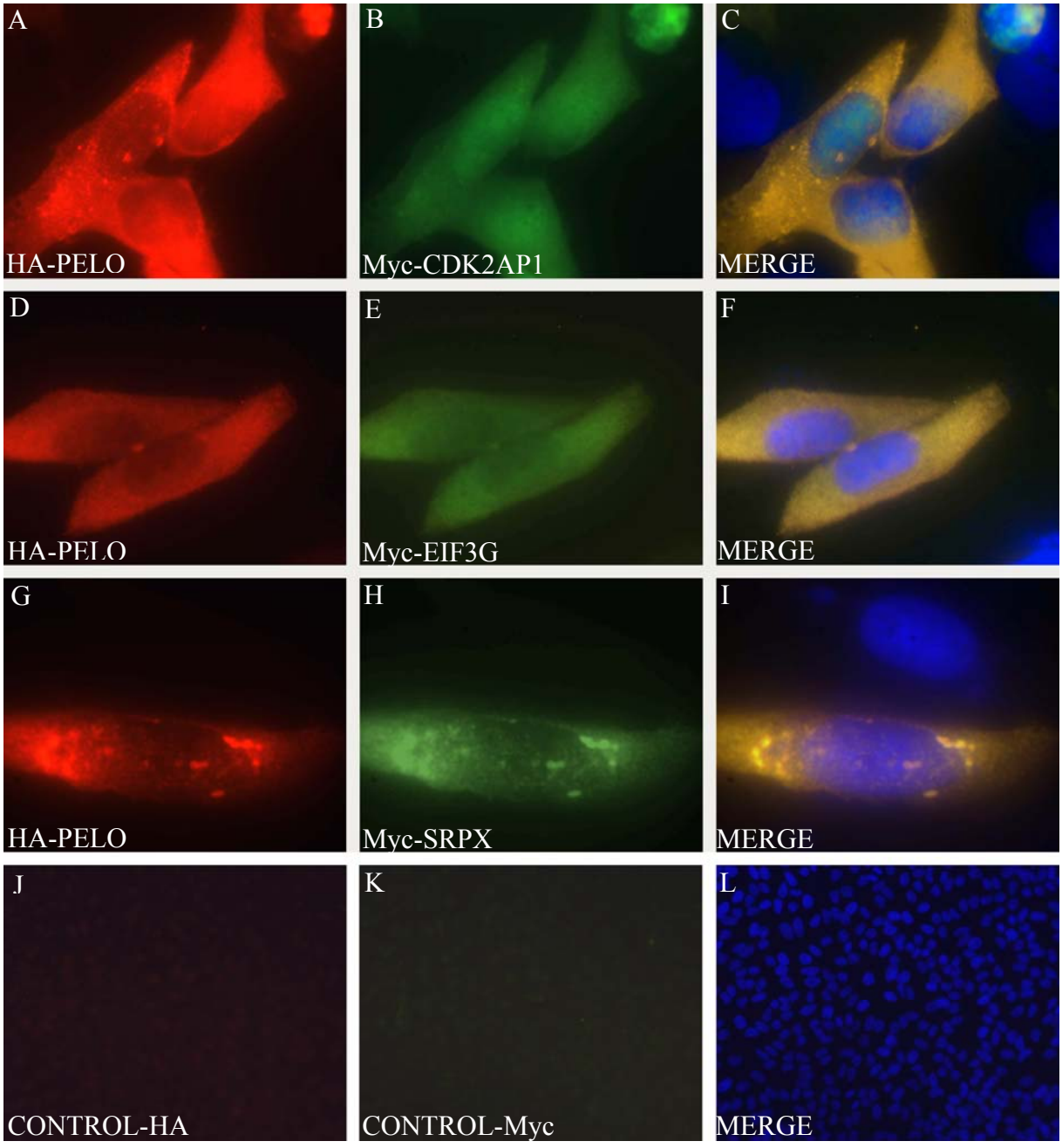

Fig. 41. Subcellular colocalization of PELO with putative interaction partners. HeLa cells were transiently cotransfected with: pCMV-HA-*PELO* and pCMV-Myc-*CDK2AP1* (A-C), pCMV-HA-*PELO* and pCMV-Myc-*EIF3G* (D-F), or pCMV-HA-*PELO* and pCMV-Myc-S*RPX* (G-I) expression constructs. The expression of fusion proteins was determined by staining with rabbit polyclonal anti-HA-tag (red signal, Cy3) and mouse monoclonal anti-c-myc (green signal, FITC) antibodies. Cells nuclei were counterstained with DAPI (blue) and analyzed under the fluorescence microscope. HA-PELO fusion protein (red) was localized exclusively in cytoplasm (A, D, G). Myc-CDK2AP1 fusion protein (green) was localized both in nucleus and in cytoplasm (B). Location of Myc-EIF3G and Myc-SRPX fusion proteins (green) was restricted to cytoplasm (E and H,

respectively). Merged images showed overlapping signals in cytoplasm of stained cells (yellow, C, F, and H). Negative control (untransfected cells incubated with primary and secondary antibodies) proved specificity of our immunostaining (J-L). A-I, 60-fold magnification; J-L, 20-fold magnification.

As shown in Figure 41 A, D, G, in all cotransfected cells, HA-PELO fusion protein (red signal) was localized exclusively in cytoplasm. Figure 41B showed that in cells cotransfected with pCMV-Myc-*CDK2AP1* and pCMV-HA-*PELO* expression constructs (Fig. 40A and 39, respectively), Myc-CDK2AP1 fusion protein (green signal) was localized in nucleus as well as in cytoplasm. Although the pattern of both fusion proteins did not overlap completely, a coincided localization was observed in cytoplasm of stained cells (yellow signal, Fig. 41C). In contrast, in cells cotransfected with pCMV-Myc-*EIF3G* and pCMV-HA-*PELO* expression constructs (Fig. 40B and 39, respectively), Myc-EIF3G fusion protein (green signal, Fig. 41E) was localized exclusively in cytoplasm and its distribution entirely overlapped with HA-PELO fusion protein (yellow signal, Fig. 41F). A similar staining pattern was observed in cells cotransfected with pCMV-Myc-*SRPX* and pCMV-HA-*PELO* expression constructs (Fig. 40C and 39, respectively). Myc-SRPX fusion protein was localized exclusively in cytoplasm and distribution of both fusion proteins overlapped completely (yellow signal, Fig. 41I). Specificity of obtained coimmunostaining was proved by negative control. As shown in Figure 41J-L, no positive signal was obtained in control staining untransfected cells incubated with anti-c-myc and anti-HA-tag primary antibodies and Cy3-conjugated anti-rabbit (Fig. 41J) and FITC conjugated anti-mouse IgG (Fig. 41K) secondary antibodies. Blue colour at overlapped picture (Fig. 41L) represented the DAPI staining of the nuclei.
In conclusion, our results confirmed subcellular colocalization between PELO and: CDK2AP1, EIF3G, and SRPX (Fig. 41) suggested that PELO may form functional complexes with these proteins in cytoplasm.

3.3.2. Coimmunoprecipitation of PELO protein with putative interaction partners

The coimmunoprecipitation assay was performed to answer the question whether in vitro protein-protein interactions would support the interactions found between PELO and candidate proteins by the yeast two-hybrid screening (Ebermann, 2005). For this experiment HeLa cells were cultured into 6-well or 100 mm plates and transiently cotransfected (2.2.15.4) with appropriate pair of expression constructs: pCMV-HA-*PELO* and pCMV-Myc-

CDK2AP1, pCMV-HA-*PELO* and pCMV-Myc-*EIF3G,* or pCMV-HA-*PELO* and pCMV-Myc-S*RPX* (3.3.1.1 and 3.3.1.2). HeLa cells support with empty pCMV-HA and pCMV-Myc expression vectors were used as a negative control. Forty-eight hrs after cotransfection, total cell proteins were isolated (2.2.12.2) and subjected to coimmunoprecipitation studies (2.2.14.2). Coimmunoprecipitates were prepared by incubating the lysates either with rabbit polyclonal anti-HA-tag (10 µl) or with mouse monoclonal anti-c-myc (10 µl) antibodies and protein-A/G or protein-G beads, respectively. After several washing steps, finally immunoprecipitated fusion proteins were eluated, separated by SDS-PAGE (2.2.12.4), transferred to a nitrocellulose membrane Hybond-C (2.2.12.5), and immunoblotted with appropriate antibodies (dilution 1:200, Fig. 42 and 43). Myc-CDK2AP1, Myc-EIF3G and Myc-SRPX fusion proteins were detected with mouse monoclonal anti-c-myc antibodies (dilution 1:200, Fig. 42), whereas HA-PELO fusion protein was probed with rabbit polyclonal anti-HA-tag antibodies (dilution 1:200, Fig. 43). Secondary antibodies were goat anti-mouse or goat anti-rabbit IgG conjugated with horseradish peroxidase, respectively. Immunoreactive polypeptides were then visualized by the SuperSignal® West Pico Chemiluminescent Substrate as previously described 2.2.12.7.

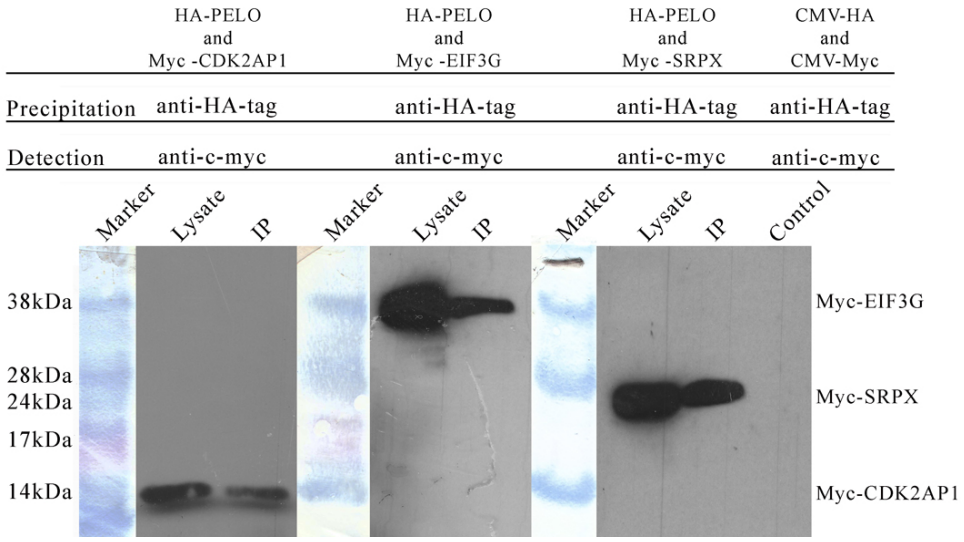

Fig. 42. Coimmunoprecipitation of PELO protein with putative interaction partners. HeLa cells were cotransfected with pCMV-HA-*PELO* and pCMV-Myc-*CDK2AP1,* pCMV-HA-*PELO* and pCMV-Myc-*EIF3G* or CMV-HA-*PELO* and CMV-Myc-*SRPX* expression constructs. Fusion proteins were coimmunoprecipitated using anti-HA-tag antibodies and visualized by Western blot analysis using anti-c-myc antibodies. In the left panel, an approximately 14 kDa Myc-CDK2AP1 fusion protein was detected by immunoblotting in the whole cell lysate and in the precipitation pellet (IP). In second panel, an approximately 38 kDa Myc-EIF3G fusion protein was detected by Western blot analysis both in cell lysate and in the precipitation pellet (IP). In third panel, an approximately 24 kDa Myc-SRPX fusion protein was visualized in the whole cell lysate as well as in the precipitation pellet (IP). Control panel shows a control experiment with cotransfection of pCMV-HA and

pCMV-Myc vectors. The whole cell lysate was incubated with dynabeads without cross-linking with antibodies, demonstrating that HA-tag and c-myc epitopes do not bind unspecific to the dynabeads. Lysate- the cell lysate before immunoprecipitation.

As shown in Figure 42, from total proteins of HeLa cells cotransfected with pCMV-HA-*PELO* and pCMV-Myc-*CDK2AP1* expression constructs, a 14 kDa Myc-CDK2AP1 fusion protein was coimmunoprecipitated together with HA-PELO using anti-HA-tag antibodies. The protein was visualized in Western blot using anti-c-myc antibodies. Similarly, from total proteins of HeLa cells cotransfected with pCMV-HA-*PELO* and pCMV-Myc-*EIF3G* or pCMV-HA-*PELO* and pCMV-*SRPX* expression constructs, the 38 kDa Myc-EIF3G or 24 kDa Myc-SRPX fusion proteins were coimmunoprecipitated together with HA-PELO using anti-HA-tag antibodies and visualized by immunobloting with anti-c-myc antibodies (Fig. 42).

For reverse coimmunoprecipitation HeLa cells were cotransfecred with pCMV-HA-*PELO* and pCMV-*CDK2AP1,* pCMV-HA-*PELO* and pCMV-Myc-*EIF3G* or pCMV-HA-*PELO* and pCMV-SRPX expression constructs. A 44 kDa HA-PELO fusion protein was coimmunoprecipitated together with Myc-CDK2AP1, Myc-EIF3G or Myc-SRPX fusion proteins using anti-c-myc antibodies. Protein was visualized in Western blot using anti-HA-tag antibodies (Fig. 43). No specific proteins were recognized in all precipitations of control (Fig. 42 and 43).

In conclusion, coimmunoprecipitation assays confirmed interactions between PELO and: CDK2AP1, EIF3G and SRPX.

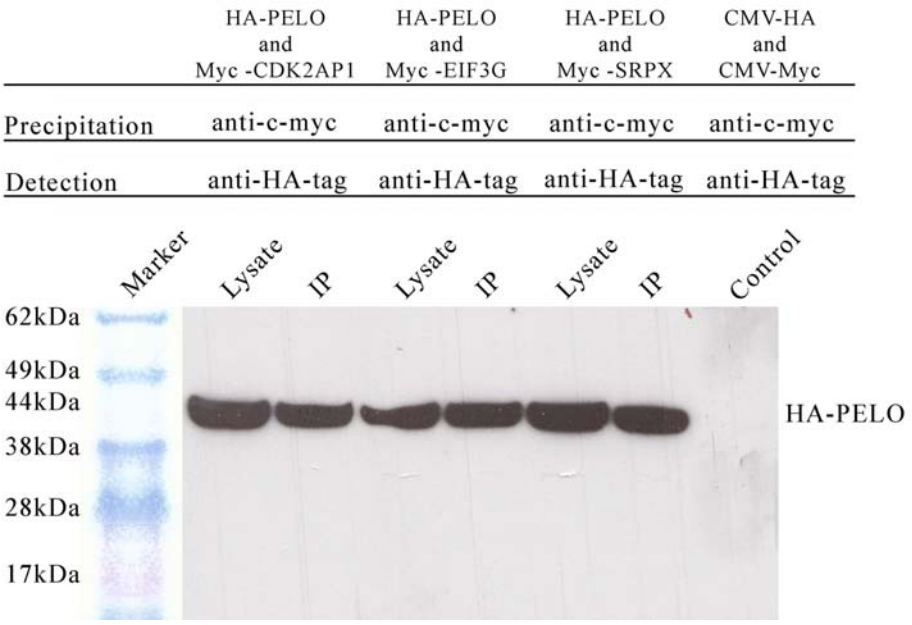

Fig. 43. Coimmunoprecipitation of PELO protein with putative interaction partners. HeLa cells were cotransfected with appropriate pair of expression constructs: pCMV-HA-*PELO* and pCMV-Myc-*CDK2AP1*,

pCMV-HA-*PELO* and pCMV-Myc-*EIF3G,* or pCMV-HA-*PELO* and pCMV-Myc-S*RPX.* An approximately 44 kDa HA-PELO fusion protein was coimmunoprecipitated using anti-c-myc antibodies and visualized by Western blot analysis using anti-HA-tag antibodies (panels I-III). Control panel shows a control experiment with cotransfection of pCMV-HA and pCMV-Myc vectors. The whole cell lysate was incubated with dynabeads without cross-linking with antibodies, demonstrating that HA-tag and c-myc epitopes do not bind unspecific to the dynabeads. Lysate, the cell lysate before immunoprecipitation.

3.3.3. Mapping of PELO interaction domains

PELO protein contains three eEF1α-like domains: eEF1_1 (1-131 aa), eEF1_2 (136-268 aa) and eEF1_3 (271-371 aa), and a putative leucine zipper motif which is located at the C-terminus (Fig. 44). To determine the regions of PELO protein involved in binding to CDK2AP1, EIF3G and SRPX proteins, several Glutathione S-transferase-*PELO* (GST-*PELO*) deletion constructs (Fig. 45) were generated and fusion proteins were overexpressed in *E. coli.* GST-PELO truncated fusion proteins were isolated and tested for ability to bind to the interaction partners of PELO in the GST Pull-down assay.

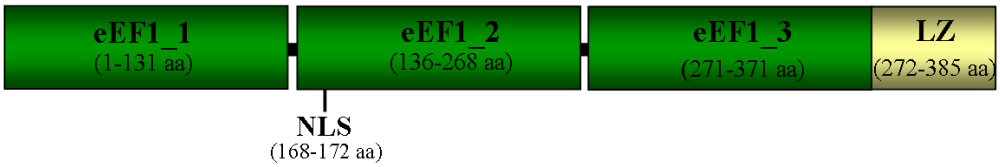

Fig. 44. Schematic representation of PELO protein structure. PELO protein contains three eEF1α-like domains, nuclear localization signal (NLS) and leucine zipper (LZ) motif. NLS is located at residues 168-172 and LZ motif is located at the C-terminus of PELO protein.

3.3.3.4.Construction of GST-*PELO*ΔeEF1_1 and GST-*PELO*ΔeEF1_3 expression constructs

To generate GST-*PELO*ΔeEF1_1 expressing construct (Fig. 45B), fragment encoding PELOΔeEF1_1 (136-385 aa) was amplified from human *PELO* cDNA using Pelo_pET_F2 and Pelo_pET_R primers. These primers contained *Eco*RI or *Xho*I restriction site at the 5'-ends, respectively. A 0.75-kb PCR product was further cloned into the pGEM-T Easy vector and sequenced. Then, clone containing correct insert sequence was digested with *Eco*RI and *Xho*I restriction enzymes and 0.75-kb *Eco*RI/*Xho*I fragment was inserted in frame into pET-41a (+) expression vector.

To construct GST-*PELO*ΔeEF1_3 expression plasmid (Fig. 45D), cDNA fragment encoding PELOΔeEF1_3 (1-268 aa) was amplified from human *PELO* cDNA using primers

Pelo_pET_F and Pelo_pET_R2. A 0.8-kb PCR fragment containing *Eco*RI and *Xho*I restriction sites was subcloned into pGEM-T Easy vector and sequenced. Subsequently, the 0.8-kb *Eco*RI/*Xho*I fragment was isolated and cloned in frame into pET-41a (+) expression vector.

Both generated constructs (GST-PELOΔeEF1_1 and GST-PELOΔeEF1_3) were sequenced by enzymatic cycle sequencing to confirm the identity, the orientation and frame of the inserts.

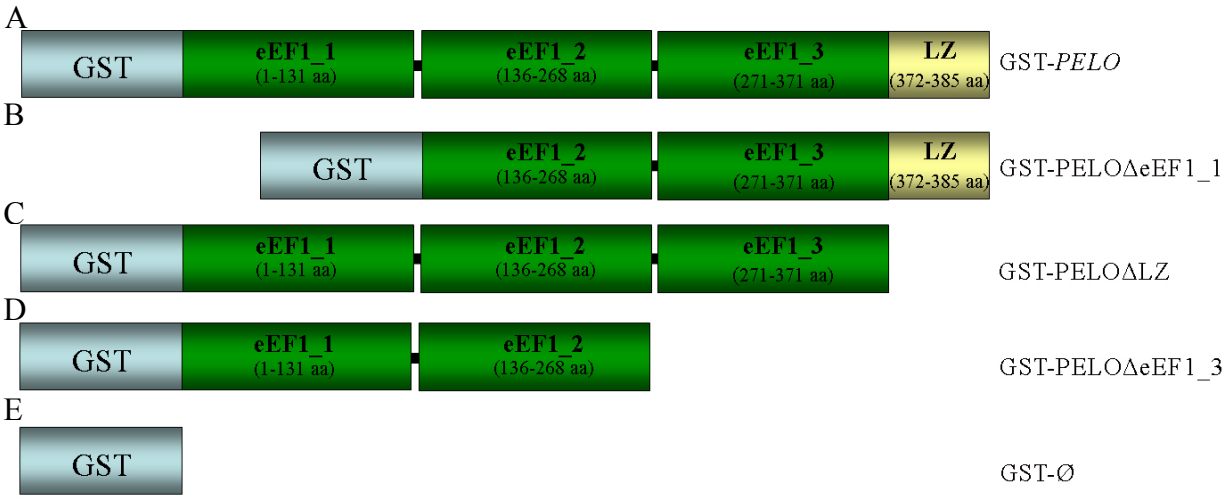

Fig. 45. Schematic representation of the constructs used for the expression of the recombinant GST-PELO fusion protein. GST-*PELO* (A) and GST-Ø (B) constructs were generously provided by L. Ebermann (Ebermann 2005). GST-PELOΔLZ (C) construct was kindly provided by N. Kirchenmayer (Kirchenmayer 2007). GST-PELOΔeEF1_1 (B) and GST-PELOΔeEF1_3 (D) constructs were generated by amplification of defined cDNA fragments and cloning them in the *Eco*RI/*Xho*I sites of the pET41a(+) expression vector. GST, Glutathione S-transferase; eEF1_1, eEF1α-like domain 1st, eEF1_2, eEF1α-like domain 2nd; eEF1_3, eEF1α-like domain 3rd; LZ, leucine zipper motif.

3.3.3.5. Generation and purification of GST-PELOΔeEF1_1 and GST-PELOΔeEF1_3 fusion proteins

GST-*PELO*ΔeEF1_1 and GST-*PELO*ΔeEF1_3 fusion constructs (Fig. 45B and D) were separately transformed (2.2.6) into competent cells BL21 and the protein expression was induced by addition of IPTG (2.2.13.1). Subsequently, recombinant GST-fusion proteins were purified from bacterial cell extract using the GST-binding kit (2.2.13.2). The expected 63 kDa GST-PELOΔeEF1_1 and 67 kDa GST-PELOΔeEF1_3 fusion proteins were electrophoresed

on SDS-PAGE gel (2.2.12.4) and visualized by Coomassie blue staining (2.2.12.6, Fig. 46). Purified GST-PELO fusion proteins were used for GST Pull-down assay.

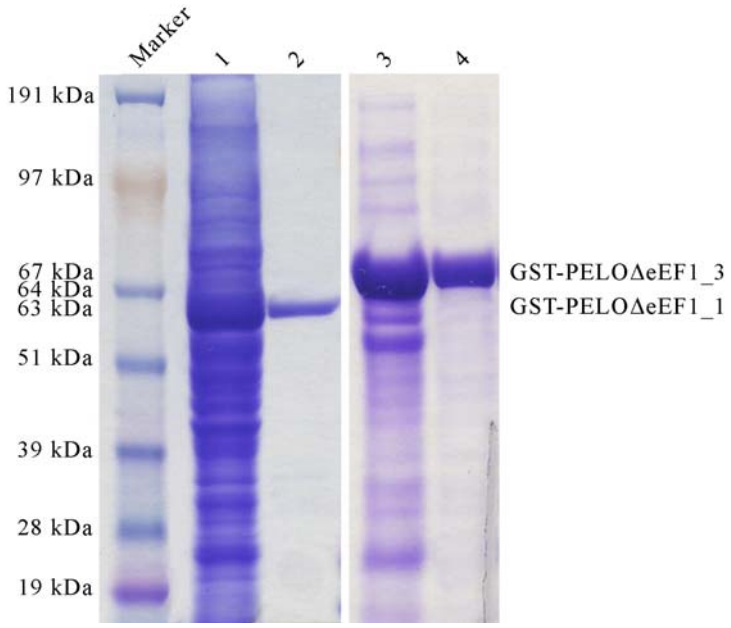

Fig. 46. SDS- PAGE gel analysis of GST-PELOΔeEF1_1 and GST-PELOΔeEF1_3 fusion proteins purified using GST-binding kit. 1, total cell proteins from an induced GST-PELOΔeEF1_1 sample; 2, purified GST-PELOΔeEF1_1 protein; 3, total cell proteins from an induced GST-PELOΔeEF1_3 sample; 4, purified GST-PELOΔeEF1_3 protein; GST, Glutathione S-transferase.

3.3.3.6. GST Pull-down assay

To determine which domain of PELO protein (Fig. 44) is responsible for binding to CDK2AP1, EIF3G and SRPX proteins, GST-PELO truncated fusion proteins (Fig. 45 and 46) were tested for ability to bind to the Myc-CDK2AP1, Myc-EIF3G and Myc-SRPX fusion proteins (Fig. 39) in the GST Pull-down assay. In all experiments purified GST protein was used as a negative control and purified GST-PELO fusion protein (containing full-length PELO) - as a positive control. Myc-CDK2AP1, Myc-EIF3G and Myc-SRPX fusion proteins were isolated (2.2.12.2) from HeLa cells transiently transfected (2.2.15.4) with pCMV-Myc-*CDK2AP1*, pCMV-Myc-*EIF3G* or pCMV-Myc-*SRPX* expression constructs, respectively (2.2.15.4; Fig. 39). The in vitro GST Pull-down assay was performed as described previously (2.2.14.1). Briefly, purified GST, GST-PELO, GST-PELOΔLZ, GST-PELOΔeEF1_1 or GST-PELOΔeEF1_3 fusion proteins were immobilized onto glutathione resin. Subsequently, these resin-bound GST or GST-fusion proteins were incubated with cellular lysate from HeLa cells transiently transfected with CMV-Myc-*CDK2AP1*, CMV-Myc-*EIF3G* or CMV-Myc-*SRPX*

constructs. After GST Pull-down, proteins remaining on the beads were resuspended with SDS sample buffer, separated by SDS-PAGE (2.2.12.4) and analyzed by Western blotting (2.2.12.5) using anti-c-myc primary antibodies (dilution 1:200) and goat anti-mouse IgG conjugated with horseradish peroxidase secondary antibodies. Immunoreactive polypeptides were then visualized by the SuperSignal® West Pico Chemiluminescent Substrate as previously described 2.2.12.7 (Fig. 47).

As shown in Fig. 47, GST-PELO, GST-PELOΔLZ and GST-PELOΔeEF1_1 recombinant proteins exhibited strong binding to 14 kDa Myc-CDK2AP1, 38 kDa Myc-EIF3G and 24 kDa Myc-SRPX fusion proteins, whereas GST-PELOΔeEF1_3 truncated fusion protein showed no interaction with above mentioned proteins. Therefore, we believe that the third eEF1α-like domain of PELO protein (eEF1_3; 271-371 aa) is responsible for the interaction with partner proteins. In the negative control of GST Pull-down assay, the GST protein was not bound to Myc-CDK2AP1, Myc-EIF3G or Myc-SRPX fusion proteins. This control confirmed specificity of GST-PELO Pull-down assay.

In conclusion, GST PELO Pull-down assay further confirmed interactions between PELO and: CDK2AP1, EIF3G and SRPX proteins, and also demonstrated that all three interaction partners bind to the same region of PELO protein (Fig. 47).

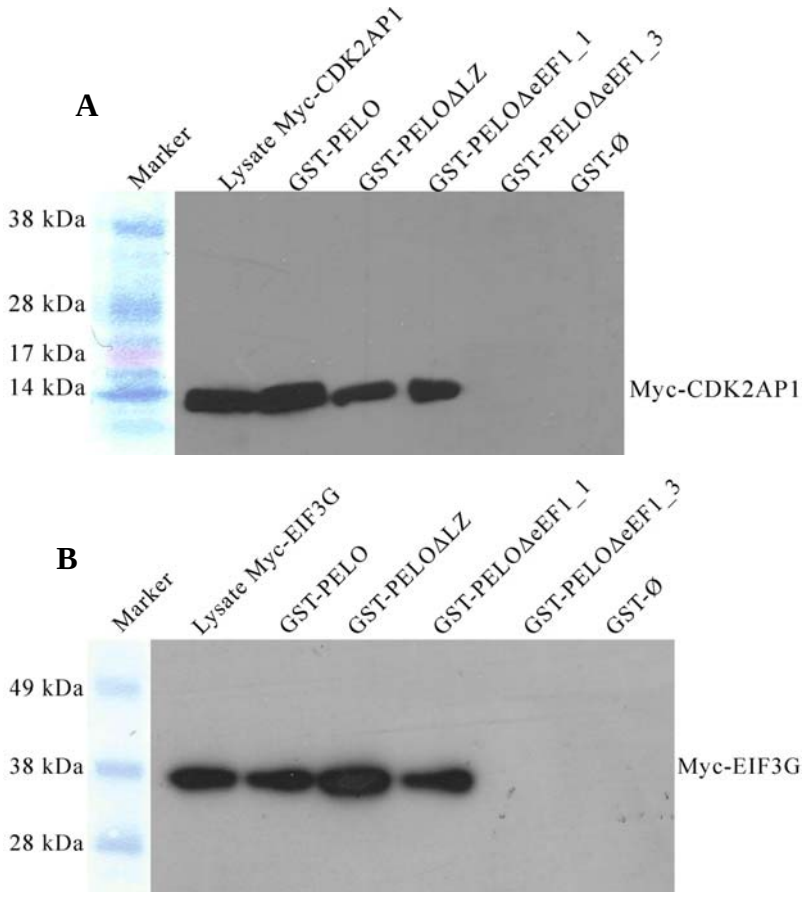

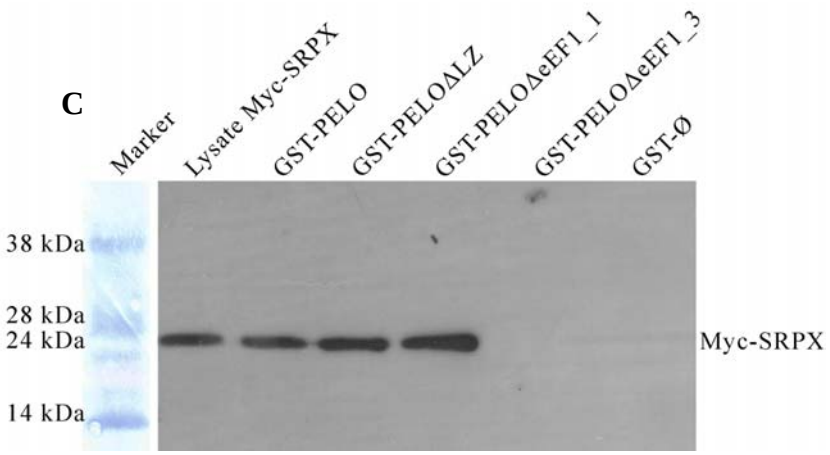

Fig. 47. GST Pull-down assay to determine the region of PELO protein involved in binding to CDK2AP1, EIF3G and SRPX proteins. GST-Ø, full-length and truncated GST-PELO fusion proteins (Fig. 45) coupled to glutathione–agarose beads were separately incubated with cellular lysate from HeLa cells transiently transfected with CMV-Myc-*CDK2AP1* (A), CMV-Myc-*EIF3G* (B) or CMV-Myc-*SRPX* (C) constructs. After incubation and several washing steps, the bound complexes were analyzed by SDS-PAGE and Western blotting using anti-c-myc antibodies. 14 kDa Myc-CDK2AP1 (A), 38 kDa Myc-EIF3G (B) and 24 kDa Myc-SRPX (C) fusion proteins were coprecipitated with GST-PELO, GST-PELOΔLZ and GST-PELOΔeEF1_1 recombinant proteins but they were not coprecipitated with GST- PELOΔeEF1_3 truncated fusion protein and with negative control (A-C). GST-Ø, negative control (only GST protein), GST-PELO, fusion protein containing full-length of PELO; GST-PELOΔLZ; truncated fusion proteins with deleted LZ motif; GST-PELOΔeEF1_1, truncated fusion proteins with deleted first eEF1α-like domain; GST-PELOΔeEF1_3, truncated fusion proteins with deleted last eEF1α-like domain; LZ, leucine zipper motif. Lisate, the cell lisate before GST Pull-down.

3.3.4. Direct visualization of PELO protein interactions using Bimolecular Fluorescence Complementation (BiFC) assay

To further support the specificity of the interactions between PELO and: CDK2AP1, EIF3G or SRPX and to determine the cellular localization of the interacting proteins, bimolecular fluorescence complementation (BiFC) assay was performed. BiFC assay has been developed for the simple and direct visualization of protein interactions in living cells (Hu *et al.* 2002). It is based on the principle of protein fragment complementation, in which an enhanced green fluorescent protein (EGFP) is divided into two parts. Each fragment itself is not fluorescent. These two fragments are fused with putative interaction partners and when the two partners interact, the two non-fluorescent fragments are brought into proximity and an intact fluorescent protein is reconstituted (Fig. 48). Hence, the reconstituted fluorescent signals reflect the interaction of two fused proteins under study. This method enables visualization of the subcellular locations of specific protein interactions in the normal cellular environment.

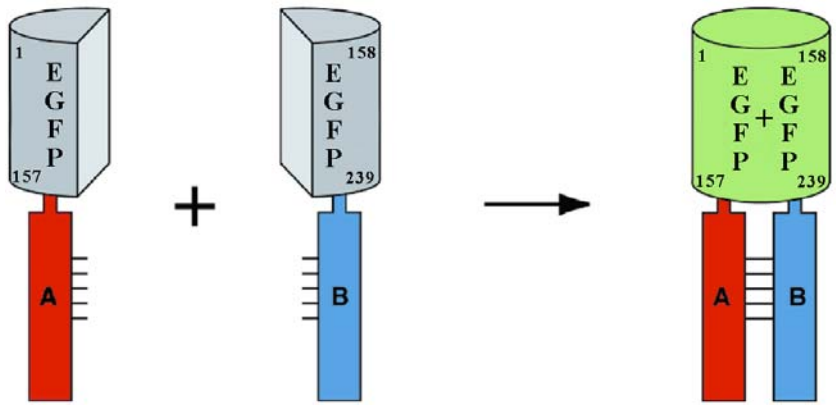

Fig. 48. Schematic representation of the principle of the BiFC assay. Two nonfluorescent fragments (EGFP$^{1\text{-}157\ aa}$ and EGFP$^{158\text{-}239\ aa}$) of the Enhanced Green Fluorescent Protein (EGFP) are fused to putative interaction partners (A and B). The association of the interaction partners allows formation of a bimolecular fluorescent complex.

3.3.4.1. Generation of EGFP expression constructs used for BiFC assay

Vectors (FPCA-V1 and FPCA-V2) used for construction of BiFC constructs were generated and kindly provided by Prof. Dr. S. Hoyer-Fender (Department of Developmental Biology GZMB, University of Göttingen, Göttingen) and they contain fragments of EGFP molecule which was split between amino acid 157 and 158.

Vector FPCA-V1 (CMV-EGFP-V1) was generated on backbone of pEGFP-N1 vector. It contains the sequence encoding COOH -terminal fragment of enhanced green fluorescent protein (EGFP 158-239 aa) which was placed downstream of the multiple cloning site (MCS) (Fig. 49A).

Vector FPCA-V2 (CMV-EGFP-V2) was generated on backbone of pQM-Ntag/B vector and it contains sequence encoding the NH_2-terminal fragment of enhanced green fluorescent protein (EGFP 1-157 aa). This fragment of EGFP was introduced upstream of the multiple cloning site (MCS) (Fig. 49B).

In both vectors, spacers were inserted between the MCS and the EGFP fragments to ensure that the orientation and arrangement of the fusions in space are optimal to bring the GFP fragments into close proximity.

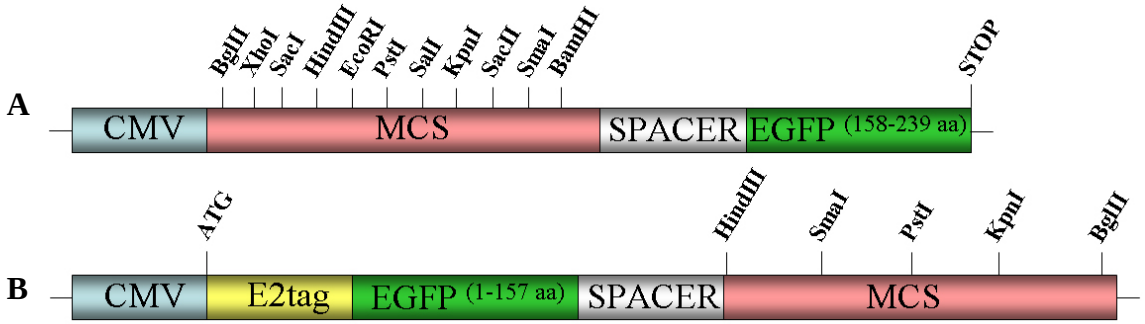

Fig. 49. Structure of FPCA-V1 (A) and FPCA-V2 (B) vectors used for generation of BiFC constructs. They contain fragment of EGFP molecule which was split between amino acid 157 and 158. ATG, translation initiation codon; CMV; CMV promoter; EGFP, enhanced green fluorescent protein; MCS, a multiple cloning site; STOP, translation termination codon.

To generate CMV-*PELO*-*EGFP*-V1 construct (Fig. 50A), human *PELO* cDNA was amplified (2.2.14.3) from human testis RNA using specific primers HPELO_LVF2 and HPELO_LVR2. A 1.1-kb *PELO* ORF fragment containing ATG codon and *Xho*I and *Bam*HI restriction sites was subcloned into pGEM-T Easy vector and sequenced. Subsequently, the 1.1-kb *Xho*I/*Bam*HI fragment was isolated and cloned in frame into the CMV-EGFP-V1 vector (Fig. 49A). Nucleotide sequence of generated CMV-*PELO*-*EGFP*-V1 construct (Fig. 50A) was confirmed by sequencing.

To generate CMV-*EGFP*-*CDK2AP1*-V2, CMV-*EGFP*-*EIF3G*-V2 and CMV-*EGFP*-*SRPX*-V2 constructs (Fig. 50B, C, D; respectively) primer pairs: CDK2AP1_LF/CDK2AP1_LR, EIF3G_LF/EIF3G_LV or SRPX_LR/SRPX_LR were used. The amplified cDNA fragments containing coding sequence of *CDK2AP1* (full-length, 1-115 aa), *EIF3G* (full-length,1-320 aa) or *SRPX* (265-464 aa) and STOP codon were subcloned into pGEM-T Easy vector, sequenced, cut out with *Hind*III and *Bgl*II restriction enzymes and then inserted in frame into CMV-EGFP-V2 vector (Fig. 49B). Nucleotide sequences of generated CMV-*EGFP*-*CDK2AP1*-V2, CMV-*EGFP*-*EIF3G*-V2 and CMV-*EGFP*-*SRPX*-V2 constructs (Fig. 50B, C, D; respectively) were confirmed by sequencing.

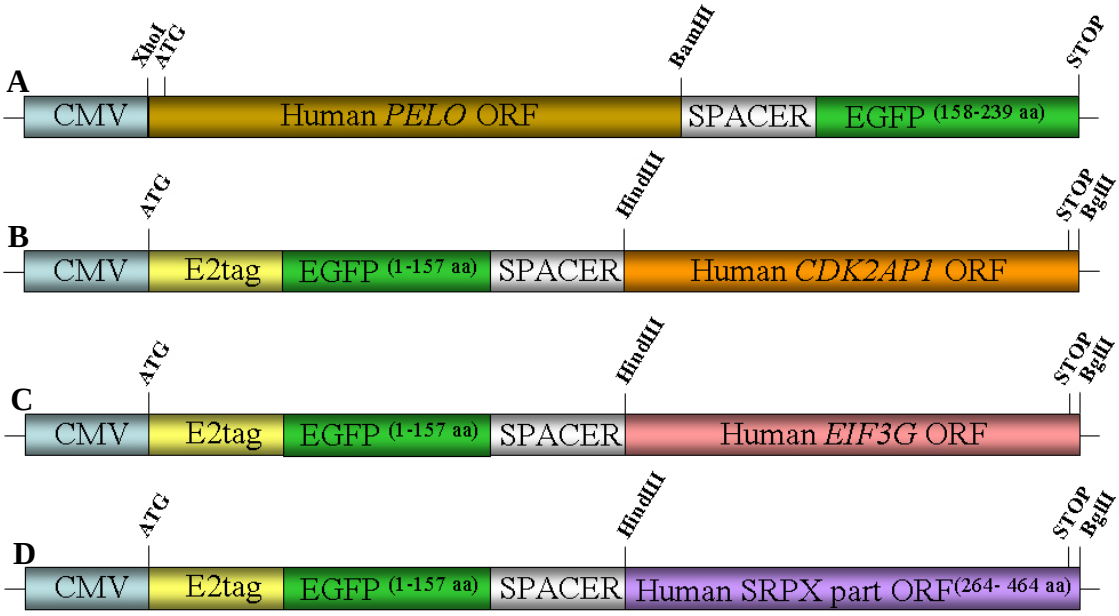

Fig. 50. Schematic representation of CMV-*PELO*-*EGFP*-V1 (A), CMV-*EGFP*-*CDK2AP1*-V2 (B), CMV-*EGFP*-*EIF3G*-V2 (C) and CMV-*EGFP*-*SRPX*-V2 (D) constructs used for BiFC assay. The cDNA sequence containing the ORF of human PELO without STOP codon was cloned in frame into the CMV-EGFP-V1 vector (A). The amplified cDNA fragments containing the ORF of CDK2AP1 (full-length, 1-115 aa, Fig. 50B), EIF3G (full-length, 1-320, Fig. 50C) or SRPX (part, 264-464 aa, Fig. 50D) without ATG codon were subcloned in frame into CMV-EGFP-V2 vector. Fusion proteins were expressed under the control of human cytomegalovirus promoter (CMV). ATG, translation initiation codon; EGFP, enhanced green fluorescent protein; ORF, open reading frame; STOP, translation termination codon.

3.3.4.2. Determination of subcellular localization of PELO-CDK2AP1, PELO-EIF3G and PELO-SRPX interaction complexes using BiFC assay

To determine cellular localization of the PELO-CDK2AP1, PELO-EIF3G or PELO-SRPX protein complexes in normal cellular environment, BiFC assay was performed. Human HeLa cells were cultured onto coverslips (2.2.15) and transiently cotransfected (2.2.15.4) with: CMV-*PELO*-*EGFP*-V1 and CMV-*EGFP*-*CDK2AP1*-V2, CMV-*PELO*-*EGFP*-V1 and CMV-*EGFP*-*EIF3G*-V2 or CMV-*PELO*-*EGFP*-V1 and CMV-*EGFP*-*SRPX*-V2 BiFC expression constructs, respectively (Fig. 50). After 24 hrs incubation at 37°C, transfected cells were moved to 30°C and let for 2 hrs. Next, the formation of the green fluorescent complexes was examined using standard fluorescence microscopy (Fig. 51A-I). To prove that fluorescent-protein fragments are not able to associate with each other efficiently in the absence of an interaction between the proteins that are fused to these fragments, negative control was performed. HeLa cells were transiently cotransfected with CMV-*PELO*-*EGFP*-V1 and CMV-

EGFP-COPS5-V2 BiFC expression construct and 24 hrs later, they were incubated 2 hrs at 30°C and observed under fluorescence microscope (Fig. 51J-L). COPS5 (COP9 constitutive photomorphogenic homolog subunit 5) is one of the eight subunits of COP9 signalosome, a highly conserved protein complex that functions as an important regulator in multiple signaling pathways (Bech-Otschir *et al.*; 2001; Tomoda *et al.,* 2002). PELO is not involved in these pathways (Kirchenmayer, 2005).

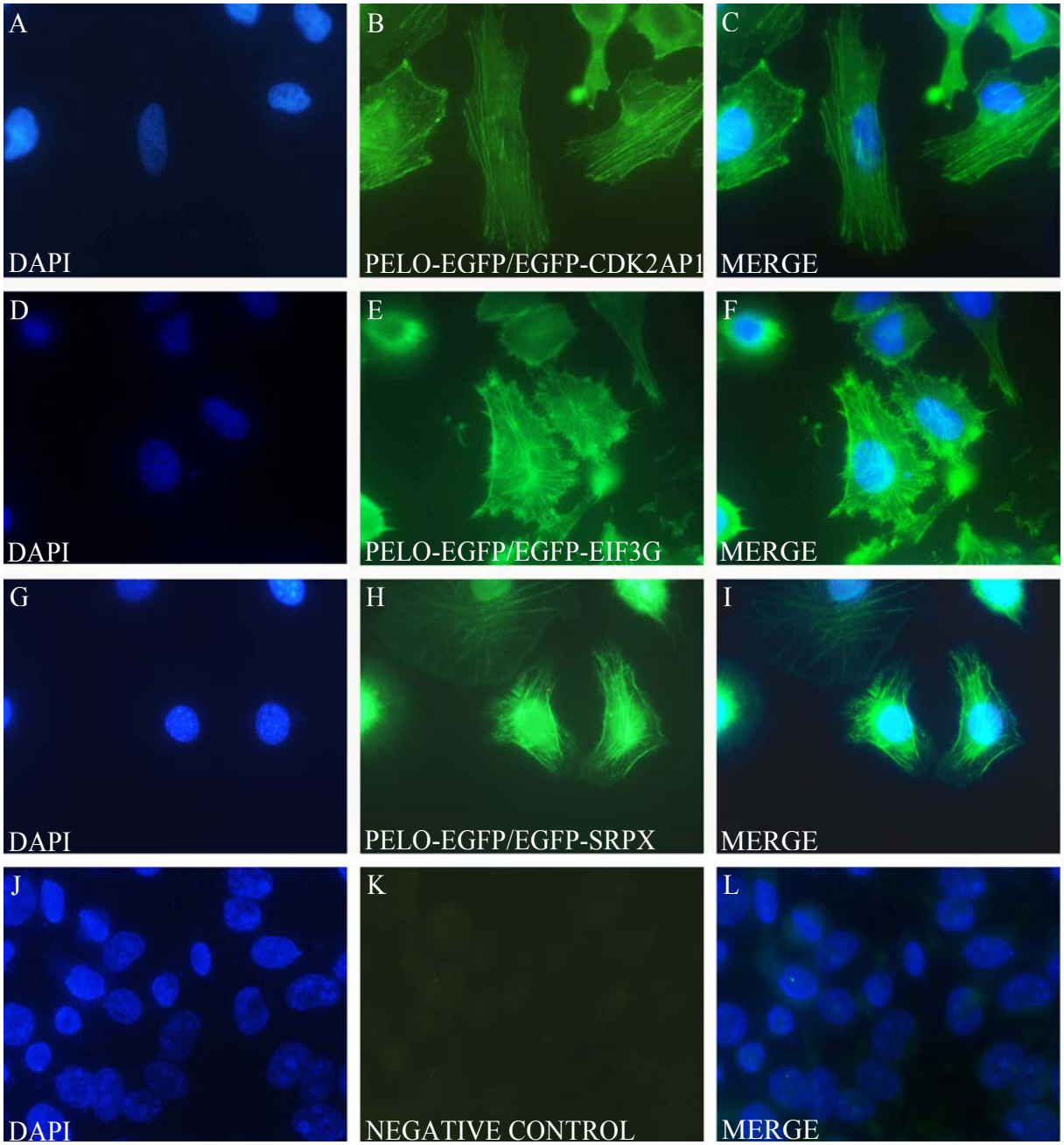

Fig 51. Determination of subcellular localization of PELO-CDK2AP1, PELO-EIF3G or PELO-SRPX interaction complexes using BiFC assay. HeLa cells were transiently cotransfected with: CMV-*PELO-EGFP*-V1 and CMV-*EGFP-CDK2AP1*-V2 (A-C), CMV-*PELO-EGFP*-V1 and CMV-*EGFP-EIF3G*-V2 (D-F) or CMV-*PELO-EGFP*-V1 and CMV-*EGFP-SRPX*-V2 (G-I) BiFC expression constructs. Twenty-four hours after transfection

cells nuclei were counterstained with DAPI (blue) and the green fluorescence emissions of the cells were analyzed under the fluorescence microscope. The images are representative of greater than 90% of the fluorescent cells in each population. The transiently cotransfected cells exhibited bright green fluorescence that was localized to cytoplasm and cytoskeleton (B, C, E, F, H, I). Negative control proved specificity of our BiFC assay (J-L). A-L, 60-fold magnification; EGFP, enhanced green fluorescent protein; negative control, HeLa cells transiently cotransfected with CMV-PELO-EGFP-V1 and CMV-EGFP-COPS5-V2 constructs.

As shown in Figure 51 A-I, green fluorescence signal was localized at the cytoskeleton and cytoplasm of the HeLa cells transiently cotransfected with: CMV-PELO-EGFP-V1 and CMV-EGFP-CDK2AP1-V2, CMV-PELO-EGFP-V1 and CMV-EGFP-EIF3G-V2 or CMV-PELO-EGFP-V1 and CMV-EGFP-SRPX-V2, respectively.

Negative control (Fig. 51J-L) exhibited no detectable fluorescence. It confirmed that the observed positive green signal depends on the physical interaction between PELO and CDK2AP1, EIF3G or SRPX proteins.

In conclusion, BiFC assay further proved the specificity of the interactions between PELO and: CDK2AP1, EIF3G or SRPX proteins, and also demonstrated that all three interaction partners form a protein complex with PELO in the cytoskeleton and maybe in the cytoplasm (Fig. 51). It should be noted that CDK2AP1, EIF3G and SRPX do not interact with each other (data not shown).

3.4. Mouse *Eif3g* gene

3.4.1. Expression analysis of mouse *Eif3g* gene by RT-PCR

In order to study the expression pattern of mouse *Eif3g* gene, RT-PCR analysis was performed with total RNA isolated from different adult mouse tissues (brain, testis, colon, stomach, spleen, heart, kidney, muscle, ovary, lung, and liver), and from embryos at different developmental stages (E9.5 to E15.5) (2.2.1.3). RT-PCR was performed using primers Eif3g-F1 and Eif3g-R1, which amplify 1-kb fragment of *Eif3g* gene. To exclude genomic contamination, our primers for RT-PCR were located in two different exons (exon 1 and 11). The quality of the RNA was proved by amplification of a 250-bp fragment of HPRT transcript (Fig. 52A, B).

RT-PCR analysis with total RNA and *Eif3g*-specific primers showed the presence of a 1-kb amplified fragment in all of the investigated tissues (Fig. 52A), and in all tested prenatal developmental stages (starting from E9.5 to E15.5) (Fig. 52B). These results suggest that the *Eif3g* transcript is expressed ubiquitously.

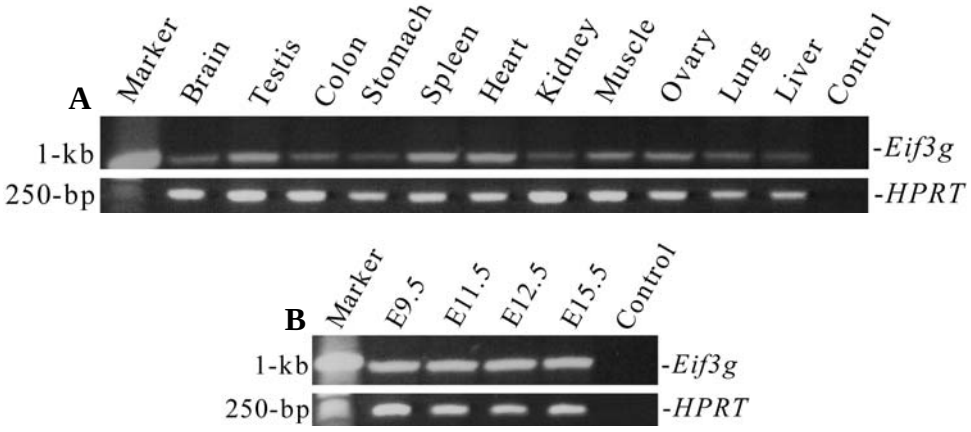

Fig. 52. RT-PCR expression analysis of *Eif3g* in different tissues **(A)**, and prenatal developmental stages **(B)**. *Eif3g*-specific primers Eif3g-F1 and Eif3g-R1 were used to amplify a 1-kb fragment of *Eif3g* gene. Expression was detected in all of examined tissues and in all studied stages of embryos. RT-PCR for HPRT transcript was performed as positive control of RNA quality. Control: negative control (no-template probe).

3.4.2. Targeted inactivation of mouse *Eif3g* gene

One of the best ways to elucidate gene function is generation of a knock-out animal model. For this purpose, *Eif3g* knock-out construct was generated in this study.

3.4.2.1. Identification of a BAC clone containing *Eif3g* genomic DNA from mouse C57BL/6J BAC library

Screening of a 129/Sv genomic mouse library (129/ola mouse cosmid, 121, RZPD, Berlin) using probes localized in 5' region (Eif3g_5 probe) and 3' region (Eif3g_3 probe) of *Eif3g* gene did not identify any positive genomic clone. Therefore, we have decided to generate *Eif3g* knock-out construct using genomic clone from the C57BL/6J strain. The mouse genome was sequenced from C57BL/6J and BAC clones containing the gene of interest could be simply identified. Clone RPCIB731H22369Q from RPCI-23 mouse BAC library was identified (http://genome.ucsc.edu) and ordered from the Resource Center and Primary Database (RZPD, Berlin).

To prove that ordered clone contains *Eif3g* genomic DNA, Southern blot analysis was performed. BAC clone was digested with *ApaI* restriction enzyme and blotted on Hybond-XL membrane. Then, the membrane was separately hybridized with 363-bp Eif3g_5 probe located in exon 1, and 586-bp Eif3g_3 probe located in exons 9 to 11 of *Eif3g* gene (Fig. 53). These probes were performed by PCR using the primers eIF3F1anew and eIF3R1anew for the Eif3g_5 probe and eIF3F2 and eIF3R2 for the Eif3g_3 probe, and genomic DNA from C57BL/6J mice as a template. Southern blot analysis and comparison of its results with known genomic structure revealed that clone RPCIB731H22369Q contains the EIF3G gene and can be used for generation of *Eif3g* knock-out construct (Fig. 53).

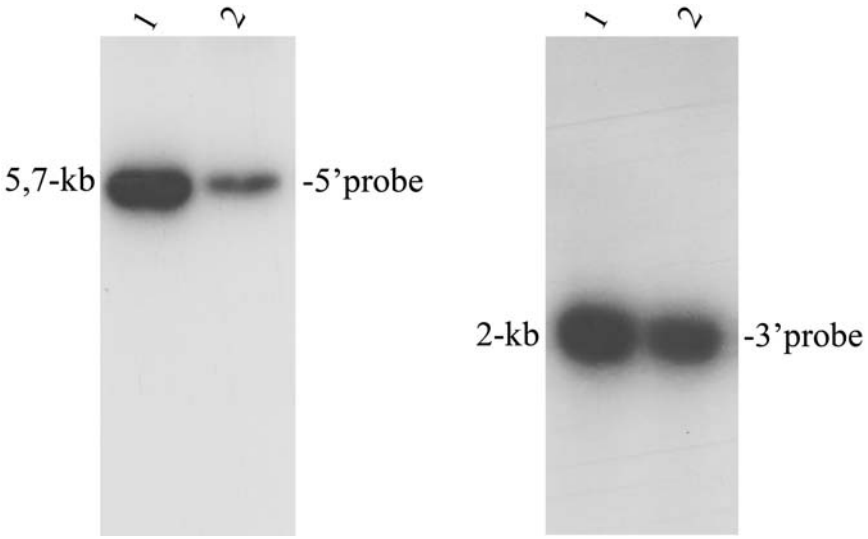

Fig. 53. Southern blot analysis of clone RPCIB731H22369Q. BAC clone was digested with *ApaI* and hybridized with 363-bp Eif3g_5 probe located in exon 1 (A) and 586-bp Eif3g_3 probe located in exons 9 to 11 (B). Southern blot hybridization confirmed that BAC clone is positive.1, BAC clone; 2, BAC clone diluted 1:10.

3.4.2.2. Construction of the *Eif3g* knock-out construct

In order to generate the *Eif3g* targeting construct, a 2.4-kb *Not*I/*Bam*HI fragment containing a sequence of exons 1 to 5 was deleted and replaced by *Neomycin phosphotransferase* gene cassette (*neo*^{r}) under the control of the *Phosphoglycerate kinase (Pgk)* promoter (Fig. 54). Deletion of exon 1, which contains the translation initiation site ATG, is predicted to generate a null allele. Introduction of a negative selection marker, the *Herpes simplex virus thymidine kinase* (Tk) gene, at the 3' end of the construct (Fig. 54) enabled us to use negative selection (Mansour *et al.,* 1998) for the proper homologous recombination event.

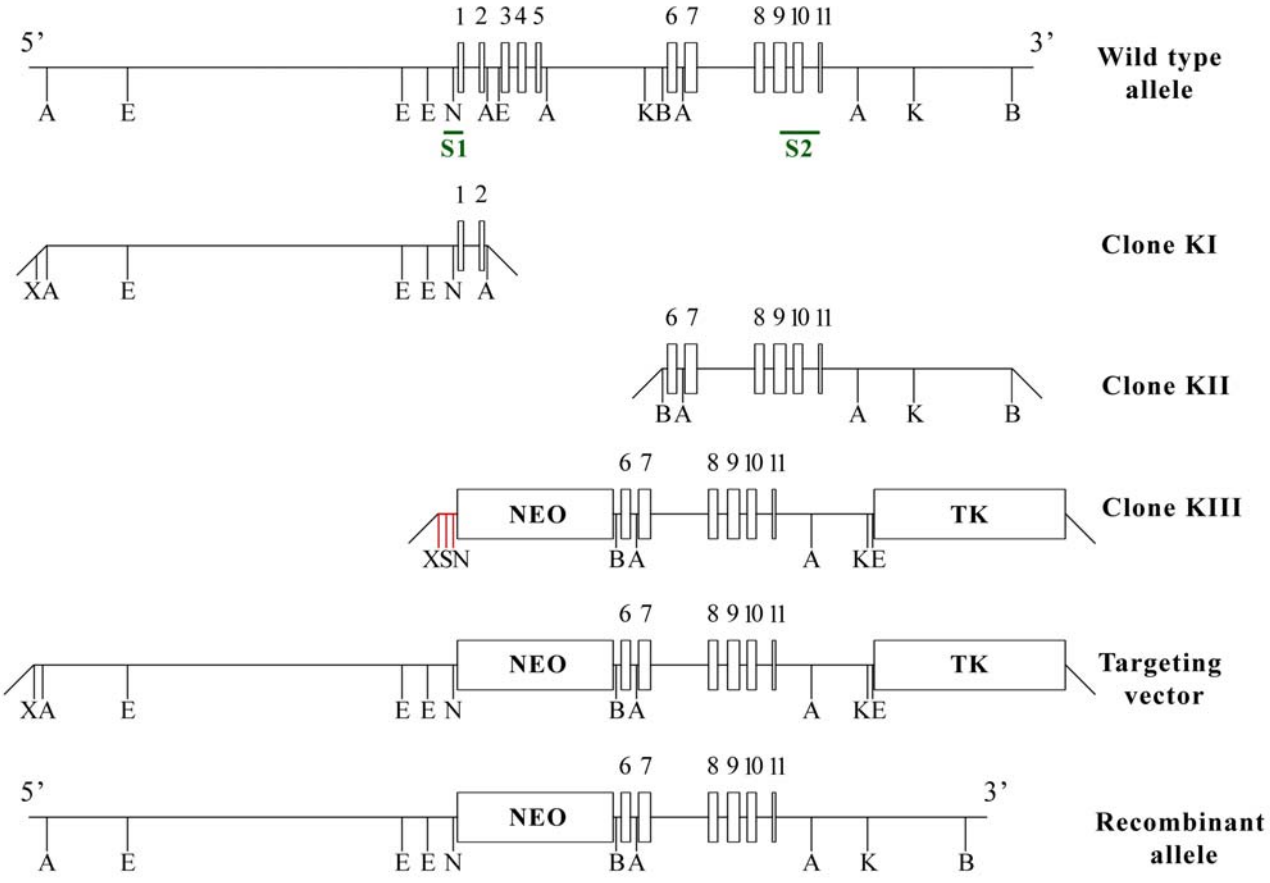

Fig. 54. Schematic representation of the targeting strategy. The structures of the wild type allele, targeting vector, and recombinant allele are shown together with the relevant restriction sites. The construct contains 5.5-kb of the 5'and 3-kb of the 3' region of *Eif3g* gene. A *pgk-neo* selection cassette (NEO) replaced a 2.4-kb *Not*I/*Bam*HI fragment containing exons 1 to 5. The 5' and 3' probes (S1 and S2, respectively) used to identify positive clones in colony hybridization are shown. Strategy to subclone the 5'and 3' flanking regions of the *Eif3g* gene in the pPNTvector (clones KI to KIII) is also shown. Modified multicloning site of pPNT vector is marked by red line. Abbreviations: TK, *Thymidine kinase* cassette; 1-11, exons 1-11; S1, Eif3_5 probe; S2, Eif3_3 probe; A, *Apa*I; B, *Bam*HI; E, *Eco*RI; K, *Kpn*I; N, *Not*I; S, *Sal*I; X, *Xho*I.

3.4.2.2.1. Modification of the cloning site of the pPNT vector

To introduce (in a proper 5'-3' orientation) a 5.5-kb *Xho*I/*Not*I fragment of clone KI (Fig. 54) into the pPNT vector (Tybulewicz *et al.,* 1991), a oligonucleotide adaptor (red line in Fig. 54, and Fig. 55) containing sequence of *Not*I*-*Xho*I-*Sal*I-*Not*I-*Xho*I* restriction sites was generated. In this adaptor at 5' and 3' end were located modified *Not*I* and *Xho*I* restriction sites, respectively. Sequence of *Not*I site was modified by changing the last guanine and cytosine to two adenines, whereas *Xho*I site was modified by replacement last cytosine by adenine (Fig. 55). After ligation with *Not*I/*Xho*I digested pPNT vector, these two altered by nucleotide substitutions sites were not longer recognized by restriction enzymes (Fig. 55). Modified pPNT vector (pPNT*) was purified and used to generate of the *Eif3g* knock-out construct.

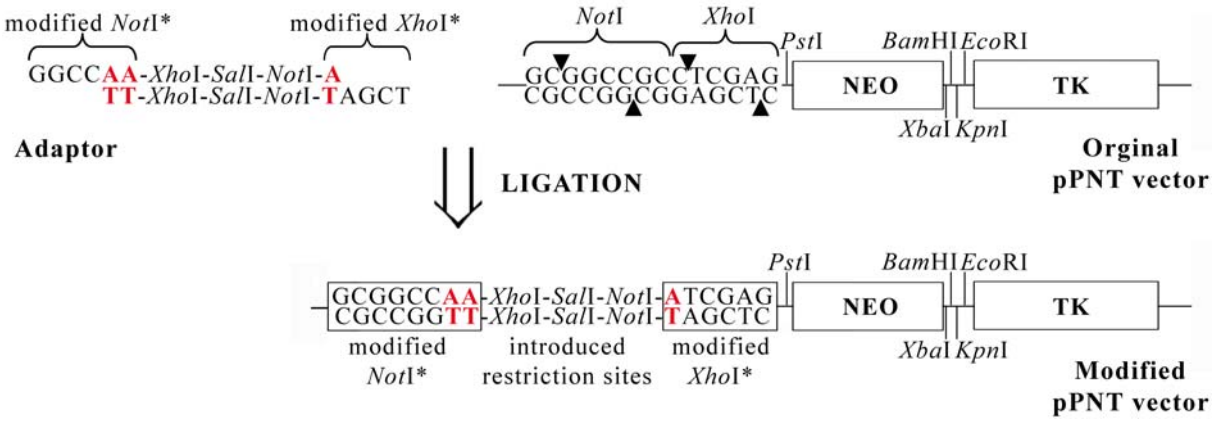

Fig. 55. Modification of the pPNT vector. To introduce (in a proper 5'-3' orientation) a 5.5-kb *Xho*I/*Not*I fragment of clone KI (Fig. 54) into the pPNT vector, a oligonucleotide adaptor containing the sequence of *Not*I*-*Xho*I-*Sal*I-*Not*I-*Xho*I* restriction sites was generated, annealed and ligated with *Not*I/*Xho*I digested pPNT vector. Orginal *Not*I and *Xho*I restriction sites located in pPNT vector were inactivated by nucleotide substitutions. *, modification. A, Adenine; C, Cytosine; G, Guanine, T, Thymine, TK; *Thymidine kinase* cassette, NEO, *Pgk-neo* selection cassette.

3.4.2.2.2. Subcloning of the 3' wing of the *Eif3g* knock-out construct into the modified pPNT vector

BAC clone (RPCIB731H22369Q) was digested with *Bam*HI restriction enzyme and restriction fragments were cloned into pZERO-2/*Bam*HI vector. Then, using the 586-bp Eif3g_3 probe (Fig. 54) a clone containing 4.2-kb *Bam*HI fragment (clone KII) was identified by colony hybridization. This 4.2-kb fragment contained exons 6 to 11 of the *Eif3g* gene. The

correct orientation of clone KII was confirmed by restriction digestion with *Kpn*I enzyme. As expected for clone in a proper 5'-3' orientation 4.5-kb and 3-kb fragments were obtained (data not shown). Then, a 3-kb *Bam*HI/*Kpn*I fragment was isolated from clone KII, purified from the agarose gel and cloned into *Bam*HI/*Kpn*I site of pPNT targeting vector (clone KIII; Fig. 54).

3.4.2.2.3. Subcloning of the 5' wing of the *Eif3g* knock-out construct into the modified pPNT vector

BAC clone (RPCIB731H22369Q) was digested with *Apa*I restriction enzyme and restriction fragments were inserted into pZERO-2/*Apa*I vector. Then, using the 363-bp Eif3g_5 probe (Fig. 54) a clone containing 5.7-kb *Apa*I fragment (clone KI) was identified by colony hybridization. This 5.7-kb fragment contained the 5'-flanking region with exon 1 of the *Eif3g* gene (Fig. 54). Restriction analysis with *Not*I enzyme confirmed correct orientation of clone KI. As expected for clone in a proper 5'-3' orientation 5.5-kb and 3.5-kb fragments were obtained (data not shown). The DNA of clone KI was further digested with *Xho*I/*Not*I enzymes and the 5.5-kb *Xho*I/*Not*I fragment was purified from the agarose gel and ligated with the *Xho*I/*Not*I digested clone KIII (Fig. 54). The resulting targeting construct (Eif3g-Neo-Tk) was subjected to multiple restriction analysis in order to confirm right orientation of both 5' and 3' wings (Fig. 56). Then, the construct was linearized at the unique *Xho*I site present at the 5´multiple cloning site and will be used for transfection of ES cells (2.2.16.1).

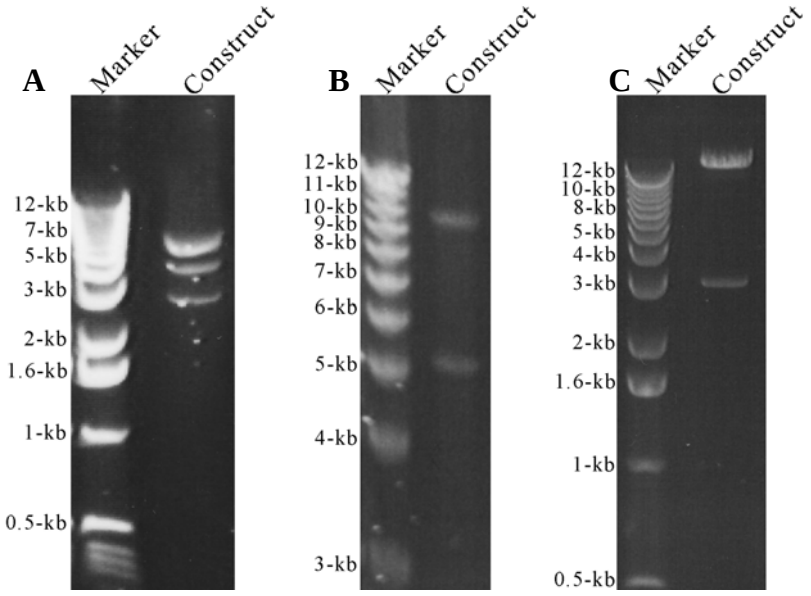

Fig. 56. Restriction analysis of the targeted vector *Eif3g*-Neo-Tk with *Eco*RI (A), *Xho*I/*Not*I (B) and *Bam*HI/*Kpn*I (C) restriction enzymes to confirm the correct orientation of the 5'and 3' fragments of the *Eif3g*

gene in pPNT vector. For the restriction enzymes sites location, please refer to Figure 52. (A) As expected by *Eco*RI digestion 6.7-kb, 5.1-kb, 3.7-kb and 0.3-kb fragments were obtained. (B) A correct site of 5' wing was confirmed by *Xho*I/*Not*I digestion. As expected two fragments 10.4-kb and 5.4-kb were obtained. (C) A correct site of 3' wing was verified by *Bam*HI/*Kpn*I digestion. As expected two fragments 12.8-kb and 3-kb were obtained.

4. DISCUSSION

4.1. Expression and functional analysis of *Insl5* gene

Insulin-like peptide 5 (INSL5), a member of insulin superfamily, was first identified through a search of the expressed sequence tags (EST) databases for novel insulin-like sequences (Conklin *et al.,* 1999; Hsu, 1999). The prepro-INSL5, a polypeptide of 135 amino acids, is characterized by a signal peptide, a B-chain, an A-chain, and a connecting C-peptide, which is the signature motif of insulin-like molecules (Conklin *et al.* 1999). The amino acid sequence of mature INSL5 peptide, which consists of the A- and the B-chain, is conserved between human and mouse. The human INSL5 has 71% identity to mouse INSL5, 40% identity to human relaxin, 34% identity to human insulin-like 3 peptide, 30% to insulin, 29% to INSL6, 29% to IGF-2, 28% to IGF-1, and 22% to INSL4 (Conklin *et al.,* 1999, Wilkinson *et al.,* 2005). The 66-amino-acid C-peptide of human INSL5 has no detectable sequence similarity to the C-peptide of other insulin family members, but has 48% identity to the 67-amino-acid C-peptide of mouse INSL5.

In human genome, some genes of insulin superfamily are closely linked. *INSL6*, I*NSL4*, relaxin-1 (*RLN1*) and relaxin-2 (*RLN2*) are mapped to chromosome 9p23-24.3, while *INSL3* and relaxin-3 are localized on chromosome 19p12-13.2, and insulin and *IGF-2* on chromosome 11p15.5. In contrast, *INSL5* and *IGF-1* are localized alone on chromosomes 1p22.3 and 12q22, respectively.

4.1.1. Expression analysis of mouse *Insl5* gene

Existing reports from several groups on the expression of *Insl5* are somewhat controversial. By Northern blot analysis human INSL5 transcripts were detected in rectum, colon and testis (Conklin *et al.,* 1999). Mouse *Insl5* gene was found to be expressed in colon, kidney, brain, and testis (Conklin *et al.,* 1999; Hsu, 1999). Northern blot analysis in our group revealed that the expression of *Insl5* is restricted to rectum. No transcript could be detected in thymus, brain and kidney (Shirneshan, 2005). Using RT-PCR, mouse *Insl5* was amplified from a wide variety of fetal and adult tissues (Fig.4). Taken together, these results suggested that *Insl5* is predominantly expressed in rectum, colon, kidney, brain and testis. However, in other tissues, *Insl5* transcript is also present, but at a very low level, which is beyond the threshold level of

Northern blot detection. Our RT-PCR analysis revealed that the expression of *Insl5* during prenatal development starts at embryonic day 11.5 and continues to later stages of embryogenesis (Fig. 4C). No expression of *Insl5* could be detected in early stages as well as in embryonic stem cells (ES). These results suggest that the expression of *Insl5* may be involved in organogenesis. To determine the expression pattern of *Insl5* during testis development and in testes of different mutant mice with spermatogenesis arrested at different stages (Lyon and Hawkes, 1970; Bennett *et al.,* 1971; Moutier, 1976; Zimmermann *et al.,* 1999; de Rooij and Boer, 2003), the RT-PCR assay was performed. The results of this study revealed that *Insl5* is expressed in germ cells as well as in somatic cells of the testis (Shirneshan, 2005) and suggested its potential role in reproductive physiology.

The cellular localization of INSL5 protein has been only determined in kidney and brain (Hsu, 1999; Liu *et al.,* 2005a,b; Dun *et al.,* 2006). By immunohistochemical analysis, INSL5 protein was exclusively detected in the specific cells of loop of Henle, suggested that INSL5 could have a regulatory role in the kidney (Hsu, 1999). The immunohistochemical detection of INSL5-immunoreactive neurons in the paraventricular, supraoptic, accessory secretory and supraoptic retrochiasmatic nuclei as well as in the hypothalamus suggested an additional neuroendocrine function for INSL5 in the mouse (Liu *et al.,* 2005a,b; Dun *et al.,* 2006). Using an other polyclonal anti-INSL5 antibody, we have detected the expression of INSL5 in the anterior hypothalamus (Fig. 8).

In conclusion, expression pattern of *Insl5* suggests a non-reproductive and reproductive role of this gene in mice (Bathgate *et al.,* 2006a,b; Haugaard-Jönsoon *et al.,* 2009).

4.1.2. Functional characterization of *Insl5* gene

4.1.2.1. Generation of *Insl5*-deficient mice

The rapid advance of molecular techniques as well as the availability of the expressed sequence tag (EST) and completing of the genome databases facilitated the identification of five novel genes : *Insl3* (Adham *et al*., 1993); *Insl4* (Chassin *et al.,* 1995); *Insl5* (Conklin *et al.,* 1999; Hsu, 1999); *Insl6* (Hsu, 1999; Lok *et al.,* 2000) and *Insl7/Rln3 (*Bathgate *et al.,* 2002a) belonging to the insulin superfamily (Bathgate *et al.,* 2006a,b). However, there is still very little information regarding functions of proteins encoded by these genes (Bathgate *et al.,* 2002a,b, 2006a,b). Mutations in some members of the insulin superfamily revealed that these

peptides are involved in reproduction functions (Zhao *et al.,* 2000; Adham *et al,*. 2000; Kappeler *et al.* 2008). For example, relaxin-deficient mice exhibit abnormalities in nipple development and the parturition process (Zhao *et al.,* 1999). Mice with deficiency of INSL3 show bilateral cryptorchidism due to defects in the development of the gubernaculum (Zimmermann *et al.,* 1999; Nef and Parada,1999; review in Hughes and Acerini, 2008). Conditional knock-out of insulin-like growth factor 1 receptor (*Igf1r*) affected female fertility in mice (Kappeler *et al.* 2008). Therefore, to understand the biological function of *Insl5* gene in mice, we have disrupted the gene by homologous recombination and generated *Insl5*-deficient mice on two different genetic backgrounds, namely on a C57Bl/6J x 129/Sv hybrid background and on a 129/Sv inbred genetic background (Shirneshan, 2005; this work).

Mice heterozygous for the *Insl5* mutant allele developed to adulthood, were fertile, and appeared phenotypically normal. The resulting progeny from heterozygous intercrosses displayed a normal Mendelian ratio of the three genotypes (section 3.1.3.1) indicating that *Insl5* is not essential for embryonic development. Northern blot analysis with total RNA isolated from adult rectum demonstrated that *Insl5* is not expressed in rectum of *Insl5*$^{-/-}$ mice (Shirneshan, 2005 and data not shown). This result supported the notion that engineered disruption of the *Insl5* had generated a null mutation. *Insl5*-deficient mice were viable and did not exhibit obvious abnormalities, although *Insl5* expression has been detected at low level in almost all tissues of wild type mice (Fig. 4A).

4.1.2.2. *Insl5*-deficient mice display an alternation in nociceptive behaviors on a hybrid background

The most interesting differences between wild type and *Insl5*$^{-/-}$ mice generated on a C57Bl/6J x 129/Sv hybrid genetic background were observed in behavior, most notably in nociceptive behaviors. Alterations in nociceptive behaviors were significant in the hot plate test and in the Hargreaves test, but not in tail flick test. One of the major differences between these tests is the level of information processing (Franklin and Abbott, 1989). The nociceptive response on the hot plate and on the Hargreaves tests has a spinal and a supraspinal part. The central pathway for processing nociceptive information starts at the level of the spinal cord. Afferents activate the dorsal horn neurons located in the superficial spinal lamina, which project in the contralateral ventrolateral tracts to supraspinal sites and activate neurons in the medulla, mesencephalon and thalamus (Willis and Westlund, 1997). The response on the tail flick test

is a spinal reflex (Franklin and Abbott, 1989). Our results suggested that the INSL5-deficiency impairs neuronal pathways involved in the central mediation of pain or in maintenance of the balance of spinal excitatory and inhibitory processes. These findings are supported by expression analysis of INSL5 in central nervous system. INSL5 showed a particular dense expression in brain areas concerned with the central mediation of antinociception such as anterior hypothalamus/preoptic area (Liu *et al.,* 2005a,b; Holden *et al.,* 2005; Mobarakeh *et al.,* 2005; Dun *et al.,* 2006), the ventral nuclei of the periaqueductal gray (Sandkühler, 1996; Ossipov *et al.,* 2000), and the pontine Kölliker-Fuss neucleus (Hodge *et al.,* 1986; Jones, 1991; Nag and Mokha, 2004). The INSL5 expression in pain processing regions of brain such as the medullary raphe nuclei (Mason, 2001), the lateral reticular nucleus (Ness *et al.,* 1998) and the nucleus of the solitary tract (Jänig, 1996) further strengthen the idea that INSL5 might be an important neuropeptide of central pain pathway, although expression was not found at the primary relays of somatic pain in the dorsal horn of the spinal cord. Nevertheless, an impairment of the antinociceptive system in the INSL5-deficient mice can explain the faster latency of the paw withdrawal response in the Hargreaves test due to impaired descending inhibitory antinociceptive inputs to spinal cord. Tail elevation behaviour in a neurological screen is an additional indicator for changes in nociceptive behaviour. Thus, increased tail elevation can be induced by dose-dependent activation of the mu opioid receptor with morphine (Zarrindast *et al.,* 2001). The decreased tail elevation seen in the neurological analysis supports the involvement of INSL5 in inhibitory antinociceptive signalling. Considering the delayed hind paw licking and shaking in the hot plate tests as delayed behavioral response of the antinociceptive system is also in accordance with the observed expression profile of INSL5 (Fig. 8). This expression pattern is also in accordance with the observed reduction of rearing activity in *Insl5*$^{-/-}$ mice, as for example the anterior hypothalamic/preoptic area is known to be involved in the control of rearing activity (Brudzynski and Mogenson, 1986).

The significant differences in nociceptive behaviors between wild type and *Insl5*-deficient mice were observed on 7-month-old animals, which were derived from F_2 generation (Fig. 6). Therefore, to provide a complete picture of differences in nociceptive behaviors in *Insl5* mutant mouse line, we have tested pain reactivity of younger (3-month old) wild type and *Insl5*-deficient mice, which were derived from subsequent generations (F_6-F_9). The nociceptive screen of these younger group of animals did not show significant differences between *Insl5*$^{-/-}$ and *Insl5*$^{+/+}$ animals (Fig. 7). These results suggest that the defect in nociceptive behaviors of *Insl5*-deficient mice is dependent of the age and the genetic

background. These findings were supported by several studies, which revealed that the behavioral phenotypes of genetically modified animals is strongly influence by the age, genetic background of the animals as well as environmental factors (Bilkei-Gorzo *et al.,* 2004, Siuciak *et al.,* 2008).

4.1.2.3. *Insl5*-deficient mice on a 129/Sv inbred background display male and female infertility and impaired glucose homeostasis

Insl5-deficient mice generated on a 129/Sv inbred genetic background showed impaired fertility and glucose homeostasis. Analysis of *Insl5*$^{-/-}$ males revealed that spermatogenesis is not affected and sperm number in the cauda epididymidis as well as in uteri of wild type females inseminated by infertile *Insl5*$^{-/-}$ males is not reduced (Fig. 10; Tab. 4). However, no sperm was observed in oviducts of females mated with *Insl5* mutant males. These results suggested that sperm of *Insl5*$^{-/-}$ are not able to migrate through the female genital tracts (Tab. 5). The impaired sperm motility was further supported by a computer assisted semen analysis (CASA) system (this phenotype will be discussed more widely in section 4.2.2.3).
Breeding of *Insl5*$^{-/-}$ males with wild type females and *Insl5*$^{-/-}$ females with wild type males revealed that the average litter size per *Insl5*-deficient male or female varied considerably, ranging from no pups born (infertile male or female group) to a smaller litter size than normal (Tab. 2). The variations in phenotype observed here might be explained by incomplete penetrance (Griffiths *et al.* 2000, Rakyan *et al.* 2002; Reinholdt *et al.,* 2006; Held *et al.,* 2006) which could be caused by environmental modifiers (such as nutrition or level of hormones during embryonic development; Juriloff and Harris, 2000, Huebner *et al.,* 2006) and epigenetic regulation of expression (e.g. histone modifications, DNA methylation, genomic imprinting by the paternal or maternal allele; Rakyan *et al.* 2002; Cisneros, 2004; Bromfield *et al.,* 2007; Han *et al.,* 2008). Incomplete penetrance of infertility was also reported in other models of genetically modified mice. For example, in mice lacking a functional aromatase (Robertson *et al.* 1999) or in transgenic mice overexpressing insulin-like growth factor binding protein-1 (IGFBP-1) in the liver (Froment *et al.* .2002), 25–30% of 3- to 6-month-old males showed impaired reproduction and spermatogenesis, whereas the other males produced offspring. Interestingly, mice homozygous for the *curly tail* (*ct*) mutation also exhibit varied expressivity of their phenotype ranged from no outward phenotype to perinatal lethality with individuals displaying the intermediate phenotypes of spina bifida, exencephaly, or only the

twist in the tail (Gruneberg, 1954). Only approximately 38% of newborn homozygotes on the inbred STOCK *ct*/J background have been found to display cranial or spinal neural tube defects.

Histological analysis of *Insl5*$^{-/-}$ ovaries revealed presence of different stages of follicle development (Fig. 11). The number of oocytes, which were isolated from superovulated and normally cycling *Insl5*$^{-/-}$ females, was not significantly different from that of wild type females. However, no 2-cell stage embryos could be found in collected embryos (E1.5) from *Insl5*-deficient females mated with wild type males. These results suggest that the maturation of oocytes might be affected in *Insl5*-deficient mice.

During prenatal development, mammalian oocytes undergo meiosis within ovarian follicles. Oocytes are arrested at the first meiotic prophase and held in meiotic arrest by the surrounding follicle cells until a preovulatory surge of LH from the pituitary stimulates the immature oocyte to resume meiosis (Fan *et al.,* 2002; Kawamura *et al.,* 2004; Downs and Chen, 2006; Chen and Downs, 2008). Meiotic arrest depends on high level of cyclic adenosine monophosphate (cAMP) within the oocyte. Therefore, oocyte meiotic resumption is associated with decreased concentration of intracellular cAMP (Conti *et al.,* 2002; Eppig *et al.,* 2004; Voronina and Wessel, 2004; Chen and Downs, 2008). INSL5 is the ligand for the G-protein-coupled receptor 142 (GPCR142) (Liu *et al.,* 2003a,b, 2005a, Bathgate *et al.,* 2005, Tregear et al., 2009), which activates the inhibitory Gi protein to cause inhibition of cAMP production (Bathgate *et al.,* 2005; Halls *et al.,* 2007). The lack of INSL5 prevents the GPCR142 receptor activation, which subsequently leads to increase of cAMP level and the arrest of oocyte maturation. Accordingly, we suggested that INSL5-deficiency causes an arrest of oocyte meiotic resumption. Kawamura *et al.* (2004) have reported that INSL3 binds to a G-protein-coupled receptor, LGR8, which is expressed in germ cells and activates the inhibitory G protein (Gi). The activation of Gi protein leads to decrease of the intracellular cAMP production. These results suggested that the INSL3 may be involved in oocyte maturation and that therefore both INSL3 and INSL5 may cooperate in initiating oocyte maturation. Furthermore, detection of INSL5 and its receptor in the hypothalamus (Fig. 8; Liu *et al.,* 2005a; Dun *et al.,* 2006) suggested that observed anomalous ovulation cycle was caused by the unsettled feedback between ovary, pituitary gland and hypothalamus. Moreover, INSL5 is closely related to the RLN3 (Bathgate *et al.,* 2002a,b, 2005; Liu *et al.,* 2005a,b) which was reported to play a key role in the regulation of the hypothalamo-pituitary-gonadal (HPG) axis (McGowan *et al.,* 2008).

A further significant difference between *Insl5*$^{-/-}$ and wild type mice was found in blood glucose level. The glucose level of INSL5-deficient mice, which are older than 6 months, was significantly higher than in control littermates. However, we only found three *Insl5*$^{-/-}$ mice with diabetes. Results of glucose tolerance test (GTT) suggest that *Insl5*$^{-/-}$ mice are less able to metabolize glucose from the bloodstream and that progressive impairment of glucose tolerance in *Insl5*$^{-/-}$ mice is age-dependent. However, results of insulin tolerance test (ITT) revealed that sensitivity to insulin is not altered in *Insl5*-deficient mice. Based on the results of ITT and GTT, we suggest that the observed higher glucose level might reflect reduced insulin secretion in *Insl5*$^{-/-}$ mice. Histological and immunohistochemical analysis revealed that mean islet area in *Insl5*$^{-/-}$ pancreas was 1.6-fold smaller than that of wild type controls. Furthermore, the number of insulin-positive β-cells was significantly decreased in the islets of *Insl5*$^{-/-}$ mice as compared to control littermates. These results suggest that the high glucose level observed in *Insl5*$^{-/-}$ mice might be due to defect in the organization of pancreatic islets and/or insulin secretion. Several lines of evidence revealed that G-protein-coupled receptors (GPCR) play an important role in regulation of islet function and insulin secretion. Quantitation of GPCR mRNA expression in islets by qRT-PCR has identified candidate receptors that might regulate insulin secretion (Regard *et al*., 2007). However the putative receptor of Insl5, namely GPCR142, was not included in this study. Analyses of knock-out mice revealed the role of some GPCRs in regulation of insulin secretion (Pedrazzini *et al*., 1998; Fagerholm *et al*., 2004).

4.2. Expression and functional analysis of *Insl6* gene

Insulin-like peptide 6 (INSL6) is another member of the insulin superfamily (Lok *et al.,* 2000; Lu *et al.,* 2005). It was identified from an expressed sequence tag database through a search for proteins containing the conserved sequence of B-chain (Hsu, 1999; Kasik *et al.,* 2000; Lok *et al.,* 2000). Human, mouse and rat INSL6 encode polypeptides of 213, 191 and 188 amino acids, respectively (Hsu, 1999; Lok *et al.,* 2000). These orthologous sequences contain the B-chain, C-peptide, and A-chain motif found in other members of the insulin family (Lok *et al.,* 2000; Lu *et al.,* 2005, Bathgate *et al.,* 2006a,b; Rosengren *et al.*, 2009). Through the B- and A-chain regions, human INSL6 has 55% identity to rat INSL6, 43% identity to human relaxin H2, 38% identity to human INSL3, 36% identity to human insulin, 36% identity to human IGF-2, 33% identity to human IGF-1, 28% identity to human INSL5, and 24% identity

to human placenta INSL4. Human and rat INSL6 has no significant sequence similarity in the C-peptide with other family members, but exhibit a significant degree of similarity (43%) with each other (Lok *et al.,* 2000). The human *INSL6* gene is located on chromosome 9 in proximity to the human relaxin genes as well as to *INSL4*. The mouse ortholog, *Insl6*, is located on chromosome 19, which also contains the single mouse relaxin gene (Lok *et al.,* 2000; Lu *et al.,* 2005, Tregear *et al.,* 2009). This observation suggests that these genes originated from a single gene that underwent duplication numerous times throughout evolution (Kasik *et al.,* 2000, Wilkinson *et al.,* 2005). The function of INSL6 is unknown. Therefore, it was chosen as the subject of our study.

4.2.1. Expression analysis of *Insl6* gene

The expression pattern of *Insl6* has been studied in mouse, rat and human (Hsu, 1999; Lok *et al.* 2000). Northern blot analysis showed that the expression of *Insl6* in mouse and human was highly restricted to testis (Hsu, 1999; Lok *et al.* 2000). In rat, *Insl6* transcript was detected in testis and prostate (Lok *et al.,* 2000). Our expression studies confirmed and extended the earlier studies. Northern blot analysis demonstrated testis-specific expression of *Insl6* (Fig. 23A). However, RT-PCR analysis revealed ubiquitous expression of *Insl6* in adult tissues as well as during fetal development (Fig. 23B, C). The discrepancy between results obtained by Northern blot and RT-PCR analysis suggested, that *Insl6* is predominantly expressed in testis. However, in other tissues, *Insl6* transcript is also present, but at a very low level, undetectable by Northern blot analysis. These findings are in agreement with results published by Lu *et al*. (2006). Using Real-time RT-PCR assay, they confirmed predominant expression of *Insl6* in mouse testis and revealed that the level of *Insl6* transcripts in other investigated tissues (intestine, thymus, kidney, uterus, ovary, spleen, breast, lung, and liver) was only 1–8% of that observed in the testis (Lu *et al.* 2006). There is only one additional member of the insulin protein superfamily known to be expressed exclusively in the testis, namely *Insl3* (insulin-like peptide 3; expressed in pre- and postnatal Leydig cells of testis). Its mRNA was also detected in theca cells of the corpus luteum, trophoblast, mammary gland and thyroid but at lower level than in Leydig cells (Pusch *at et.,* 1996; Bathgate *et al.,* 1996; Zimmermann *et al.,* 1997, Ivell and Bathgate, 2002; Hughes and Acerini, 2008).

Expression analysis of *Insl6* in testes of different mutant mice, in which spermatogenesis is arrested at different stages of germ cell development (Fig. 23E) and testes of mice from

different postnatal developmental stages (Fig. 23D) revealed that *Insl6* is expressed exclusively in germ cells. Failure to detect the *Insl6* transcript in testes of W/W^v mutant mice (Fig. 23E), which lack all germ cells (de Rooij and Boer, 2003), suggested that *Insl6* is not expressed in Sertoli and Leydig cells. Moreover, first appearance of *Insl6* transcript in testicular RNA at stage P15 of mouse development (Fig. 23D), when about 82% of tubules contain pachytene spermatocytes (Nebel *et al.,* 1961; Silver, 1995), clearly demonstrate that the expression of *Insl6* gene starts at meiotic stages of spermatogenesis. These results are consistent with immunohistochemical data showing that the INSL6 protein is expressed in spermatogenic cells from pachytene spermatocytes to the spermatid stage (Lu *et al.,* 2006). Many genes, whose expression is restricted to meiotic and/or postmeiotic germ cells, have been reported to play an important role during spermatogenesis (Liu *et al.,* 1998; Romanienko and Camerini-Oterio, 2000; Kawamata and Nishimori, 2006). Therefore, expression pattern of *Insl6* suggests that this gene may play role in male germ cell development.

4.2.2. Functional characterization of *Insl6* gene and its role in spermatogenesis

4.2.2.1. Generation of *Insl6*-deficient mice

To understand the biological function of *Insl6* gene in mice, we have disrupted the gene by homologous recombination (Fig. 24) and generated *Insl6*-deficient mice on two different genetic backgrounds, namely on a C57Bl/6J x 129/Sv hybrid background and on a 129/Sv inbred genetic background.

Mice heterozygous for the *Insl6* mutant allele developed to adulthood, were fertile, and appeared phenotypically normal. The resulting progeny from heterozygous intercrosses displayed a normal Mendelian ratio of the three genotypes (Tab. 8) indicating that *Insl6* is not essential for embryonic development. By Northern blot and RT-PCR analysis with total RNA isolated from adult testis, we clearly showed that *Insl6* is not expressed in testis of $Insl6^{-/-}$ mice (Fig. 27). These results supported that engineered disruption of the *Insl6* has generated a null mutation. *Insl6*-deficient mice were viable and did not exhibit obvious abnormalities, although Insl6 expression has been detected at low level in all tissues in wild type mice (Fig. 23B).

Lok *et al*. (2000) have mapped human *INSL6* gene to the 9p24 region, which also contains an autosomal testis-determining factor (TDFA/SRA2) locus (Hoo *et al.,* 1989; Bennett *et al.,*

1993; Ion *et al.,* 1998; Blecher *et al.,* 2007). Interestingly, failure of testis development has been associated with rearrangement of the 9p24.1 region (Ion *et al.,* 1998). Moreover, several cases of sex reversal with gonadal dysgenesis have been reported in translocation or terminal deletion of the distal chromosome 9p region (Flejter *et al.,* 1998). Therefore, we have suggested the INSL6 might be involved in gonadal differentiation and/or testis development.

4.2.2.2. Inactivation of *Insl6* disrupts the progression of spermatogenesis at late meiotic prophase

Male infertility was the most apparent phenotype of Insl6-*deficient* mice. Breeding of *Insl6*$^{-/-}$ males with wild type females revealed that the average litter size per male varied considerably, ranging from no pups born (infertile male group) to a smaller litter size than normal (Tab. 9). Our study has also shown that the absence of *Insl6* does not significantly affect female reproduction (Tab. 9). This result is consistent with the expression profile of *Insl6* mRNA in mouse tissues, which is strong in germ cells of the mature testis but weak in ovaries (Fig. 23A, B). The variability in the expression of fertility impairment is only shown among Insl6-*deficient* mice with a hybrid C57BL/6J x 129/Sv genetic background but not in those with the inbred 129/Sv genetic background (data not shown). Furthermore, a high incidence of male infertility was observed among lnsl6$^{-/-}$ mice in the F_2 generation, which contains a high level of genetic variability between offspring (Silver, 1995; Krameret *et al.,*1998; Packert and Kuhn, 1998). The decreased incidence of male infertility in subsequent generations would impose a selection bias against that genotype (Kelada *et al.,* 2001; Moritorio *et al.,* 2003). Therefore, the partial penetrance of male infertility among Insl6$^{-/-}$ mice most probably reflects the segregation of genetic modifiers on the hybrid genetic background (e.g. presence or absence of polymorphic alleles at other gene loci, genetic background effect; Reinholdt, 2006). The background related differences in male infertility phenotypes have been reported in other targeted mice. Mice carrying targeted null mutations for the Pou-homeodomain (*Spnn-1*), the transition protein-1 (*Tnp-1*), -2 (*Tnp-2*), mitochondrial capsule protein (*Smcp*) and the desert hedgehog gene (*Dhh*) are infertile only if these mutations are maintained in the 129/Sv genetic background (Pearse *et al.,* 1997; Yu *et al.,* 2000; Adham *et al.,* 2001; Nayernia *et al.,* 2002). Moreover, males deficient for the sperm protein 1 (SED1) show a similar variation in fertility impairment in outbreed background (Ensslin and Shur, 2003).

Partially compromising of spermatogenesis in infertile *Insl6*-deficient mice may be based on the involvement of other members of the insulin superfamily in that process. The increase of *Insl3* expression during spermatogenesis (Balvers *et al.,* 1998; Adham *et al.,* 2000; Kawamura et al., 2004) and its role in the suppression of germ cell apoptosis (Kawamura *et al.,* 2004) raises the possibility that INSL3 may partially compensate for the lack of INSL6 and that therefore both INSL3 and INSL6 cooperate in male germ cell development. Several studies reported that one gene can partially compensate for loss of function of an other related gene (Carpentier *et al.,* 2004; Towne *et al.,* 2008; Singh *et al.,* 2009). For instance, *Nl1* mutant mice show the variability in the expression of fertility impairment because another related peptide (neprilysin) may partially compensate the loss of NL1 (Carpentier *et al.,* 2004).

Histological analysis of testis sections from wild type and *Insl6* knock-out mice (Fig. 31, 33), as well as analysis of different parameters of sperm collected from $Insl6^{+/+}$ and $Insl6^{-/-}$ males (Fig. 28 and Tab. 9-11), suggested that INSL6 modulates two different processes related to fertility, spermatogenesis and sperm motility.

Based on progression of the first wave of spermatogenesis in juvenile wild type and $Insl6^{-/-}$ mouse testes (Fig. 32 and 33) and expression pattern of different meiotic and postmeiotic-specific genes (Fig. 36), we propose that the INSL6-deficiency causes an arrest of spermatogenesis at late stages of meiotic prophase. These findings mostly agree with the results of RNA (Fig. 23) and immunostaining (Lu *et al.,* 2006) analyses, which showed that the Insl6 expression starts at pachytene spermatocyte stage. Enhanced apoptosis observed in $Insl6^{-/-}$ testes of the postnatal days 20 and 25 (Fig. 35C-F), which mainly lacked round spermatids (Fig. 33C-F and 35C-F), suggested that the INSL6 deficiency resulted in a cease the meiotic division and an increase in apoptotic cell death. Several knock-out mouse strains exhibit an increase of apoptotic cell death of spermatogenic cells. For instance, spermatogenesis in *CREM*-mutant mice is arrested at postmeiotic stage, and the degraded germ cells undergo apoptosis (Blendy *et al.,* 1996; Nantel *et al.,* 1996). A-*myb* mutant males show meiotic arrest at the pachytene stage and an increase of apoptotic cells (Toscani *et al.,* 1997). Similar the knock-out of *Ddx25* gene resulted in apoptosis of male germ cells (Gutti *et al.,* 2008). Furthermore, the double knock-out mouse model with targeted disruption of the *Pex7* and *Abcd1* genes revealed spermatogenesis arrest and increased apoptosis of male germ cells (Brites *et al.,* 2009). These results suggest that germ cells lacking a gene that is essential for normal spermatogenesis undergo apoptosis just after the arresting step (Tanaka *et al.,* 2000). Therefore, the increase in apoptotic germ cells in *Insl6*-deficient testes is most likely

due to the fact that INSL6-signalling is essential for progress of spermatogenesis rather than for survival of male germ cells.

The insulin superfamily ligands are structurally related to each other and mediate many of biological effects on cellular metabolism and proliferation through binding and activation of their receptors (Lok *et al.,* 2000; Hsu *et al.,* 2003b, 2005; Bathgate *et al.,* 2005, 2006a,b; Van Der Westhuizen *et al.,* 2007; Tregear *et al.,* 2009). Members of insulin superfamily mediate the signaling pathways by endocrine, paracrine and autocrine mechanisms (Kumagai *et al.,* 2002; Hsu *et al.,* 2003b; Kawamura *et al.,* 2004; Halls *et al.,* 2007a,b; Van Der Westhuizen *et al.*, 2007). For instance, Leydig cell-derived INSL3 acts as an endocrine hormone to activate the leucine rich repeat containing G-protein-coupled receptor 8 (LGR8) in the gubernaculum (Overbeek *et al.,* 2001; Kumagai *et al.,* 2002, reviw in Huges and Acerini, 2008) and as a paracrine factor to induce its receptor in male germ cells (Kawamura *et al.,* 2004). The INSL6-receptor and signaling has not yet been identified (Bathgate *et al.,* 2005, 2006a,b). The expression of *Insl6* in meiotic and postmeiotic germ cells and the failure of germ cells to progress prior the first meiotic division suggested possible autocrine actions of INSL6 on the germ cells. In addition to a putative autocrine action of INSL6 on germ cells, the intimate proximity of germ cells to Sertoli cells renders the Sertoli cells a further likely candidate for the paracrine actions of INSL6 (Lu *et al.,* 2005, 2006). Sertoli cells secret a variety of endocrine and paracrine factors that regulate spermatogenesis (Shabanowitz *et al.,* 1986; Skinner, 1991; Rassoulzadegan *et al.,* 1993; reviewed in Russell, 1993; Syed and Hecht, 1997; Vincent *et al.,* 1998; Lilienbaum *et al.,* 2000; Vidal *et al.,* 2001). Therefore, INSL6 loss might alter Sertoli cell functions that are required for the maintenance of spermatogenesis.

The production of *Insl6*-null mice constitutes an important step in the understanding of the physiological function of INSL6 in mammals. INSL6-deficiency has been proven to impair normal fertilization processes, at the level of both: spermatogenesis and sperm motility. Further studies will be necessary to precisely determine the molecular basis of the fertility defect and INSL6-signaling.

4.2.2.3. The role of *Insl5* and *Insl6* in spermatogenesis

Male germ cell differentiation (spermatogenesis) is a highly regulated, complex process that requires cooperation of germ cells and testicular somatic cells. Spermatogenesis can be subdivided into 3 main phases: (i) spermatogonial proliferation, (ii) meiosis of spermatocytes

and (iii) spermiogenesis, a morphological process converting haploid spermatids to spermatozoa (Leblond and Clermont, 1952; Chung *et al.,* 2004). In a cross section of the testis the spermatogenic stem cells, spermatogonia and somatic Sertoli cells are situated on the basal lamina of the seminiferous tubule. The Sertoli cells surround completely the germ cells beyond the onset of meiosis. The next layer is formed by spermatocytes while haploid spermatids and elongated spermatids are situated in the adluminal compartment (Fig. 57).

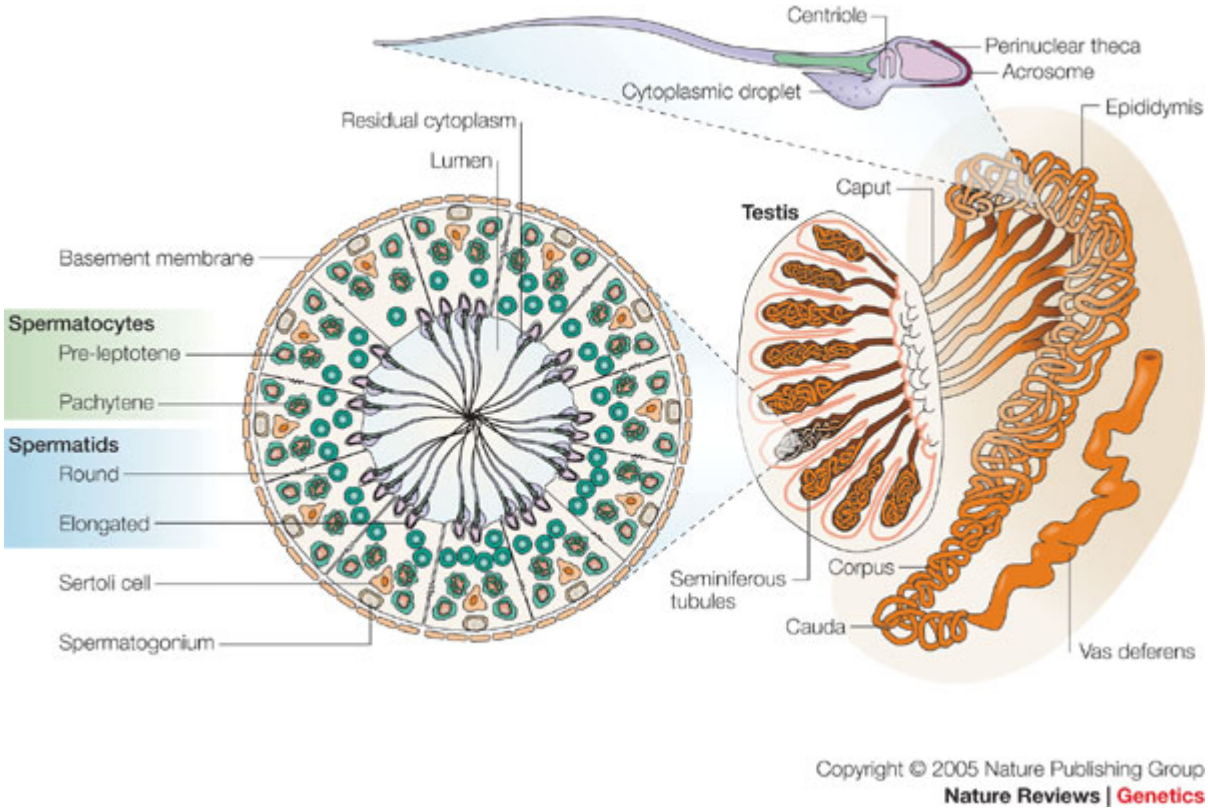

Fig. 57. A cross section of a seminiferous tubule showing cells from the various stages of the spermatogenic pathway, from the spermatogonium stem cell to the elongating spermatid (left panel). In the maturing spermatid, most of the cytoplasm is extruded as a cytoplasmic droplet as it is displaced by the perinuclear theca (top panel). The sperm are matured through a caput-to-cauda gradient of RNases, glycosidases and proteases, where approximately 80% of the sperm achieve competence for motility (right panel) (published by Krawetz, 2005)

During spermatogenesis male germ cells undergo a complex differentiation, where morphological alterations lead to the formation of differentiated sperm. Spermatogenesis starts when a spermatogenic stem cell (called As spermatogonia) gives rise to two daughter cells after initial division (Russell *et al.,* 1990; de Rooij, 1998, 2001). One of these cells remains as a stem cell while the other enters spermatogenesis as a differentiating spermatogonia [called Apr (paired) and further Aal (aligned) spermatogonia]. Then, nearly all Aal spermatogonia differentiate into A1 spermatogonia. They divide mitotically six times

giving rise A2-A4, intermediate, and B-type spermatogonia which can be identified based on morphological criteria (Oakberg, 1971; Russell *et al.,* 1990; de Rooij, 1998; Chiarini-Garcia and Russel, 2001). A characteristic feature of spermatogenesis is that after mitotic and meiotic divisions the dividing germ cells fail to complete cytokinesis resulting in formation of cytoplasmic bridges that interconnect a large number of cells (Burgos and Fawcett, 1955; Fawcett *et al.,* 1959). Kinetic analyses reveal that hundreds or even thousands of cells theoretically may be connected by bridges at the completion of spermatogenesis (Dym and Fawcett, 1971). After the final mitotic division of type B spermatogonia preleptotene spermatocytes are formed, which initiate meiosis and give rise to leptotene and zygotene spermatocytes. These cells differentiate into pachytene and diplotene spermatocytes followed by meiotic divisions. After the meiotic division, the germ cells enter spermiogenesis, the haploid phase of spermatogenesis, where round spermatids differentiate into elongated spermatids and ultimately spermatozoa.

During spermiogenesis, spermatids undergo a complex restructuring program in which the acrosome and sperm tail are formed, DNA is tightly packed leading to a drastic reduction in the size of the nucleus, mitochondria are rearranged along the neck and middle piece of the tail, surface and transmembrane structures (e.g., receptors and ion channels) for zona pellucida binding and signaling are synthesized and eventually most of the cytoplasm is removed to facilitate motility (Fawcett *et al.,* 1959; Russell *et al.,* 1990). Spermatogenesis culminates in spermiation, when mature spermatozoa are released from Sertoli cells into the lumen of the seminiferous epithelium (Russell *et al.,* 1990; de Rooij, 1998, 2001). The interval of time between the formation of subsequent cohorts of new A1 spermatogonia is always similar in particular species and is called the duration of the epithelial cycle.

Numerous genes have been shown to be involved in regulation of spermatogenesis. Disruption or incorrect activity of these genes might lead to impaired spermatogenesis, abnormal sperm function and male infertility. Mouse models for azoospermia (Kuo *et al.,* 2005, 2007), asthenozoospermia (Pilder *et al.,* 1997; Roy *et al.,* 2009) or teratozoospermia (Mendoza-Lujambio *et al.,*2002; Fujita *et al.,* 2007) are widely described in literature. Therefore, generation of knock – out mice seems to be a powerful tool to study the function of the gene which could be involved in spermatogenesis.

The defects in spermatogenesis of *Insl5*- and *Insl6*-deficient mice suggest a role of *Insl5* and *Insl6* in reproduction. The arrest of spermatogenesis at late prophase I and an increase of apoptotic cells suggested a role of *Insl6* in regulation of the first meiotic division. However,

further analyses are needed to determine the molecular role of INSL6-signaling in this process. Results of immunostainning of germ cells with anti-SYCP3 antibody revealed that chromosomal synapsis and disynapsis occurred normally during meiotic prophase. The down regulation of meiotic and postmeiotic genes such as *Ccna1, Acr, Tnp2* in *Insl6*-deficient testes cannot be explained by the regulatory role of the INSL6 on the expression of these genes, but rather by the decreasing number of meiotic and postmeiotic germ cells. The comparison of the expression profile of wild type and *Insl6*$^{-/-}$ testes at postnatal day 15 using microarray technique may help to identify genes, which are regulated by INSL6-signaling.

The male germ cell development is normally progressed in *Insl5*-deficient testis. However, impairment of sperm motility was observed in sperm isolated from *Insl5*-deficient epididymis. Furthermore, sperm of infertile *Insl5*$^{-/-}$ males were not able to migrate to the oviduct. Such phenotype was also observed in infertile *Insl6*$^{-/-}$ mice. These results raise the possibility that both INSL5 and INSL6 cooperate in sperm motility. The striking feature of reduced sperm motility can be either due to a possible structural defect (e.g. defects in ultrastructure of flagella or abnormally shaped sperm) or to a functional blockade in a physiological process leading to the promotion of sperm motility (Held *et al.,* 2006). Based on the fact that the members of the relaxin-like subfamily activate the G-protein-coupled receptors (Hsu *et al.,* 2003, 2005; Bathgate *et al.,* 2005; Tregear *et al.,* 2009), suggests that the impairment in sperm motility of *Insl5*- and *Insl6*-deficient mice is due to defects in accumulation of cyclic adenosine monophosphotase (cAMP) in sperm. The increase of intracellular cAMP is necessary for the proper coordinated beating of sperm flagellum (Tash and Means, 1982, Opresko *et al.,* 2005).

4.3. Characterization of the interactions between PELO and CDK2AP1, EIF3G and SRPX

4.3.1. The function of PELO in different species

The function of PELO has been studied in *Drosophila melanogaster*, *Saccharomyces cerevisiae* and *Mus musculus*. Mutations in the *D. melanogaster* pelota gene or in the *S. cerevisiae* homologous gene, *Dom34*, cause defects of spermatogenesis and oogenesis in *Drosophila* (Eberhart and Wasserman, 1995) and delay of growth and failure of sporulation in yeast (Davis and Engebrecht, 1998).

Furthermore, Xi *et al.* (2005) have reported the unexpected new role of *Drosophila* pelota in controlling germline stem cell (GSC) self-renewal. In the *Drosophila* ovary, GSC self-renewal is controlled by both extrinsic and intrinsic factors (Xi *et al.,* 2005). GSCs reside in a structure called the germarium, which is at the anterior end of an ovariole (Lin, 2002). At the anterior tip of the germarium, three types of somatic cells, cap cells and inner sheath cells, constitute a niche that supports two or three GSCs. One GSC divides to generate two daughter cells: the daughter cell maintaining contact with the cap cells renews itself as a stem cell, while the daughter cell moving away from the cap cells differentiates into a cystoblast. The cystoblast divides four times with incomplete cytokinesis to form a 16-cell cyst, in which one cell becomes an oocyte and the rest becomes nurse cells (Fig. 58; Xi *et al.,* 2005).

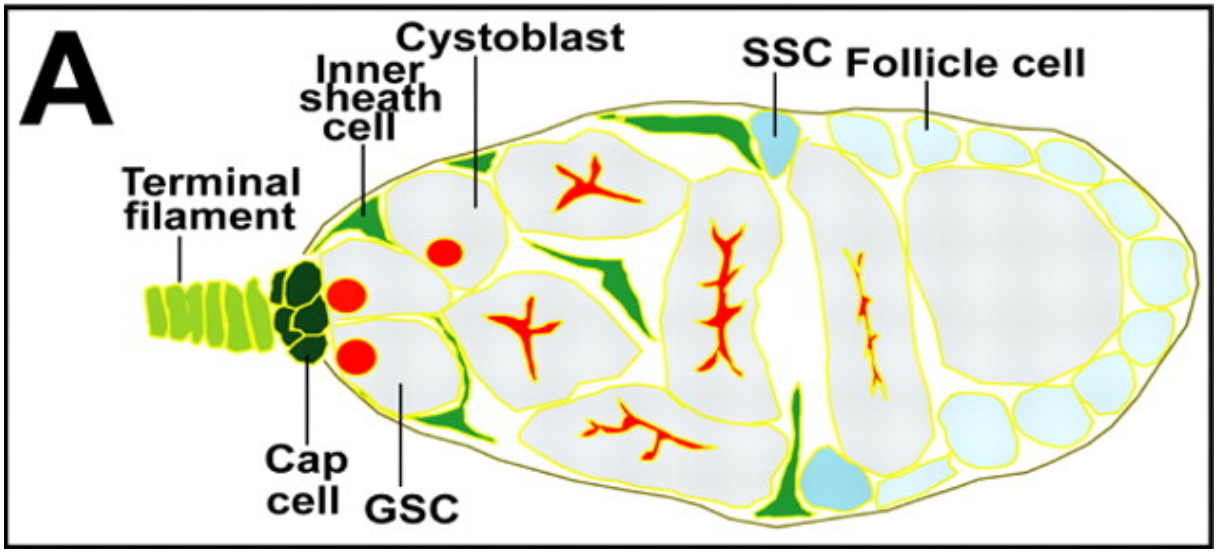

Fig. 58. Schematic diagram of the germarium. Red circles indicate spectrosomes (GSCs and cystoblasts) and branched red structures indicate fusomes (germ cell cysts) (published by Xi *et al.,* 2005).

Bone morphogenic protein (BMP)/dpp produced from cap cells functions as short-range signal that directly repress the transcription of differentiation-promoting gene *bam* in GSCs to maintain their self-renewal, and also allow cystoblasts lying one cell diameter away to differentiation (Chen and McKearin, 2003; Song *et al.,* 2004). Overexpression of *bmp/dpp* in the inner sheath cells of germarium of transgenic flies leads to repression of the *bam* expression in all GSCs daughter cells. The maintenance of self-renewal and blocking of germ cell differentiation in all GSCs daughter cells results in the formation of GSC-like tumors and consequently in female sterility (Song *et al.,* 2004).

In genetic screen to identify genes which are potentially involved in *Bmp* signaling in GSCs, Xi *et al.* (2005) has identified *Pelo* as a dominant suppressor of the *bmp/dpp* overexpression

induced GSC tumor phenotype. Mutation of *Pelo* gene in transgenic ovary, which overexpresses *bmp/dpp* signals, induces the expression of differentiation-promoting genes in GSCs and thereby rescues *Bmp/dpp* overexpression-induced female infertility. These results indicate that *Pelo* is required intrinsically for controlling GSC self-renewal by repression of differentiation-promoting genes. They also support that expression of *Pelo* is regulated by *Bmp* signaling. Furthermore, this report found that *Pelo* downregulates the expression of *Dad* gene, which is one of *Bmp*-target genes in GSC. The *Dad* is the orthologous gene of mammalian *Smad* gene.

Recently, *yeast* protein DOM34, the pelota orthologous protein, has been described to play a critical role in a newly identified mRNA decay pathway called No-Go decay (NGD) (Fig. 59; Doma and Parker, 2006; Passos *et al.,* 2009). This pathway clears cells from mRNAs inducing translational stalls through endonucleolytic cleavage. In all organisms, the amount of each mRNA is tightly controlled by the rates of both transcription and decay processes. Large-scale analyses indicate that as many as half of all changes in the amounts of mRNA in some responses can be attributed to altered rates of decay (Garneau *et al.,* 2007). Normal mRNAs undergo decay by three different pathways: the deadenylation-dependent, deadenylation-independent, and endonucleasemediated decays (Garneau *et al.,* 2007). In addition to turnover of normal mRNAs, mRNAs that undergo abnormal translation in the cytoplasm are targeted for degradation by the mRNA-surveillance pathways (Clement and Lykke-Andersen, 2006; Tollervey, 2006). At least three mRNA-surveillance pathways have been described. The nonsense-mediated decay (NMD) targets mRNAs with premature translation-termination codons (Gonzalez *et al.,* 2001; Wilusz *et al.,* 2001), while the nonstop decay (NSD) targets mRNAs lacking termination codons (van Hoof *et al.,* 2002; Vasudevan *et al.,* 2002). More recently, a new surveillance pathway, termed no-go decay, was identified in Saccharomyces cerevisiae (Doma and Parker, 2006). It targets mRNAs with translation-elongation stalls. In contrast to the former two surveillance pathways, the no-go decay involves endonucleolytic cleavage of the mRNA in the vicinity of the stalled ribosome (Clement and Lykke-Andersen, 2006; Doma and Parker, 2006). This is reminiscent of NMD in *D. melanogaster* (Gatfield and Izaurralde, 2004). Although the full mechanism of no-go decay is not well understood, it appears that mRNA surveillance based on translation elongation rates is a conserved process (Doma and Parker, 2006). In the no-go decay, stalled ribosomes on an mRNA are detected, and the mRNA is endonucleolytically cleaved near the stall site (Doma and Parker, 2006; Garneau *et al*., 2007). The 5' fragment of the mRNA is

degradated by the cytoplasmic exosome and 3' fragment is degradated by the 5' to 3' exonuclease *Xm1*. It was shown that two *S. cerevisiae* proteins, DOM34 and HBS1 (Hsp70 subfamily B suppressor 1), are required for the initial endonucleolytic cleavage (Doma and Parker, 2006). Each of *Dom34* and *Hbs1* is related to the translation termination factors *eRF1* and *eRF3*, respectively.

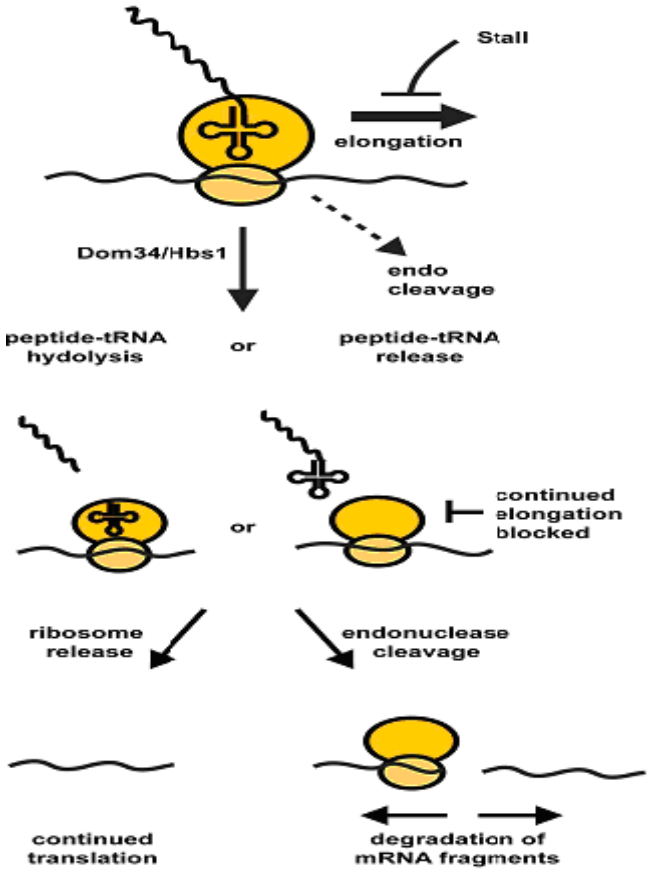

Fig. 59. A model for NGD (published by Passos *et al.,* 2009)

Physiological function of PELO in mouse was investigated by generation of a conventional knockout mouse (Adham *et al.,* 2003). These analyses revealed that PELO null embryos die after the initiation of gastrulation (E6.5), a particularly active period of cell division characterised by a very short cell cycle (as short as 2 hrs) (Snow, 1977; Hogan *et al.,* 1994). The PELO role in control of cellular proliferation was obtained from the results of *in vitro* culture of blastocysts. While the inner cell mass (ICM) of *Pelo*$^{+/+}$ and *Pelo*$^{+/-}$ blastocysts continued to expand throughout the 7-day culture period, *Pelo*$^{-/-}$ ICM cells failed to proliferate. In contrast, *Pelo* $^{-/-}$ trophoblast cells continued to grow in size through 7 days of culture. These results demonstrate that the death of PELO-deficient cells is restricted to the

rapidly dividing cells of the ICM. The survival of mitotically inactive *Pelo*$^{-/-}$ trophoblast cells further argues that PELO is required selectively in cells undergoing mitosis.

4.3.2. PELOTA is interacting with CDK2AP1, EIF3G and SRPX

Early developmental lethality of the *Pelo*-deficient embryos and the failure to establish *Pelo*$^{-/-}$ homozygous mouse lines prevented us to define the exact role of *Pelo* gene. Therefore, to get more information about the function of pelota, we have generated pelota conditional knock-out mice (work in progress) and identified the putative interaction partners of pelota.
The results of several groups demonstrated that identification of interaction partners let to propose a physiological function of investigated protein. For example, *BRCA-1* gene (breast cancer 1) was identified by Miki *et al.* (1994), who supposed that it could be a tumor suppressor gene. Further analyses revealed that BRCA-1 protein contains cysteine-rich zinc-binding motif known as the RING-Finger motive which mediates protein-protein interactions (Saurin *et al.,* 1996; Borden *et al.,* 1998). Moreover, it was reported that BRCA-1 is a part of a macromolecular complex including human RAD51 and BRCA1 that plays a role in DNA repair. To understand the function of this BRCA1, Houvras *et al.* (2000) started to search for proteins capable of interacting with the BRCA-1 RING domain. Using Yeast-Two hybrid, ATF1 was identified as a putative interaction partner of BRCA1 protein. ATF1 is transcription factor that bind a consensus CRE (TGACGTCA) and mediate transcriptional activation in response to cAMP and Ca^{2+} (Liu *et al.,* 1993a,b). Based on these a specific physical association between the BRCA1 RING domain and ATF1 it has been demonstrated that BRCA-1 is a transcriptional coactivator that can modulate the activity of ATF1. Summarized, Houvras *et al.* (2000) demonstrated by using interaction study connection between the role of BRCA1 cossing breast cancer and its function in DNA-repair system.

In order to find out putative interaction partners of PELO protein, the yeast two-hybrid screening was performed (Ebermann, 2005). Several PELO binding partners were identified, which were classified according to their structure and function. In the present study, we were concentrated to confirmed the interactions between human PELO and putative interacting proteins, CDK2AP1, EIF3G and SRPX. To prove interactions between human PELO and CDK2AP1, EIF3G and SRPX, we have used coimmunoprecipitation assay, GST-Pull down assay and BiFC assay.

Coimmunoprecipitation assay proved the specificity of interaction between PELO and CDK2AP1, EIF3G and SRPX. To determine the regions of PELO protein involving in the binding to CDK2AP1, EIF3G and SRPX proteins, several Glutathione S-transferase-*PELO* (GST-*PELO*) deletion constructs were generated and fusion proteins were used for GST-Pull down assay. GST-Pull down assay further confirmed the specificity of interactions between PELO and CDK2AP1, EIF3G and SRPX proteins, and also demonstrated that all three interaction partners bind to the same region of PELO protein, namely domain eEF1_3 (Fig. 47).

BiFC assay further proved the specificity of the interactions between PELO and CDK2AP1, EIF3G and SRPX proteins. All three interacting partners form a protein complex with PELO in the cytoskeleton (Fig. 51). This confirmed our subcellular localization studies, which demonstrated that Pelo is localized with the cytoskeleton and (Buyandelger, 2006).

Human *SRPX/DRS/ETX1* was temporarily supposed and later excluded as a candidate gene for X-linked retinitis pigmentosa (Meindl *et al.,* 1995). *SRPX* gene was originally isolated as a suppressor gene of v-src transformation (Pan *et al.,* 1996; Inoue *et al.,* 1998). Expression of *SRPX* mRNA is markedly downregulated in a variety of human cancer cell lines and tissues, suggesting the potential role of this gene as a tumor suppressor (Yamashita *et al.,* 1996; Mukaisho *et al.,* 2002; Shimakage *et al.,* 2000, 2002; *Kim et al.,* 2003). *SRPX* encodes 464 aa protein, which consists a transmembrane domain, a short intracellular domain in the C-terminus, and three consensus repeat (CRs) designated as sushi motifs (Norman *et al.,* 1991). They are conserved in the extracellular domain of the selecin family of adhesion molecules and complement-binding proteins (Lasky, 1992; Kansas,1996, Rubinfeld *et al.,*1997). The transmembrane domain of SRPX shares sequence similarity with three repetitive elements of the putative tumor suppressor gene, DRO1, the mRNA expression of which is downregulated by some known oncogenes including β-catenin, activated H-ras and c-myc. It was also revealed that ectopic expression of the SRPX protein induced apoptosis associated with the activation of caspase-12 (like), -9 and -3 in various human cancer cell lines (Tambe *et al.,* 2004). The release of cytochrome c from the mitochondria into the cytoplasm was not observed in the apoptosis induced by *SRPX*. Instead, the SRPX protein interacted with ASY/Nogo-B/RTN-xS, an apoptosis inducing protein localized in the endoplasmic reticulum (ER) (Chen *et al.,* 2000; Tagami *et al.,* 2000, Li, *et al.,* 2001). Co-expression of these genes was shown to increase the efficiency of apoptosis. These findings indicated that SRPX induces apoptosis via a novel ER-mediated pathway and suggested that this pathway might

contribute to the suppression of tumor formation (Tambe *et al.,* 2007). Generated *Srpx* knock-out mice confirmed that *Srpx* gene plays a role as a tumor suppressor. Between 7 and 12 months after birth, malignant tumors including lymphomas, lung adenocarcinomas and hepatomas were generated in about 30% of the *Srpx*-deficient mice, whereas no tumors were found in any of the wild-type mice during the same period of time (Tambe *et al.,* 2007). *Srpx* null embryonic fibroblasts also showed enhanced sensitivity to transformation by v-src oncogene (Tambe *et al.,* 2007). Reintroduction of *Srpx* into a tumor cell line derived from the tumor of a *Srpx* null mouse led to the suppression of tumor formation in nude mice, which was accompanied by enhanced apoptosis and the activation of caspase-9 and -3. Furthermore, overexpression of *Srpx* into this cell line enhanced sensitivity to apoptosis mediated by caspase-3, -9 and -12 under low serum culture conditions (Tambe *et al.,* 2007). The present results thus indicate that *Srpx* contributes to the suppression of malignant tumor formation, and this suppression is closely correlated with *Srpx*-mediated apoptosis.

Translational control plays an important role in the regulation of gene expression in eukaryotes. The initiation phase of translation is one of the points at which changes in the rate of protein synthesis occur. Initiation of translation begins with dissociation of 80 S ribosomes into 40 and 60 S subunits. The 40 S subunit then binds a ternary complex consisting of eukaryotic initiation factor 2 (eIF2), GTP, and methionyl-tRNAi (Met-tRNAi). This 40 S preinitiation complex recognizes the m^7G-capped end of a mRNA, binds to the mRNA, and scans toward the end until it forms a stable complex at the first AUG initiation codon (Block *et al.,* 1998; Mayeur *et al.,* 2003). Subsequently, the 60 S subunit joins to form the 80 S initiation complexes. The various reactions in the initiation pathway are promoted by 11 or more soluble proteins called eIFs (Block *et al.,* 1998, Mayeur *et al.,* 2003, Kim *et al.,* 2006). The largest of them, eIF3 (eukaryotic translation initiation factor 3), is a complex of 12 or more polypeptides and plays a central role in the the process (Block *et al.,* 1998; Lagirand-Cantaloube *et al.,* 2008). EIF3 binds to 40 S ribosomal subunits in the absence of other translational components and helps maintain 40 S and 60 S ribosomal subunits in a dissociated state. It stabilizes methionyl-tRNA binding to 40 S subunits and contributes to mRNA binding through its interaction with the eIF4G subunit of the mRNA m^7G-cap binding protein complex, eIF4F and with eIF4B. EIF3 also may be involved in the recognition of the initiation codon (de Quintoet *et al.,* 2001, Martineau *et al.,* 2008). eIF3 is the largest of the eukaryotic translation initiation factors, with an apparent mass of about 700 kDa and comprises at least 12 subunits (de Quintoet *et al.,* 2001; Lagirand-Cantaloube *et al.,* 2008;

Martineau *et al.*, 2008). One of these units is EIF3G which was shown (in our thesis) to be an interacting partner of PELO.

EIF3G is highly conserved 320 aa polypeptide, which is widely expressed in fetal and postnatal tissues (Hou *et al.,* 2000). EIF3G has been reported to strongly associate with eIF3a (p170) and bind to 18S rRNA and β-globin mRNA through a RRM (RNA-recognition motif) domain at the C-terminal region (Block *et al.,* 1998; Hou *et al.,* 2000). The physiological function of the *Eif3g* gene in mammals is not characterized and no report about generation and characterization of *Eif3g* knock-out mice was founding literature. It was reported that eIF3g interacts directly with erythroid protein 4.1 (4.1R), which is 80-kDa a cytoskeletal protein (Hou *et al.,* 2000). This interaction suggests that 4.1R may act as an anchor protein that links the cytoskeleton network to the translation apparatus. The accumulation of *Dom34/Pelo* in polyribosomes in yeast (Davis and Engebrecht, 1998) suggested that DOM34 is involved in translation process. The specific interaction between PELO and EIF3G further supports the involvement of both proteins in complex, which initiate the translation process. The localization PELO-EIF3G interacting proteins at the cytoskeleton network similar to that of EIF3G-4.1R complex suggests the presence of these three proteins in protein complex of translation apparatus.

CDK2AP1 was initially identified as a cancer-related gene by using hamster oral cancer model (Todd *et al.,* 1995). *CDK2AP1* is a highly conserved and ubiquitously expressed gene located on human chromosome 12q24 and is a 115 aa nuclear polypeptide that is down regulated in ~70% of oral cancers (Tsuji *et al.,* 1998; Shintani *et al.,* 2001; Choi *et al.,* 2009). It was shown, that CDK2AP1 has a role in TGF-β induced growth arrest, cisplatin induced genotoxicity, and cellular apoptosis (Matsuo *et al.,* 2000; Shintani *et al.,* 2000, 2001; Kohno *et al.,* 2002; Figueiredo *et al.,* 2005; Peng *et al.,* 2006). Furthermore, it was demonstrated that overexpression of *Cdk2ap1* in a transgenic mouse model resulted in gonadal atrophy, seminiferous tubule degeneration, and folliculogenesis abnormalities *in vivo* (Figueiredo *et al.,* 2006).

Cdk2ap1 has been identified as one of stem cell specific genes that are enriched in both embryonic and adult stem cells (Ramalho-Santos *et al.,* 2002). It has been reported by microarray analysis that *Cdk2ap1* has been categorized as one of genes that are expressed in early stage preimplantation embryos and its expression gradually decreases as the embryo further develops (Sharov *et al.,* 2003). Analysis of *Cdk2ap1* knock-out mice revealed that *Cdk2ap1*$^{-/-}$ embryos died after implantation. Comparison of *Cdk2ap1*$^{-/-}$ and *Pelo*$^{-/-}$ mice

revealed an overlapping phenotype. Deletion of both genes results in similar phenoypes, namely early embryonic lethality after implantation. Results of interaction studies and the phenotypic similarity of *Pelo* and *Cdk2ap1* knock-out mice suggest that both protein are involved in the same pathway that regulate the early embryonic development. Interestingly, CDK2AP1 was also identified as a core component of MBD-NuRD protein complexes, which promote *Oct4* promoter methylation during differentiation of embryonic stem cell (ES). *Oct4* is a known master regulator of stem cell renewal and differentiation. The downregulation of *Oct4* by MBD-NuRD complex leads to differentiation of ES cells (Ovitt *et al.,* 1998; Pesce *et al.,* 2001; Watson *et al.,* 2001).

Analysis of *Cdk2ap1*$^{-/-}$ stem cells revealed that ES cells lack the ability to differentiate in the absence of LIF. These studies have also shown that CDK2AP1 negatively regulates the expression of Oct4 during differentiation (Deshpande *et al.,* 2008). The function of CDK2AP1 requires a direct interaction with *Mbd3* in the MBD-NuRD complexes (Fig. 60). The failure of the *Mdb*-Cdk2ap1 interaction results in hypomethylation of the *Oct4* promoter and deregulation of *Oct4* expression in differentiating EB (embryoid bodies) (Deshpande *et al.*, 2008). In contrast to the function of CDK2AP1 in repression of pluripotent genes, it has been shown that pelota is repressed expression of differentiating genes in pluripotent germline stem cells of *Drosophila melanogaster*. We hypothesed that the interaction of pelota with CDK2AP1 in cytoplasm may prevent the CDK2AP1 to interact with the Mbd3 in the nucleus and thereby disrupt the formation of the repressor complex MBD-NuRD, which represess the expression of the pluripotent gene Oct4.

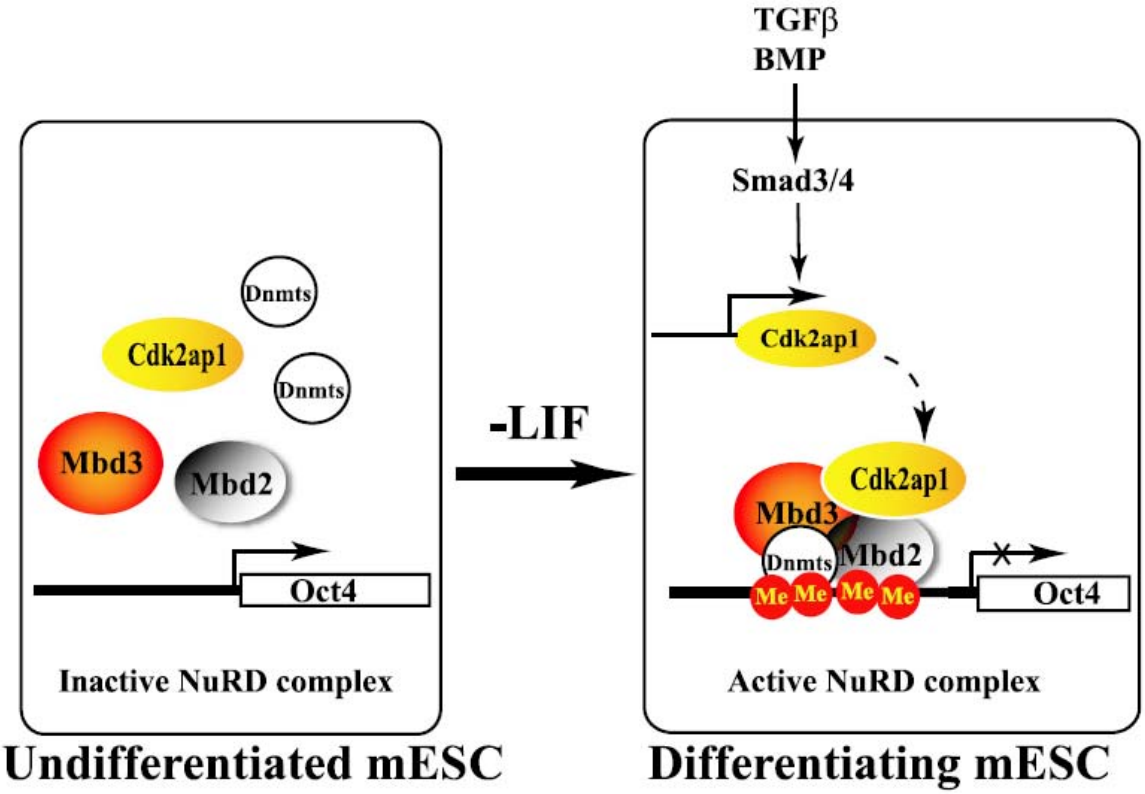

Fig. 60. Schematic for the role of Cdk2ap1 as a component of the NuRD complex and in mediation of extracellular signals. Up-regulation of *Cdk2ap1* in mESC by TGF_-Smad pathway, accompanied by an initiating event that brings together the NuRD complex, results in hypermethylation of the Oct4 promoter. Cdk2ap1 potentially functions as a Velcro factor to keep the members of the NuRD complex together. Increase in methylation (*Me*) of the *Oct4* promoter then results in the down-regulation of *Oct4* expression and loss of self-renewal potential.

5. SUMMARY

The aims of the study were to determinate expression and function of two members of insulin – like family, namely *Insl5* and *Insl6* and to verify the interactions between PELO and its putative partners CDK2AP1, EIF3G and SRPX.

To investigate the consequence of *Insl5* inactivation, *Insl5*-deficient mice on the hybrid C57BL/Jx129/Sv and inbred 129/Sv genetic background have been analysed. This study shown, that the absence of *Insl5* in both genetic backgrounds does not significantly affect the health. The most interesting differences between *Insl5*$^{-/-}$ and wild type mice on the hybrid genetic background were observed in behaviours, especial in nociceptive behaviours. Thus, *Insl5*$^{-/-}$ mice show delayed latency for antinociceptive behaviour and show faster paw withdraw latency potentially due to impairment of descending inhibitory antinociceptive inputs to the spinal cord. These results suggest that the *Insl5*-deficiency impairs neuronal pathways involved in the central mediation of pain or maintenance of the balance of spinal excitatory and inhibitory processes. These findings are supported by expression analysis of INSL5 in central nervous system. INSL5 showed a particular dense expression in brain areas concerned with the central mediation of antinociception such as anterior hypothalamus/preoptic area, the ventral nuclei of the periaqueductal gray and the pontine Kölliker-Fuse nucleus.

Insl5$^{-/-}$ mice on the inbred 129/Sv background display male and female infertility. This phenotype was not observed in the *Insl5*$^{-/-}$ mice on the hybrid background. Histological analysis of testes isolated from *Insl5*-deficient mice revealed the presence of all stages of spermatogenesis. Number of epididymal spermatozoas in *Insl5*$^{-/-}$ mice was not significantly different from that of wild type mice. Analysis of sperm parameters revealed that sperm of *Insl5* null mice had impaired sperm motility. Histological analysis of ovaries isolated from *Insl5*$^{-/-}$ mice revealed the presence of all stages of follicle development. To further analyse the reproductive defect in infertile *Insl5*$^{-/-}$ females, the number of oocytes, collected from females after and without superovulation, were counted and no significant differences were observed between *Insl5*$^{-/-}$ and control mice. However, most E1.5 embryos collected from *Insl5*$^{-/-}$ females inseminated by wild type males were at 1-cell stage in contrast to 2 cell-stage embryos observed in control females. These results suggest that the infertility of *Insl5*$^{-/-}$ females may be due to defect in oocyte maturation.

The glucose level of *Insl5*-deficient mice was significantly higher than in control litter mates. Results of glucose tolerance test (GTT) suggest impaired ability to metabolize glucose from bloodstream in *Insl5*$^{-/-}$ mice and that progressive defect of glucose tolerance in *Insl5*$^{-/-}$

mice is age-dependent. However, results of insulin tolerance test (ITT) revealed that sensitivity to insulin is not altered in *Insl5*-deficient mice. Based on the results of GTT and ITT, we suggest that the higher glucose level might reflect reduced insulin secretion in *Insl5*$^{-/-}$ mice. These findings were supported by histological and immunohistological analyses. Results of these studies revealed that the mean islet area in *Insl5*$^{-/-}$ pancreas was 1.6-fold smaller than that of wild type. Furthermore, the numbers of insulin positive ß-cells was significantly decreased in islets of *Insl5*$^{-/-}$ mice compared to control litter mates. These results suggest that the high glucose level in *Insl5*$^{-/-}$ mice might be due to defect in the developmental of pancreatic islets and/or insulin secretion.

Analyses of *Insl6* expression revealed that *Insl6* is predominantly expressed in male germ cells. Expression of *Insl6* is first detected in mouse testis at postnatal day 15, when the first wave of spermatogenesis progresses to pachytene spermatocytes.

To elucidate the role of INSL6 in germ cell development, we generated *Insl6*-deficient mice. The majority of the *Insl6*-deficient males on a hybrid genetic background exhibited impaired fertility, whereas females were fertile. The sperm number was significantly reduced probably due to apoptotic events. Also the motility of spermatozoa was drastically affected. Analysis of germ cell development during the juvenile life of *Insl6*$^{-/-}$ mice, showed an arrest of first wave of spermatogenesis in late meiotic prophase. RNA analysis revealed a significant decrease in expression of late meiotic- and post meiotic-specific marker genes, whereas expression of early meiotic-specific genes remains unaffected in the *Insl6*$^{-/-}$ testes. These results demonstrated that INSL6 is required for the progression of spermatogenesis.

The third aim of this study is concentrated to verify the interaction between pelota protein (PELO) and three proteins, namely cyclin-dependent kinase 2 associated protein 1 (CDK2AP1), eukaryotic translation initiation factor 3, subunit G (EIF3G) and Sushi- repeat-containing protein X-linked (SRPX). These three putative interaction partners of PELO have been identified in the yeast two-hybrid screening. Results of coimmunoprecipitation assay confirmed the specific interaction of CDKAP1, EIF3G and SRPX with PELO. GST-Pull down assay further supported the specific binding of PELO with its interaction partners and demonstrated that the third eEF1α-like domain of PELO protein is responsible for the interaction with partner proteins. To further support the specificity of interaction between PELO and its putative partners and to determine the subcellular localization of the interacting proteins, bimolecular fluorescence complementation assay (BiFC) was performed. Results of BiFC assay demonstrated the cytoskeleton-associated localization of PELO and CDK2AP1, EIF3G, SRPX, respectively protein complexes.

6. REFERENCES

Adham I.M., Burkhardt E., Benahmed M., Engel W.(1993) Cloning of a cDNA for a novel insulin-like peptide of the testicular Leydig cells. *J Biol Chem.* **268**:26668-26672.

Adham I.M., Emmen J.M.A. Engel W. (2000) The role of the testicular factor INSL3 in establishing the gonadal position *Mole Cell End.* **160**:11-16.

Adham I.M., Nayernia K., Burkhardt-Göttges E., Topaloglu Ö., Dickens C., Holstein A.F. Engel W. (2001) Teratozoospermia in mice lacking the transition protein 2 (TNP2). *Mol Hum Reprod*. **7**:513-520

Adham I.M., Sallam M.A., Steding G., Korabiowska M., Brinck U., Hoyer-Fender S., Oh C., Engel W. (2003) Disruption of the pelota gene causes early embryonic lethality and defects in cell cycle progression. *Mol Cell Biol*. **23**:1470-1476.

Ahrén B., Pacini G. (2003) Signals adapting the beta cells to changes in insulin sensitivity. *International Congress Series.* **1253**:105-113.

Ahlgren U., Jonsson J., Jonsson L., Simu K., Edlund H. (1998) β-cell-specific inactivation of the mouse *Ipf1/Pdx1* gene results in loss of the β-cell phenotype and maturity onset diabetes. *Genes Dev.* **12**:1763–1768.

Araki E., Lipes M.A., Patti M.E., Brüning J.C., Haag B., Johnson R.S., Kahn C.R. (1994) Alternative pathway of insulin signalling in mice with targeted disruption of the IRS-1 gene. *Nature*. **372**:186-190.

Ascoli M. (1981) Characterization of several clonal lines of cultured Leydig tumor cells: gonadotropin receptors and steroidogenic responses. *Endocrinology*. **108**:88-95.

Avruch J. (1998) Insulin signal transduction through protein kinase cascades. *Mol Cell Biochem*. **182**:31-48.

Baker J., Hardy M.P., Zhou J., Bondy C., Lupu F., Bellve A.R., Efstratiadis A. (1996) Effects of an *Igf1* gene null mutation on mouse reproduction. *Mol Endocrinol.* **10**:903-918.

Balvers M., Spiess A.N., Domagalski R., Hunt N., Kilic E., Mukhopadhyay A.K., Hanks E., Charlton H.M., Ivell R. (1998) Relaxin-like factor expression as a marker of differentiation in the mouse testis and ovary. *Endocrynology.* **139**:2960-2970.

Bandyopadhyay G., Standaert M.L., Sajan M.P., Karnitz L.M., Cong L., Quon M.J., Farese R.V. (1999) Dependence of insulin-stimulated glucose transporter 4 translocation on 3-phosphoinositide-dependent protein kinase-1 and its target threonine- 410 in the activation loop of protein kinase C-ζ. *Mol Endocrinol*. **13**:1766-1772.

Bathgate R.A., Balvers M., Hunt N., Ivell R. (1996) Relaxin-like factor gene is highly expressed in the bovine ovary of the cycle and pregnancy: sequence and messenger ribonucleic acid analysis. *Biol Reprod*. **55**:1452–1457.

Bathgate R.A., Samuel C.S., Burazin T.C., Layfield S., Claasz A.A., Reytomas I.G., Dawson N.F., Zhao C., Bond C., Summers R.J., Parry L.J., Wade J.D., Tregear G.W. (2002a) Human relaxin gene 3 (H3) and the equivalent mouse relaxin (M3) gene. Novel members of the relaxin peptide family. *J Biol Chem.* **277**:1148-1157.

Bathgate R.A., Scott D., Chung S., Ellyard D., Garreffa A., Tregear G. (2002b) Searching the human genome database for novel relaxin- and insulin-like peptides. *Letter Pept Sci.* **8**:129-132.

Bathgate R.A., Samuel C.S., Burazin T.C., Gundlach A.L., Tregear G.W. (2003) Relaxin: new peptides, receptors and novel actions. *Trends Endocrinol Metab.* **14**:207-213.

Bathgate R.A., Ivell R., Sanborn B.M., Sherwood O.D., Summers R.J. (2005) Receptors for relaxin family peptides. *Ann N Y Acad Sci.* **1041**:61–76.

Bathgate R.A., Hsueh A.J., Sherwood O.D. (2006a) Physiology and molecular biology of the relaxin peptide family. In: Knobil E., Neill J.D., eds. Physiology of reproduction. *3rd ed. San Diego: Elsevier.* pp. 679–770.

Bathgate R.A., Ivell R., Sanborn B.M., Sherwood O.D., Summers R.J. (2006b). International Union of Pharmacology LVII: recommendations for the nomenclature for receptors for relaxin family peptides. *Pharmacol Rev.* **58**:7-31.

Bech-Otschir D., Kraft R., Huang X., Henklein P., Kapelari B., Pollmann C., Dubiel W. (2001) COP9 signalosome-specific phosphorylation targets p53 to degradation by the ubiquitin system. *EMBO J.* **20**:1630–1639.

Bell G.I., Swain W.F., Pictet R.L., Cordell B., Goodman H.M., Rutter W.J. (1979) Nucleotide sequence of a cDNA clone encoding human preproinsulin. *Nature.* **282**:525-527.

Bell G.I., Merryweather J.P., Sanchez-Pescador R., Stempien M.M., Priestley L., Scott J., Rall L.B. (1984) Sequence of a cDNA clone encoding human preproinsulin-like growth factor II. *Nature*. **310**:775-777.

Bender A., Beckers J., Schneider I., Hölter S.M., Haack T., Ruthsatz T., Vogt-Weisenhorn D.M., Becker L., Genius J., Rujescu D., Irmler M., Mijalski T., Mader M., Quintanilla-Martinez L., Fuchs H., Gailus-Durner V., Hrabé de Angelis M., Wurst W., Schmidt J., Klopstock T. (2008) Creatine improves health and survival of mice. *Neurobiol Aging.* **29**:1404-1411.

Bennett W.I., Gall A.M., Southard J.L., Sidman R.L. (1971) Abnormal spermiogenesis in quaking, a myelin-deficient mutant mouse. *Biol Reprod.* **5**:30-58.

Bennett C.P., Docherty Z., Robb S.A., Ramani P., Hawkins J.R., Grant D. (1993) Deletion 9p and sex reversal. *J. Med. Genet.* **30**:518-520.

Bilkei-Gorzo A., Racz I., Michel K., Zimmer A., Klingmüller D., Zimmer A. (2004) Behavioral phenotype of pre-proenkephalin-deficient mice on diverse congenic background. *Psychopharmacology (Berl).* **176**:343-52.

Birnboim H.C., Doly J. (1979) A rapid alkaline extraction procedure for screening recombinant plasmid DNA. *Nucleic Acids Res*. **7**:1513-1523.

Blecher S.R., Erickson R.P. (2007) Genetics of sexual development: a new paradigm. *Am J Med Genet.* **143**:3054-3068.

Blendy J.A., Kaestner K.H., Weinbauer G.F., Nieschlag E., Schutz G. (1996) Severe impairment of spermatogenesis in mice lacking the CREM gene. *Nature.* **380**:162–165.

Block KL, Vornlocher H.P, Hershey J.W.B. (1998) Characterization of cDNAs encoding the p44 and p35 subunits of human translation initiation factor *eIF3. J Biol Chem.* **273**:31901–31908.

Blundell T.L., Humbel R.E. (1980) Hormone families: pancreatic hormones and homologous growth factors. *Nature***. 287**:781-787.

Bondy C.A., Zhou J., Arraztoa J.A. (2006) Growth Hormone, Insulin-Like Growth Factors, and the Ovary. In: Knobil E., Neill J.D. (eds.) Physiology of reproduction. *3rd ed. San Diego: Elsevier.* 527–546.

Bradford M.M. (1976) A rapid and sensitive method for the quantitation of microgram quantities of protein utilizing the principle of protein-dye binding. *Anal Biochem.* **72**:248-254.

Brandt B., Roetger A., Bidart J.M., Packeisen J., Schier K., Mikesch J.H., Kemming D., Boecker W., Yu D., Buerger H. (2002) Early placenta insulin-like growth factor (pro-EPIL) is overexpressed and secreted by c-erbB-2-positive cells with high invasion potential. *Cancer Res.* **62**:1020-1024.

Brites P., Mooyer P.A.W., el Mrabet L., Waterham H.R., Wanders R.J.A. (2009) Plasmalogens participate in very-long-chain fatty acid-induced pathology. *Brain.* **132**:482–492.

Bromfield J., Messamore W., Albertini D.F. (2007) Epigenetic regulation during oogenesis. *Reprod Fert Dev.* **20**:74-80.

Brudzynski S.M., Mogenson G.J. (1986) Decrease of locomotor activity by injections of carbachol into the anterior hypothalamic/preoptic area of the rat. *Brain Res.* **376**:38-46.

Bullesbach E.E., Schwabe C. (2002) The primary structure and the disulfide links of the bovine relaxin-like factor (RLF). *Biochemistry.* **41**:274-281.

Bult C.J., White O., Olsen G.J., Zhou L., Fleischmann R.D., Sutton G.G., Blake J.A., Fitzgerald L.M., Clyton R.A., Cocayne J.D., Kerlavage A.R., Dougherty B.A., Tomb J.F., Adams M.D., Reich C.I., Overbeek R., Kirkness E.F., Weinstock K.G., Merrick J.M., Glodeck A., Scott J.L., Geoghagen G.S., Venter J.C. (1996) Complete genome sequence of the methanogenic archeon *Methanococcus jannaschii*. *Science.* **237**:1058-1073.

Burazin T.C., Bathgate R.A., Macris M., Layfield S., Gundlach A.L., Tregear G.W. (2002) Restricted, but abundant, expression of the novel rat gene-3 (R3) relaxin in the dorsal tegmental region of brain. *J Neurochem.* **82**:1553-1557.

Burgess W., Liu Q., Zhou J., Tang Q., Ozawa A., Van Hoy R., Arkins S., Dantzer R., Kelley K. (1999) The immune–endocrine loop during aging: role of growth hormone and insulin-like growth factor-I. *Neuroimmunomodulation.* **6**:56–68.

Burgos M.H., Fawcett D.W. (1955) Studies on the fine structure of the mammalian testis. *J Biophys Biochem Cytol.* **1**:287-300.

Burkhardt E., Adham I.M., Brosig B., Gastmann A., Mattei M.G., Engel W. (1994) Structural organization of the porcine and human genes coding for a Leydig cell-specific insulin-like peptide (LEY I-L) and chromosomal localization of the human gene (INSL3). *Genomics.* **20**:13-19.

Busch S.J., Sassone-Corsi P. (1990) Dimers, leucine zippers and DNA-binding domains. *Trends Genet*. **6**:36-40.

Buyandelger B. (2006) PhD Thesis. The University of Göttingen. Expression and functional analyses of murine Pelota (*Pelo*) gene.

Cantley J., Choudhury A.I., Asare-Anane H., Selman C., Lingard S., Heffron H., Herrera P., Persaud S.J., Withers D.J. (2007) Pancreatic deletion of insulin receptor substrate 2 reduces beta and alpha cell mass and impairs glucose homeostasis in mice. *Diabetologia.* **50**:1248-1256.

Carpentier M., Guillemette C., Bailey J.L., Boileau G., Jeannotte L., DesGroseillers L., Charron J. (2004) Reduced fertility in male mice deficient in the zinc metallopeptidase NL1. *Mol Cell Biol.* **24**:4428-4437.

Castrillon D.H., Gonczy P., Alexander S., Rawson R., Eberhart C.G., Viswanathan S., DiNardo S., Wasserman S.A. (1993) Toward a molecular genetic analysis of spermatogenesis in *Drosophila melanogaster*: characterization of male-sterile mutants generated by single P element mutagenesis. *Genetics*. **135**:489-505.

Chan S.J., Steiner D.F. (2000) Insulin through the ages: phylogeny of a growth promoting and metabolic regulatory hormone. *Amer Zool.* **40**:213-222.

Chan S.J, Nakagawa S., Steiner D.F. (2007) Complementation analysis demonstrates that insulin cross-links both alpha subunits in a truncated insulin receptor dimer. *J Biol Chem.* **282**:137-154.

Chaplan S.R., Bach F.W., Pogrel J.W., Chung J.M., Yaksh T.L. (1994) Quantitative assessment of tactile allodynia in the rat paw. *J Neurosci Methods*. **53**:55-63.

Chassin D., Laurent A., Janneau J.L., Berger R., Bellet D. (1995) Cloning of a new member of the insulin gene superfamily (INSL4) expressed in human placenta. *Genomics*. **29**:465-70.

Chen M.S., Huber A.B., van der Haar M.E., Frank M., Schnell L., Spillmann A.A., Christ F., Schwab M.E. (2000) Nogo-A is a myelinassociated neurite outgrowth inhibitor and an antigen for monoclonal antibody IN-1. Nature, **403**:434–439.

Chen,M.S., Huber,A.B., van der Haar,M.E., Frank,M., Schnell,L., Spillmann,A.A., Christ,F. and Schwab,M.E. (2000) Nogo-A is a myelinassociated neurite outgrowth inhibitor and an antigen for monoclonal antibody IN-1. Nature, 403, 434–439.

Chen D., McKearin D. (2003). Dpp signaling silences bam transcription directly to establish asymmetric divisions of germline stem cells. *Curr. Biol.* 13:1786-1791.

Chen K., Knorr C., Moser G., Gatphayak K., Brening B. (2004) Molecular characterization of the porcine testis-specific phosphoglycerate kinase 2 (PGK2) gene and its association with male fertility. *Mamm Genome*. **15**:996-1006.

Chen J., Downs S.M. (2008) AMP-activated protein kinase is involved in hormone-induced mouse oocyte meiotic maturation in vitro. *Dev Biol.* **313**:47–57.

Chiarini-Garcia H., Russel L.D. (2001) High resolution light microscopic characterization of mouse spermatogonia. *Biol Reprod.* **85**:1170-1178.

Chien A., Edgar D.B., Trela J.M. (1976) Deoxyribonucleic acid polymerase from the extreme thermophile Thermus aquaticus. *J Bacteriol.* **127**:1550-1557.

Chomczynski P., Sacchi N. (1987) Single step method of RNA isolation by acid guanidine thiocyanate-phenol-chloroform extraction. *Anal Biochem*. **162**:156-159.

Chubb C. (1992) Oligotriche and quaking gene mutations. Phenotypic effects on mouse spermatogenesis and testicular steroidogenesis. *J Androl.* **13**:312-317.

Chung S.S.W., Sung W., Wang X., Wolgemuth D.J. (2004) Retinoic acid receptor is required for synchronization of spermatogenic cycles and its absence results in progressive breakdown of the spermatogenic process. *Dev Dyn.* **230**:754-766.

Cicero T.J., Davis L.A., LaRegina M.C., Meyer E.R., Schlegel M.S. (2002) Chronic opiate exposure in the male rat adversely affects fertility. *Pharmacol Biochem Behav.* **72**:157-163.

Cisneros F.J. (2004) DNA methylation and male infertility. *Front Biosci*. **9**:1182-1200.

Clark J.M. (1988) Novel non-templated nucleotide addition reactions catalyzed by procaryotic and eucaryotic DNA polymerases. *Nucleic Acids Res.* **16**:9677-9686.

Clement S.L., Lykke-Andersen J. (2006). No mercy for messages that mess with the ribosome. *Nat. Struct. Mol. Biol.* 13:299–301.

Clermont Y. (1972) Kinetics of spermatogenesis in mammals seminiferous epithelium cycle and spermatogonial renewal. *Physiol Rev.* **52**:198–236.

Choi M.G., Sohn T.S., Park S.B., Paik Y.H., Noh J.H., Kim K.M., Park C.K., Kim S. (2009) Decreased Expression of $p12^{DOC-1}$ Is Associated with More Advanced Tumor Invasion in Human Gastric Cancer Tissues. *Eur Surg Res.* **42**:223-229.

Combettes-Souverain M., Issad T. (1998) Molecular basis of insulin action. *Diabetes Metab*. **24**:477-489.

Conklin D., Lofton-Day C.E., Haldeman B.A., Ching A., Whitmore T.E., Lok S., Jaspers S. (1999) Identification of INSL5, a new member of the insulin superfamily. *Genomics.* **60**:50-56.

Conti M., Anderson C.B., Richard F., Mehats C., Chun S.Y., Horner K., Jin C., Tsafriri A. (2002) Role of cyclic nucleotide signaling in oocyte maturation. *Mol Cell Endocrinol.* **187**:153–159.

Costa G.L., Weiner M.P. (1994) Polishing with T4 or *Pfu* polymerase increases the efficiency of cloning of PCR fragments. *Nucleic Acids Res.* **22**:2423.

Dagert M., Ehrlich S.D.. (1979) Prolonged incubation in calcium chloride improves the competence of *Escherichia coli* cells. *Gene*. **6**:23-28.

D'Amour F.E., Smith D.L. (1941) A method for determining loss of pain sensation. *J Pharmacol Exp Ther.* **72**:74-79.

Danielson L.A., Sherwood O.D., Conrad K.P. (1999) Relaxin is a potent renal vasodilator in conscious rats. *J Clin Invest.* **103**:525–533.

Daughaday W.H., Rotwein P. (1989) Insulin-like growth factors I and II: peptide, messenger ribonucleic acid and gene structures, serum, and tissue concentrations. *Endocr. Rev.* **10**:68–91.

Davis L., Engebrecht J. (1998) Yeast *dom34* mutants are defective in multiple developmental pathways and exhibit decreased levels of polyribosomes. *Genetics.* **149**:45–56.

DeFea K., Roth R.A. (1997) Modulation of insulin receptor substrate-1 tyrosine phosphorylation and function by mitogen-activated protein kinase. *J Biol Chem*. **272**:31400-31406

de Kretser D.M., Kerr J.B. (1988). The cytology of the testis. In: Knobil E., Neill J.D. (eds.) The physiology of reproduction. *Raven Press, New York.* pp. 837–932.

Denhardt D.T. (1966) A membrane-filter technique for the detection of complementary DNA. *Biochem Biophys Res Commun.* **23**:641-646.

de Pablo F., de la Rosa E.J. (1995) The developing CNS: a scenario for the action of proinsulin, insulin and insulin-like growth factors. *Trends Neurosci.* **18**:143-150.

de Rooij D.G. (1998) Stem cells in the testis. *Int J Exp Pathol.* **79**:67-80.

de Rooij D.G. (2001) Proliferation and differentiation of spermatogonial stem cells. *Reproduction.* **121**:347-354.

de Rooij D.G., de Boer P. (2003) Specific arrest of spermatogenesis on genetically modified and mutant mice. *Cytogenet Genome Res.* **103**:267-276.

de Quinto S.L., Lafuente E., Martínez-Salas E. (2001) IRES interaction with translation initiation factors: functional characterization of novel RNA contacts with eIF3, eIF4B, and eIF4GII. RNA *Cambridge University Press*. **7**:1213–1226.

Deshpande A.M., Dai Y.S., Kim Y., Kim J, Kimlin L., Gao K., Wong D.T.W.W. (2008) Cdk2ap1 is required for epigenetic silencing of *Oct4* during murine embryonic stem cell differentiation. *J Biol Chem.* **284:**6043–6047.

Dierich A., Parvinen M., Sassone-Corsi P. (1996) Spermiogenesis deficiency and germ-cell apoptosis in CREM-mutant mice. *Nature.* **380**:159–162.

Doma M.K., Parker R. (2006) Endonucleolytic cleavage of eukaryotic mRNAs with stalls in translation elongation. *Nature* 440:561–564.

Downs S.M., Chen J. (2006) Induction of meiotic maturation in mouse oocytes by adenosine analogs. *Mol Rep Dev.* **73**:1159–1168.

Duguay S.J., Jin Y., Stein J., Duguay A.N., Gardner P.G., Steiner D.F. (1998) Post-translational processing of the insulin-like growth factor-2 precursor. *J Biol Chem.* **273**:18443-18451.

Dun S.L., Brailoiu E., Wang Y., Brailoiu G.C., Liu-Chen L.Y., Yang J., Chang J.K., Dun N.J. (2006) Insulin-like peptide 5: expression in the mouse brain and mobilization of calcium. *Endocrinology*. **147**:3243–3248.

Dym M., Fawcett D.W. (1971) Further observation on the numbers of spermatogonia, spermatocytes and spermatids connected by intercellular bridges in the mammalian testis. *Biol. Reprod.* **4**:195-215.

Ebermann L. (2005) MSc Thesis. The University of Göttingen. Identification and characterization of putative interaction partners of Pelota.

Eberhart C.G., Wasserman S.A. (1995) The pelota locus encodes a protein required for meiotic cell division: an analysis of G2/M arrest in *Drosophila* spermatogenesis. *Development*. **121**:3477-3486.

Eddy N.P., Leimbach D. (1953) Synthetic analgesics (II), dithienylbutenyl and dithienylbutylamines. *J Pharmacol Exp Ther.* **107**:385– 389.

Eldar-Finkelman H., Krebs E.G. (1997) Phosphorylation of insulin receptor substrate 1 by glycogen synthase kinase 3 impairs insulin action. *Proc Natl Acad Sci USA*. **94**:9660-9664.

Embury S.H., Dozy A.M., Kan Y.M. (1980) Molecular mechanism in alpha-thalasemia: racial differences in alpha globin gene organization. *Ann NY Acad Sci.* **344**:31-40.

Ensslin M.A., Shur B.D. (2003) Identification of mouse sperm SED1, a bimotif EGF repeat and discoidin domain protein involved in sperm-egg binding. *Cell* **114**:405-417.

Eppig J.J., Viveiros M.M., Marin-Bivens C., de La Fuente R. (2004) Regulation of mammalian oocyte maturation, In: Leung P.C.K., Adashi E.Y. (eds.), The ovary, second edition. *Elsevier/Academic Press, San Diego*, pp. 113–129.

Escalier D. (2001) Impact of genetic engineering on the understanding of spermatogenesis. *Hum Reprod Update.* **7**:191-210.

Evans M.J., Kaufman M.H. (1981). Establishment in culture of pluripotential cells from mouse embryos. *Nature*. **292**:154-156.

Fagerholm V., Grönroos T., Marjamäki P., Viljanen T., Scheinin M., Haaparanta M.(2004) Altered glucose homeostasis in alpha2A-adrenoceptor knockout mice. *Eur J Pharmacol*. **505**:243-52.

Fan H., Li M., Tong C., Chen D., Xia G., Song X., Schatten H., Sun Q. (2002) Inhibitory effects of cAMP and protein kinase C on meiotic maturation and MAP kinase phosphorylation in porcine oocytes. *Mol Rep Dev.* **63**:480–487.

Fawcett J., Rabkin R. (1995) The processing of insulin-like growth factor-I (IGF-I) by a cultured kidney cell line is altered by IGF-binding protein-3. *Endocrinology.* **136**:1340-1347.

Feinberg A. P., Vogelstein B. (1984) A technique for radiolabeling DNA restriction endonuclease fragments to high specific activity. *Anal Biochem.* **123**:6-13.

Figueiredo M.L., Kim Y, John M.A.R.S., Wong D.T.W.W. (2005) p12CDK2-AP1gene therapy strategy inhibits tumor growth in an in vivo mouse model of head and neck cancer. *Clin Cancer Res.***11**:3939-3948.

Flejter W.L., Fergestad J., Gorski J., Varvill T., Chandrasekharappa S. (1998) A gene involved in XY sex reversal is located on chromosome 9, distal to marker D9S1779. *Am J Hum Genet.* **63**:794–802.

Fowler K.J., Clouston W.M., Fournier R.E., Evans B.A. (1991) The relaxin gene is located on chromosome 19 in the mouse. *FEBS Lett.* **292**:183-186.

Franklin K.B.J., Abbott F.V. (1989) Techniques for assessing the effects of drugs on nociceptive responses. In: Boulton A.A., Baker G.B., Greenshaw A.J., eds. Neuromethods 13; Psychopharmacology. *Clifton NJ USA: Humana Press.* pp. 145-216.

Frolova L., Le Goff X., Rasmussen H.H., Cheperegin S., Drugeon G., Kress M., Arman I., Haenni A.L., Celis J.E., Philippe M., Justesen J., Kisselev L. (1994) A highly conserved eukaryotic protein family possessing properties of polypeptide chain release factor. *Nature*. **372**:701-703.

Froment P., Seurin D., Hembert S., Levine J.E., Pisselet C., Monniaux D., Binoux M., Monget P. (2002) Reproductive abnormalities in human IGF binding protein-1 transgenic female mice. *Endocrinology*. **143**:1801-1808.

Fujita E., Tanabe Y., Hirose T., Aurrand-Lions M., Kasahara T., Imhof B.A., Ohno S., Momoi T. (2007) Loss of partitioning-defective-3/isotype-specific interacting protein (par-3/ASIP) in the elongating spermatid of RA175 (IGSF4A/SynCAM)-deficient mice. *Am J Pathol.* **171**:1800-1810.

Gailus-Durner V., Fuchs H., Becker L., Bolle I., Brielmeier M., Calzada-Wack J., Elvert R., Ehrhardt N., Dalke C., Franz T.J., Grundner-Culemann E., Hammelbacher S., Hölter S.M., Hölzlwimmer G., Horsch M., Javaheri A., Kalaydjiev S.V., Klempt M., Kling E., Kunder S., Lengger C., Lisse T., Mijalski T., Naton B., Pedersen V., Prehn C., Przemeck G., Racz I., Reinhard C., Reitmeir P., Schneider I., Schrewe A., Steinkamp R., Zybill C., Adamski J., Beckers J., Behrendt H., Favor J., Graw J., Heldmaier G., Höfler H., Ivandic B., Katus H., Kirchhof P., Klingenspor M., Klopstock T., Lengeling A., Müller W., Ohl F., Ollert M., Quintanilla-Martinez L., Schmidt J., Schulz H., Wolf E., Wurst W., Zimmer A., Busch D.H., de Angelis M.H. (2005) Introducing the German Mouse Clinic: open access platform for standardized phenotyping. *Nat Methods*. **2**:403-404.

Galic S., Hauser C., Kahn B.B., Haj F.G., Neel B.G., Tonks N.K., Tiganis T. (2005) Coordinated regulation of insulin signaling by the protein tyrosine phosphatases PTP1B and TCPTP. *Mol Cell Biol.* **25**:819-829.

Galy B., Hölter S.M., Klopstock T., Ferring D., Becker L., Kaden S., Wurst W., Gröne H.J., Hentze M.W. (2006) Iron homeostasis in the brain: complete iron regulatory protein 2 deficiency without symptomatic neurodegeneration in the mouse. *Nat Genet*. **38**:967-969.

Gambineri A., Patton L., De Iasio R., Palladoro F., Pagotto U., Pasquali R. (2007) Insulin-like factor 3: a new circulating hormone related to luteinizing hormone-dependent ovarian hyperandrogenism in the polycystic ovary syndrome. *J Clin Endocrinol Metab.* **92**:2066-2073.

Garneau N.L., Wilusz J., Wilusz C.J. (2007). The highways and byways of mRNA decay. *Nat. Rev. Mol. Cell Biol.* **8**:113–126.

Gatfield D., Izaurralde E. (2004). Nonsense-mediated messenger RNA decay is initiated by endonucleolytic cleavage in *Drosophila*. *Nature.* **429**:575–578.

Geenen, V., Kecha, O., Brilot, F., Charlet-Renard, C., and Martens, H. (1999). The thymic repertoire of neuroendocrine-related self antigens: biological role in T-cell selection and pharmacological implications. *Neuroimmunomodulation.* **6**:115–125.

Gershoni J.M., Palade G.E. (1982) Electrophoretic transfer of proteins from sodium dodecyl sulfate-polyacrylamide gels to a positively charged membrane filter. *Anal Biochem.* **124**:396-405.

Goldstein B.J. (2003) Protein-tyrosine phosphatases and the regulation of insulin action. In: LeRoith D., Taylor S.I., Olefsky J.M., (eds), *Diabetes mellitus: a fundamental and clinical text;* **3**:255.

Gonzalez C.I., Bhattacharya A., Wang W., Peltz, S.W. (2001). Nonsense-mediated mRNA decay in Saccharomyces cerevisiae. *Gene.* **274**:15–25.

Goto M., Koji T., Mizuno K., Tematu M., Koikeda S., Nakane P.K., Mori N., Masamune Y., Nakanishi Y. (1990) Transcription switch of two phosphoglycerate kinase genes during spermatogenesis as determined with mouse testis sections in situ. *Exp Cell Res.* **186**:273-278.

Greene N.D., Copp A.J. (1997) Inositol prevents folate-resistant neural tube defects in the mouse. *Nature Med.* **3**:60-66.

Griffiths A.J.F., Miller J.H., Suzuki D., Lewontin R.C., Gelbart W.M., (2000) An introduction to genetic analysis. *W.H. Freeman and Company, San Francisco.*

Grunberg H. (1954) Variation within inbred strains of mice. *Nature.* **173**:674-676.

Gutti R.V., Tsai-Morris C., Dufau M.L. (2008) Gonadotropin-regulated testicular helicase (DDX25), an essential regulator of spermatogenesis, prevents testicular germ cell apoptosis. *J Biol Chem.* **283**:17055–17064.

Grzmil P., Boinska D., Kleene K.C., Adham I.M., Schlüter G., Kämper M., Buyandelger B, Meinhardt A., Wolf S., Engel W. (2008) *Prm3*, the fourth gene in the mouse protamine gene cluster, encodes a conserved acidic protein that affects sperm motility. *Biol Reprod.* **78**:958-67.

Halls M.L., Bathgate R.A., Summers R.J. (2007a) Comparison of signaling pathways activated by the relaxin family peptide receptors, RXFP1 and RXFP2, using reporter genes. *J Pharmacol Exp Ther.* **320**:281–290.

Halls M.L., van der Westhuizen E.T., Bathgate R.A., Summers R.J. (2007b) Relaxin family peptide receptors – former orphans reunite with their parent ligands to activate multiple signalling pathways. *Br J Pharmacol.* **150**:677-691.

Han Z., Mtango N.R., Patel B.G., Sapienza C., Latham K.E. (2008) Hybrid vigor and transgenerational epigenetic effects on early mouse embryo phenotype. *Biol Reprod.* **79**:638-648.

Hargreaves K., Dubner R., Brown F., Flores C., Joris J. (1988) A new and sensitive method for measuring thermal nociception in cutaneous hyperalgesia. *Pain*. **32**:77-88.

Haugaard-Jönsson M.L., Hossain M.A., Daly N.L., Craik D.J., Wade J.D., Rosengren K.J. (2009) Structure of human insulin-like peptide 5 and characterization of conserved hydrogen bonds and electrostatic interactions within the relaxin framework. *Biochem J.* **419**:619–627.

Held T., Paprotta I., Khulan J., Hemmerlein B., Binder L., Wolf S., Schubert S., Meinhardt A., Engel W., Adham I.M. (2006) *Hspa4l*-deficient mice display increased incidence of male infertility and hydronephrosis development. *Mol Cell Biol.* **26**:8099-8108.

Herrera P.L., Orci L., Vassalli J.D. (1998) Two transgenic approaches to define the cell lineages in endocrine pancreas development. *Mol Cell Endocrinol.* **140**:45–50.

Hinton P., Peterson C., Dahly E., Ney D. (1998) IGF-I alters lymphocyte survival and regeneration in thymus and spleen after dexamethasone treatment. *Am J Physiol.* **274**:912–920.

Hodge C.J., Apkarian A.V., Stevens R.T. (1986) Inhibition of dorsal-horn cell responses by stimulation of the Kolliker-Fuse nucleus. *J Neurosurg.* **65**:825-833.

Hodge R. (1994) Reparation of RNA gel blots. *Methods Mol Biol*. **28**:49-54.

Holden J.E., Farah E.N., Jeong Y. (2005) Stimulation of the lateral hypothalamus produces antinociception mediated by 5-HT1A, 5-HT1B and 5-HT3 receptors in the rat spinal cord dorsal horn. *Neuroscience* **135**:1255-1268.

Hofmann H.A., De Vry J., Siegling A., Spreyer P., Denzer D. (2003) Pharmacological sensitivity and gene expression analysis of the tibial nerve injury model of neuropathic pain. *Eur J Pharmacol.* **470**:17-25.

Hogan B., Beddington R., Costantini F., Lacy E. (1994) Manipulating the mouse embryo. A laboratory manual, second edition. *Cold Spring Harbor Laboratory Press, Cold Spring Harbor.*

Hoo J.J., Salasfsky I.S., Lin C.C., Pinsky L. (1989) Possible location of a recessive testis forming gene on 9p24. *Am J Hum Genet Suppl.* **45**:A78.

Hossain M.A., Bathgate R.A., Kong C.K., Shabanpoor F., Zhang S., Haugaard-Jçnsson L.M., Rosengren K.J., Tregear G.W., Wade J.D. (2008) Synthesis, conformation, and activity of human insulin-like peptide 5 (INSL5). *Chembiochem.* **9**:1816-1822.

Hotamisligil G.S., Peraldi P., Budavari A., Ellis R., White M.F., Spiegelman B.M. (1996) IRS-1-mediated inhibition of insulin receptor tyrosine kinase activity in TNF-α- and obesity-induced insulin resistance. *Science*. **271**:665-668.

Hou C., Tang C.C, Roffler S.R., Tang T.K. (2000) Protein 4.1R binding to eIF3-p44 suggests an interaction between the cytoskeletal network and the translation apparatus. *Blood.* **96**:747-753

Houvras Y., Benezra M., Zhang H., Manfredi J.J., Weber B.L. Licht D.J. (2000) BRCA1 physically and functionally interacts with ATF1. *J Biol Chem.* **275**:36230-36237.

Hsu, S.Y. (1999) Cloning of two novel mammalian paralogs of relaxin/insulin family proteins and their expression in testis and kidney. *Mol Endocrinol*. **13**:2163–2174.

Hsu S.Y., Nakabayashi K., Nishi S., Kumagai J., Kudo M., Sherwood O.D., Hsueh A.J. (2002) Activation of orphan receptors by the hormone relaxin. *Science.* **295**:671-674.

Hsu S.Y. (2003a) New insights into the evolution of the relaxin-LGR signaling system. *Trends Endocrinol Metab.* **14**:303-309.

Hsu S.Y., Nakabayashi K., Niski S., Kumagai J., Kudo M., Bathgate R.A., Sherwood O.D., Hsueh A.J.W. (2003b) Relaxin signaling in reproductive tissues. *Mol Cell Endocrinol.* **202**:165-170.

Hsu S.Y., Semyonov J., Park J., Chang C.L. (2005) Evolution of the signaling system in relaxin-family peptides. *Ann NY Acad Sci.* **1041**:520–529.

Hu G. (1993) DNA polymerase-catalyzed addition of nontemplated extra nucleotides to the 3' end of a DNA fragment. *DNA Cell Biol.* **12**:763-770.

Hu C.D., Chinenov Y., Kerppola T.K. (2002). Visualization of interactions among bZIP and Rel family proteins in living cells using bimolecular fluorescence complementation. *Mol Cell* **9:**789-798.

Huebner A., Mann P., Rohde E., Kaindl A.M., Witt M., Verkade P., Jakubiczka S., Menschikowski M., Stoltenburg-Didinger G., Kohler K. (2006) Mice lacking the nuclear pore complexprotein ALADIN show female infertility but fail to develop a phenotype resembling human tripe A syndrome. *Mol Cell Biol.* **26**:1879-1887.

Hudson P., Haley J., John M., Cronk M., Crawford R., Haralambidis J., Tregear G., Shine J., Niall H. (1983) Structure of a genomic clone encoding biologically active human relaxin. *Nature.* **301**:628-631.

Hudson P., John M., Crawford R., Haralambidis J., Scanlon D., Gorman J., Tregear G., Shine J., Niall H. (1984) Relaxin gene expression in human ovaries and the predicted structure of a human preprorelaxin by analysis of cDNA clones. *EMBO J.* **3**:2333-2339.

Hughes I.A., Acerini C.L. (2008) Factors controlling testis descent. *Eur J Endocrinol.* **159**:75–82.

Inoue H., Pan J. and Hakura A. (1998) Suppression of v-Src transformation by the drs gene. J. Virol., **72**:2532–2537.

Ion R., Telvi L., Chaussain J.L., Barbet J.P., Nunes M., Safar A., Rethore M.O., Fellous M., McElreavet K. (1998) Failure of testicular development associated with a rearrangement of 9p24.1 proximal to the *SNF2* gene. *Hum Genet.* **102**:151–156.

Ivell R., Bathgate R.A.D. (2002) Reproductive biology of the relaxin-like factor (RLF/INSL3). *Biol Reprod.* **67**:699-705.

Janneau J.L., Maldonado-Estrada J., Tachdjian G., Miran I., Motte N., Saulnier P., Sabourin J.C., Cote J.F., Simon B., Frydman R., Chaouat G., Bellet D. (2002) Transcriptional expression of genes involved in cell invasion and migration by normal and tumoral trophoblast cells. *J Clin Endocrino Metabo.* **87**:5336-5339.

Jansen M., van Schaik F.M.A., Ricker A.T., Bullock B., Woods D.E., Gabbay K.H., Nussbaum A.L., Sussenbach J.S., Van de Brande J.L. (1983) Sequence of cDNA encoding human insulin-like growth factor I precursor. *Nature.* **306**:609-611.

Jänig W. 1996 Neurobiology of visceral afferent neurons: neuroanatomy, functions, organ regulations and sensations. *Biol Psychol*. **42**:29-51.

Jones S.L. (1991) Descending noradrenergic influences on pain. *Prog Brain Res.* **88**:381-394.

Joyner A.L. (2000) Gene targeting. a practical approach second edition. *Oxford University Press, New York.*

Juriloff D.M., Harris M.J. (2000) Mouse models for neural tubes closure defects. *Hum Mol Genet.* **9**:993-1000.

Kadowaki T. (2000) Insights into insulin resistance and type 2 diabetes from knockout mouse models. *J Clin Invest*. **106**:459-465.

Kallnik M., Elvert R., Ehrhardt N., Kissling D., Mahabir E., Welzl G., Faus-Kessler T., Hrabe de Angelis M., Wurst W., Schmidt J., Hölter S.M. (2007) Impact of IVC housing on emotionality and fear learning in male C3HeB/FeJ and C57BL/6J mice. *Mamm Genome.* **18**:173-186.

Kansas G.S. (1996) Selectins and their ligands: current concepts and controversies. *Blood.* **88**:3259–3287.

Kappeler1 L., de Magalhaes Filho C., Dupont J., Leneuve P., Cervera P., Loudes C., Blaise A., Klein R., Epelbaum J., Le Bouc Y., Holzenberger M. (2008) Brain IGF-1 receptors control mammalian growth and lifespan through a neuroendocrine mechanizm. *PLoS Biol.* **6**:2144-2151.

Kasik J., Muglia L., Stephan D.A., Menon R.K. (2000) Identification, chromosomal mapping and partial characterization of mouse *Insl6*: a new member of the insulin family. *Endocrinology.* **141**:458-461.

Kastner P., Mark M., Leid M., Gansmuller A., Chin W., Grondona J.M., Decimo D., Krezel W., Dierich A., Chambon P. (1996) Abnormal spermatogenesis in RXR beta mutant mice. *Genes Dev.* **10**:80–92.

Kawamata M., Nishimori K. (2006) Mice deficient in *Dmrt7* show infertility with spermatogenic arrest at pachytene stage. *FEBS Lett.* **580**:6442–6446.

Kawamura K., Kumagai J., Sudo S., Chun S., Pisarska M., Morita H., Toppari J., Fu P., Wade J.D., Bathgate R.A., Hsueh A.J.W. (2004) Paracrine regulation of mammalian oocyte maturation and male germ cell survival. *Proc Natl Acad Sci.* **101:**7323-7328.

Kayampilly P.P., Menon K.M.J. (2009) Follicle-stimulating hormone inhibits adenosine 5'-monophosphate-activated protein kinase activation and promotes cell proliferation of primary granulosa cells in culture through an Akt-dependent pathway. *Endocrinology.* **150**:929–935.

Kelada S.N., Shelton E., Kaufmann R.B., Khoury M.J. (2001) δ-aminolevulinic acid dehydratase (ALAD) genotype and lead toxicity. *Am J Epidem.* **154**:1-13.

Kido Y., Nakae J., Accili D. (2001) Clinical review 125: the insulin receptor and its cellular targets. *J Clin Endocrinol Metab.* **86**:972.

Kim C.J., Shimakage M., Kushima R., Mukaisho K., Shinka T., Okada Y. Inoue,H. (2003) Down-regulation of drs mRNA in human prostate carcinomas. *Hum Pathol.,* **34**:654–657.

Kim J.T., Kimb K.D., Songb E.Y., Leeb H.G., Kimb J.W., Kimc J.W., Chaec S.K., Kimd E., Leea M., Yanga Y., Lima J.S. (2006) Apoptosis-inducing factor (AIF) inhibits protein synthesis by

interacting with the eukaryotic translation initiation factor 3 subunit p44 (eIF3g). *FEBS Lett.* **580**:6375–6383.

Kirchenmayer N. (2007) MSc Thesis. The University of Köln. Untersuchungen zur Interaktion zwischen Pelota und putativen Interaktionspartnern.

Kizawa H., Nishi K., Ishibashi Y., Harada M., Asano T., Ito Y., Suzuki N., Hinuma S., Fujisawa Y., Onda H., Nishimura O., Fujino M. (2003) Production of recombinant human relaxin 3 in AtT20 cells. *Requl Pept.* **113**:79-84.

Kohno Y., Patel V., Kim Y., Tsuji T., Chin B.R., Sun M., Bruce Donoff R., Kent R., Wong D., Todd R. (2002) Apoptosis, proliferation and *p12(doc-1)* profiles in normal, dysplastic and malignant squamous epithelium of the Syrian hamster cheek pouch model. *Oral Oncol.***38**:274-280.

Kramer M.G., Vaughn T.T., Pletscher L.S., King-Ellison K., Adams E., Erikson C., Cheverud J.M. (1998) Genetic variation in body weight gain and composition in the intercross of large (LG/J) and small (SM/J) inbred strains of mice. *Genet Mol Biol.* **21**:211-218.

Krawetz S.A. (2005) Paternal contribution: new insights and future challenges. *Nat Rev Genet.* **6**:633-642.

Kremling H., Kemie S., Wilhelm K., Adham I.M., Hameister H., Engel W. (1991) Mouse proacrosin gene: nucleotide sequence, diploid expression, and chromosomal localization. *Genomics.* **11**:828–834.

Kubota N., Terauchi Y., Tobe K., Yano W., Suzuki R., Ueki K., Takamoto I., Satoh H., Maki T., Kubota T., Moroi M., Okada-Iwabu M., Ezaki O., Nagai R., Ueta Y., Kadowaki T., Noda T. (2004) Insulin receptor substrate 2 plays a crucial role in beta cells and the hypothalamus. *J Clin Invest.* **114**:917-924.

Kulkarni R.N., Brüning J.C., Winnay J.N., Postic C., Magnuson M.A., Kahn C.R. (1999) Tissue-specific knockout of the insulin receptor in pancreatic β cells creates an insulin secretory defect similar to that in type 2 diabetes. *Cell*. **96**:329-39.

Kumagai J., Hsu S.Y., Matsumi H., Roh J.S., Fu P., Wade J.D., Bathgate R.A., Hsueh A.J. (2002) INSL3/Leydig insulin-like peptide activates the LGR8 receptor important in testis descent. *J Biol Chem.* **277**:31283–31286.

Kuo Y.M., Duncan J.L., Westaway S.K., Yang H., Nune G., Xu E.Y., Hayflick S.J., Gitschier J. (2005) Deficiency of pantothenate kinase 2 (*Pank2*) in mice leads to retinal degeneration and azoospermia. *Hum Mol Genet.* **14**:49-57.

Kuo Y.M., Hayflick S.J., Gitschier J. (2007) Deprivation of pantothenic acid elicits a movement disorder and azoospermia in a mouse model of pantothenate kinase-associated neurodegeneration. *J Inherit Metab Dis.* **30**:310-317.

Kuramochi-Miyagawa S., Kimura T., Ijiri T.W., Isobe T., Asada N., Fujita Y., Ikawa M., Iwai N., Okabe M., Deng W., Lin H., Matsuda Y., Nakano T. (2004) Mili, a mammalian member of piwi family gene, is essential for spermatogenesis. *Development.* **131**:839-849.

Laemmli U.K. (1970) Cleavage of structural proteins during the assembly of the head of the bacteriophage T4. *Nature.* **227**:680-685.

Lagirand-Cantaloube J., Offner N., Csibi A., Leibovitch M.P., Batonnet-Pichon S., Tintignac L.A., Segura C.T. Leibovitch S.A. (2008) The initiation factor eIF3-f is a major target for Atrogin1/MAFbx function in skeletal muscle atrophy *EMBO J.* **27**:1266–1276.

Laird P.W., Zijderveld A., Linders K., Rudnicki M.A., Jaenisch R., Berns A. (1991) Simplified mammalian DNA isolation procedure. *Nucleic Acids Res*. **19**:4293.

Lalouel J.M., White R. (1990) Analysis of genetic linkage. In: Emery A.E.H., Rimoin D.L., Sofaer J.A., Black I., McKusick V.A., eds. Principles and practice of medical genetics, vol. 1. *Churchill-Livingston Inc., New York.* pp. 149-164.

Lammers J.H., Offenberg H.H., van Aalderen M., Vink A.C., Dietrich A.J., Heyting C. (1994) The gene encoding a major component of the lateral elements of synaptonemal complexes of the rat is related to X-linked lymphocyte-regulated genes. *Mol Cell Biol.* **14**:1137-1146.

Lamothe B., Baudry A., Desbois P., Lamotte L., Bucchini D., de Meyts P., Joshi R.L. (1998) Genetic engineering in mice: impact on insulin signalling and action. *Biochem J*. **335**:193-204.

Laurent A., Rouillac C., Delezoide A.L., Giovangrandi Y., Vekemans M., Bellet D., Abitbol M., Vidaud M. (1998) Insulin-like 4 (INSL4) gene expression in human embryonic and trophoblastic tissues. *Mol Reprod Dev*. **51**:123-1239.

Leblond and Clermont (1952) Spermiogenesis of the rat, mouse, hamster, and guinea pig as revealed by the periodic acid-fuchsin sulfurous acid technique. *Am J Anat.* **90**:167-216.

Lebrun P., Mothe-Satney I., Delahaye L., Van Obberghen E., Baron V. (1998) Insulin receptor substrate-1 as a signaling molecule for focal adhesion kinase $pp125^{FAK}$ and $pp60^{src}$. *J Biol Chem*. **273**:32244-32253.

Li J., DeFea K., Roth R.A. (1999) Modulation of insulin receptor substrate-1 tyrosine phosphorylation by an Akt/phosphatidylinositol 3-kinase pathway. *J Biol Chem*. **274**:9351-9356.

Li,Q., Qi,B., Oka,K., Shimakage,M., Yoshioka,N., Inoue,H., Hakura,A.,Kodama,K., Stanbridge,E.J. and Yutsudo,M. (2001) Link of a new type of apoptosis-inducing gene ASY/Nogo-B to human cancer. *Oncogene* **20**:3929–3936.

Lilienbaum A., Sage J., Memet S., Rassoulzadegan M., Cuzin F., Israel A. (2000) NF-kappa B is developmentally regulated during spermatogenesis in mice. *DevDyn.* **219**:333-340.

Lin, H. (2002). The stem-cell niche theory: lessons from flies. *Nat. Rev. Genet.* **3:**931-940.

Liu D., Matzuk M.M., Sung W.K., Guo Q., Wang P., Wolgemuth D.J. (1998) Cyclin A1 is required for meiosis in the male mouse. *Nat. Genet.* **20**:377–380.

Liu J., LeRoith D. (1999) Insulin-like growth factor I is essential for postnatal growth in response to growth hormone. *Endocrinology.* **140**:5178-5184.

Liu, C., Chen, J., Sutton, S., Roland, B., Kuei, C., Farmer, N., Sillard, R., and Lovenberg, T. W. (2003a) Identification of relaxin-3/INSL7 as a ligand for GPCR142. *J Biol Chem.* **278:**50765-50770.

Liu C., Eriste E., Sutton S., Chen J., Roland B., Kuei C., Farmer N., Jornvall H., Sillard R., Lovenberg T.W. (2003b) Identyfication of relaxin-3/INSL7 as an endogenous ligand for the orphan G-protein-coupled receptor GPCR135. *J Biol Chem.* **278**:50754-50764.

Liu C., Chen J., Kuei C., Sutton S., Nepomuceno D., Bonaventure P., Lovenberg T.W. (2005a) Relaxin-3/insulin-like peptide 5 chimeric peptide, a selective ligand for G protein-coupled receptor (GPCR)135 and GPCR142 over leucine-rich repeat-containing G protein-coupled receptor 7. *Mol Pharmacol* **67**:231-240.

Liu C., Kuei C., Sutton S., Chen J., Bonaventure P., Wu J., Nepomuceno D., Wilkinson T., Bathgate R.A., Eriste E., Sillard R., Lovenberg T.W. (2005b) INSL5 is a high affinity specific agonist for *GPCR142 (GPR100). J Biol Chem.* **280**:292-300.

Lok S., Johnston D.S., Conklin D., Lofton-Day C.E., Adams R.L., Jelmberg A.C., Whitmore T.E., Schrader S., Griswold M.D., Jaspers S.R. (2000) Identification of INSL6, a new member of the insulin family that is expressed in the testis of the human and rat. *Biol Reprod.***62**:1593–1599.

Lu C., Lam H.N., Menon R.K. (2005) New members of the insulin family: regulators of metabolism, growth and now… reproduction. *Pediatr Res.* **57**:70R-73R.

Lu C., Walker W.H., Sun J., Weisz O.A., Gibbs R.B., Witchel S.F., Sperling M.A., Menon R.K. (2006) Insulin-like peptide 6: characterization of secretory status and posttranslational modifications. *Endocrinology.* **147**:5611-5623

Lyon M.F., Hawkes S.G. (1970) X-linked gene for testicular feminization in the mouse. *Nature.* **227**:217-1219.

Lyon M.F., Searle A.G. (1989) Genetic variants and strains of the laboratory mouse, 2nd edition. *Oxford University Press.*

Lasky L.A. (1992) Selectins: interpreters of cell-specific carbohydrate information during inflammation. *Science.* **258**:964–969.

Mansour S.L., Thomas K.R., Capecchi M.R. (1998) Disruption of the proto-oncogene int-2 in mouse embryo-derived stem cells: a general strategy for targeting mutations to non-selectable genes. *Nature.* **336**:348-352.

Martin G.R. (1981) Isolation of a pluripotent cell line from early mouse embryos cultured in medium conditioned by teratocarcinoma stem cells. *Proc Natl Acad Sci USA.* **78**:7634-7638.

Martineau Y., Derry M.C., Wang X., Yanagiya A., Berlanga J.J., Shyu A., Imataka H., Gehring K., Sonenberg1 N. (2008) Poly(A)-binding protein-interacting protein 1 binds to eukaryotic translation initiation factor 3 to stimulate translation. *Mol Cell Biol.* **28**:6658–6667.

Mason P. (2001) Contributions of the medullary raphe and ventromedial reticular region to pain modulation and other homeostatic functions. *Annu Rev Neurosci.* **24**:737-777.

Massicotte G., Parent A., St-Louis J. (1989) Blunted responses to vasoconstrictors in mesenteric vasculature but not in portal vein of spontaneously hypertensive rats treated with relaxin. *Proc Soc Exp Biol Med.* **190**:254–259.

Matsuo K, Shintani S, Tsuji T, Nagata E., Lerman M., McBride J., Nakahara Y., Ohyama H., Todd R., Wong D.T. (2000) p12(DOC-1), a growth suppressor, associates with DNA polymerase a/primase. *FASEB J.* **14**:1318-1324.

Mayeur G.L., Fraser C.S., Peiretti F., Block K.L., Hershey J.W.B. (2003) Characterization of *eIF3k*:a newly discovered subunit of mammalian translation initiation factor *eIF3. Eur J Biochem.* **270**:4133–4139

McCarrey J.R., Berg W.M., Paragioudakis S.J., Zhang P.L., Dilworth D.D., Arnold B.L., Rossi J.J. (1992) Differential transcription of *Pgk* genes during spermatogenesis in the mouse. *Dev Biol.* **154**:160-168.

McGowan B.M., Stanley S.A., Smith K.L., White N.E., Connolly M.M., Thompson E.L., Gardiner J.V., Murphy K.G., Ghatei M.A., Bloom S.R. (2005) Central relaxin-3 administration causes hyperphagia in male Wistar rats. *Endocrinology.* **146**:3295–3300.

McGowan B.M., Stanley S.A., Smith K.L., Minnion J.S., Donovan J., Thompson E.L., Patterson M., Connolly M.M., Abbott C.R., Small C.J., Gardiner J.V., Ghatei M.A., Bloom S.R. (2006) Effects of acute and chronic relaxin-3 on food intake and energy expenditure in rats. *Requl Pept.* **136**:72–77.

McGowan B.M., Stanley S.A., Donovan J., Thompson E.L., Patterson M., Semjonous N.M., Gardiner J.V., Murphy K.G., Ghatei M.A., Bloom S.R. (2008) Relaxin-3 stimulates the hypothalamic-pituitary-gonadal axis. *Am J Physiol Endocrinol Metab.* **295**:278-286.

McKern N.M., Lawrence M.C., Streltsov V.A., Lou M.Z., Adams T.E., Lovrecz G.O., Elleman T.C., Richards K.M., Bentley J.D., Pilling P.A., Hoyne P.A., Cartledge K.A., Pham T.M., Lewis J.L., Sankovich S.E., Stoichevska V., Da Silva E., Robinson C.P., Frenkel M.J., Sparrow L.G., Fernley R.T., Epa V.C., Ward C.W. (2006) Structure of the insulin receptor ectodomain reveals a folded-over conformation. *Nature.* **443**:218-221.

Meetei A.R., Rao M.R.S. **(**1996) Cloning of cDNA encoding rat spermatidal protein TP2 and expression in *Escherichia coli*. *Protein Expr Purif.* **8**:409-415.

Mendoza-Lujambio I., Burfeind P., Dixkens C., Meinhardt A., Hoyer-Fender S., Engel W., Neesen J. (2002) The Hook1 gene is non-functional in the abnormal spermatozoon head shape (azh) mutant mouse. *Hum Mol Genet.* **11**:1647-1658.

Meindl A., Carvalho M.R.S., Herrmann K., Lorenz B., Achatz H., Lorenz1 B., Apfelstedt-Sylla E., Wittwer B., Ross M., Meitinger T.(1995) A gene (SRPX) encoding a sushi-repeat-containing protein is deleted in patients with X-linked retinitis pigmentosa. *Hum Mol Gen.***4**:2339-2346.

Mobarakeh J.I.., Takahashi K., Sakurada S., Nishino S., Watanabe H., Kato M., Naghdi N., Yanai K. (2005) Enhanced antinociception by intracerebroventricularly administered orexin A in histamine H1 or H2 receptor gene knockout mice. *Pain*. **118**:254-262.

Moritorio M.L., White E., Newcomb P.A. (2003) Selection bias in the assessment of gene-environment interaction in case-control studies. *Am J Epidemiol.* **158**:259-263.

Moutier R. (1976) New mutations causing sterility restricted to the male rats and mice. In: Antikatzides T., Erichsen S., Spiegel A., (eds.). The laboratory animal in the study of reproduction. *Gustav Fischer Verlag, Stuttgart.* pp. 115-117.

Mukaisho K., Suo M., Shimakage M., Kushima R., Inoue H. Hattori,T. (2002) Down-regulation of drs mRNA in colorectal neoplasms. *J Cancer Res*. **93**:888–893.

Nag S, Mokha S.S. (2004) Estrogen attenuates antinociception produced by stimulation of Kolliker-Fuse nucleus in the rat. *Eur J Neurosci.* **20**:3203-3207.

Nantel F., Monaco L., Foulkes N.S., Masquilier D., LeMeur M., Henriksen K., Dierich A., Parvinen M., Sassone-Corsi P. (1996) Spermiogenesis deficiency and germ-cell apoptosis in CREM-mutant mice. *Nature.* **380**:159–162.

Nayernia K., Nieter S., Kremling H., Oberwinkler H., Engel W. (1994) Functional and molecular characterization of the transcriptional regulatory region of the proacrosin gene. *J Biol Chem*. **269**:32181-32186.

Nayernia K., Adham I.M., Burkhardt-Göttges E., Neesen J., Rieche M., Wolf S., Sancken U., Kleene K., Engel W. (2002) Asthenozoospermia in mice with targeted deletion of the sperm mitochondrion-associated cysteine-rich protein (Smcp) gene. *Mol Cell Biol.* **22**:3046-3052.

Nebel B.R., Amarose A.P., Hacket E.M. (1961) Calendar of gametogenic development in the prepuberal male mouse. *Science.* **134**:832-833.

Nef S., Parada L.F. (1999) Cryptorchidism in mice mutant for *Insl3*. *Nat Genet.* **22**:295-299.

Ness T.J., Follett K.A., Piper J., Dirks B.A. (1998) Characterization of neurons in the area of the medullary lateral reticular nucleus responsive to noxious visceral and cutaneous stimuli. *Brain Res*. **802**:163-174.

Norman D.G., Barlow P.N., Baron M., Day A.J., Sim R.B. and Campbell I.D. (1991) Three-dimensional structure of a complement control protein module in solution. *J Mol Biol*. **219**:717–725.

Oakberg E.F. (1956) Duration of spermatogenesis in the mouse and timing of stages of the cycle of the seminiferous epithelium. *Am J Anat.* **99**:507-516.

O'Dell S.D., Day I.N. (1998) Insulin-like growth factor II (IGF-II). *Int J Biochem Cell Biol.* **30**:767-771.

Ogawa W., Matozaki T., Kasuga M. (1998) Role of binding proteins to IRS-1 in insulin signalling. *Mol Cell Biochem*. **182**:13-22.

Opresko L.K., Brokaw C.J. (2005) cAMP-dependent phosphorylation associated with activation of motility of Ciona sperm flagella. *Gamete Res.* **8**:201-218.

Ossipov M.H., Lai J., Malan T.P., Porreca F. (2000) Spinal and supraspinal mechanisms of neuropathic pain. *Ann NY Acad Sci.* **909**:12-24.

Ott J. (1991) Penetrance. In: Ott J., Analysis of human genetic linkage, revised edition. *The Johns Hopkins University Press, Baltimore*. pp. 146-164.

Overbeek P.A., Gorlov I.P., Sutherland R.W., Houston J.B., Harrison W.R., Boettger-Tong H.L., Bishop C.E., Agoulnik A.I. (2001) A transgenic insertion causing cryptorchidism in mice. *Genesis.* **30**:26-35.

Ovitt C.E., Scholer H.R. (1998) *Mol. Hum. Reprod. The* molecular biology of Oct-4 in the early mouse embryo. **4**:1021–1031.

QIAEX II Handbook. (1999) *Qiagen*.

QIAquick Spin Handbook. (2002) *Qiagen.*

QIAGEN Plasmid Purification Handbook. (2003) *Qiagen*.

Packert G., Kuhn D.T. (1998) The tumorous-head-1 locus affects bristle number of the Drosophila melanogaster cuticle. *Genetics.* **148**:743-752.

Pan J., Nakanishi K., Yutsudo M., Inoue H., Li Q., Oka K., Yoshioka N. Hakura A. (1996) Isolation of a novel gene down-rgulated by v-src. *FEBS Lett,* **383**:21–25.

Parra M.T., Viera, A., Góme R., Page J., Benavente R., Santos J.L., Rufas J.S., Suja J.A. (2003) Involvement of the cohesin RAD21 and SCP3 in monopolar attachment of sister kinetochores during mouse meiosis I. *J Cell Sc.* **17**:1221-1234.

Parvinen M., Hecht N.B. (1981) Identification of living spermatogenic cells of the mouse by transillumination-phase contrast microscopic technique for 'in situ' analyses of DNA polymerase activities. *Histochemistry.* **71**:567-579.

Passos D.O., Doma M.K., Shoemaker C.J., Muhlrad D., Greek R., Weissman J., Hollien J., Parker R. (2009) Analysis of Dom34 and its function in No-Go Decay.(manuscript, not published yet).

Pearse RV, Drolet DW, Kalla KA, Hooshmand F, Bermingham JR, and Rosenfeld MG (1997) Reduced fertility in mice deficient for the POU protein sperm-1. *Natl Acad Sci USA* **94**:7555-7560 .

Pedrazzini T, Seydoux J, Künstner P, Aubert JF, Grouzmann E, Beermann F, Brunner HR (1998) Cardiovascular response, feeding behavior and locomotor activity in mice lacking the NPY Y1 receptor.*Nat Med.* **4**:722-726.

Peng H., Shintani S., Kim Y., Wong D.T. (2006) Loss of p12CDK2-AP1 expression in human oral squamous cell carcinoma with disrupted transforming growth factor-beta-Smad signaling pathway. *Neoplasia.* **8**:1028-1036.

Pesce M., Scholer H.R. (2001) Oct-4: gatekeeper in the beginnings of mammalian development. *Stem Cells* (*Dayton*) **19:**271–278.

Pictet R., Rutter W. (1972) Development of the embryonic pancreas. In Steiner D, Frenkel M. (eds.) *Handbook of physiology***.** *Am Physiol Soc*. 25-66.

Pilder S.H., Olds-Clarke P., Orth J.M., Jester W.F., Dugan L. (1997) Hst7: a male sterility mutation perturbing sperm motility, flagellar assembly, and mitochondrial sheath differentiation. *J Androl.* **18**: 663-671.

Pusch W, Balvers M, Ivell R 1996 Molecular cloning and expression of the relaxin-like factor from the mouse testis. *Endocrinology*. **137**:3009–3013.

Ragan M.A., Logsdon Jr J.M., Sensen C.W., Charlebois R.L., Doolittle W.F. (1996) An archeobacteria homolog of pelota, a meiotic cell division protein in eukaryotes. *FEMS Microbiol Lett.* **114**:151-155.

Rakyan V.K., Blewitt M.E., Druker R., Preis J.I., Whitelaw E. (2002) Metastable epialleles in mammals. *Trends Genet.* **18**:348–351.

Ramalho-Santos M., Yoon S., Matsuzaki Y., Mulligan R.C., Melton D.A. (2002) "Stemness": transcriptional profiling of embryonic and adult stem cells. *Science*. **298**:597–600.

Rassoulzadegan M., Paquis-Flucklinger V., Bertino B., Sage J., Jasin M., Miyagawa K., van Heyningen V., Besmer P., Cuzin F. (1993). Transmeiotic differentiation of male germ cells in culture. *Cell.* **75**:997-1006.

Ravichandran L.V., Esposito D.L., Chen J., Quon M.J. (2001) Protein kinase C-ζ phosphorylates IRS-1 and impairs its ability to activate PI 3-kinase in response to insulin. *J Biol Chem*. **276**:3543–3549.

Ravnik S.E., Wolgemuth D.J. (1999) Regulation of meiosis during mammalian spermatogenesis: the A-type cyclins and their associated cyclin-dependent kinases are differentially expressed in the germ-cell lineage. *Dev Biol.* **207**:408–418.

Ravnik, S.E., Wolgemuth D.J. (1996) The developmentally restricted pattern of expression in the male germ line of a murine cyclin A, cyclin A2, suggests roles in both mitotic and meiotic cell cycles. *Dev Biol.* **173**:69–78.

Regard J.B., Kataoka H., Cano D.A., Camerer E., Yin L., Zheng Y.W., Scanlan T.S., Hebrok M. Coughlin S.R. (2007) Probing cell type-specific functions of Gi in vivo identifies GPCR regulators of insulin secretion. *J Clin Invest*. **117**:4034-43.

Reinecke M., Collet C. (1998) The phylogeny of the insulin-like growth factors. *Int Rev Cytol.* **183**:1-94.

Reinholdt L.G., Munroe R.J., Kamdar S., Schimenti J.C. (2006) The mouse *gcd2* mutation causes primordial germ cell depletion. *Mech Dev.* **123**:559-569.

Robertson K.M., O'Donnell L., Jones M.E., Meachem S.J., Boon W.C., Fisher C.R., Graves K.H., McLachlan R.I., Simpson E.R. (1999) Impairment of spermatogenesis in mice lacking a functional aromatase (cyp 19) gene. *Proc Natl Acad Sci USA.* **96**:7986-7991.

Romanienko P.J., Camerini-Otero R.D. (2000) The mouse *Spo11* gene is required for meiotic chromosome synapsis. *Mol Cell* **6**:975-987.

Romrell L.J., Bellvé A.R., Fawcett D.W. (1976) Separation of mouse spermatogenic cells by sedimentation velocity. A morphological characterization. *Dev Biol.* **49**:119–131.

Rosengren K.J., Bathgate R.A., Craik D.J., Daly N.L., Haugaard-Jönsson L.M., Hossain M.A., Wade J.D. (2009) Structural insights into the function of relaxins. *Ann NY Acad Sci.* **1160**:20-26.

Roy A., Lin Y.N., Agno J.E., DeMayo F.J., Matzuk M.M. (2009) Tektin 3 is required for progressive sperm motility in mice. *Mol Reprod Dev.* **76**:453-459.

Rubinfeld B., Robbins P., El-Gamil M., Albert I., Porfiri E. Polakis P. (1997) Structure-function relationships of the complement components. *Science*. **275**:1790–1792.

Russell L.D., Ettlin R.A., Sinha Hikim A.P., Clegg E.D. (1990) Histological and histopathological evaluation of testis. *Clearwater, USA: Cache River Press.* pp. 120-161.

Russel L.D. (1993). Morphological and functional evidence for Sertoli-germ cell relationship. In: Russell L.D., Griswold M.D. (eds). The Sertoli Cell. *CacheRiver Press, Clearwater*. pp. 365-390.

Saiki R.K., Gelfand D.H., Stoffel S., Scharf S.J., Higuchi R., Horn G.T., Mullis K.B., Erlich H.A. (1988) Primer directed enzymatic amplification of DNA with a thermostable DNA polymerase. *Science.* **239**:487-491.

Sallam M.A.A. (2001) PhD Thesis. The University of Göttingen. Expression and function of mouse Pelota gene.

Saltiel A.R., Kahn C.R. (2001) Insulin signalling and the regulation of glucose and lipid metabolism. *Nature.* **414**:799-806.

Sambrook J., Fritsch E.F., Maniatis T. (1989) Molecular cloning: a laboratory manual. *Cold Spring Harbor Laboratory, New York, USA.*

Samuel C.S., Zhao C., Bathgate R.A., Du X., Summers R.J., Amento E.P., Walker L.L., McBurnie M., Zhao L., Tregear G.W. (2005) The relaxin gene-knockout mouse: a model of progressive fibrosis. *Ann NY Acad Sci.* **1041**:173–181.

Sandkühler J. (1996) The organization and function of endogenous antinociceptive systems. *Prog Neurobiol*. **50**:49-81.

Sanger F., Nicklen S., Coulson A.R. (1977) DNA sequencing with the chain terminating inhibitors. *Proc Natl Acad Sci USA*. **74**:5463-5467.

Saunders P.T.K., Millar M.R., Maguire S.M., Sharpe R.M. (1992) Stage-specific expression of rat transition protein 2 mRNA and possible localization to the chromatoid body of step 7 spermatids by in situ hybridization using a nonradioactive riboprobe. *Mol Reprod Dev.* **33**:385-391.

Schlessinger J. (2000) Cell signaling by receptor tyrosine kinases. *Cell.* **103**:211-225.

Schneider I., Tirsch W.S., Faus-Kessler T., Becker L., Kling E., Busse R.L., Bender A., Feddersen B., Tritschler J., Fuchs H., Gailus-Durner V., Englmeier K.H., Hrabé de Angelis M., Klopstock T. (2006) Systematic, standardized and comprehensive neurological phenotyping of inbred mice strains in the German Mouse Clinic. *J Neurosci Methods.* **157**:82-90.

Seller M.J., Embury S., Polani P.E., Adinolfi M. (1979). Neural tube defects in curly-tail mice. II. Effect of maternal administration of vitamin A. *Proc R Soc Lond B Biol Sci.* **206**:95-107.

Shabanowitz R.B., DePhilip R.M., Crowell J.A., Tres L.L., Kierszenbaum A.L. (1986) Temporal appearance and cyclic behavior of Sertoli cell-specific secretory proteins during the development of the rat seminiferous tubule. *Bio lReprod.* **35**:745-60.

Shamsadin R., Adham I.M., von Beust G., Engel W. (2000) Molecular cloning, expression and chromosome location of the human pelota gene PELO. *Cytogenet Cell Genet*. **90**:75-78.

Shamsadin R., Adham I.M., Engel W. (2002) Mouse pelota gene (*Pelo*): cDNA cloning, genomic structure, and chromosomal localization. *Cytogenet Genome Res*. **97**:95-99.

Sharov AA, Piao Y, Matoba R, Dudekula DB, Qian Y. (2003) Transcriptome analysis of mouse stem cells and early embryos. *PLoS Biol* 1:E74

Sherwood O.D. (1994) Relaxin. In: Knobil E., Neill J.D., eds. Physiology of reproduction. *Raven Press, New York.* pp. 861-1009.

Sherwood O.D. (2004) Relaxin's physiological roles and other diverse actions. *Endocr rev.* **25**:205-234.

Shih D.M., Kleene K.C. (2002) A study by in situ hybridization of the stage of appearance and disappearance of the transition protein 2 and the mitochondrial capsule seleno-protein during spermatogenesis in the mouse. *Mol Reprod Dev.* **33**:222-227.

Shimakage M., Kawahara K., Kikkawa N., Sasagawa T., Yutsudo M., Inoue,H. (2000) Downregulation of drs mRNA in human colon adenocarcinomas. *Int J Cance.* **87**:5–11.

Shimakage M., Takami K., Kodama K., Mano M., Yutsudo M. Inoue,H. (2002) Expression of drs mRNA in human lung adenocarcinomas. *Hum Pathol.* 33:615–619.

Shintani S., Ohyama H., Zhang X., McBride J., Matsuo K., Tsuji T., Hu M.G., Hu G., Kohno Y., Lerman M., Todd R., Wong D.T. (2000) p12(DOC-1) is a novel cyclin-dependent kinase 2-associated protein. *Mol. Cell. Biol.* **20**:6300–6307.

Shintani S., Mihara M., Terakado N., Nakahara Y., Matsumura T., Kohno Y., Ohyama H., McBride J., Kent R., Todd R., Tsuji T., Wong D.T.W.W. (2001) Reduction of p12DOC-1 expression is a negative prognostic indicator in patients with surgically resected oral squamous cell carcinoma. Clin Cancer Res **7**:2776–2782.

Shirneshan K. (2005) PhD Thesis. The University of Göttingen. Expression, functional and regulation analysis of selected genes from the Insulin family.

Silver L.M. (1995) Mouse Genetics: concepts and applications. *Oxford University Press.*

Singh A.P., Harada S., Mishina Y. (2009) Downstream genes of *Sox8* that would affect adult male fertility. *Sex Dev.* **3**:16-25.

Siuciak J.A., McCarthy S.A., Chapin D.S., Martin A.N., Harms J.F., Schmidt C.J. (2008) Behavioral characterization of mice deficient in the phosphodiesterase-10A (PDE10A) enzyme on a C57/Bl6N congenic background. *Neuropharmacology*. **54**:417-427.

Skinner M.K. (1991). Cell-cell interactions in the testis. *Endocr Rev.* **12**:45-77.

Snow M.H.L. (1977) Gastrulation in the mouse: growth and regionalisation of the epiblast. *J Embryol Exp Morphol*. **42**:293–303.

Song X., Wong M.D., Kawase E., Xi R., Ding B.C., McCarthy J.J. and Xie T. (2004). Bmp signals from niche cells directly repress transcription of a differentiation-promoting gene, bag of marbles, in germline stem cells in the Drosophila ovary. *Development* **131:** 1353-1364.

Southern E.M. (1975) Detection of specific sequences among DNA fragments separated by gel electrophoresis. *J Mol Biol.* **98**:503-517.

Spanel-Borowski K., Schäfer I., Zimmermann S., Engel W., Adham I.M. (2001) Increase in final stages of follicular atresia and premature decay of corpora lutea in *Insl3*-deficient mice. *Mol Reprod Dev.* **58**:281-286.

Summers S.A., Kao A.W., Kohn A.D., Backus G.S., Roth R.A., Pessin J.E., Birnbaum M.J. (1999) The role of glycogen synthase kinase 3β in insulinstimulated glucose metabolism. *J Biol Chem.* **274**:17934-17940.

Sutton S.W., Bonaventure P., Kuei C., Roland B., Chen J., Nepomuceno D., Lovenberg T.W., Liu C. (2004) Distribution of G-protein-coupled receptor (GPCR)135 binding sites and receptor mRNA in the rat brain suggests a role for relaxin-3 in neuroendocrine and sensory processing. *Neuroendocrinology*. **80**:298-307.

Sweeney C., Murphy M., Kubelka M., Ravnik S.E., Hawkins C.F., Wolgemuth D.J., Carrington M. (1996) A distinct cyclin A is expressed in germ cells in the mouse. *Development.* **122**:53–64.

Syed V., Hecht N. (1997) Up-regulation and down-regulation of genes expressed in co-culture of rat Sertoli cells and germ cells. *Mol Reprod Dev.* **47**:380-389.

Tagami S., Eguchi Y., Kinoshita M., Takeda M. Tsujimoto Y. (2000) A novel protein, RTN-xS, interacts with both Bcl-xL and Bcl-2 on endoplasmic reticulum and reduces their anti-apoptotic activity. *Oncogene*s, **19:**5736–5746.

Tambe Y., Isono T., Haraguchi S., Yoshioka-Yamashita A., Yutsudo M., Inoue H. (2004) A novel apoptotic pathway induced by the drs tumor suppressor gene. *Oncogene.* **23**:2977–2987.

Tambe Y., Yoshioka-Yamashita A., Mukaisho K., Haraguchi S., Chano T., Isono T., Kawai T., Suzuki Y., Kushima R., Hattori T., Goto M., Yamada S., Kiso M., Saga Y., Inoue1 H. (2007) Tumor prone phenotype of mice deficient in a novel apoptosis-inducing gene, drs. *Carcinogenesis.* **28**:777–784.

Tamemoto H., Kadowaki T., Tobe K., Yagi T., Sakura H., Hayakawa T., Terauchi Y., Ueki K., Kaburagi Y., Satoh S., Sekihara H., Yoshioka S., Horikoshi H., Furuta Y., Ikawa Y., Kasuga M., Yazaki Y., Aizawa S. (1994) Insulin resistance and growth retardation in mice lacking insulin receptor substrate-1. *Nature*. **372**:182-186.

Tanaka S.S., Toyooka Y., Akasu R., Katoh-Fukui Y., Nakahara Y., Suzuki R., Yokoyama M., Noce T. (2000) The mouse homolog of Drosophila Vasa is required for the development of male germ cells. *Genes Dev.* **14**:841-853.

Tanaka M., Iijima N., Miyamoto Y., Fukusumi S., Itoh Y., Ozawa H., Ibata Y. (2005) Neurons expressing relaxin 3/INSL 7 in the nucleus incertus respond to stress. *Eur J Neurosci.* **21**:1659-1670.

Tanti J.F., Gremeaux T., van Obberghen E., Le Marchand-Brustel Y. (1994) Insulin receptor substrate 1 is phosphorylated by the serine kinase activity of phosphatidylinositol 3-kinase. *Biochem J.* **304**:17-21.

Tanti J.F., Gremeaux T., van Obberghen E., Le Marchand-Brustel Y. (1994) Serine/threonine phosphorylation of insulin receptor substrate 1 modulates insulin receptor signaling. *J Biol Chem*. **269**:6051-6057.

Tash J.S., Means A.R. (1982) Regulation of protein phosphorylation and motility of sperm by cyclic adenosine monophosphate and calcium. *Biol Reprod.* **26**:745–763.

Todd R., McBride J., Tsuji T., Donoff R.B., Nagai M., Chou M.Y., Chiang T., Wong D.T. (1995) Deleted in oral cancer-1 (doc-1), a novel oral tumor suppressor gene *FASEB J.* **9**:1362–1370.

Tollervey D. (2006). RNA lost in translation. *Nature.* **44**0:425–426.

Tomoda K., Kubota Y., Arata Y., Mori S., Maeda M., Yoshida M., Yoneda-Kato N., Kato J.Y. (2002) The cytoplasmic shuttling and subsequent degradation of p27Kip1 mediated by Jab1/CSN5 and the COP9 signalosome complex. *J Bio Chem.* **277**:2302–2310.

Toscani A., Mettus R.V., Coupland R., Simpkins H., Litvin J., Orth J., Hatton K.M., Reddy P.R. (1997) Arrest of spermatogenesis and defective breast development in mice lacking A-myb. *Nature.* **386**:713 – 717.

Towne C.F., York I.A., Neijssen J., Karow M.L., Murphy A.J., Valenzuela D.M., Yancopoulos G.D., Neefjes J.J., Rock K.L. (2008) Puromycin-sensitive aminopeptidase limits MHC class I presentation in dendritic cells but does not affect CD8 T cell responses during viral infections. *J Immunol.* **180**:1704-1712.

Tregear G.W., Bathgate R.A., Hossain M.A., Lin F., Zhang S., Shabanpoor F., Scott D.J., Ma S., Gundlach A.L., Samuel C.S., Wade J.D. (2009) Structure and activity in the relaxin family of peptides. *Ann NY Acad Sci.* ***1160***:5-10.

Tsuji T., Duh F.M., Latif F., Popescu N.C., Zimonjic D.B., McBride J., Matsuo K., Ohyama H., Todd R., Nagata E., Terakado N., Sasaki A., Matsumura T., Lerman M. I., Wong D.T. (1998) Cloning, mapping, expression, function, and mutation analyses of the human ortholog of the hamster putative tumor suppressor gene Doc-1. *J. Biol. Chem.* **273**:6704–6709.

Tybulewicz V.L., Crawford C.E., Jackson P.K., Bronson R.T., Mulligan R.C. (1991) Neonatal lethality and lymphopenia in mice with a homozygous disruption of the c-abl protoncogene. *Cell*. **65**:1153-1163.

Van Der Westhuizen E.T., Summers R.J., Halls M.L., Bathgate R.A., Sexton P.M. (2007) Relaxin receptors - new drug targets for multiple disease states. *Curr Drug Targets.* **8**:91-104.

van Hoof A., Frischmeye P.A., Dietz H.C., Parker, R. (2002) Exosome-mediated recognition and degradation of mRNAs lacking a termination codon. *Science.* **295**:2262–2264.

Vasudevan S., Peltz S.W., Wilusz C.J. (2002). Non-stop decay - a new mRNA surveillance pathway. *Bioessays.* **24**:785–788.

Vidal F., Lopez P., Lopez-Fernandez L.A., Ranc F., Scimeca J.C., Cuzin F., Rassoulzadegan M. (2001) Gene trap analysis of germ cell signaling to Sertoli cells: NGF-TrkA mediated induction of *Fra1* and *Fos* by post-meiotic germ cells. *J Cell Sci.* **114**:435-443.

Vincent S., Segretain D., Nishikawa S., Nishikawa S.I., Sage J., Cuzin F., Rassoulzadegan M. (1998) Stage-specific expression of the Kit receptor and its ligand (KL) during male gametogenesis in the mouse: a Kit-KL interaction critical for meiosis. *Development.* **125**:4585-4593.

Voronina E., Wessel G.M. (2004) Regulatory contribution of heterotrimeric G-proteins to oocyte maturation in the sea urchin. *Mech Dav.* **121**:247-259.

Waters S.H., Distel R.J., Hecht N.B. (1985) Mouse testes contain two size classes of actin mRNA that are differentially expressed during spermatogenesis. *Mol Cell Biol*. **5**:1649-1654.

Watson C.M., Tam P.P. (2001) Cell lineage determination in the mouse. *Cell Struct. Funct.* **26:**123–129.

White M.F. (1997) The insulin signalling system and the IRS proteins. *Diabetologia*. **40** Suppl:S2-17.

White M.F. (1998) The IRS-signaling system: a network of docking proteins that mediate insulin and cytokine action. *Recent Prog Horm Res*. **53**:119-138.

Wilkinson T.N., Speed T.P., Tregear G.W., Bathgate R.A. (2005) Evolution of the relaxin-like peptide family. *BMC Evol Biol.* **5**:14.

Wilkinson T.N., Bathgate R.A. (2007) The evolution of the relaxin peptide family and their receptors. *Adv Exp Med Biol.* **612**:1-13.

Willis W.D., Westlund K.N. (1997) Neuroanatomy of the pain system and of the pathway that modulate pain. *J Clin Neurophysiol.* **14**:2-31.

Wilusz C.J., Wormington M., Peltz S.W. (2001). The cap-to-tail guide to mRNA turnover. *Nat. Rev. Mol. Cell Biol.* **2**:237–246.

Withers D.J., Gutierrez J.S., Towery H., Burks D.J., Ren J.M., Previs S., Zhang Y., Bernal D., Pons S., Shulman G.I., Bonner-Weir S., White M.F. (1998) Disruption of IRS-2 causes type 2 diabetes in mice. *Nature.* **391**:900-904.

Withers D.J., Burks D.J., Towery H.H., Altamuro S.L., Flint C.L., White M.F. (1999) Irs-2 coordinates Igf-1 receptor-mediated β-cell development and peripheral insulin signaling. *Nat Genet*. **23**:32-40.

Withers D.J., White M.F. (2000) Perspective: the insulin signaling system - a common link in the pathogenesis of type 2 diabetes. *Endocrinology*. **141**:1917-1921.

Wojtusciszyn A., Armanet M., Morel P., Berney T., Bosco D. (2008) Insulin secretion from human beta cells is heterogeneous and dependent on cell-to-cell contacts. *Diabetologia.* **51**:1843-1852.

Xi R., Doan C., Liu D., Xie T. (2005) Pelota controls self-renewal of germline stem cells by repressing a Bam-independent differentiation pathway. *Development.* **132**:5365-74.

Yamashita A., Hakura A., Inoue,H. (1999) Suppression of anchorageindependent growth of human cancer cell lines by the drs gene. *Oncogene*. **18:**4777–4787.

Yenush L., White M.F. (1997) The IRS-signalling system during insulin and cytokine action. *Bioessays*. **19**:491-500.

Yoshioka H., Geyer C.B., Hornecker J.L., Patel K.T., McCarrey J.R. (2007) In vivo analysis of developmentally and evolutionarily dynamic protein-DNA interactions regulating transcription of the *Pgk2* gene during mammalian spermatogenesis. *Mol Cell Biol.* **27**:7871–7885.

Yu Y.E., Zhang Y., Unni E., Shirley C.R., Deng J.M., Russell L.D., Weil M.W., Behringer R.R., Meistrich M.L. (2000) Abnormal spermatogenesis and reduced fertility in transition nuclear protein 1-deficient mice. *Proc Natl Acad Sci USA*. **97**:4683-4688.

Zarrindast M.R., Alaei-Nia K., Shafizadeh M. (2001) On the mechanism of tolerance to morphine-induced Straub tail reaction in mice. *Pharmacol Biochem Behav.* **69**:419-424.

Zhao L., Roche P.J., Gunnersen J.M., Hammon E., Tregear G.W., Wintour E.M., Beck F. (1999) Mice without a functional relaxin gene are unable to deliver milk to their pups. *Endocrinology.* **140**:445-453.

Zhao M., Shirley C.R., Mounsey S., Meistrich M.L. (2004) Nucleoprotein transitions during spermiogenesis in mice with transition nuclear protein TNP1 and TNP2 mutations. *Biol Reprod.* **71**:1016–1025.

Zimmermann S., Schöttler P., Engel W., Adham I.M. (1997) Mouse Leydig insulin-like (Ley I-L) gene: structure and expression during testis and ovary development. *Mol Reprod Dev.* **47**:30–38.

Zimmermann S., Steding G., Emmen J.M., Brinkmann A.O., Nayernia K., Holstein A.F., Engel W., Adham I.M. (1999) Targeted disruption of the *Insl3* gene causes bilateral cryptorchidism. *Mol Endocrinol.* **13**:681-691.

7. PUBLICATIONS AND PRESENTATIONS

Publications

Dabrowska G., Dzialuk A., **Burnicka O.**, Jankowski W., Gugnacka-Fiedor W., Goc A. (2006) Genetic Diversity of Postglacial Relict Shrub *Betula Nana* Revealed by RAPD Analysis.

Burnicka-Turek O., Shirneshan K., Paprotta I., Grzmil P., Meinhardt A., Engel W., Adham IM (2009) Inactivation of Insulin-like factor 6 (*Insl6*) Disrupts the Progression of Spermatogenesis at Late Meiotic Prophase. **Manuscript submitted and accepted for publication in *Endocrinology***.

Presentations- Posters

Bubnicka O., Marszal J., Dabrowska G. 2003. The Analysis of The Plant Genome of The Population of *Betula nana* in The Linie Reserve Using RAPD-PCR Method. 1st Conference of The Polish Society for Plant Experimental Biology, September, Olsztyn, Poland.

Buyandelger B., **Burnicka O.,** Hartung M., Ebermann L., Sallam M., Engel W., Adham I.M. 2006. The Role of Pelota (*Pelo*) during The Cell Cycle. 17th Annual Meeting of the German Society of Human Genetics, March, Heidelberg.

Burnicka O., Buyandelger B., Ebermann L., Sallam M., Engel W., Adham I.M. 2007. Functional Analysis of Pelota during The Cell Cycle. 18th Annual Meeting of the German Society of Human Genetics, March, Bonn.

Burnicka O., Shirneshan K., Dutschmann M., Racz I., Fuchs H., Barakat A., Engel W., Adham I.M. 2008. Analysis of The Physiological Role of Insulin-like Factor 5. 19th Annual Meeting of the German Society of Human Genetics, April, Hannover.

ACKNOWLEDGEMENTS

There are many people to whom I wish to thank and who helped me, taught me and encouraged me along the way.

I wish to express my deepest gratitude to Prof. Dr. med. W. Engel for the chance he gave me, to make my PhD study in the Institute of Human Genetics. I would like to thank for his permanent support, encouragement, valuable scientific discussions, supervision and for always being ready to lend a helping hand in all situations involving not only the work. I am also indebted to him for editing my thesis, despite having a very busy schedule.

My particular gratitude goes to my supervisor Prof. Dr. I.M. Adham for his invaluable support, stimulating advises and for being so enthusiastic, an endless resource of ideas (it is truly inspiring). His door has always been open for answering my questions, listening and taking the time to explain. Thank you for the long hours at your office that were filled with sparkling (and sometimes emotional) scientific disputes and ideas; for your patience with my 'the' and 'a' in English and for all the corrections and revisions made to the text that is about to be read.

I sincerely thank Prof. Dr. S. Hoyer-Fender to be my co-referee. I also extend my sincere thanks to Prof. Dr. V. Lipka and Prof. Dr. P. Kappeler for the accepting to be my examiners and Prof. Dr. D. Doenecke and Prof.Dr.I. Feußner for the accepting to be committee members for managing to read the whole thesis so thoroughly, despite having a very busy schedule.

I would like to warmly thank my friend Dr. Pawel Grzmil who asked the "hard" questions when they were needed and helped make sense of my results along the way. Thank you for sharing of your vast knowledge in many subjects, help with proof-reading of my thesis, patience, providing me criticism and advices in the right proportions and for teaching me how to tackle a scientific topic from the right perspective. Your constant support and enthusiasm has brightened many a dark unproductive days.

I am indeed thankful to Dr. M. Dutschmann for his excellent collaboration regarding *Insl5* immunohistochemistry analysis. I am also very thankful to Prof. Dr. A. Meinhardt for his cooperation regarding the spermatogenesis study.

I would also like to thank PD Dr. Annie Goc for her help, friendly relationship, proof-reading the manuscript and for good time spend together at different occasions.

A particular note of thanks must go to Dr. A. ul-Mannan and his lovely wife, Shahnoor Shah for stimulating talks (not only scientific) and for their good friendship. I will miss our lunch time a lot.

While this PhD has been one of the most challenging experiences of my life, it has also been one of the most rewarding thanks to the wonderful friends I have made along the way. Therefore, I would like to appreciate all of the former and current members of lab. 108 for their numerous advices, constant support, fantastic work atmosphere and for the great time we had over the last few years. You guys make terrible experiments appear like a walk in the park.
Especially, I thank: Amal (for your fantastic positive attitude to hard work and for being so friendly and supportive), Gonjee (for your enthusiasm and your sweet personality), Ilona (for your help and providing friendly atmosphere), Khulan (for support, "opening my eyes" and creating a lovely and pleasant environment in the lab), Mahmoud (for all your help in many different ways, support, stimulating discussions and friendship, it has been a great opportunity to know you), Meike (for our laugh, your exuberance and for breaking one of cultural stereotypes of Germans) and Ogie (for our discussions about Polish and Mongolian cultures and for all the great times we have had together in the lab and in the "real world").

I would like to thank all my institute colleagues and co-workers for being so friendly and helpful during my stay. It has been a pleasure working in such an inspiring and friendly atmosphere as you have created in the Institute of Human Genetics. Special thanks to Agusia (for being sources of energy, happiness and laughter every day), Birgit (for all nice conversations and your humour, which have given me so many bright moments), Janine (for your technical support in some experiments performed in this work), Krishna (for friendship, inspiration and shared knowledge), Leticia (for your friendship, support, and nice company) and Sofia (for opportunity to know your culture and country better).

Most especially, let me thank one of my "best lab friend", Tatjana (Tania) for her kindness, support, care, friendship and for supplying me with encouragement when I needed it over these past years. Thank you for all laughs and for our somewhat repetitive but always entertaining talks about everything from science to childbirth. A big warm Polish hug for you!

Many thanks to Christina for help and professional technical assistance, for never giving up on all my different cloning- and transfection strategies (We made it!), and for being a great person to work with. I hope that you don't have nightmares with me and minipreps☺.

Thanks to my students, Ann Christin, Martina, Meike, Nadine and Sasha for their contribution to the project and for nice time spend together.

I am grateful to the secretaries: Mrs. P. Albers and Mrs. A. Winkles at the Institute of Human Genetics for excellent administrative assistance and for kind and friendly attitude.

I would also like to thank Jutta, Stephan and Tony for their technical assistance in generation and breeding of knock-out mice.

A huge thanks to my wonderful friends all over the world who tried to keep patient in the case I forgot again a birthday, or again had no time to meet because important experiments were waiting for me, or invited us to so many dinners and managed to be there for me and to cheer me up every time I needed a good friend. This work would for sure not have been done without your friendship.
Particularly, I would like to warmly thank: Oli and Wackowi, Jarkowi, Karolinie, Mackowi, Mariuszowi and Pawlowi for the special Polish spirit.

Extra special thanks to my best friend Ewa for always making me smile and for lively discussions regarding everything within this universe! Thank you for making my life happier, brighter and for your understanding. I hope once I finish my PhD thesis I can repay you support, help and love in some way.

I would like to thank all of the Polish friends, which I made during these five years in Göttingen, for the extraordinary time we have spent here. You know who you are! However, there are a few persons I would like to mention by name: Asia and Lukasz, Asia and Lukasz, Dominika and Mirek, Halinka and Kazik, Iwona and Artur, Renata and Pawel, Agnieszka, Aneta, Ania, Ania, Irmina and Marzena for their encouragement, continued moral support, humour (sometimes ironic) and friendship. Thanks for long movie nights and for making the weekends and social events the best ever, I am so proud to have you as my friends.

Of course none of this would ever have been possible without my family! Mum, Dad, Oskar, Grandma, Grandpa, Marietta, Bozena, Zuzia, Milenka, Leszek, Jurand and Marcin, what can I say? I left Poland five years ago and have missed you all everyday, but with that distance has come an appreciation of how lucky I am to have such a loyal, generous and supportive family. You can't possibly know how much those phone calls mean to me, especially when I was on my own and in need of a little lift. However, it is the self-belief you have always instilled into me that allowed me to pursue and then conquer this challenge.
Special thanks go to my "family through marriage": Mum, Dad, Beatka, Gosia, Ilonka, Olenka, Wikusia, Adam, Bodzio, Krzysiek and Mariusz. Nothing would have been possible without your continuous support, help, love, caring and your faith in us.

Finally, and the most importantly I would like to thank Kazik, my husband, best friend, confidant and voice of reason. While I may have been able to do this on my own, I doubt I would be as sane if not for his undying love, support and belief, not to mention his snuggles. Together we conquer the world darling!!!

Curriculum vitae

Personal Details:

Name	Ozanna Burnicka-Turek
Date of Birth	3rd July 1980
Place of Birth	Bydgoszcz, Poland
Nationality	Polish
Sex:	Female
Martial Status:	Married
Permanent Address:	Boh. Westerplatte Street 5/5
	85 – 827 Bydgoszcz, Poland
E-mail:	oburnic@gwdg.de; ozborn@wp.pl

Educational Background:

1987 – 1999	Primary and Secondary School, Bydgoszcz, Poland
May 1999	High School Diploma
1999 – 2004	Studies of Biology at Nicolas Copernicus University, Faculty of Biology and Earth Sciences, Torun, Poland. Specialization: Molecular Biology - Genetics
2002 – 2004	Experimental Work Performed for Masters Thesis in The Laboratory of Genetics, The Institute of Genetics and Molecular Biology at Nicolas Copernicus University in Torun, Poland Scientific supervision: PD. Dr. Anna Goc
July 2004	Master of Science. Dissertation for MSc Thesis: **"The Analysis of The Plant Genome of The Population of *Betula nana* in The Linie Reserve Using RAPD Method "**
2004 – Present	PhD studies at the Georg-August University Göttingen, Institute of Human Genetics, under the supervision of Prof. Dr. med. W. Engel Dissertation for PhD Thesis: **"Functional Analysis of *Insl5* and *Insl6* Genes and Verification of Interactions between Pelota and its Putative Interacting Proteins"**